AD-A172 245 SEAT EXPERIMENT RESULTS OF FULL-SCALE TRANSPORT AIRCRAFT CONTROLLED IMPAC (U) RMS TECHNOLOGIES INC TREVOSE PA M R CANNON ET AL JUL 86 TR-85413 1/3

UNCLASSIFIED DOT/FAA/TT-85/25 DTFA03-81-C-00040 F/G 1/3 NL

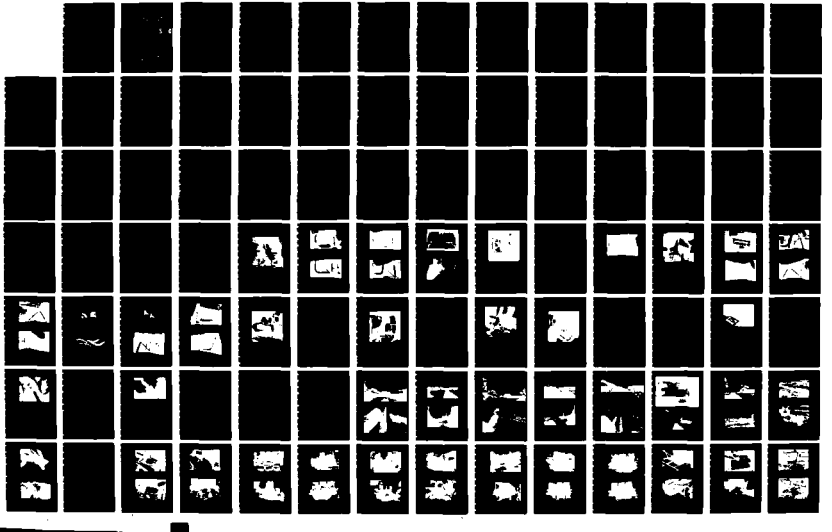

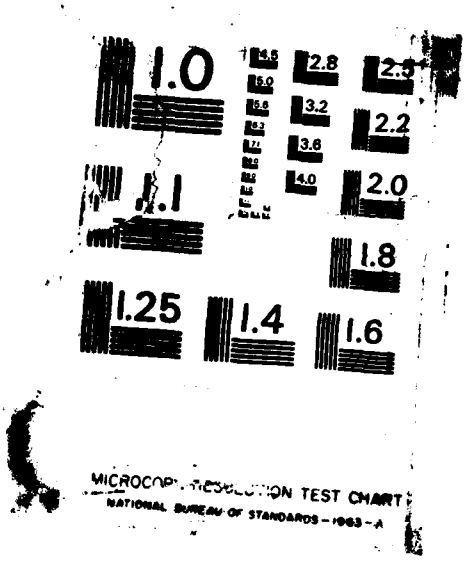
1.0
1.1
1.25
1.4
1.6
1.8
2.0
2.2
2.8
3.2
3.6
4.0
MICROCOPY RESOLUTION TEST CHART
NATIONAL BUREAU OF STANDARDS - 1963 - A

DOT/FAA/CT-85/25

FAA TECHNICAL CENTER
Atlantic City Airport
N.J. 08405

Seat Experiment Results Full-Scale Transport Aircraft Controlled Impact Demonstration

Mark R. Cannon
Richard E. Zimmermann

RMS Technologies, Inc./Simula Inc.
Trevose, PA/Tempe, AZ

July 1986

Final Report

U.S. Department of Transportation
Federal Aviation Administration

NOTICE

This document is disseminated under the sponsorship of the Department of Transportation in the interest of information exchange. The United States Government assumes no liability for the contents or use thereof.

The United States Government does not endorse products or manufacturers. Trade or manufacturer's names appear herein solely because they are considered essential to the object of this report.

Technical Report Document Page

1. Report No.	2. Government Accession No.	3. Recipient's Catalog No.
DOT/FAA/CT-85/25	AD-A172245	

4. Title and Subtitle
Seat Experiment Results of Full-Scale Transport Aircraft Controlled Impact Demonstration

5. Report Date
July 1986

6. Performing Organization Code

8. Performing Organization Report No.
TR-85413

7. Author(s)
Mark R. Cannon and Richard E. Zimmermann

10. Work Unit No. (TRAIS)

9. Performing Organization Name and Address
Simula Inc.
10016 S. 51st St.
Phoenix, AZ 85044

RMS Technologies, Inc.
1200 Church St.
Mt. Laurel, NJ 08054

11. Contract or Grant No.
DTFA03-81-C-00040

13. Type of Report and Period Covered
Final
January 1985 - July 1985

12. Sponsoring Agency Name and Address
Federal Aviation Administration
Technical Center
Atlantic City Airport, New Jersey 08405

14. Sponsoring Agency Code
ACT-330

15. Supplementary Notes

16. Abstract

This report describes the results of the Federal Aviation Administration (FAA) seat experiments tested in the joint FAA/NASA Controlled Impact Demonstration (CID). Twenty-three seats were placed on the test aircraft. Thirteen seats were modifications of existing transport seats which were designed structurally to improve their crashworthiness. The remaining experiments were unmodified standard seats which included seven light and heavy-weight forward-facing seats, two aft-facing seats, and one flight attendant seat. Three additional seat experiments were placed onboard the test aircraft: two by NASA, and one by a private contractor.

Onboard instrumentation was placed at specific locations to obtain data pertaining to airframe structural loads and seat/occupant response. Accelerometers were attached to the airframe and floor structure, the seat experiments, and the anthropomorphic dummies occupying the seats. The data base resulting from the test was intended for validating crash prediction models and occupant/seat dynamic simulation models. Keywords:

17. Key Words
Transport Seats
Crashworthiness
Human Tolerance
Impact Dynamics
Crash Environment
~~Seat Experiments~~
Controlled Impact
Demonstration

18. Distribution Statement
This document is available to the U.S. public through the National Technical Information Service, Springfield, Virginia 22161

19. Security Classif. (of this report)	20. Security Classif. (of this page)	21. No. of Pages	22. Price
Unclassified	Unclassified	251	

Form DOT F 1700.7 (8-72)

PREFACE

This report describes the Controlled Impact Demonstration (CID) seat experiments conducted by Simula Inc. and RMS Technologies, Inc. under Federal Aviation Administration (FAA) Technical Center Contract DTFA03-81-C-00040. The objective was to demonstrate the performance of standard and modified transport seats in the crash environment caused by the CID. Technical monitor for the FAA Technical Center was Mr. Dick Johnson, FAA Transport Program Manager. The contractor's technical monitor was Mr. Roger Lloyd, Program Manager.

TABLE OF CONTENTS

TABLE OF CONTENTS (CONTD)

LIST OF FIGURES

LIST OF FIGURES (CONTD)

LIST OF FIGURES (CONTD)

LIST OF FIGURES (CONTD)

LIST OF TABLES

EXECUTIVE SUMMARY

The objective of the FAA/NASA Controlled Impact Demonstration (CID) of a Boeing 720 was to demonstrate the performance of an antimisting fuel additive. Other objectives were to obtain data pertaining to airframe structural loads and seat/occupant response, and to demonstrate crashworthy seat experiments. The FAA placed nine standard transport seats and one flight attendant seat onboard the aircraft. Twelve transport seats and one flight attendant seat were modified to improve their structural crashworthiness and were also placed onboard. Three additional seat experiments were conducted by NASA and a private contractor.

A total of 352 data channels were used for recording measured accelerations and loads on the airframe and floor structure, the seat experiments, and the anthropomorphic dummies occupying the seats. Of these, 179 channels were dedicated to the FAA crashworthiness seat experiments. The collected data were intended to validate crash prediction models and seat/occupant dynamic simulation models.

The CID resulted in a fuselage fracture and a posttest fire. The fire severely damaged several of the seat experiments. The crash impact condition was not severe enough to conclusively evaluate the difference between the standard and modified seats. However, a significant quantity of data was obtained showing the interaction between the aircraft floor, seats, and dummies in a mild, survivable crash. Additionally, a majority of the onboard camera film survived the fire and allowed observations to be made of the seats' performance during the impact.

INTRODUCTION

This report describes the results of the Federal Aviation Administration (FAA) crashworthiness seat experiments tested in the joint FAA/NASA Controlled Impact Demonstration (CID) of a Boeing 720 on December 1, 1984, at the NASA Dryden Flight Research Facility, Edwards Air Force Base, California.

The objective of the CID was to demonstrate the performance of an antimisting fuel additive. Other objectives were to obtain data pertaining to airframe structural loads and crashworthiness. Both the FAA and NASA installed seat experiments aboard the aircraft. This report covers the FAA seat experiments. A total of 352 data channels were used to measure pertinent accelerations and loads. Of these, 179 channels were dedicated to the FAA crashworthiness seat experiments.

The experiments were centered around existing standard transport seats and modifications made to those seats that improved their crashworthiness. Details concerning the development of the modified seats, the rationale, assumptions, criteria, and performance testing are in a separate report entitled Seat Experiments for the Full-Scale Transport Aircraft Controlled Impact Demonstration (DOT/FAA/CT-84/10). This report contains discussions of all the work pertaining to the seat experiments up to the actual crash test.

The crash test resulted in a fuselage fracture and a posttest fire. The fire severely damaged several of the seat experiments.

However, the crash impact condition was not severe enough to conclusively evaluate the difference between the standard and modified seats. A significant quantity of data was obtained showing the interaction between the aircraft floor, seats and dummies, and is presented herein.

Additionally, Program SOM-TA (Seat Occupant Model - Transport Aircraft) was used to model the seat experiments and then compared to the actual test data. After satisfactory correlation between the data and SOM-TA simulations was obtained, the simulations were used to predict data not available from the test.

DEVELOPMENT OF SEAT EXPERIMENTS

The seat modifications were developed in a multistep process. First, standard seats were subjected to both static and dynamic destructive testing to determine the ultimate structural strengths and failure modes. Then, concepts for improving the structural integrity in a crash were developed. Layouts of promising concepts were prepared to examine their feasibility, and finite element models were used to analyze the structural stresses resulting in the proposed modifications. Detailed designs for the modification components were then prepared. The necessary parts were fabricated, the seats modified accordingly, and static verification tests conducted to show that the modified structure performed as anticipated. Dynamic verification tests were also conducted to further establish confidence in the design. Finally, additional indentical seats were modified and installed on the test aircraft.

SEAT PROCUREMENT.

The following seats were selected and procured for the modification program:

- Weber P/N 819493, triple-occupant seat - 20 ea.
- Weberlite 4000, triple-occupant seat - 10 ea.
- UOP Model 901, triple-occupant seat - 14 ea.
- Trans-Aero Model 90835-4, flight attendant seat - 4 ea.

In each case, equal quantities of right- and left-hand passenger seats were purchased.

The Weber P/N 819493 seat was selected because it was representative of seat designs on early, narrow-bodied aircraft such as the Boeing 707/720 and Douglas DC-8 aircraft, and presented a baseline consistent with the airframe. The seat has a tubular steel leg structure typical of many transport seats. A later design, the Weberlite 4000 is very similar to the Weber P/N 819493 in appearance, but is approximately 30 lb lighter. Therefore, it was chosen as a sample of a modern lightweight structure with a design similar to the older seats. The UOP Model 901 seat was selected because it is also a modern lightweight seat, but the leg construction uses built-up sheet metal members rather than steel tubing. The Trans-Aero Model 90835-4 flight attendant seat is used on the Boeing 737, and was selected as a representative of present day flight attendant seats. Flight attendant seats from the era of the Boeing 727 were not included because there was not enough space available to mount more flight attendant seats.

DESTRUCTIVE TESTS.

Two destructive tests were run: static and dynamic. The static tests permitted the application of loads at controlled rates so that the sequence and mode of failure could be easily observed. The dynamic tests were conducted to observe the effects of an actual crash condition.

STATIC TESTS. The destructive static tests were conducted at Simula Inc. Sections of heavy-duty Brownline floor track having the same critical dimensions as the track in the test aircraft were attached to a rigid fixture mounted in a rigid loading frame. No attempt was made to simulate the flexibility of an aircraft floor. The seat was placed on the fixture and body blocks in accordance with NAS 809 were then secured to the seats with the lap belts. The blocks were slightly modified to better approximate the actual geometry of an occupant under loaded conditions.

Hydraulic cylinders were connected to each of the body blocks, with load cells at the interfaces. The cylinders were connected to a common hydraulic power unit so that the same pressure would be applied to each cylinder and approximately the same load would be applied to each body block. The presence of three load cells permitted recording the exact load applied to each of the body blocks.

The cylinders were used to apply loads in the three most critical directions: forward, downward and sideward. String potentiometers were connected to points of interest on the structure to record displacement as deformation occurred. In most cases, the motion of the rear transverse seat pan tube was measured in the forward and downward directions at the center of each seat position while the lateral displacement was measured at one end of the tube.

Force and deflection data were recorded on magnetic tape as the load was increased to ultimate failure. Later, these data were digitized, processed, and plotted in the form of applied force versus deflection curves for the different seat positions. Numerous pretest and posttest photographs of the seat were taken. Although the seats were tested to destruction, all of the standard seats successfully demonstrated the ability to resist a 9-G static load.

DYNAMIC TESTS. Dynamic tests were conducted at the FAA Civil Aeromedical Institute in Oklahoma City. The seats were mounted on a sled which is accelerated by a falling weight. The sled impacts an array of wires which are pulled through a selected arrangement of pins and absorb the energy necessary to stop the sled with the desired deceleration. Redundant tiedown straps are attached to the dummies in case of ultimate seat failure.

The seats were installed on sections of floor track which were mounted on load cells so the floor reaction forces could be measured. The tracks could also be pitched and rolled 10 degrees to simulate floor warpage. One track was pitched, and the other was rolled.

Instrumented anthropomorphic dummies were installed in the seats and secured with lap belts. The belts were instrumented with tensiometers. High-speed motion pictures were taken during the test, while still photographs were taken before and after the test. The tests were conducted with a 9-G, 50-ft/sec pulse equivalent to that used by CAMI in prior seat testing. This pulse was chosen because it allowed a sufficiently long 9-G deceleration to be applied to the seat and dummies, such that the maximum response of the seat was tested. The current standards require seats to sustain a 9-G forward static load without failing. The test pulse was intended to test the seats' capabilities at a 9-G forward inertial load. This pulse initiated ultimate failures on all the standard seats tested.

MODIFICATION PROCESS.

ASSUMPTIONS. Assumptions were made during the conceptual design of the seat modifications to ensure that changes made would not render the seat incompatible or unreasonable in terms of general configuration, weight, cost, and comfort. It was assumed that the envelope of any seat must be reasonably similar to that of existing transport seats: it must permit the same seating density and provide the same amount of space for the occupant and carry-on luggage. Most significantly, the space beneath the seat must remain available for luggage and for the feet of an occupant in the seat to the rear.

Another assumed requirement was that of minimal weight increase. This is implied by the current trend of weight reductions in transport seats to reduce operating costs. Earlier triple-occupant seats such as the Weber P/N 819493 and Hardman Model 8727 seats weigh between 80 and 90 lb. The Weberlite 4000, a more recent seat, weighs 55 lb, and the latest UOP 910 composite seat is advertised as weighing 42 lb.

In view of this trend, considerable resistance can be expected to any design change which would require increased seat weight. Therefore, it was concluded that design concepts involving appreciable weight increases were not worth pursuing. This did not prevent modifying the seats to comply with design criteria, but emphasis had to be placed on energy-absorbing (load-limiting) capability rather than on rigid structural strength.

A similar situation was assumed to exist relative to cost. It was therefore determined that design concepts be limited to those which could be mass produced using conventional materials.

It was assumed that a survivable crash need not be limited to one in which no serious airframe rupture or breakage occurred. In a large transport aircraft, survivable volumes for a large percentage of the occupants could be maintained even if the fuselage separated completely.

It was assumed that any changes made to the seat cushion, backrest cushion, or their respective angles and heights that would appreciably reduce comfort were impermissible.

It was assumed that compatibility with existing seat tracks and airframes was highly desirable. While a greater degree of crashworthiness would be obtained if the floor and tracks were reinforced, such reinforcement might be quite expensive; a design which could be used with the existing airframe structures would have a much higher probability of being placed into service.

Crashworthiness could also be improved if the floor tracks were symmetric with respect to the passenger seating position. The current asymmetry of the tracks in the B720 and 727 causes the window-side legs of the triple-passenger seat to support twice as much load as the aisle-side legs. Consequently, under crash loading conditions the window-side seat experiences greater deformation, and, as tests have shown, is the first to fail. Due to the asymmetry, three occupants in the seat do not necessarily constitute the worst loading condition on the seat legs. Under a forward load, even more load is transferred to the windowside legs if the aisle-side seat is empty. It was assumed that many new seats would still need to be designed in the present asymmetric fashion, since the new generation aircraft such as the Boeing 757 and 767 use this asymmetric track configuration, and will probably be in service for 10 to 20 years. Therefore, no changes in leg location were made on any of the experimental seats.

DESIGN GOALS. Current transport seat design requirements set forth in NAS Specification 809 are ultimate loads of 9.0 G forward, 1.5 G sideward, 6.0 G downward, and 2.0 G upward. The present standards require these load factors be applied statically to the seat. Successful resistance of these loads demonstrates that the seat possesses the minimum strength required in the various directions. However, in the crash environment, loads are applied dynamically, and the seat and occupant respond differently than under a static load situation. Because of the dynamic response of the nonrigid system consisting of occupant and seat, the peak G can impose loads on the floor surface which exceed the loads experienced during a static test. This was verified by the aforementioned dynamic tests.

As a result of these considerations, the seat modification activity of the project was designed to demonstrate the feasibility of improving crash survivability through minor modifications such as load limiting, while not increasing weight or cost significantly.

Seat design criteria of 18 G forward, 10 G sideward, 10 G downward, and 6 G upward were proposed under this program. Dynamic criteria and corresponding pulse shapes were also defined. Details concerning the rationale for these criteria are presented in the aforementioned report DOT/FAA/CT-84/10. For an occupant to survive exposure to these G loads and related environment, the seat must either have sufficient strength to sustain the loads, or be designed to deform, and thereby limit the forces acting on it. The latter approach is preferable, to the extent that existing seat tracks and floor structures in transport aircraft may not support these loads, and increasing the floor strength of the aircraft would not be an acceptable solution because of the expense. Since none of the loads contained in the proposed seat design criteria exceed human tolerance levels, the only purpose of energy absorption is to limit the loads imposed on the structure and thus avoid the additional weight associated with a design that could sustain the unattenuated G loads. However, seat designs which feature controlled forward deformation or stroking must be evaluated with respect to injuries that might result from increasing the occupant impact envelope.

A more crashworthy transport seat for use in existing aircraft could require some energy-absorbing stroke in the forward direction. This reflects past conclusions, as is evidenced by the fact that all energy absorbing transport seats which were tested or produced in the past had energy-absorbing stroke in the forward direction. Approximately 12 in. of stroke is required to accommodate the recommended forward criteria of 18 G, 50 ft/sec if the seat is designed to stroke at 9 G, in order for the resulting floor reactions to be compatible with the floor strength. Unfortunately, this much space is simply not available. A 6-in. forward stroke, which was assumed to be more reasonable, can accommodate an input pulse of 18 G and 35 ft/sec but not 18 G and 50 ft/sec. Previous energy-absorbing seats described in DOT/FAA/CT-84/10 were also designed with a 6-in. forward stroke. However, this was done at a time when the pitch (spacing) of the seats was generally greater than it is now. Present day interior arrangements would be somewhat less conducive to a stroke of 6 in. To this extent, serious thought must be given to stroking designs which might result in occupant injuries. Therefore, given the limited amount of space available in current transport aircraft, the selection of a maximum forward stroking distance involves some difficult tradeoffs. At impact, three adults seated behind a seat which is empty, partially occupied, or occupied by one or more children, could possibly be injured, trapped, or impeded in their egress. In a crash with inertial loads of over 9 G, the seat would stroke forward while the one in front of the three adults may not. Undesirable as this result is, it would most likely be less lethal to the overall group of passengers than a situation where seats break loose.

In other words, while a few people may be impeded by the stroking seats, a much larger number will benefit because of their presence. Also, any passengers trapped as discussed above would probably have been much more seriously injured (and perhaps also trapped) if their seat failed completely, which it would do if subjected to an environment which caused an energy absorbing seat

to stroke. Therefore, passengers will have a better chance of surviving the crash provided that a fire does not occur. These are difficult but necessary choices to consider when dealing with the closely spaced seating in transport aircraft.

Another element which is a very important factor in crashworthy design is floor warpage. Under some crash conditions, the floor under the seat is likely to deform. Adequate strength or load-limiting features capable of supporting crash loads are of little value if the seat structure cannot conform to floor deformations without failure. In addition to improving the capability of the seats to sustain crash loads on a flat floor or test fixture, it was determined that the ability of the seat to survive floor warpage could be improved. A series of tests conducted by the FAA showed that many current transport seats do not have release mechanisms designed into them to assure that the floor attachments will remain intact if the floor is deformed. Some of the seats have rear-leg track fittings attached by a single bolt, which permits rotation about the pitch axis. However, the front-leg fittings are not released in this manner, nor is there any provision for relative motion about the roll axis for either set of fittings. Even without floor deformation, this lack of a roll release has been shown to be a cause of attachment failure in lateral testing.

Furthermore, if a transport seat has too great a torsional rigidity about the pitch axis, the four legs may not remain attached to the floor even if the attachment fittings are released in both the pitch and roll axes. At least one of the fittings (or some portion of the leg structure) may fail if the floor is deformed in a manner which causes one of the fittings to significantly move out of plane with respect to the other three fittings. Some modifications which allow twisting about the pitch axis were considered necessary to be compatible with representative floor warpage conditions. Ideally, a seat should be designed with releases in the structure to permit twisting about the pitch axis without failing. An alternate solution is provided incorporating energy absorbers in the rear legs. Then one leg can extend and all four fittings can remain attached if the floor is deformed.

Thus, the design goals selected for the seat experiments consisted of the criteria described in Reference 1, together with the provision that the floor track fittings have a roll release, and that the seat also be able to sustain out-of-plane warpage of the floor. All of these considerations are directed towards increasing the probability of seat retention during a survivable crash of significant severity.

STATIC VERIFICATION TESTS. After the seats were modified, they were statically tested. The tests were performed to assure that the seat had the strength characteristics predicted by the design and analysis effort. They also demonstrated the proper operation of the energy absorbers. The same test procedure previously featured in the destructive static tests was used. However, if the seat successfully sustained the design loads, it was not necessarily pulled to destruction. This allowed the seat to be used in other static tests. (No dynamic test specimen was subjected to prior tests.)

DYNAMIC VERIFICATION TESTS. Dynamic verification tests were also conducted at CAMI. The tests were conducted in the same manner as the initial destructive tests. Again, only the forward test was conducted because of the limited number of test specimens.

The deceleration pulse in the dynamic verification tests was exactly the same as in the destructive dynamic tests even though it did not utilize the full energy-absorbing capability of the modified seats. It did allow a direct comparison between the performance of unmodified and modified seats under identical test conditions. No dynamic tests were conducted on the flight attendant seats.

After dynamic and static verification tests were conducted with the modified seat designs, additional seats were modified for installation aboard the test aircraft. Two samples of each modification were fabricated and instrumented prior to shipment to the test site.

SEAT EXPERIMENTS

STANDARD SEATS.

As previously mentioned, the standard seat experiments aboard the test aircraft were chosen to represent several types of seats: older seats still in use and more modern seats. These seats are listed in table 1 along with the item letter used to identify them on the test aircraft, and are described as follows.

TABLE 1. STANDARD SEAT EXPERIMENTS

Item	Quantity	Description	No. of Occupants
A	2	Weberlite 4000	3
B	2	UOP Model 901	3
C	2	Weber P/N 819493	3
D	2	Hardman/UOP Aft-Facing Model 9777	2
S	1	Trans-Aero Model 90835-6	2

WEBERLITE 4000. The seat pan structure consists of front and rear aluminum tubes which run the entire width of the seat assembly and are connected by tubular spreaders placed between each seating position and on each end. The two center spreaders consist of a tube riveted to front and rear fittings. The front fitting is a forged eye-fitting through which lies the front tube. The rear fitting holds the rear tube and also branches upward to support the seat backs and provide them with a pivot point. The rear fittings also have a seat belt attachment point forged into them. The two end spreaders are constructed of an oval-shaped tube welded to a "C"-shaped bracket which slips around bolts to the front tube. The rear of the spreaders is welded to a short cylinder which slips inside the rear tube, and is bolted into place through the walls of the tube. The two outside seat belt fittings are anchored with nut plates at the juncture of the cylinders and the rear tube.

The seat pans consist of flexible, plasticized fabric stretched between the front and rear tubes. The pans are attached by stretcher bars which run through hems in the fabric and bolt to each tube.

The leg structure consists of front and rear legs of square steel tubing connected by a diagonal brace of the same material. Welded to the top of each leg is a "C"-shaped bracket which straddles and bolts to either the front or the rear tube. Views of the seat and leg structure are in figures 1 and 2. The weight of the seat as shown is 63 lb.

The rear legs are attached to the track with a forged fitting manufactured by Ancra Corporation. The forging is made of 4140 steel which is heat treated between 180 and 200 ksi. A detented locking plunger slides up and down on the front of this forging, and an antirattle mechanism is attached to the rear. The fitting is attached to the seat leg with a single bolt, which provides a release about the pitch axis.

The front legs are attached with single studs. The stud is affixed to a steel bracket which is welded into the tubular leg. The stud has no locking mechanism, and is held in the track only as long as the rear fitting and seat structure keep it in the proper longitudinal position.

UOP MODEL 901. The seat pan assembly is built around aluminum front and rear tubes which are connected by four forged aluminum supports. The front of each support rests on top of the front tube and is attached by two bolts running through the support and the tube. The rear of each support has a semicircular cut-out that slips over the rear tube and attaches with one bolt. Three of the supports have cantilevered rear extensions which provide a pivot and anchor point for the armrests and seat backs. The seat cushions rest on perforated aluminum sheets which are riveted to the front tube in front, and wrapped around a small aluminum tube which slips in between the cantilevered extensions in the rear. Figure 3 shows the basic seat structure. The seat weight as shown is 64 lb.

The leg assembly consists of front and rear legs of formed stainless steel sheet, which are connected diagonally by a square aluminum tube. The front legs cradle and bolt to the front tube, while the rear legs are held to the rear tube by steel straps which are wrapped around the tube and bolted to the

legs. Each rear leg is connected to the diagonal tube by a steel fitting which is riveted to the leg and the tube, and is also bolted to the steel strap.

The rear legs are attached to the floor track by a fitting consisting of two studs and a lever-operated plunger. The plunger moves in and out of the track and is in the front of the fitting. The fitting is attached to the leg by a single bolt.

The front legs are attached to the track by a single stud which is incorporated in an antirattle mechanism. The stud is bolted to a yoke, which is attached to both the front leg and diagonal tube by a single bolt. An aluminum strap connects the front stud and rear fitting in order to transfer the loads from the tubular diagonal brace to the plunger.

WEBER P/N 819493. The seat pan assembly is built around aluminum front and rear tubes connected with four spreader tubes. The spreader tubes are connected to the front and rear tubes with forged aluminum fittings. Cantilevered extensions of the fittings, which are attached to the rear tube, support a smaller tube which provides a pivot and anchor point for the seat backs. Perforated aluminum sheets riveted to the three tubes which traverse the width of the seat support the bottom seat cushions. Figure 4 shows the basic seat structure. The seat weight as shown is 97 lb.

The leg assemblies are fabricated of square 4130 steel tubing, and have been heat treated between 125 and 140 ksi. Welded steel fittings on the legs are bolted to the front and rear tubes of the seat pan.

The rear legs are attached to the track with a forged fitting manufactured by Ancra Corporation. The forging is made of 4140 steel which has been heat treated between 180 and 200 ksi. A detented locking plunger slides up and down on the front of this forging, and an antirattle mechanism is attached to the rear. The fitting is attached to the seat leg with a single bolt, which provides a release about the pitch axis.

The front legs are attached with single studs. The stud is fixed to a steel bracket which is welded into the tubular leg. This stud has no locking mechanism, and is held in the track only as long as the rear fitting and seat structure keep it in the proper longitudinal position.

HARDMAN/UOP AFT-FACING MODEL 9777. This is a double-occupant aft-facing seat and was not involved in the modification process, but was placed on the test aircraft as a standard, aft-facing seat experiment. The seat pan assembly has four forged aluminum supports connecting the front and rear lateral aluminum tubes. Unlike the triple-occupant seats, this seat has a tray placed between the two seat positions, and because it is aft-facing, the Hydrolock recline adjustments have been replaced by two solid aluminum rods to brace each seat back.

The leg assembly consists of formed stainless steel sheet front and rear legs connected diagonally by a square aluminum tube. The front and rear legs cradle and bolt through the lateral seat pan tubes and are reinforced by riveted doublers where they connect to the track fittings. Figure 5 shows the seat structure. As shown, the seat weighs 57 lb.

The front legs (relative to the aircraft) attach to the floor track by a single stud which has a "screw-down" antirattle mechanism similar to that on the UOP 901 seat. The rear track fitting (relative to the aircraft) consists of two studs and a screw-operated cam plunger which moves in and out of the track between the two studs.

TRANS-AERO MODEL 90835-6. The flight attendant seat structure is made up of a foam core seat pan installed on rails for folded storage when not in use. The seat pan itself consists of a sheet metal face over the foam core. A spar tranverses the seat pan about 1 in. forward of the pivot arm attach points. A steel frame is attached to the spar and around the periphery of the top face (figure 6). The bottom and sides of the seat pan are covered by a decorative, thermoplastic sheet with a recessed handle. At each rear corner of the seat pan is a roller on a bracket that attaches to the rear and sides of the seat pan frame (figure 7).

The rollers travel inside a vertical extruded track on either side of the seat pan. A pivot arm is attached to the seat pan on the sides just behind the seat pan spar, and to the side rail above the stopping point of the roller. The pivot arm is spring-loaded to fold the seat against the wall when it is not held down by an occupant sitting in it. The seat weighs 13 lb.

The seat is designed to be wall mounted with a separate seat back cushion and restraint system attached directly to the aircraft wall. The side rails are connected to the wall with bolts through six holes in each rear flange: four near the top and two near the bottom. Because the seat was not designed for specific use on the test aircraft, an adapter made of aluminum channel was designed so the seat could be attached to the bulkhead (figure 8).

MODIFIED SEATS.

As discussed in the "Standard/Modified Seat Development" section, the objective of the seat experiments was to modify the seats to withstand an 18-G, 35-ft/sec pulse. The downward and lateral strength objectives, both 10 G (static), were still assumed to apply. However, in the design of the modifications, it was found that the lateral bracing required to meet the design objective might entail an unacceptable weight penalty, depending on the seat structure. Therefore, the criterion was reduced to a lower G-level to accommodate the particular structure being modified. Since the standard seats had a lateral strength of at least 3 G, it was felt that the modification should at least demonstrate the impact of doubling the lateral strength to 6 G. The seat modifications are listed in table 2 and are matched to the item letter used to identify them on the test aircraft. A brief description of each follows, but a more thorough description and justification of the designs is contained in DOT/FAA/CT-84/10.

PROTOTYPE TRACK FITTINGS. All of the seat modifications were fitted with three-button prototype track fittings which were designed to improve seat retention by withstanding higher loads and allowing floor deformation without failing. The prototype fitting was tested and compared with four standard two-button track fittings that are currently used on transport seats. Compared to the strongest standard fitting, the prototype fitting was 1000 lb stronger in the upward direction and had equal strength in the forward direction.

TABLE 2. MODIFIED SEAT EXPERIMENTS

Item	Quantity	Description	No. of Occupants
E	2	Weberlite MOD	3
F	2	UOP MOD I	3
G	2	Weber MOD I	3
H	2	UOP MOD II	3
I	2	Weber MOD II	3
K	1	Weber Aft MOD	3
P	1	Weber Standard with Simula Track Fittings	3
T	1	Trans-Aero MOD	2

Furthermore, the fitting is made out of a ductile material and is designed to deform extensively without fracture. This provides a plastic hinge that allows more than 30 degrees of track roll or leg bending without failure (figure 9).

WEBERLITE MOD. The structure of the seat is shown in figure 10. Energy absorbers made of round stainless steel tubing and designed to begin elongating at specific loads were encased in square, aluminum tube housings and replaced the seat's rear legs and diagonal struts. Stronger front legs and lateral bracing were also added. The weight of the seat was 68 lb.

UOP MOD I. The diagonal struts were replaced with compressive, inversion-tube energy absorbers and stronger rear legs were installed. The original front legs were retained but extended and reinforced to attach to the prototype track fittings. Figure 11 shows the modified seat structure. Its weight was 67 lb.

WEBER MOD I. Instead of integrating the energy absorbers into the leg structure, the restraint system was modified (figure 12) so the lap belts actuated a wire-bending energy absorber at a specific load. A reinforced leg structure replaced the original structure (figure 13) and the seat pans were replaced with stronger ones. The seat weighed 100 lb. It was especially heavy because the concept was an add-on rather than a new design. Appreciable weight savings could be anticipated if the energy absorber was designed as an integral part of the seat.

UOP MOD II. This modification used rear-leg energy absorbers which incorporated an inversion tube and a die being pulled through a tube. A stronger diagonal strut was used and the original front legs were extended and reinforced (figure 14). The seat weighed 67 lb.

WEBER MOD II. Like the UOP MOD II, this modification also used rear leg energy absorbers. However, the concept of tandem inversion tube energy absorbers was tested. The entire leg assembly was replaced with a stronger one; the seat pans were also replaced with stronger versions. Figure 15 shows the seat leg structure. The seat weighed 89 lb.

WEBER AFT MOD. This modification used the four spreader and armrest tubes from the Weber P/N 819493 seat, but the remainder of the seat was completely revised. Because the seat became aft-facing, reinforced seat backs were installed along with appropriate bracing to support them. A reinforced leg structure was used and compressive tandem inversion tube energy absorbers were used as front legs (relative to the aircraft). The inefficiencies involved in turning a forward-facing seat into a rear-facing seat caused the seat to weigh 88 lb. The seat is shown in Figure 16.

WEBER P/N 819493 WITH SIMULA TRACK FITTINGS. The only change made to the original seat was the addition of doublers and clevises to the legs to accomodate the prototype track fittings (figure 17).

TRANS-AERO MOD. The pivot arm bracket (figure 18), pivot arm assembly (figure 19) and seat pan roller bracket (figure 20) were reinforced to increase the seat's downward static strength from 7.5 to 10 G. From the standpoint of outward appearance, the change to the original seat was unnoticeable. The modification added 2.8 oz to the 13-lb seat.

ADDITIONAL SEAT EXPERIMENTS.

Additional seat experiments were placed onboard the test aircraft by other organizations.

UOP MODEL 910 - ITEM J. This seat was purchased by the FAA and shipped directly to NASA Dryden for placement on the test aircraft. The seat leg structure is not unlike that of the UOP Model 901 seat, but the seat pan is fabricated of lightweight composite material (figure 21). The seat was installed because it represents the state of the art in transport aircraft seats.

NASA SEAT EXPERIMENTS. NASA installed two seats onboard the aircraft. One was a standard Burns-Aero Airest 2000 seat (figure 22), and the other was a modification to that seat using a crushable graphite tube energy absorber (figure 23).

FRENCH SEAT. A seat manufactured by Sicma Aero Seats, Inc. of France was installed by Dynamic Science (figure 24). Since the onboard instrumentation had already been assigned when the seat was installed, the seat was supported by its own instrumentation system.

SEAT EXPERIMENTS SETUP

FLOOR PLAN.

The seat experiments were placed aboard the aircraft as shown in figure 25. A right-hand and left-hand configuration of each seat type was included, except for the aft-facing Weber, the Weber with Simula fittings, and the UOP 910 seats. As illustrated in figure 25, the seats were placed with most of the seat pairs separated: one in the forward cabin and one in the aft cabin. This was done since it was believed that the test could provide the opportunity to obtain data for two different crash environments for one seat type. The body station numbers in figure 25 reference the location of the seats' front legs.

The seats were spaced in an attempt to minimize interaction between experiments. While there is obvious interaction between seat/occupant systems in a real crash due to the close spacing, or in cases where the seats are designed to stroke forward, it was felt that little could be learned in this test if close spacing was used, due to the fact that the seat designs were all different. The fact that not all seats were modified to stroke was a further complication. If load was transferred from one seat to another due to extensive dummy/seat contact, there would be no way of determining how the seat would have performed had the load not been transferred. (A closely spaced test with identical seats would of course be meaningful; the load transferred to the seat ahead could be presumed to be approximately offset by load applied to the seat by the occupants behind it). To limit interaction between seat experiments, the spacing was arranged to prevent or at least limit head and torso impact of the dummies into the next seat. It was not possible to space the seats to prevent arm and leg impact.

It was also desirable to limit seat experiment interaction because computer simulations with Program SOM-TA were planned for the postcrash analysis. The response of the structure by itself is of interest. Dummy impact on the rear of a seat would provide input to the accelerometers that would not be simulated in the analysis and would interfere with correlations.

ANTHROPOMORPHIC DUMMIES.

Eleven instrumented 50th-percentile anthropomorphic dummies were used in the seat experiments. Nine of these were Part 572 dummies from Humanoid Systems and the other two were made by Sierra. They were dressed in tight-fitting thermal underwear (with sleeves and legs cut off) to obtain a realistic coefficient of friction between the dummy and seat upholstery (figure 26). The joints of the dummies were adjusted so that the limbs would just barely move under the influence of gravity. They were positioned in the seats shown in figure 27. The triple-passenger seats had the instrumented dummy in the center position, the Hardman aft-facing seat and rear flight attendant seat had the instrumented dummy in the aisle position, and one instrumented dummy was placed in the pilot's seat. The remainder of the seats were occupied by uninstrumented Model 500H dummies manufactured by Med-d-Trane. They were not anthropomorphic dummies, but did have the proper mass and physical dimensions to apply the proper inertial loads to the seats. There was one exception: the standard Weber seat with Simula fittings (Seat P) had an infant dummy in the aisle seat position (figure 28); it represented a six-month old, 14.7-lb

child. Paper targets were positioned on he head, shoulder, and knee of all the dummies to facilitate evaluating motion observed with the available camera coverage.

All the dummies were secured in their respective seats with new FAA approved lap belts, pulled as tightly as possible by hand. The belts were Model No. 449470 from American Safety Equipment Corporation.

SECONDARY RESTRAINTS.

A secondary restraint system was installed on each seat experiment to keep the seat in position in case of failure. This was done to prevent one failure from initiating a succession of failures as seats contacted one another. The components of the secondary restraint system consisted of polyester slings and expanding-tube energy absorbers. The slings were cinched about the waists of the dummies, and connected to the energy absorbers, which were in turn connected to floor track fittings. The attachment to the dummies is illustrated in figure 29. The energy absorbers were designed to stroke at a load of 6000 lb for a distance of 6 in. An energy absorber in the unstroked and stroked position is illustrated in figure 30. This system used two energy absorbers per seat, and would therefore limit the load applied to a typical experimental seat to 12000 lb if the seat were to fail. The secondary restraint system was installed with 6 in. of slack so that it would not interfere with the energy-absorbing function of the modified seat.

The system was tied to the dummies, because this appeared to be the most reliable means of restraining both the seat and dummy should the seat fail. The installation shown in figure 29 is typical of the restraint system used on the various seat configurations.

INSTRUMENTATION

The aircraft floor, experimental seats, and dummies were instrumented with Endevco Model 7264-200 and 2260A-250 accelerometers, and LeBow Model 3419 lap belt tensiometers. To obtain various data requirements with limited data channels, the instruments were distributed unequally among the seats. Simula was responsible for installing seat and dummy instrumentation. NASA Dryden was responsible for installation of the floor and fuselage instrumentation and NASA Langley was responsible for data acquisition and processing.

The direction designations used by NASA Langley for the accelerometers were N (normal), L (longitudinal) and T (transverse). The normal direction is vertical and the transverse direction is lateral. Three types of accelerometer configurations were used. The "normal" accelerometers were uniaxial and measured only in the vertical direction. These were commonly the Model 2260A-250. The "biaxial" accelerometers measured the vertical and longitudinal (N and L) directions. The "triaxial" accelerometers measured all three (N, L, and T) directions. The accelerometers were oriented so that the downward direction was positive for vertical accelerations, "forward" was positive for longitudinal accelerations, and "right" was positive for lateral accelerations.

FLOOR ACCELEROMETERS.

The floor accelerometers were divided among the different seat experiments at the locations shown in figure 31. The normal accelerometers were mounted on the seat track directly behind the seats' aisle-side rear leg (figure 32) and the biaxial and triaxial accelerometers were mounted beneath the floor on the inboard floor beams where the beams intersected the floor track (figure 33). It was assumed that the vertical accelerations would experience the most variation throughout the aircraft, so every seat location had a normal accelerometer on the floor. The longitudinal accelerations would vary to a lesser degree, and the lateral accelerations even further since the floor beams were relatively rigid in the lateral direction. As figure 31 illustrates, the distribution of the floor accelerometers was prioritized according to these assumptions; 20 vertical, 11 longitudinal, and 7 lateral accelerometers.

SEAT ACCELEROMETERS.

Every seat except seats P and K had a triaxial accelerometer mounted on the rear lateral seat pan tube near the aisle leg (figures 34 and 35). Some seats had an additional longitudinal accelerometer (notated as EXL in the appendix data) placed near the window leg because the assymetry of the seat structure could cause variations in longitudinal accelerations along the width of the seat. It was assumed the aisle side of the seats would, in most cases, experience higher decelerations than the window side, since the window side leg assembly would be subject to a greater load and experience more deformation. The triaxial accelerometer was placed on the aisle side because more output was expected and because the accelerometers were in line with floor accelerometers and would give the best correlation of input versus output for the structure. The seat accelerometers were mounted near the intersection of the rear legs and rear tube to attempt to measure a representative acceleration of the structure independent of the free vibration response of any of the seat components.

DUMMY ACCELEROMETERS.

Each of the eleven anthropomorphic dummies was instrumented with a triaxial accelerometer in the pelvis. Three dummies had additional accelerometers placed in their head and thorax. Figure 36 shows the locations of the dummy accelerometers.

LAP BELT TENSIOMETERS.

The lap belt restraint on each anthropomorphic dummy was equipped with tensiometers. The rear flight attendant and pilot dummy had additional tensiometers on their shoulder restraints. The tensiometers used were known to produce erroneous readings under certain conditions where a load was applied to the base of the device as tension was applied to the belt on which it was installed. In the intended application, the thigh and/or pelvis of the dummy would apply a load to the base of the tensiometer. As a solution, guide blocks (figure 37) were installed to suspend the tensiometers on the belts and prevent them from experiencing load other than that provided by belt tension.

DATA ACQUISITION.

Data from the sensors aboard the aircraft were collected and processed by two onboard data acquisition systems (DAS). It was filtered, multiplexed, then digitized and sampled for onboard recording and telemetrization to a ground station. The accelerations from the dummies' head, chest, and pelvis were filtered at 180 Hz. Floor and seat accelerations and lap belt loads were filtered at 100 Hz. After filtering, the 180 and 100 Hz data were digitized, then sampled approximately every 1 and 2 milliseconds, respectively.

The range of each data channel was dependent on the instruments' placement and orientation, as shown in table 3.

TABLE 3. INSTRUMENTATION RANGE*

Location	Orientation	Range
Dummy - Head, Thorax, Pelvis	N, L	± 150 G
Thorax, Pelvis	T	± 50 G
Seat and Floor	N	± 150 G
	L	± 100 G
	T	± 50 G
Lap Belt		0 to 1500 lb

*N = Normal (vertical), L = Longitudinal, T = Transverse (lateral)

Each instrumentation channel had an 8-bit word assigned to it for digitizing its output. Using this 8-bit format allowed $256(2^8)$ discrete units to measure the full range of each accelerometer or load cell. For example, if an accelerometer was set to 300-G full range (± 150 G), the smallest measurable acceleration would be (300/256) G or 1.17 G. Likewise, an accelerometer set to ±100 G would have a resolution no better than (200/256) G or 0.78 G.

After the CID data was made available for analysis, it was discovered that this instrumentation ranging procedure was not consistent. Figure 38 is an example of this. Three acceleration plots from floor-mounted vertical accelerometers are shown with the smallest measurable G and the resulting ranges. Similar occurences were found throughout the seat and dummy data. This does not invalidate the data, but it does require an explanation in the Data Interpretation section concerning the inaccuracies inherent in the CID data.

CID FLIGHT

TEST AIRCRAFT.

The aircraft used in the Controlled Impact Demonstration was a Boeing 720 that originally belonged to the FAA and had outlived its serviceable life. Though obsolete, the aircraft was representative in design and construction of transports currently in service, and thus yielded pertinent data for the structural and seat experiments.

PLANNED IMPACT SCENARIO.

Since the impact of the aircraft had to satisfy the structural and seat experiments and the antimisting fuel additive experiment, it was determined that the aircraft would first touch down in a wheels-up landing to obtain the structural data, then slide through obstacles to open the wing tanks and spill the fuel.

It was planned that the aircraft would impact at 150 knots with a sink rate of 17 ft/sec, a glide path of 3.3° to 4.0°, and a nose-up attitude of 1° (figure 39). This would be a symmetric impact prior to the obstacles, a series of large, steel, wing-opening devices (figure 40), allowing the fuselage to slide between them. Beyond the wing openers was a 1200-ft long by 300-ft wide, packed bed of railroad rock to provide an ignition source for the spilled fuel. Additionally, powered landing lights were placed in the aircraft's slide-out path and jet-fueled flame generators were mounted in the tail cone to assist in igniting the fuel.

IMPACT TEST.

The CID flight was under the ground-based control of a NASA test pilot and was accompanied by a Beech King Air, acting as chase, in case an abort required a landing. Two helicopters and an Orion P-3 over the impact area provided photographic coverage along with over 50 ground-based cameras. A final calibration of the instrumentation was performed before take-off.

On final approach to the impact site, the aircraft had a speed of 144 to 148 knots, an approximate sink rate of 17 ft/sec, and a pitch attitude of 0°. It was experiencing roll oscillations which caused the left outboard engine to touch ground first (figures 41 and 42), 410 ft short of the target. This initiated a left yawing motion of the aircraft. The forward portion of the fuselage (approximately B.S. 540) then touched down (figures 43 and 44) and the aircraft continued to yaw as it slid through the wing openers (figure 45). A fire erupted when a wing opener impacted the right inboard engine. The right wing, having been failed by the obstacles, separated, lifted upward as the aircraft continued to slide (figure 46), then plummeted into the ground (figure 47) and slid under the fuselage. In the meantime, fuel entered the cargo area of the aircraft through holes left by the wing openers and began burning. Since the crash fire rescue team was concentrating on saving the contents of the cabin, it was not discovered until much later that a major source of the fire was in the cargo area. The main locations of fire damage occurred where the fire had burned up through the floor, into the cabin, then out through the roof.

POSTTEST OBSERVATIONS

FUSELAGE.

According to the onboard films and outside cameras there was no discernable damage to the aircraft from the ground impact that affected the seats. It appeared that the seats were mostly influenced by the obstacle impact and slide-out along the rocky impact area.

One of the obstacles penetrated the fuselage and weakened it. As the aircraft continued to slide, a fracture occurred at approximately body station 920 (figure 48). The fuselage and floor aft of the break shifted upward (figure 49), and the hub of a landing gear struck the underside of the floor structure (figure 50). The seat located at the floor break was thrown over onto its back, and the seat above the hub impact point had a track fitting dislodged.

Damage by the fire was substantial. Six seats were entirely destroyed. Three seats were located at the forwardmost hole in the roof created by the fire, and three seats were at the aftmost hole. The middle hole was where the fuselage broke (figure 51). A convenient aspect of the fire was that the holes in the roof facilitated removal of the seats and dummies (figure 52).

SEATS.

An in-place examination of the seats after the test showed that all the dummies with remaining belts (some were completely burned) stayed restrained in the seats by the lap belts; no belt failures occurred. In general, all the seats experienced fire damage in various degrees; some seats were completely destroyed and some were only singed.

A common occurrence found on three seats was the deformation of the right side of the center seat pan. Figure 53 shows the locations of these seats and figures 54-56 show the seat pans. Onboard films showed the dummies in these seats leaning to the right and bouncing during the obstacle impact and slideout. The accelerometers from seats H/R and B/L indicated peak vertical accelerations of 40 G with 10-msec durations.

The following observations were made of the seats.

SEAT A/R. The fire caused the underfloor structure in front of the seat and in the aisle to collapse, leaving the seat tilted forward and toward the aisle. Fire damage extended to melting two of the plasticized seat pans, burning the upholstery off the seat backs and scorching the food trays. There was no impact-related damage (figure 57).

SEAT E/L. This seat was across the aisle from seat A/R and was found in a similar orientation, due to the floor collapsing. It also sustained similar fire damage; one of the plasticized seat pans had melted and the upholstery was blackened (figure 58).

SEAT C/L. No damage from the impact was sustained by the seat. However, the fire destroyed both outboard and inboard seat backs and part of the center one (figure 59).

SEATS G/R, B/R AND H/L. The fire burned through the cabin floor at these three seat locations, leaving a hole. All that remained of these seats was the steel parts and the thick aluminum forgings that had not completely melted.

SEATS F/R, I/L, D/R AND D/L. These seats were not damaged by the impact, but received various degrees of fire damage. Generally, the seat back upholstery was burned away and the seat structure remained intact (figures 60-63).

SEAT P/R. The seat backs and armrests were destroyed, as well as the infant seat (except its steel frame). There was no impact-related damage (figure 64).

SEAT K/L. The fire melted the seat pans and partially melted the seat backs and leg structure. There was no damage from the impact (figure 65).

SEAT C/R. All the aluminum in the seat pan and leg structure was melted; only the steel legs remained. The seat backs were partially destroyed and no damage was caused by the impact (figure 66).

SEAT G/L. The outboard seat pan structure was destroyed, as was half of the seat back and both lap belt energy absorbers. The rest of the seat was generally scorched. There was no impact-related damage (figure 67).

SEATS E/R, H/R AND I/R. There was no damage to these seats from the impact. The seat back tops and food trays were partially burned and overall, the seats were singed (figures 68-70).

SEAT A/L. As a result of the impact with the wing openers, a floor break occurred directly beneath this seat, causing it to be thrown upward and flipped over onto its back, landing in an orientation 90 degrees counterclockwise from its original position. All the dummies remained strapped in the seat. There was only minor bending of the seat leg structure (figure 71), and a piece of broken floor track stayed attached to the outboard rear track fitting (figure 72). The inboard front track button (or stud) was broken and appeared to have been torn out of the floor track (figures 73 and 74).

SEAT B/L. During the obstacle impact, a landing gear hub struck the underside of the floor structure directly beneath the outboard track cover bar that connects the front and rear seat legs. The floor broke and assumed the shape of an inverted V. Since the track cover bar was lying flush over the floor track, it also assumed the same shape (figure 75). The deformation of the floor also caused the outboard front track fitting to come loose from the floor track (figure 76), leaving the seat supported by three legs.

Lateral loading caused the inboard rear leg to buckle (figure 77) and the outboard rear leg to bend slightly. It is not possible to show conclusively whether the seat was supported by three or four legs when the leg buckling occurred. The vertical and lateral seat accelerations (figure 78) indicate the vertical impact which dislodged the front outboard track fitting could have occurred before the lateral pulse which bent the legs. On the other hand, seat J/L, a seat two rows to the rear with a similar leg construction, failed due to the lateral accelerations. All the other adjacent seats were modifications built to withstand at least 6 G, twice the strength of seats B/L and J/L. The modified seats did not experience any deformation.

The front seat pan tube was deformed downward at both window and aisle seat positions (figure 79) and the rear seat pan tube was similarly deformed at the aisle seat position (figure 80). Since the fire had discolored the tubes at these locations, the deformations can be attributed to the heat softening the metal.

SEAT F/L. This seat was only damaged by the fire. The seat backs were partially burned and the leg structure was singed (figure 81).

SEAT J/L. Examination of the onboard films revealed that this seat failed laterally after the impact with the wing openers. Originally, posttest observations indicated the seat legs might have buckled due to a combination of the floor sagging beneath the seat and the intense heat. However, one film which has a view of the inboard dummy head and seat back, and the power pallet directly behind the seat, shows the dummy and seat disappearing from view and the pallet remaining in place. This implies the seat was not affected by a floor fracture. A posttest examination confirmed this; the floor beneath the seat was intact.

A second film shows the inboard dummy falling sideways across the aisle and striking a battery pallet. When closely examined, the film briefly shows the heads of the other two dummies falling backwards. The seat's failure is also substantiated by the direction in which the seat's legs were deformed (figure 82). As shown, the seat pan was forced toward the aisle. If the sagging floor and heat had caused the seat to fail and placed it in the position in which it was found (figure 83), the legs would have bent in the opposite direction.

The floor sag and heat did distort the seat legs further so it was not possible to determine the degree of deformation caused by the lateral G load.

This seat did not have any instrumentation, and the closest accelerometers were those on seat F/L immediately in front. The lateral accelerations from seat F/L after the obstacle impact are shown in figure 84.

NASA SEATS AND THE FRENCH SEAT. The entire contents of the cabin at these three seat locations were consumed by the fire. All that remained were the steel parts of the seats.

FORWARD FLIGHT ATTENDANT SEAT - ITEM S. This seat had little fire damage and no impact-related damage (figure 85).

REAR FLIGHT ATTENDANT SEAT MOD - ITEM T. It appeared that the left-hand (as referenced sitting in the seat) seat pivot support bracket melted, releasing the pivot arm and the left side of the seat. The weight of the seat and two dummies was then transferred to the right-hand support bracket. At some time after this, if not immediately, the right-hand bracket failed due to the additional load and the heat softening the bracket. The seat suffered extensive fire damage (figure 86).

DATA.

Data from the accelerometers and lap belt tensiometers over a time interval of one second (1000 milliseconds) are presented in appendices A through E. Time zero (0 msec) begins at 9 hours 22 minutes and 11 seconds, or 33731 seconds. This is the elapsed time referenced from 12:00 midnight.

A comparison was made between the instrumentation data and stop-motion analyses of the ground-based cameras to create table 4, which shows the approximate times the sequence of impact events occurred.

TABLE 4. TIME SEQUENCE OF IMPACT EVENTS

Event	Clock Time	Equivalent Seconds	Equivalent Msec In Appendices
-	9.22.11	33731	0
No. 1 Engine/Ground Impact	9.22.11.06	33731.06	60
Fuselage/Ground Impact	9.22.11.53	33731.53	530
No. 3 Engine/Obstacle Impact	9.22.12.92	33732.92	not shown

The data shown in the appendices is presented for only the ground impact. Data gathered from the CID does include the obstacle impact and continues beyond after the aircraft came to rest. Generally, because of the yaw and slide-out along the rock bed, the longitudinal and lateral accelerations were higher after the obstacle impact than after the ground impact.

Examination of the data revealed that some of the channels experienced a shift in the zero point prior to the impact, causing the resulting data to be offset by the amount of shift. This data is most likely valid since, in most cases, it has approximately the same shape trace as adjacent data. It only needs to be corrected by the amount of shift.

Other channels experienced extraneous noise prior to the impact. It is possible this noise was superimposed on the data, thus invalidating it.

Additionally, some channels show the data inverted with respect to the abscissa. In table 5, these anomalies are indicated for the channels they pertain to, along with the actual ranges (± G or lb) measured from the data plots in the appendices.

The inconsistencies in the data channels should not detract from the fact that there was general agreement between accelerometers. As an example, the floor, seat, and pelvis vertical accelerations on seat A/R (figure A-3) between 400 and 600 milliseconds, integrate to velocity changes of -15.8 to -9 ft/sec, -16.5 to -10.3 ft/sec, and -17.6 to -11.2 ft/sec, respectively.

Inverted channels should not be dismissed, as figure A-4 illustrates. Although the floor acceleration plot is inverted, its signature (without being inverted) matches closely with the seat acceleration plot. This similarity of signatures is a general and quick method of checking the validity of the majority of acceleration channels at a seat location or

TABLE 5. STATUS OF DATA CHANNELS

Channel	Seat	Location	Orientation	Range (± G)	Zero Shift	Extraneous Data	Inverted Data
1	Pilot	Floor	N	170			x
2			L	107	x		x
3			T	53	x	x	x
4		Seat	N	170			
5			L	122		x	x
6			T	64			x
7		Pelvis	N	128			x
8			L	136	x	x	
9			T	49			
10		Belt	L	0-1792 lb			
11			R	0-1792 lb			
12		Harness	L	0-1920 lb			
13			R	0-1664 lb			
14	E/L	Floor	N	128			
15			L	102			
16		Seat	N	145	x		
17			L	92			
18			T	47	x	x	
19			L		No available data		
20		Pelvis	N		No available data		
21			L	147			
22			T	53			

TABLE 5. STATUS OF DATA CHANNELS (CONTD)

Channel	Seat	Location	Orientation	Range (± G)	Zero Shift	Extraneous Data	Inverted Data
23		Belt	L	0-2133 lb	x	x	
24			R	0-2133 lb	x	x	
25	G/R	Floor	N	90			
26		Seat	N	145			
27			L	95		x	
28			T	39	x	x	x
29	H/L	Floor	N	150			
30			L	105	x		
31			T	52	x		
32		Seat	N	140	x	x	
33			L	83	x	x	
34			T	44	x		
35			L	81			
36		Pelvis	N	124	x	x	
37			L	124	x	x	
38			T	51		x	
39		Chest	N	133			
40			L	132			
41		Head	N	135			
42			L	108			
43		Belt	L	0-1760 lb			
44			R	0-1872 lb			

TABLE 5. STATUS OF DATA CHANNELS (CONTD)

Channel	Seat	Location	Orientation	Range (± G)	Zero Shift	Extraneous Data	Inverted Data
45	F/R	Floor	N	170			x
46		Seat	N	150			
47			L	100	x		
48			T	48			
49	D/L	Floor	N	224	x	x	
50			L	112			
51			T	53	x	x	
52		Seat	N	140			
53			L	87	x		
54			T	49	x		
55			L	83			
56		Pelvis	N	136			
57			L	154	x	x	
58			T	44			
59		Chest	N	126		x	
60			L	143	x	x	
61		Head	N	139			
62			L	151	x		
63		Belt	L	0-1792 lb			
64			R	0-1749 lb			
65	G/L	Floor	N	140			
66			L	83			

TABLE 5. STATUS OF DATA CHANNELS (CONTD)

Channel	Seat	Location	Orientation	Range (± G)	Zero Shift	Extraneous Data	Inverted Data
67		Seat	N	134			
68			L	100			
69			T	38	x		
70			L	87			
71		Pelvis	N	132			
72			L	111			
73			T	40			
74		Belt	L	0-1664 lb			
75			R	0-1920 lb			
76	E/R	Floor	N			No available data	
77		Seat	N	128			
78			L	100			
79			T	47			
80	B/L	Floor	N	209			x
81		Seat	N	128			
82			L	81			
83			T	59	x		
84	I/R	Floor	N	150			
85			L	92			
86		Seat	N	154	x		
87			L	75			x
88			T	47			

TABLE 5. STATUS OF DATA CHANNELS (CONTD)

Channel	Seat	Location	Orientation	Range (± G)	Zero Shift	Extraneous Data	Inverted Data
89			L	111			
90		Pelvis	N	115		x	
91			L	126	x	x	
92			T	37		x	
93		Belt	L	0-1835 lb	x		
94			R	0-1835 lb			
105	F/A	Floor	N	226			x
106			L	107	x	x	x
107			T	64			x
108		Seat	N	150			x
109			L	68	x		
110			T	52			
111		Pelvis	N			No available data	
112			L	124	x	x	
113			T	48			
114		Belt	L	0-1856 lb			
115			R	0-1792 lb			
116		Harness	L	0-1813 lb			
117			R	0-1813 lb			
186	A/R	Floor	N	132			
187			L	83			
188			T	39			

TABLE 5. STATUS OF DATA CHANNELS (CONTD)

Channel	Seat	Location	Orientation	Range (± G)	Zero Shift	Extraneous Data	Inverted Data
189		Seat	N	124			
190			L	100			
191			T	64			
192			L	68	x		
193		Pelvis	N	128	x	x	
194			L	128	x	x	
195			T	36		x	
196		Belt	L	0-1963 lb			
197			R	0-1750 lb			
198	C/L	Floor	N	124			x
199		Seat	N	150			
200			L	82			
201			T	46			
202	B/R	Floor	N	166		x	
203			L	90	x		
204		Seat	N	79			x
205			L	75			
206			T	53			
207			L	83		x	
208		Pelvis	N	128	x	x	
209			L	119	x	x	
210			T	45	x	x	

TABLE 5. STATUS OF DATA CHANNELS (CONTD)

Channel	Seat	Location	Orientation	Range (± G)	Zero Shift	Extraneous Data	Inverted Data
211		Chest	N	125	x	x	
212			L			No available data	
213			T	41		x	
214		Head	N	133		x	
215			L	126		x	
216		Belt	L	0-1728 lb			
217			R	0-1632 lb			
218	I/L	Floor	N	37			
219		Seat	N	115			
220			L	75		x	
221			T	45			
222	C/R	Floor	N	154			
223			L	96			
224			T	43			
225		Seat	N	117			
226			L	90			
227			T	34			
228			L	70			
229		Pelvis	N	122	x	x	
230			L	134	x	x	
231			T	38	x	x	
232		Belt	L	0-1792 lb			

TABLE 5. STATUS OF DATA CHANNELS (CONTD)

Channel	Seat	Location	Orientation	Range (± G)	Zero Shift	Extraneous Data	Inverted Data
233			R	0-1792 lb			
234	A/L	Floor	N	140			x
235		Seat	N	140	x	x	
236			L	87	x	x	
237			T	49	x	x	
238	H/R	Floor	N	150			x
239		Seat	N	136			
240			L	75			
241			T	49	x		
242	F/L	Floor	N	128	x		
243			L	111			
244			T	55	x		
245		Seat	N	117			x
246			L	90			
247			T	47			x
248			L	94			
249		Pelvis	N	154	x	x	
250			L	150	x	x	
251			T	41	x	x	
252		Belt	L	0-1813 lb			
253			R	0-2005 lb			
254	D/R	Floor	N	128			x

TABLE 5. STATUS OF DATA CHANNELS (CONTD)

Channel	Seat	Location	Orientation	Range (± G)	Zero Shift	Extraneous Data	Inverted Data
255		Seat	N	136			
256			L	128			
257			T	66			

between seat locations. A further demonstration is a comparison of the lateral accelerations on seat A/L (figure C-14) and the seat across the aisle, E/R (figure C-15).

DATA INTERPRETATION.

The format of the CID digital data is comprised of a series of 8 bits (one word) that give the digital equivalent of an analog signal. Since each 8-bit word is discrete, the full range of an accelerometer or load cell signal is divided into discrete levels. As an example, an acceleration signal with a range of ±150 G is divided into 256 levels. The first is -150 G, the second is -148.83 G (1.17 G increments), the third is -147.66 G, the 128th is 0 G, and the 256th level is +150 G. If an analog signal being digitized lies between two levels, the digital result will always default to the lower level. In this example, an analog signal of 0.8 G, which lies between the levels of 0 G and 1.17 G, will be assigned a digital value of 0 G. Likewise, 2.0 G (analog) will become 1.17 G (digital).

Since this sort of resolution imparts error into the data, and as mentioned, the resolution is not the same for all data channels, interpretation of the CID data needs to be performed using the method shown in the following examples.

Graph A of figure 87 is a typical acceleration trace. Measuring the smallest distance from one level to another shows that the resolution of this particular data channel is 0.5 G. Since the analog signal always defaults to the lower digital value, this trace is actually a plot of minimum acceleration values. Thus, every acceleration that was actually output by the accelerometer lies between the value shown on graph A and 0.5 G above that value. This is illustrated in graph B, where every value from graph A has been increased 0.5 G and the area between the two traces has been shaded. The shaded area is the resolution band, and the actual acceleration trace lies somewhere in that band.

It should be noted that as the data is sampled, it is recorded point by point, and data between points is lost. If plotted, the recorded data would actually result in a series of dots. Instead, the dots or data points have been connected by straight lines to create a continuous curve. It is possible that the accelerations occurring between points could deviate outside the interconnecting lines.

Data resolution becomes especially significant when determining velocity changes. As an example, the velocity change calculated from the acceleration trace in graph A of figure 88 is approximately -15.8 ft/sec. (Velocity change is defined as the difference in areas above and below the abscissa circumscribed by an acceleration-versus-time curve.) If the resolution band is drawn in as shown in graph B, and the upper trace used, the new velocity change is -9.4 ft/sec. Thus, the actual velocity change over the 200 milliseconds shown is between -15.8 and -9.4 ft/sec.

If velocity changes are to be calculated from any of the acceleration-versus-time curves from the CID data, it must be remembered that the velocity change uncertainty is proportional to the product of the resolution and the time interval. In the example from figure 88, the data channel has a resolution of 1.0 G. This, multiplied by the duration (.200 sec) and a conversion factor (32.2 ft/sec^2 per G), yields an uncertainty of 6.4 ft/sec.

A simple rule to follow is to calculate the velocity change from the trace and use this result as the lower value. Then, add the uncertainty to the result and use this sum as the upper value. In the previous case, -15.8 ft/sec (lower value) + 6.4 ft/sec (uncertainty) = -9.4 ft/sec (upper value).

FILMS.

Review of the onboard films revealed considerable motion of the dummies during impact and slideout. However, it is apparent from the photos that the forward inertial loads were not particularly high. The dummies did not fold or jackknife over the lap belts as they have been observed to do in laboratory tests with a 9-G forward deceleration, and their legs and arms did not flex to a fully extended and straightened position. Even if the seats had been placed at a more conventional and closer spacing or pitch, there would have been little or no contact between the dummies and the seat ahead of them.

In general, the longitudinal and lateral accelerations appeared larger during the obstacle impact and slideout. However, except for the few individual cases mentioned in a prior section, these accelerations only caused intermittent jostling of the dummies, without having any influence on the seats.

CONCLUSIONS

The test objectives which involved the recording of data pertaining to the airframe structural floor loads and seat occupant responses during impact were met. However, because of the mild impact conditions, the objective to demonstrate the performance between the standard and modified seat designs was not completely satisfied.

Acceleration data were obtained during impact from accelerometers installed within the cabin floor, seat and anthropomorphic dummy locations. The individual acceleration pulses recorded at these locations during both the ground impact and subsequent obstacle impact were essentially triangular in shape occurring within a 100 to 200 millisecond period.

A plot distribution of the peak accelerations measured at instrumented seat/floor locations is provided in figure 89. The peak vertical cabin floor accelerations were measured in the 2 to 10 G range with levels as high as 14 G recorded at the pilot cockpit floor area. The peak floor accelerations recorded in the lateral/longitudinal directions were in the 2 to 8 G range.

Recorded acceleration data obtained from the instrumented cabin seats and anthropomorphic dummies did demonstrate some of their dynamic capabilities and responses, but the duration as well as the amplitude of all accelerations must be considered to fully understand the significance of each measurement. Vertical accelerations recorded at all of the instrumented passenger seat structures were generally between 4 and 6 G, lasting between 100 and 200 milliseconds. The longitudinal accelerations varied between 1 and 2 G for 100 to 200 milliseconds, occasionally peaking to 4 G for 5 to 10 milliseconds. There were a few deviations up to 12 and 25 G. Since these were of very short durations and were not seen in any of the adjacent data, they are suspected of being in error. Nevertheless, the few milliseconds over which they occurred made them inconsequential. Lateral seat accelerations were mostly of the same magnitude and duration as the longitudinal accelerations. The rear flight attendant seat did experience a lateral peak of 4 G with a 300-millisecond duration.

As observed from the aforementioned floor data, the pilot seat accelerations were somewhat different from those of the cabin seats. Vertical accelerations peaked at 15 G on the seat and 18 G in the pelvis, each with a duration of 90 milliseconds. The longitudinal accelerations peaked up to 11 G on the seat and 6 G in the pelvis, with durations lasting 10 milliseconds. Lateral accelerations of 4 G and 120 milliseconds were consistent between floor, seat, and pelvis.

Demonstrating a variance in performance between the installed standard seats and modified energy-absorbing seat designs (as accomplished in previous laboratory testing) was not successful because of the mild conditions of ground impact (17 ft/sec). Low acceleration levels were withstood by all the seats without any reported failures. No modified seat experienced stroking of its energy absorber devices. Also, no standard seats experienced crash impact damage except for seat J and seats A and B which were located where the floor was broken due to the obstacle impact. Even though standard seat J did fail laterally (the seat was not in full view in any of the onboard films), it was not possible to correlate the adjacent acceleration data with the point of seat failure.

The subject test did provide a data base for floor, seat, and dummy responses resulting from a mild survivable crash. This data can be expected to be of value in the support of future research, as associated with analytical crash models and improvements in overall cabin restraint system performance. The selected test conditions did not provide data to conclusively evaluate the difference in performance between modified and standard seats. The results

and previous development work leading to the CID experiments (including the dynamic testing of the standard and modified seats), clearly demonstrated the potential effectiveness of the seat modifications under more severe impact conditions.

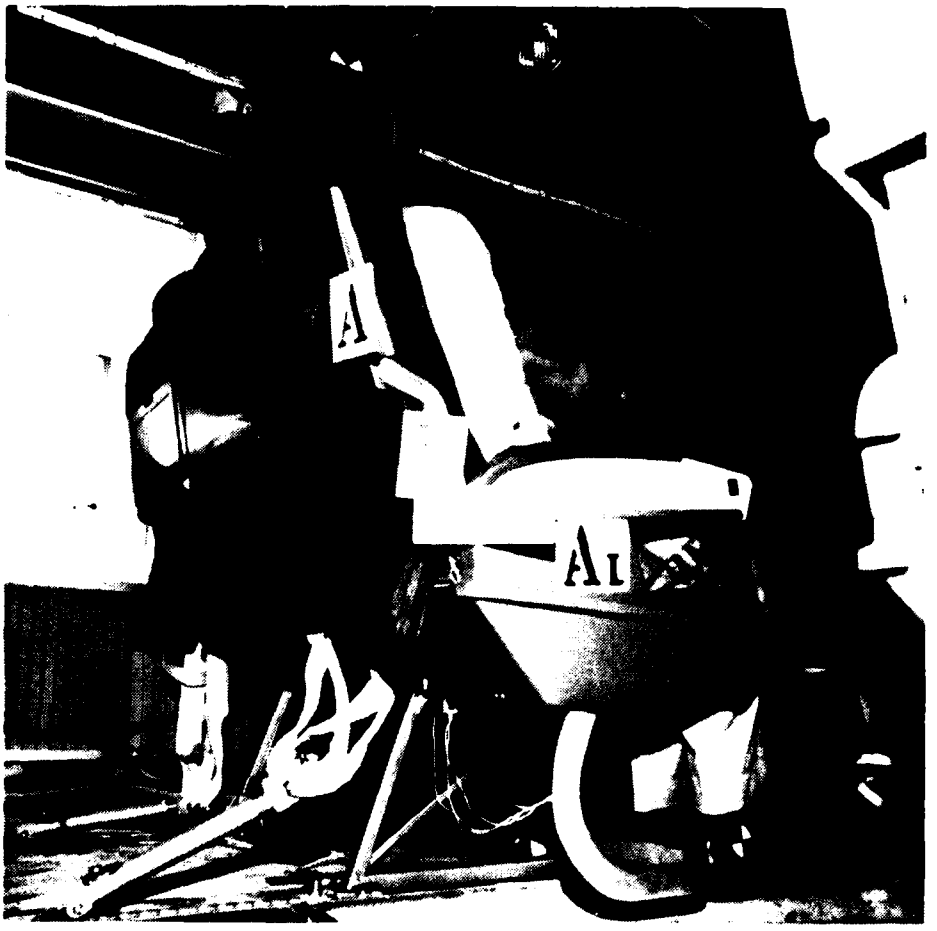

Figure 1. Weberlite 4000 transport seat.

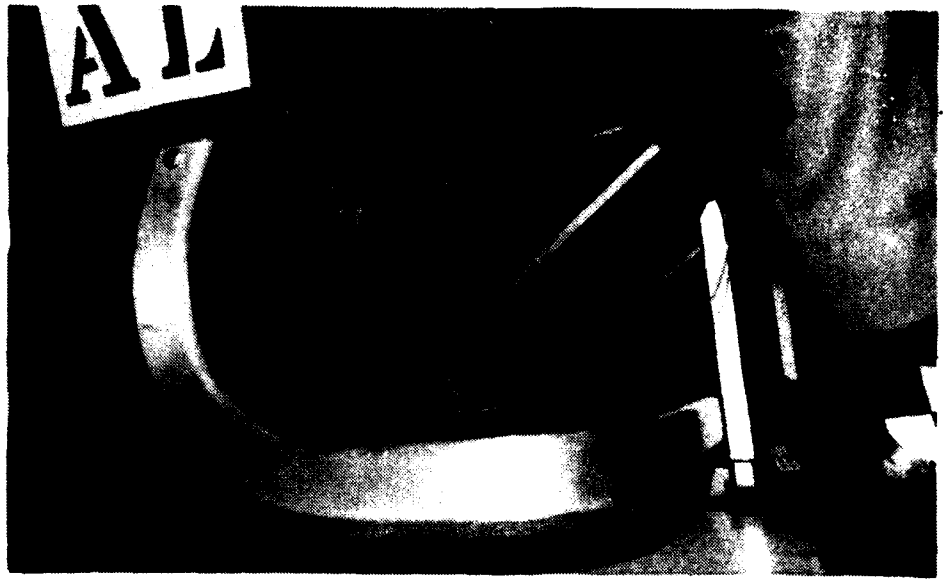

Figure 2. Weberlite 4000 seat leg structure.

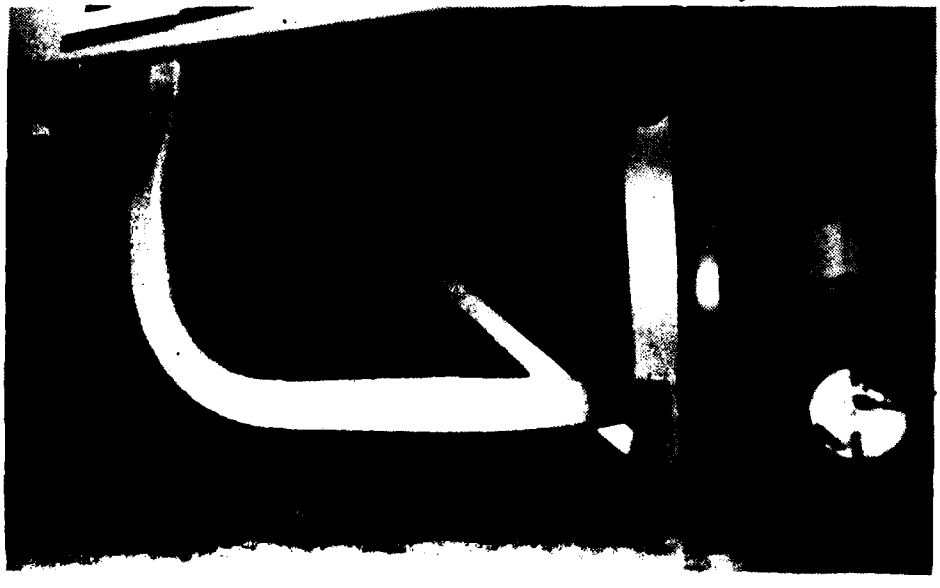

Figure 3. UOP Model 901 transport seat.

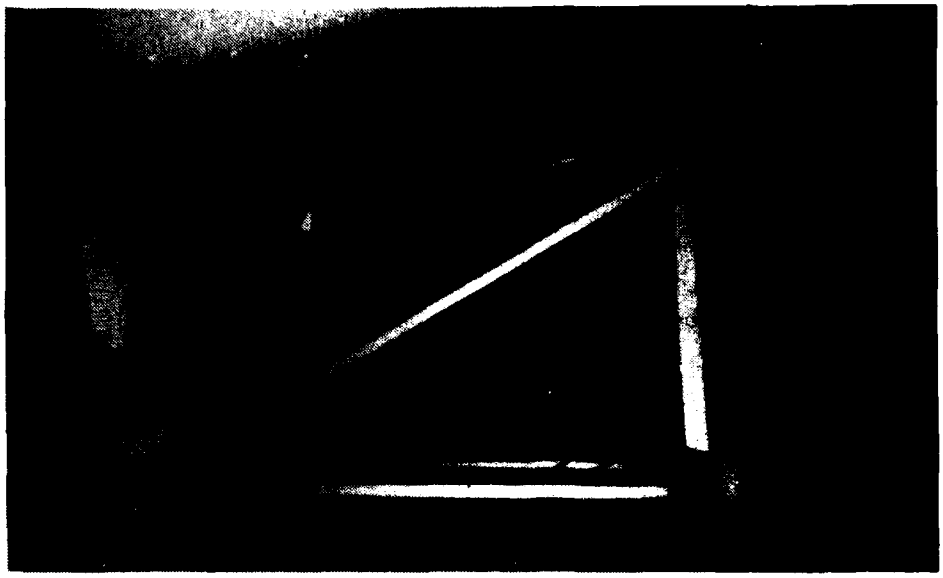

Figure 4. Weber P/N 819493 transport seat.

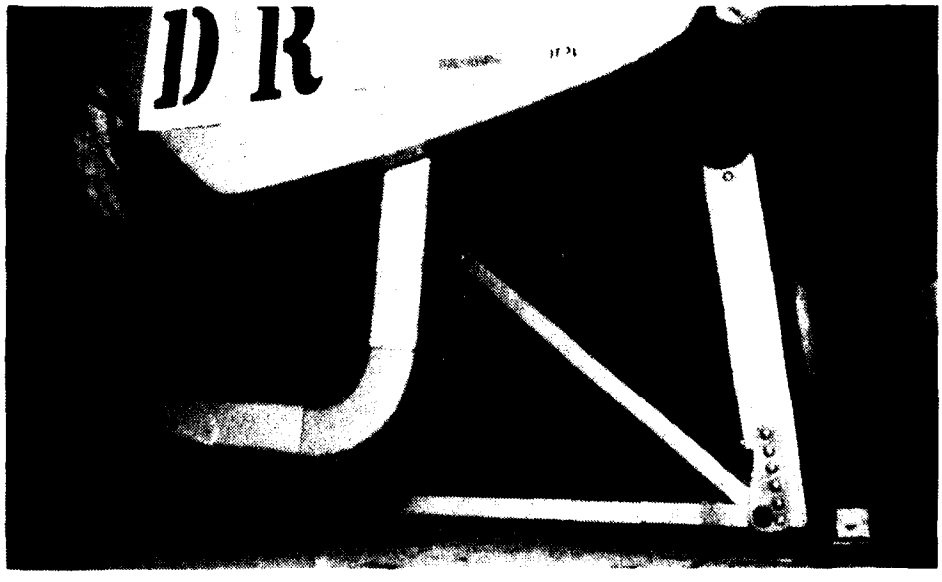

Figure 5. Hardman/UOP Aft-Facing Model 9777 transport seat.

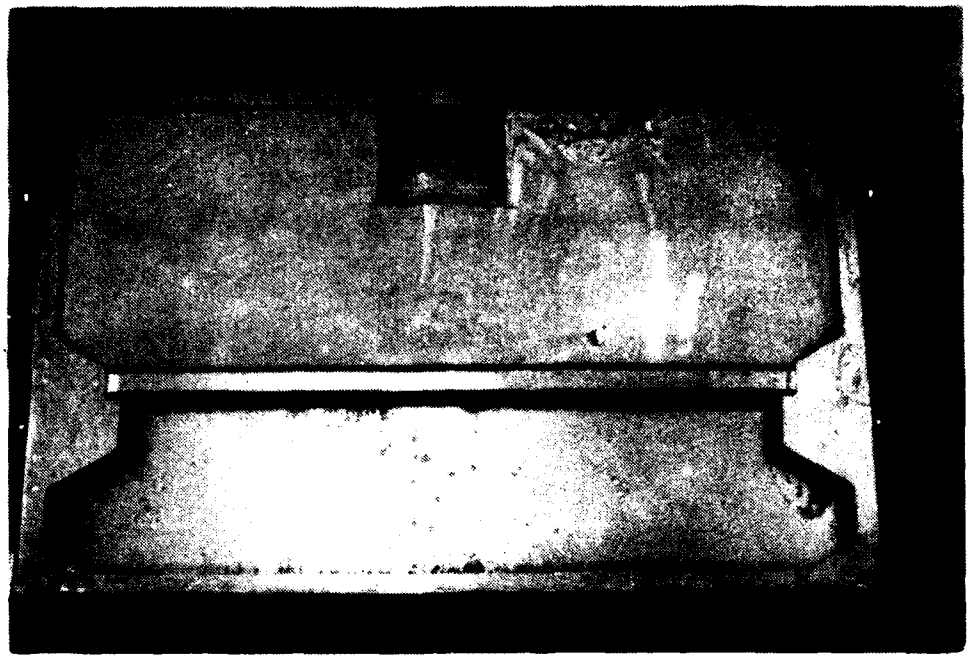

Figure 6. Framework of Trans-Aero flight attendant seat pan.

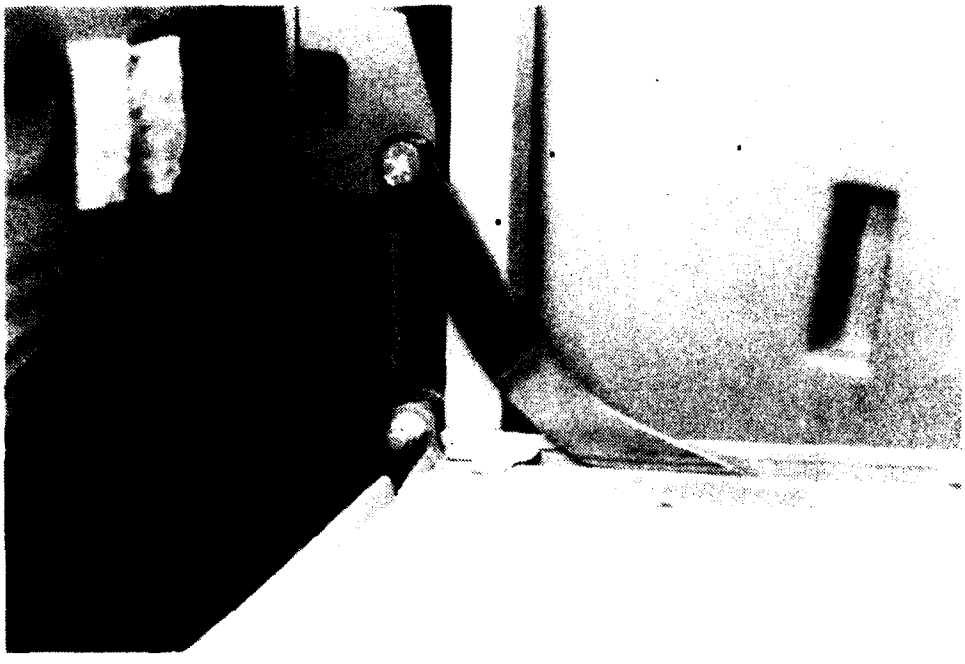

Figure 7. Pivot arm and roller bracket of Trans-Aero flight attendant seat.

Figure 8. Bulkhead adapter for Trans-Aero flight attendant seat.

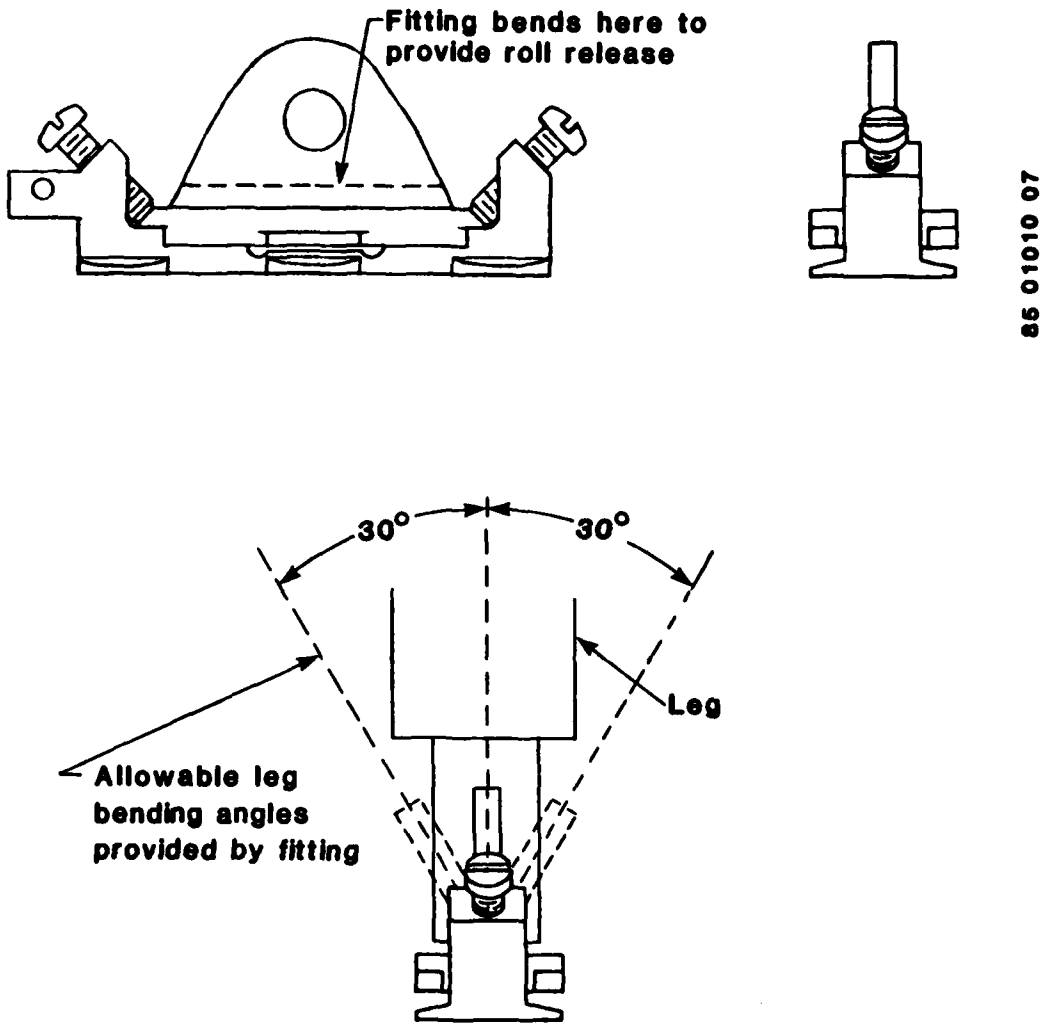

Figure 9. Prototype track fitting.

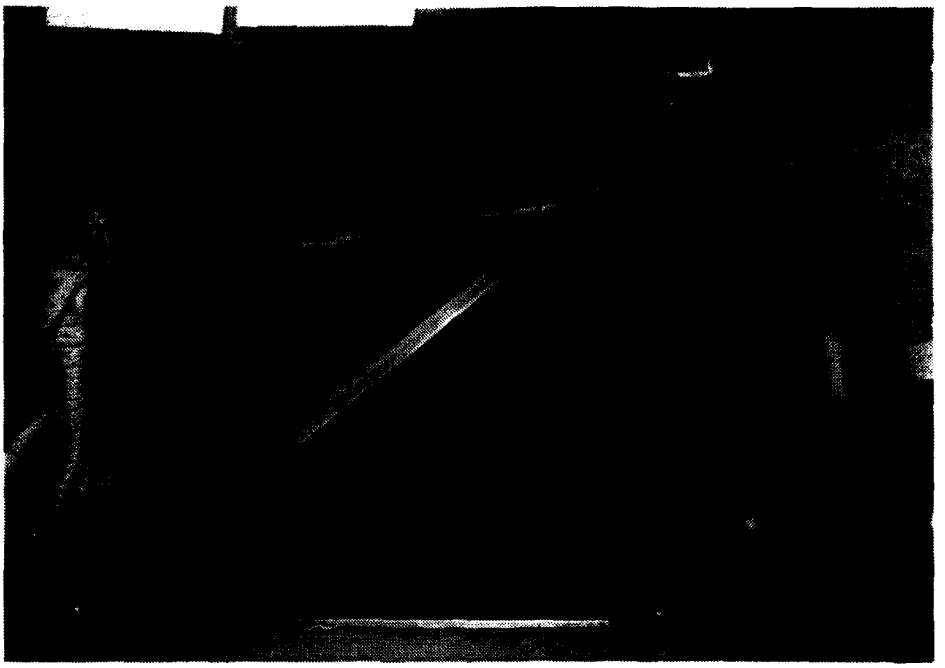

Figure 10. Weberlite MOD seat.

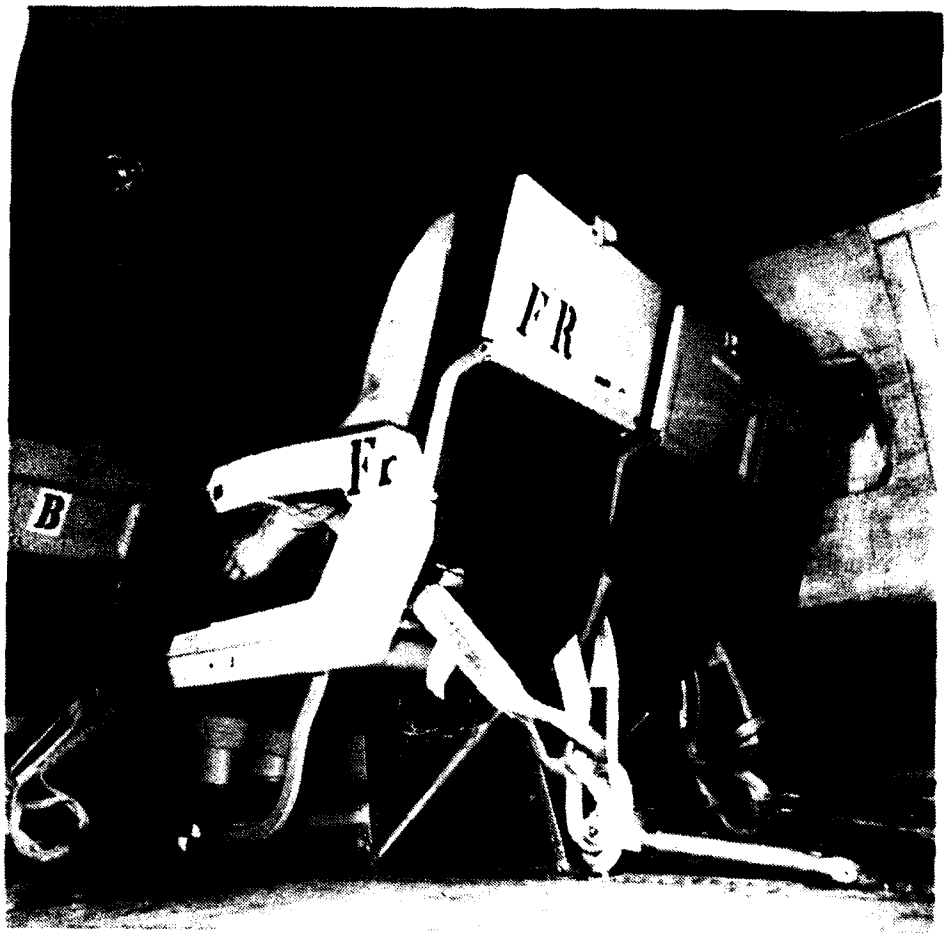

Figure 11. UOP MOD I seat.

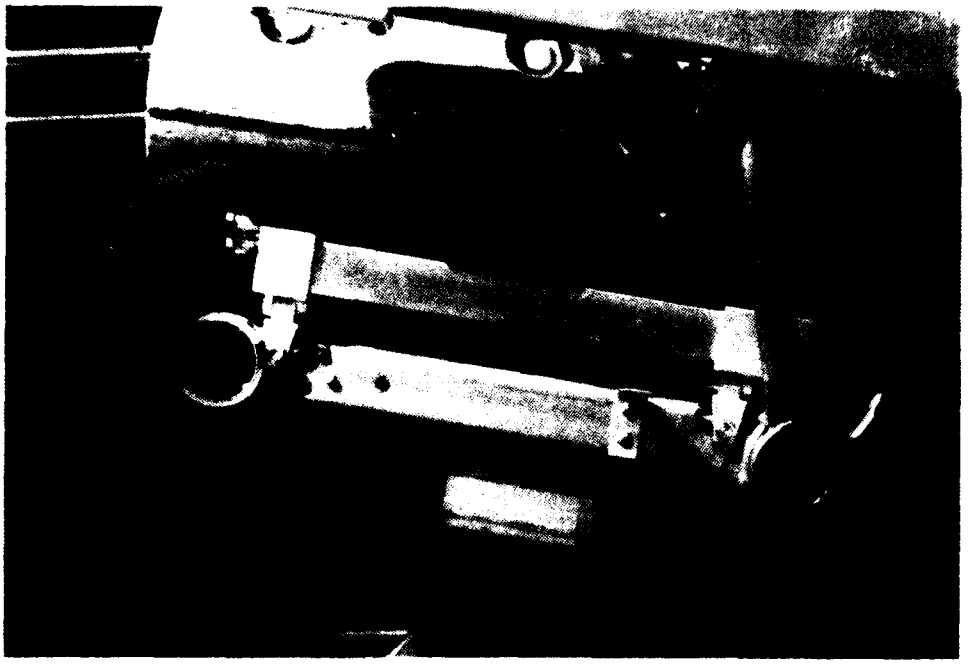

Figure 12. Weber MOD I lap belt energy absorber.

Figure 13. Weber MOD I seat.

Figure 14. UOP MOD II seat.

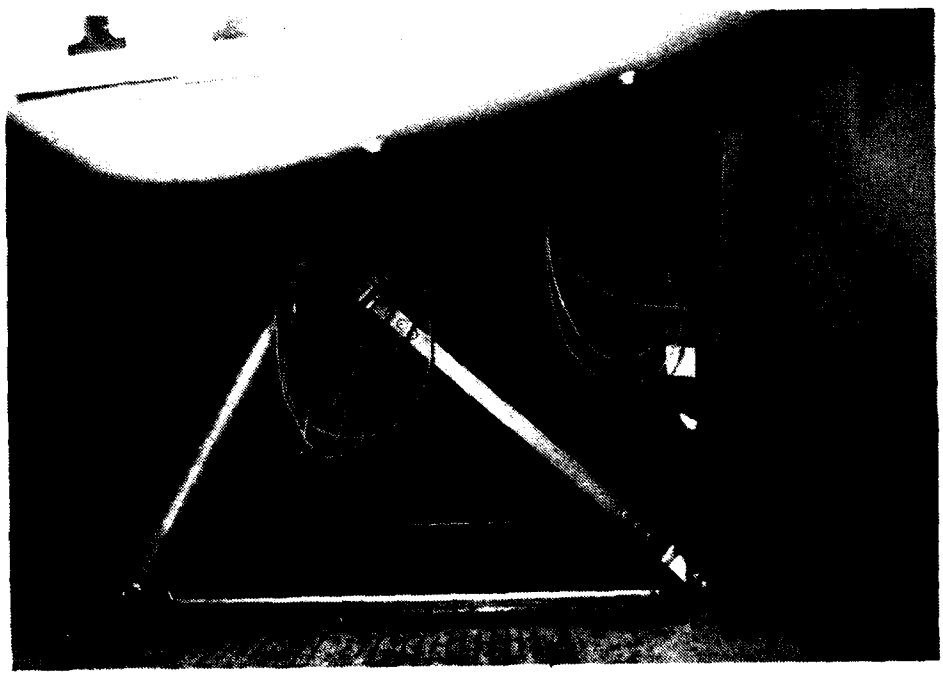

Figure 15. Weber MOD II seat.

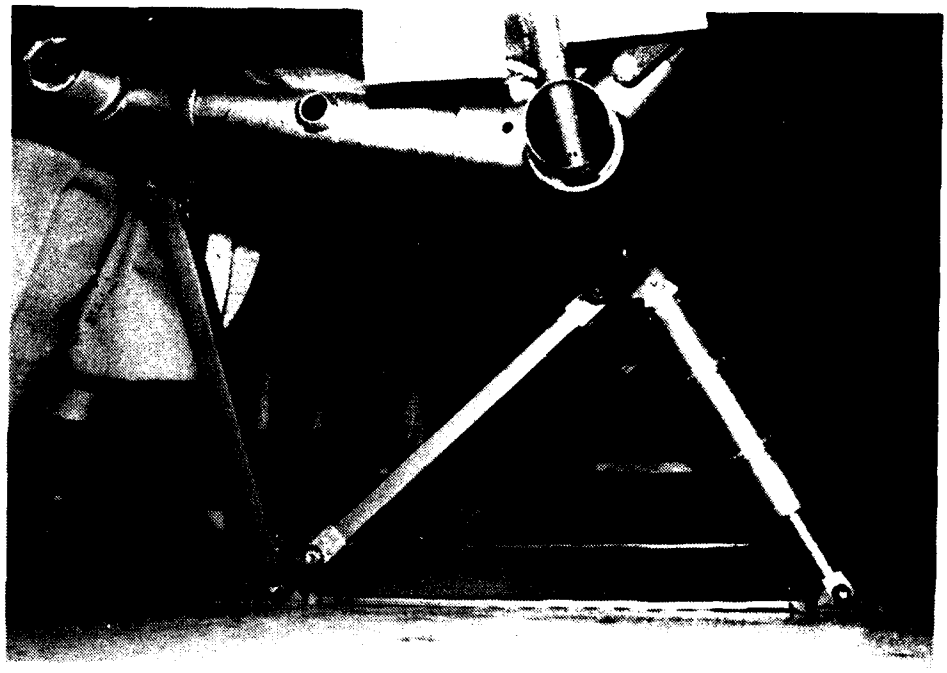

Figure 16. Weber Aft MOD seat.

Figure 17. Weber Standard with Simula track fittings.

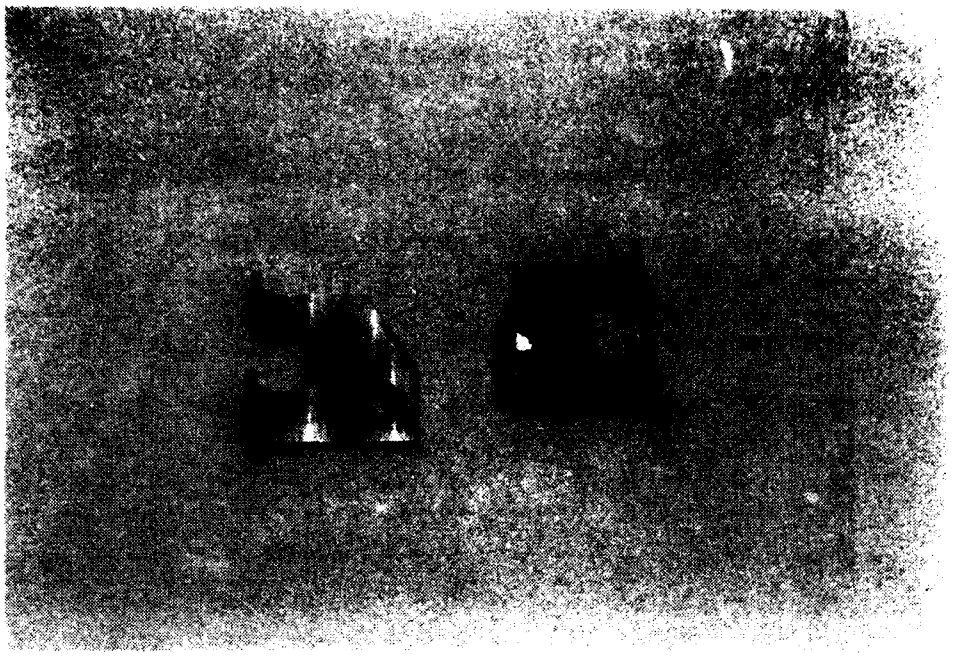

Figure 18. Modified (left) and standard pivot arm brackets for Trans-Aero flight attendant seat.

Figure 19. Modified (top) and standard pivot arm assemblies for Trans-Aero flight attendant seat.

Figure 20. Modified (left) and standard seat pan roller brackets for Trans-Aero flight attendant seat.

Figure 21. UOP Model 910 composite transport seat.

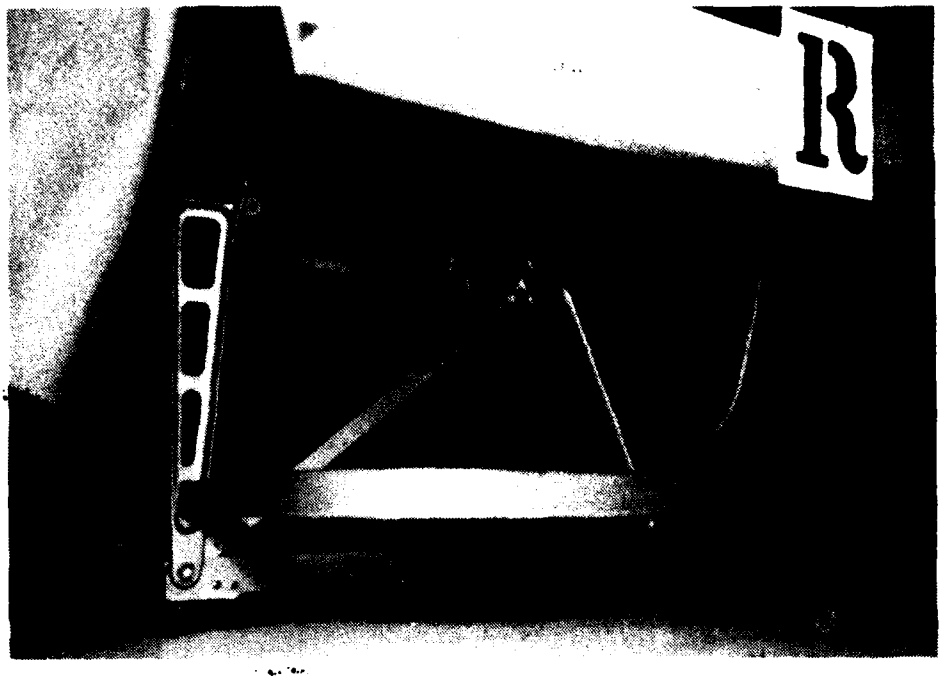

Figure 22. Standard Burns-Aero Airest 2000 transport seat.

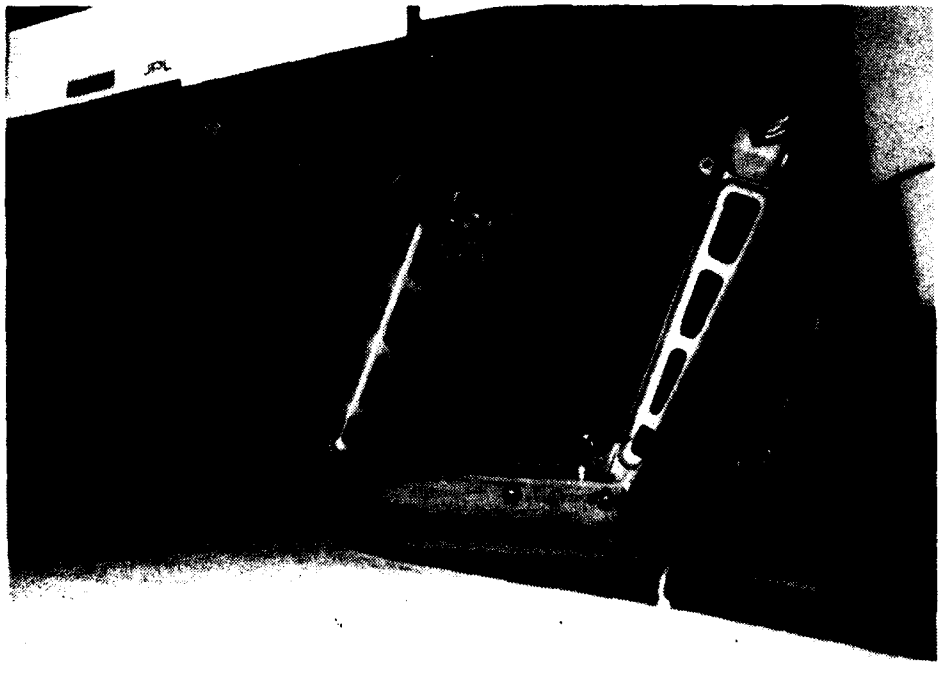

Figure 23. NASA modification of the Airest 2000 seat.

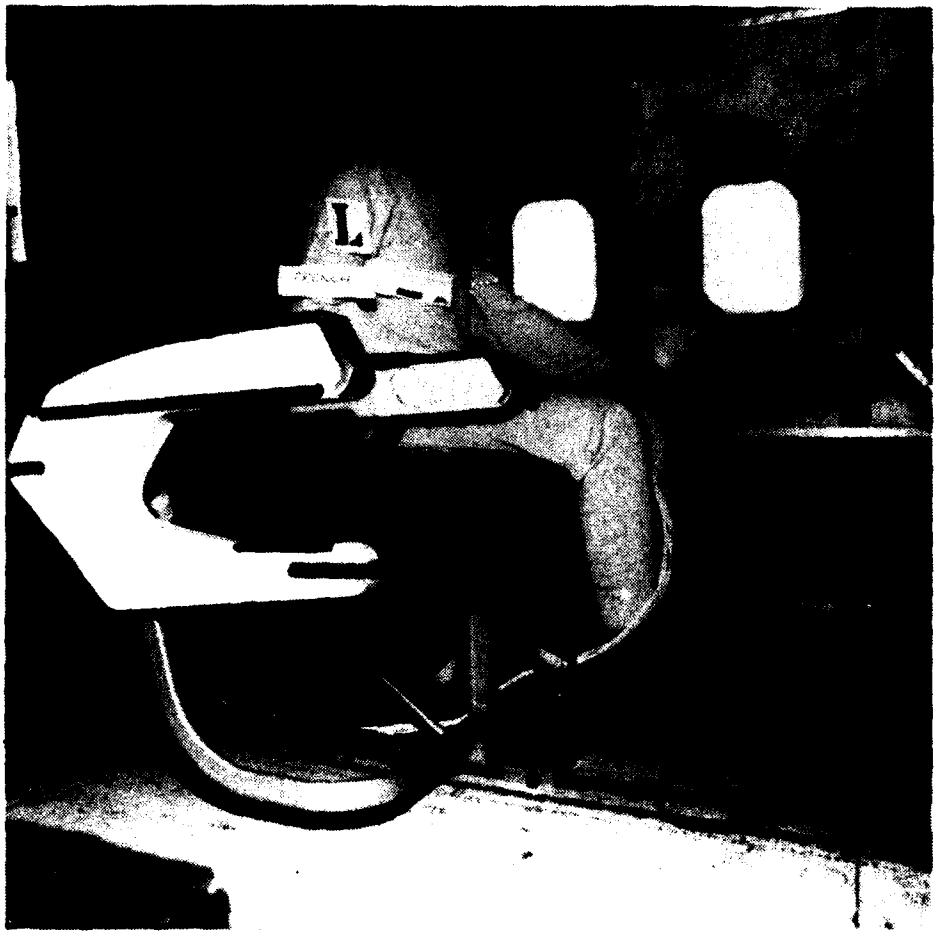

Figure 24. Standard Sicma Aero transport seat.

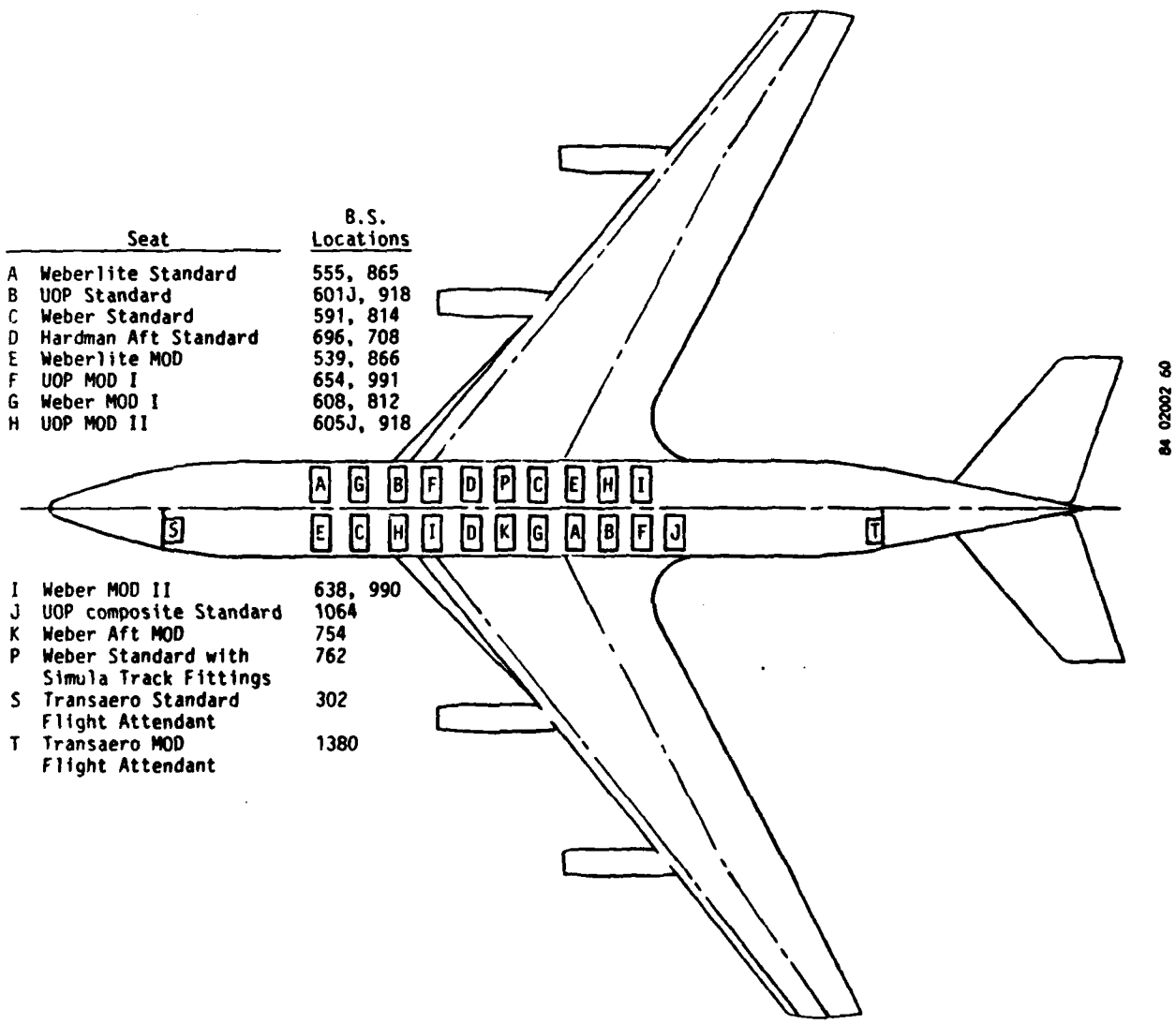

Figure 25. Position of seat experiments aboard aircraft.

Figure 26. Anthropomorphic dummy.

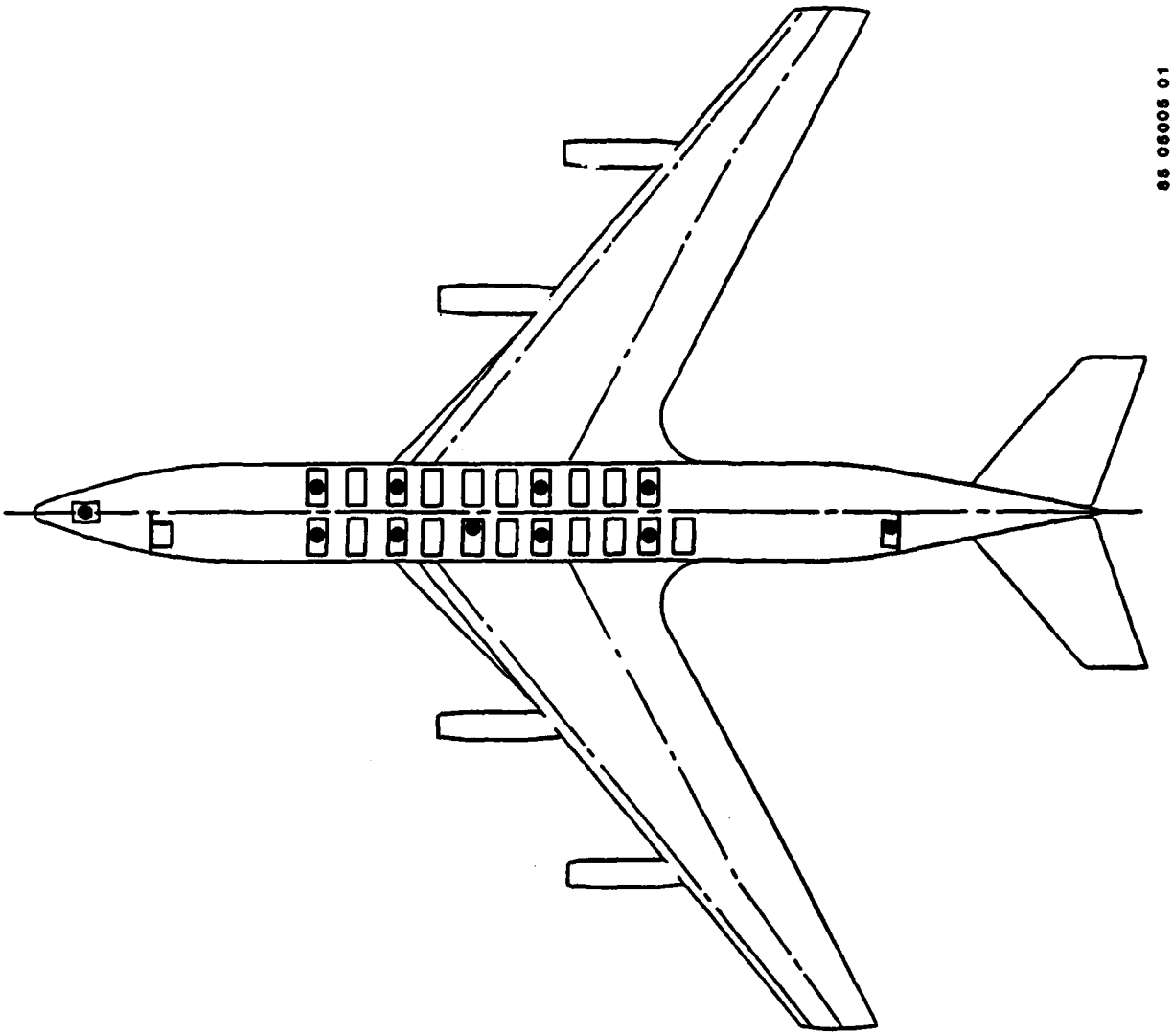

Figure 27. Location of anthropomorphic dummies in aircraft.

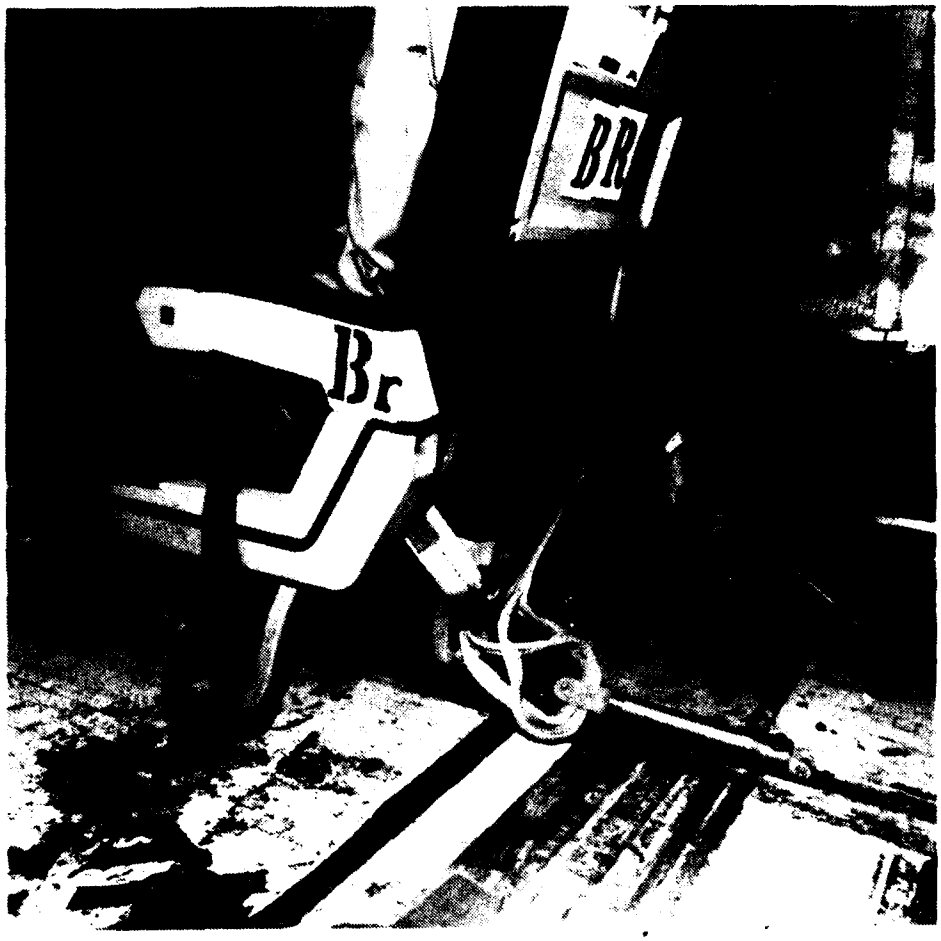

Figure 29. Secondary restraint system.

Figure 28. Infant dummy.

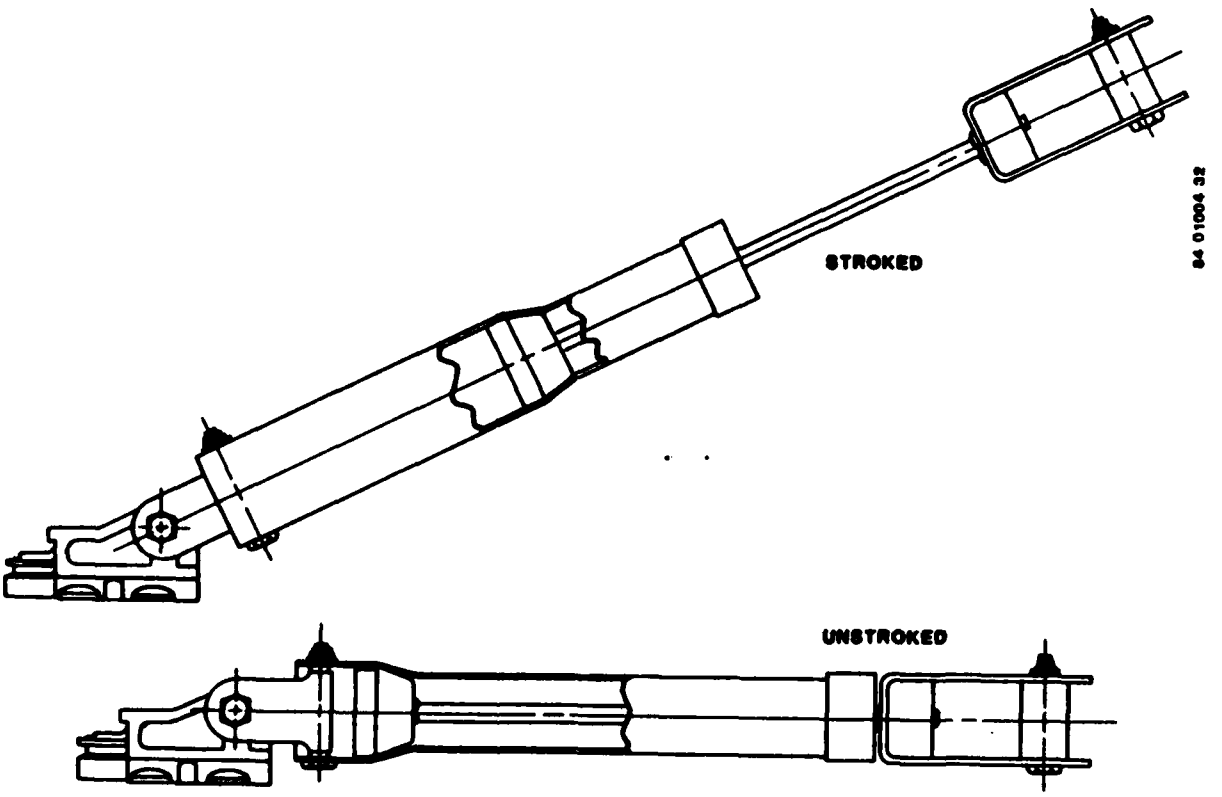

Figure 30. Secondary restraint system energy absorber.

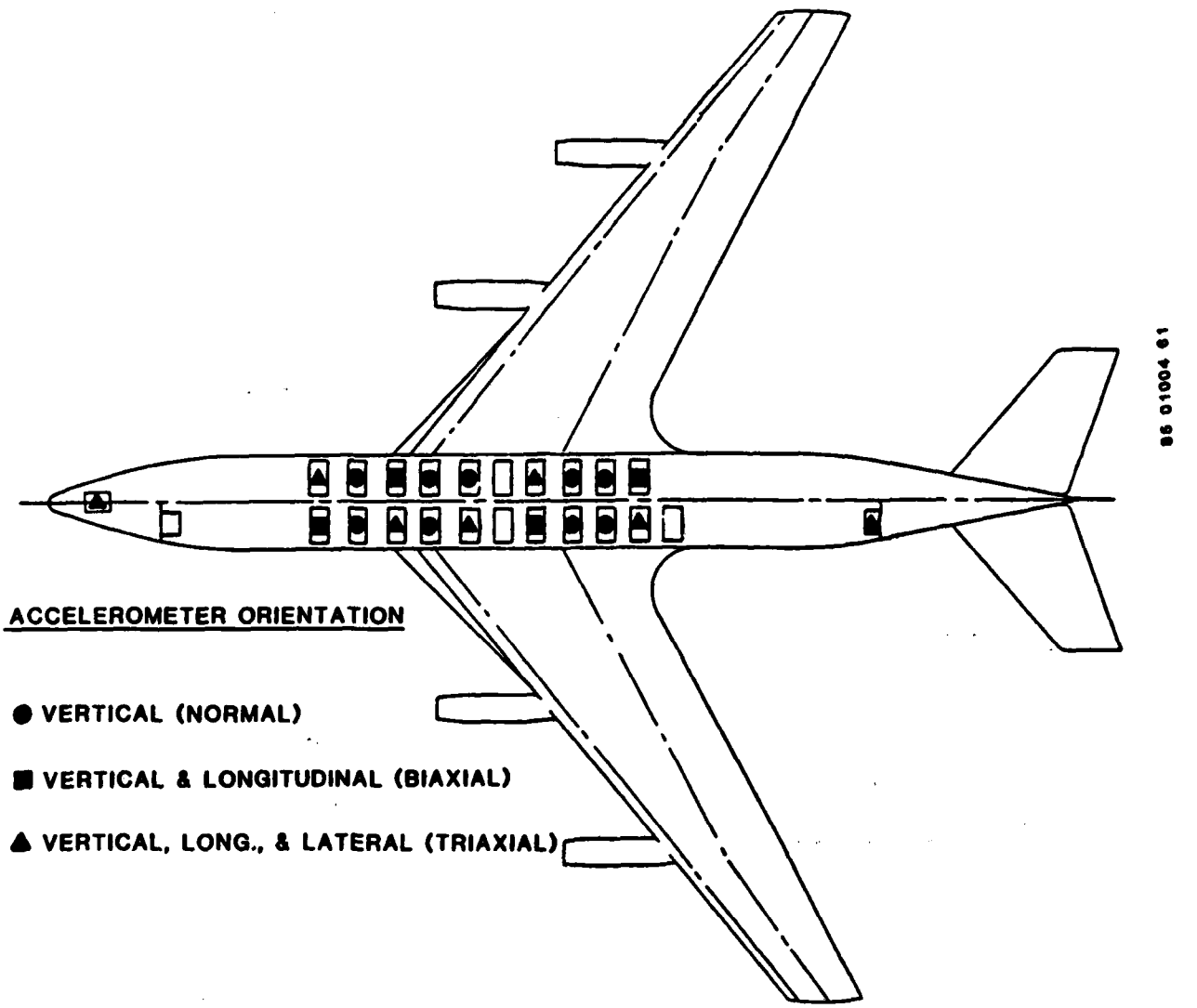

Figure 31. Location of floor accelerometers.

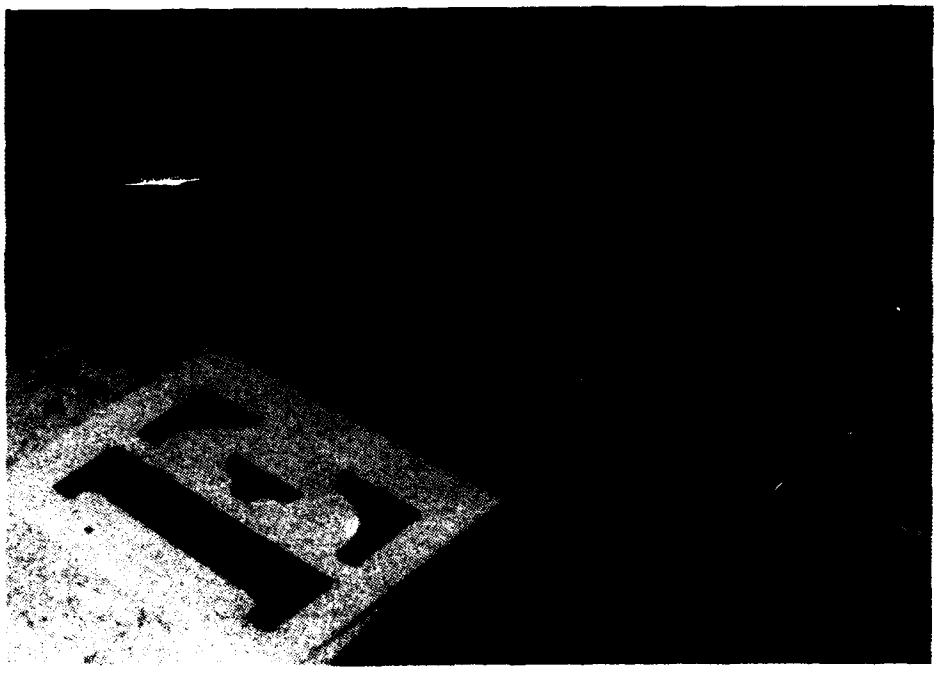

Figure 32. Typical mounting location of floor normal accelerometer.

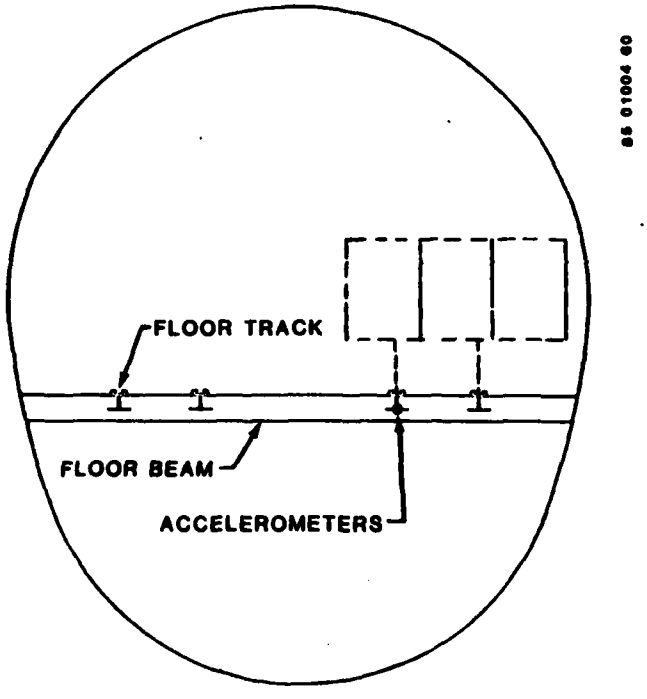

Figure 33. Typical mounting location of floor biaxial and triaxial floor accelerometers.

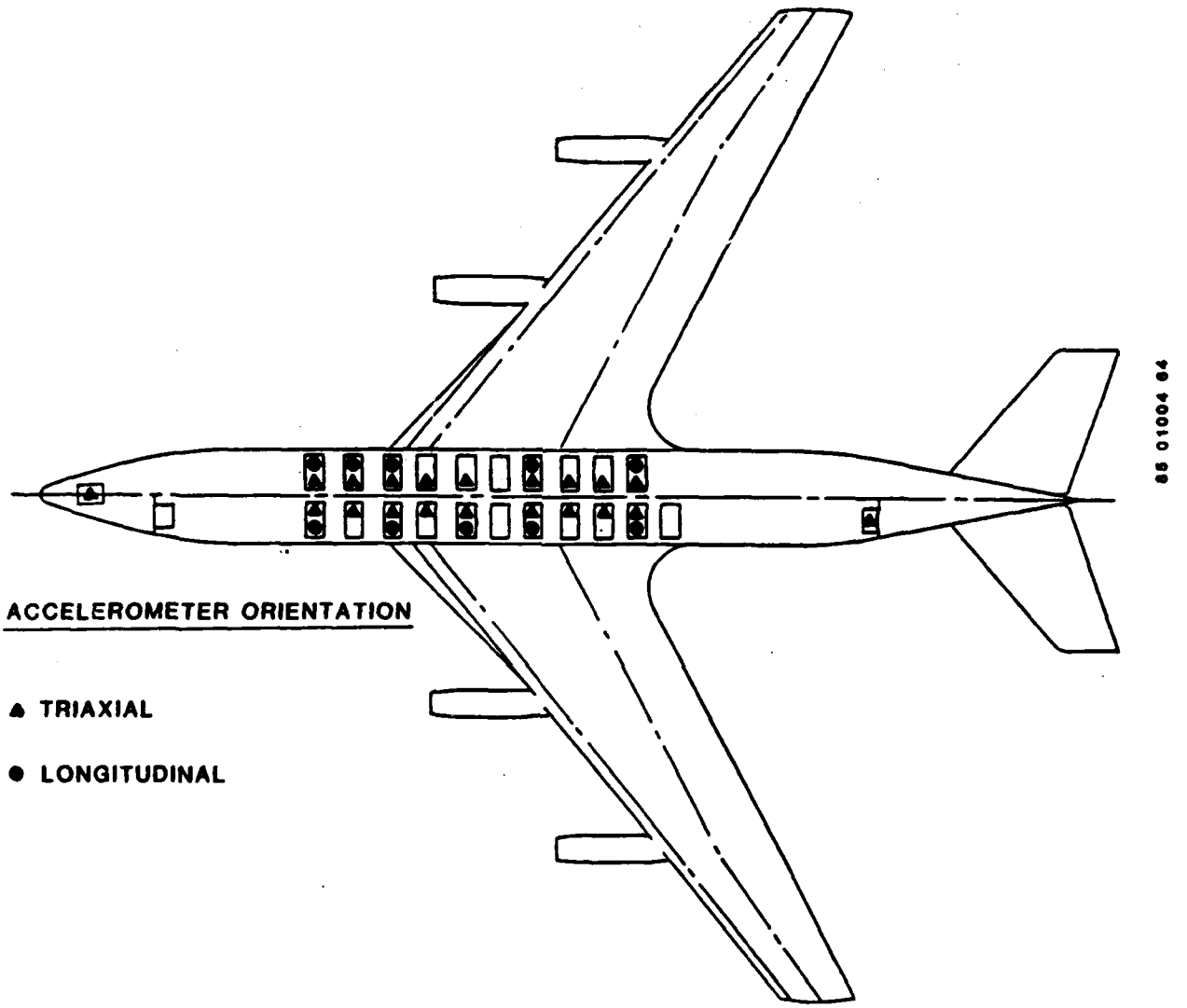

Figure 34. Location of seat accelerometers.

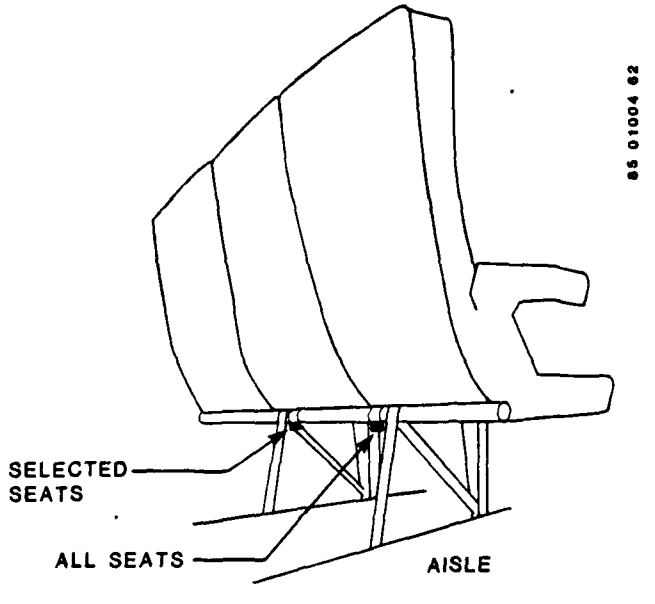

Figure 35. Typical seat accelerometer mount and mounting positions.

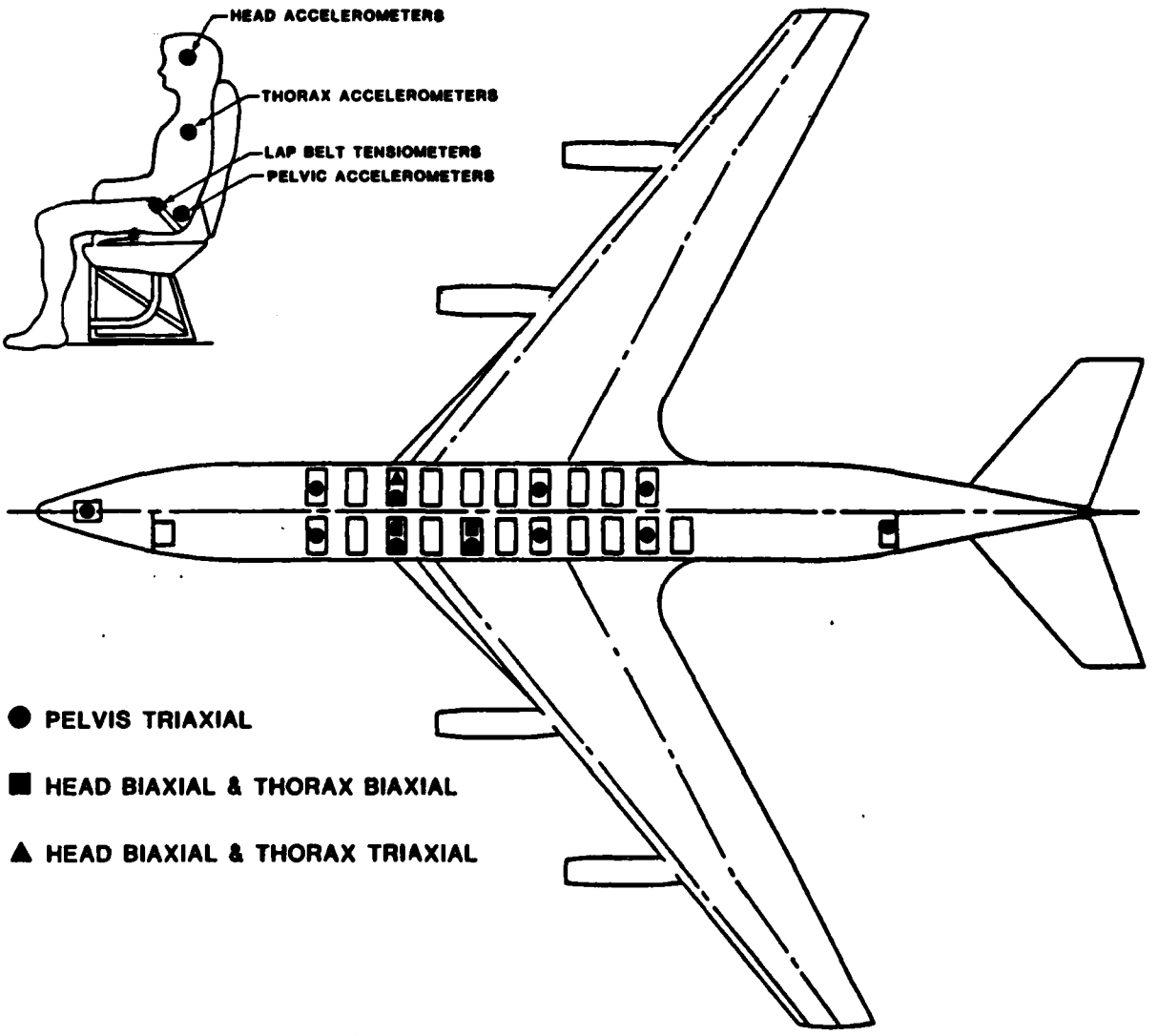

Figure 36. Location of dummy accelerometers.

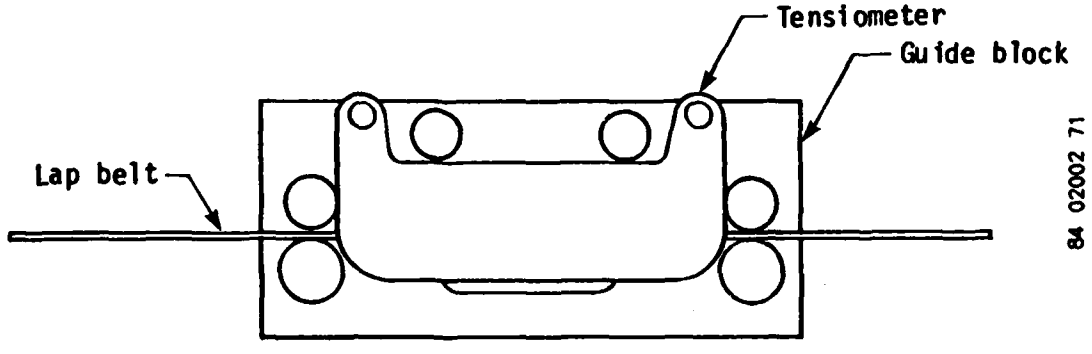

Figure 37. Installation and sketch of lap belt tensiometer guide block.

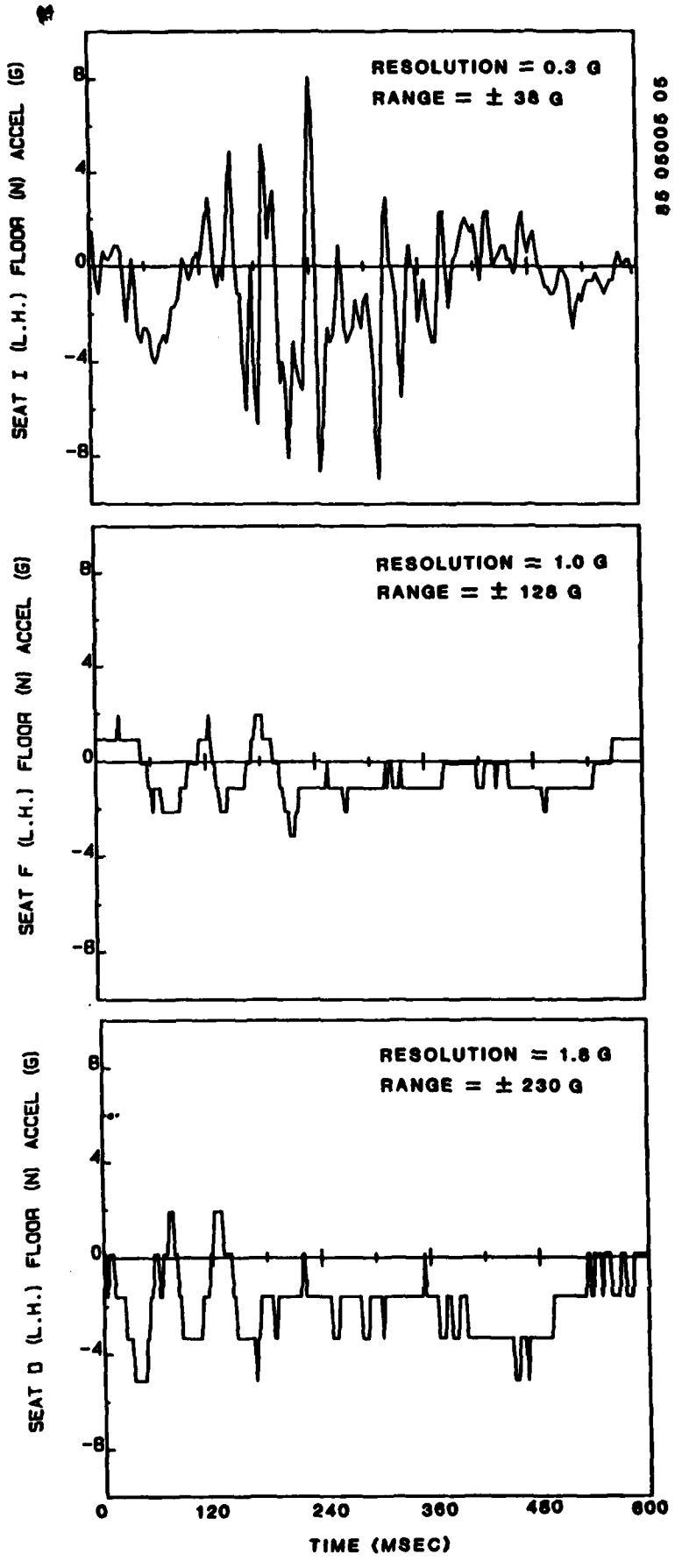

Figure 38. Example of inconsistent CID data ranging.

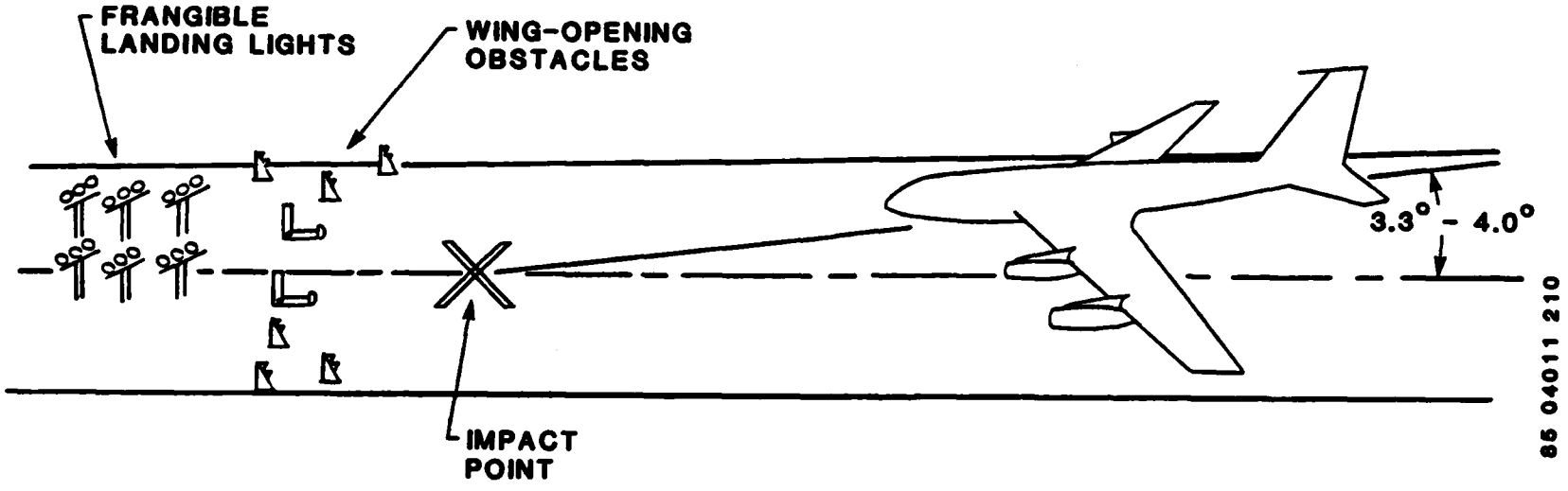

Figure 39. Planned CID impact scenario.

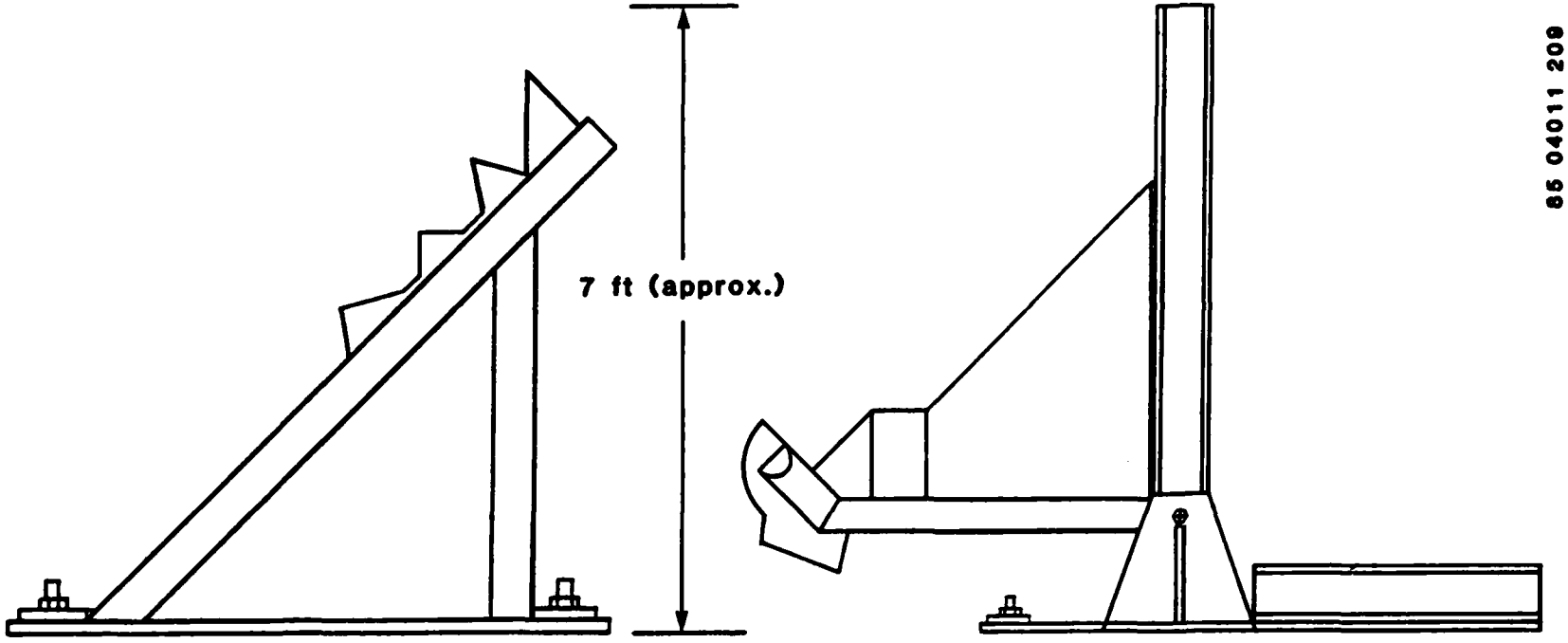

Figure 40. Wing-opening obstacles for fuel spillage.

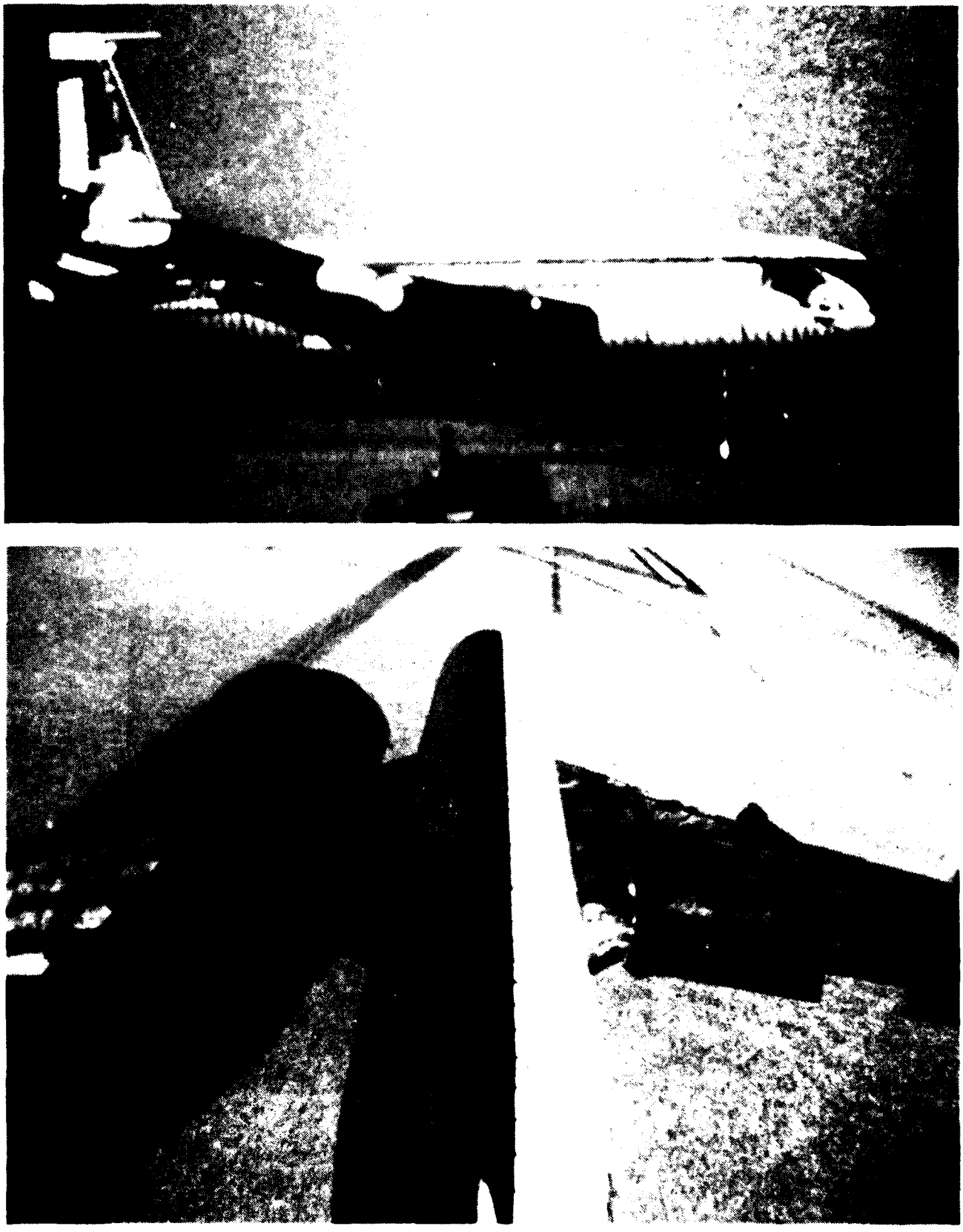

Figure 41. Left wing impact - side and top views.

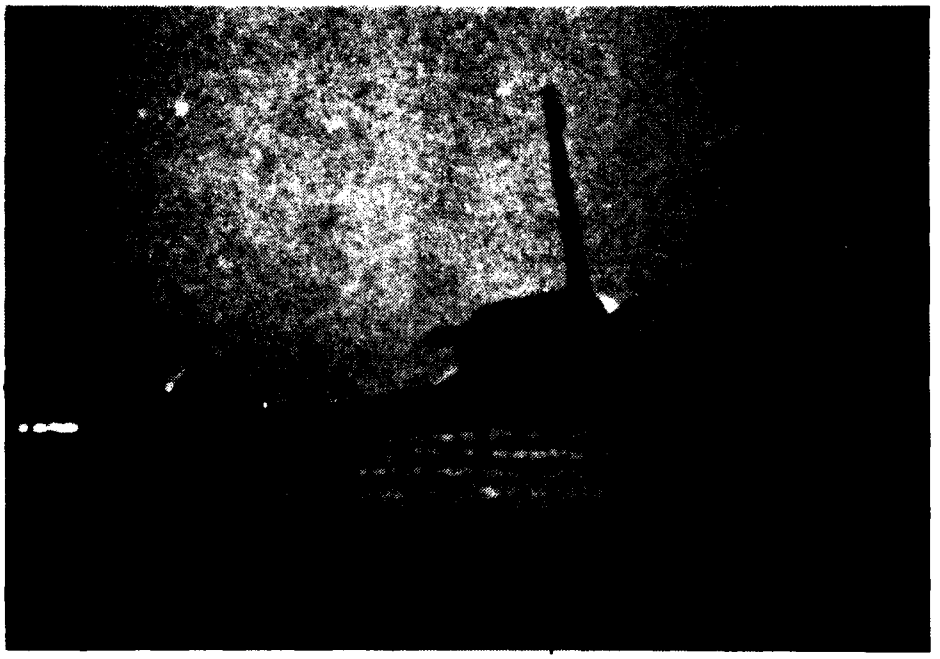

Figure 42. Left wing impact - front and rear views.

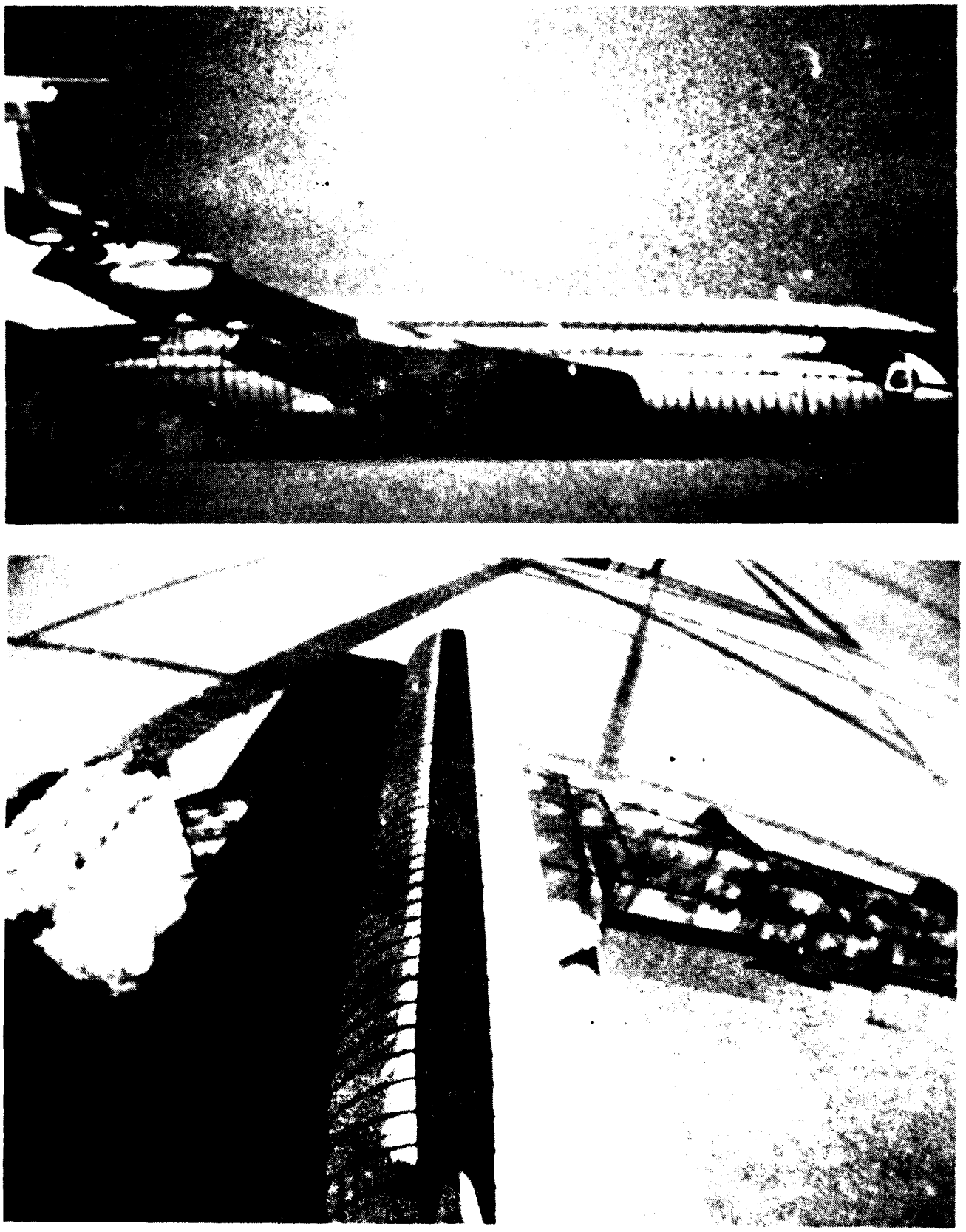

Figure 43. Fuselage impact - side and top views.

Figure 44. Fuselage impact - front and rear views.

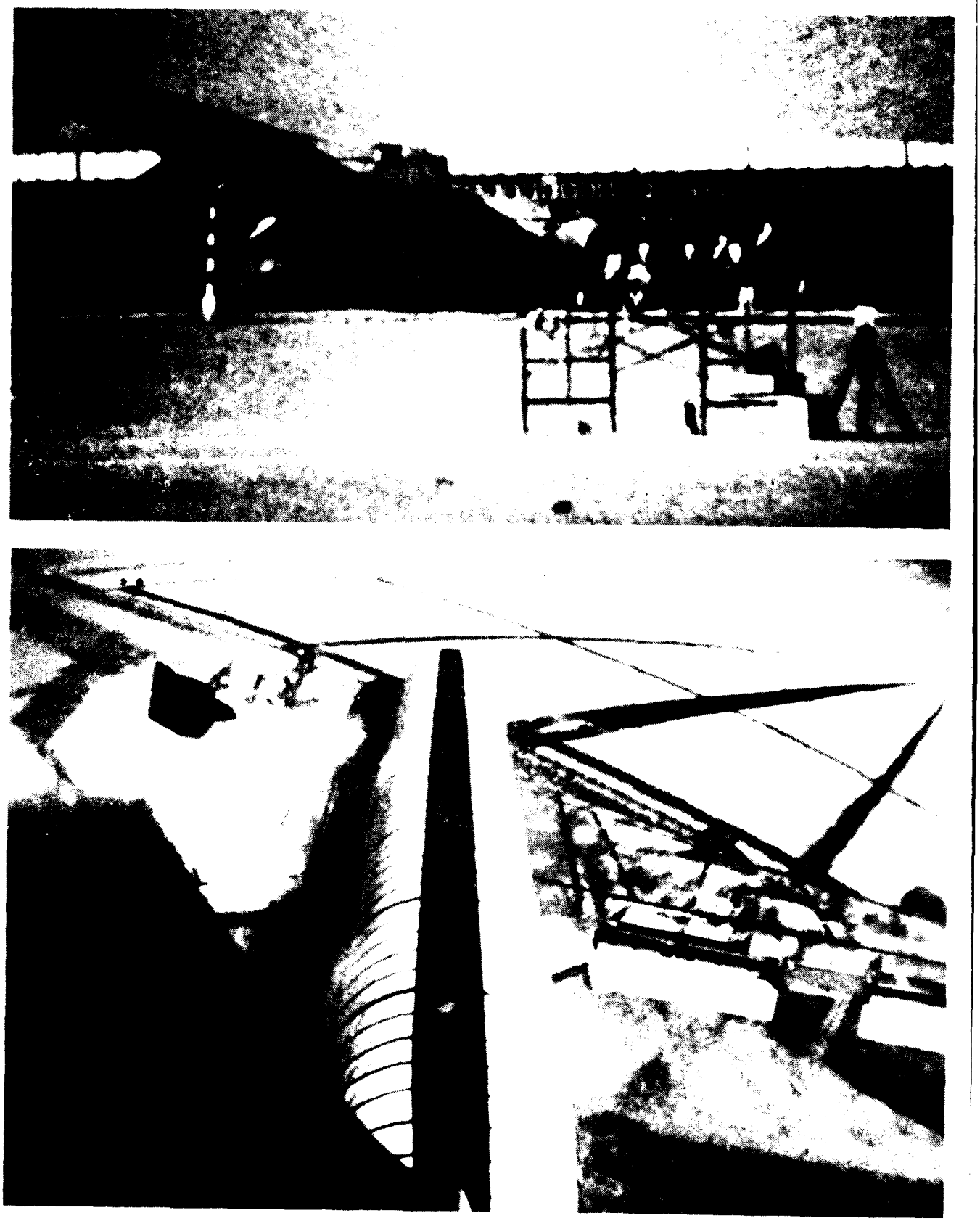

Figure 45. Wing opener (obstacle) impact - side and top views.

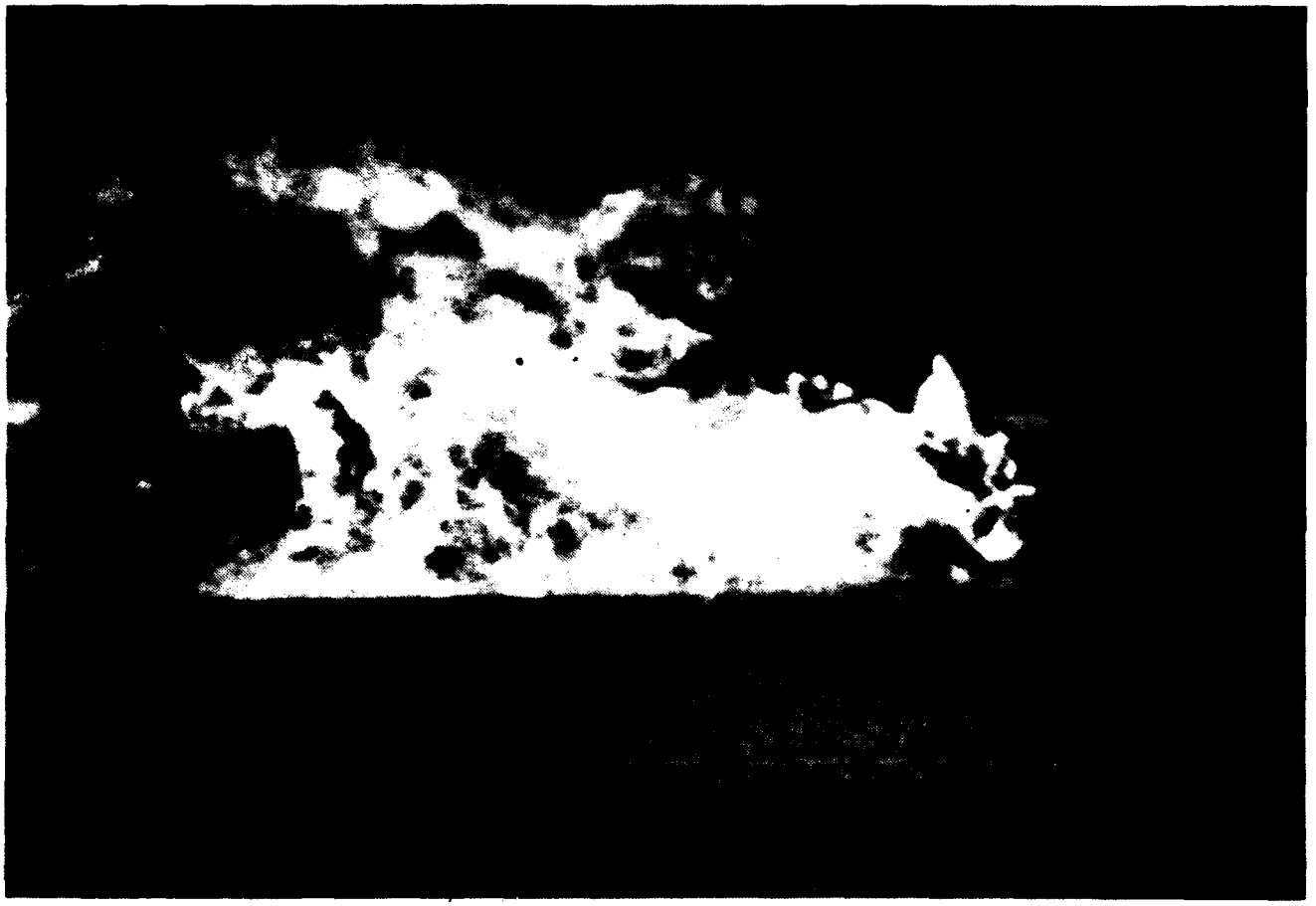

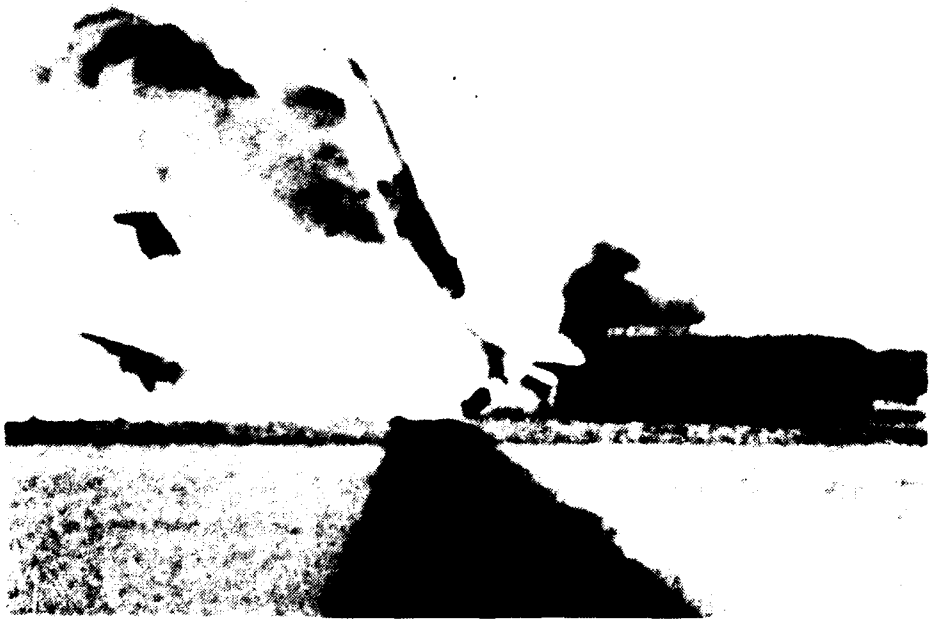

Figure 46. Right wing failure - side and front views.

Figure 47. Right wing/ground impact - front view.

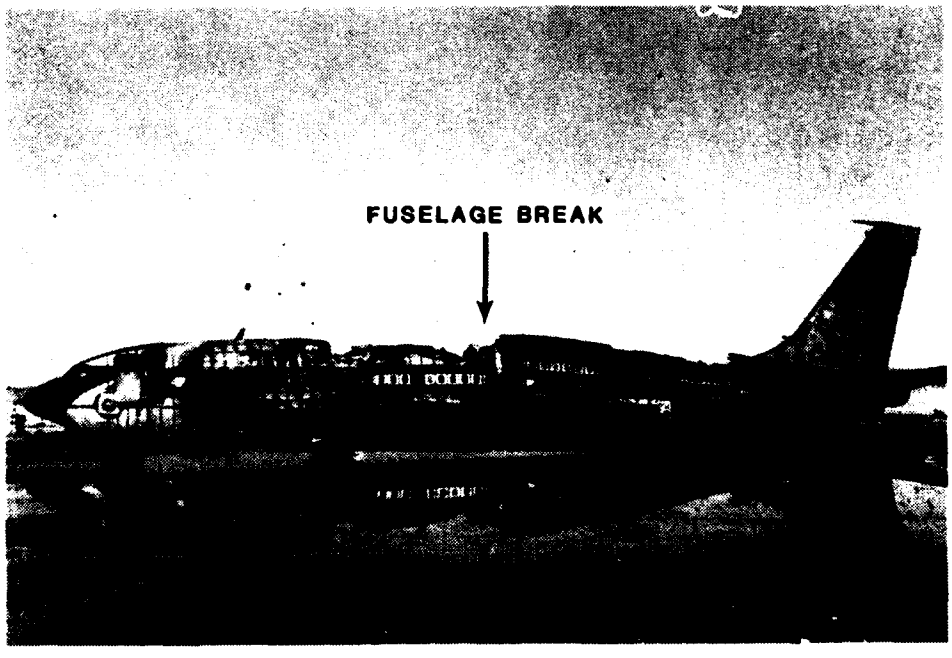

Figure 48. Posttest view of aircraft.

Figure 49. Location of floor break at B.S. 920.

Figure 50. Location of gear hub impact point.

Figure 51. Overhead view of aircraft showing roof damage.

Figure 52. Seat and dummy removal.

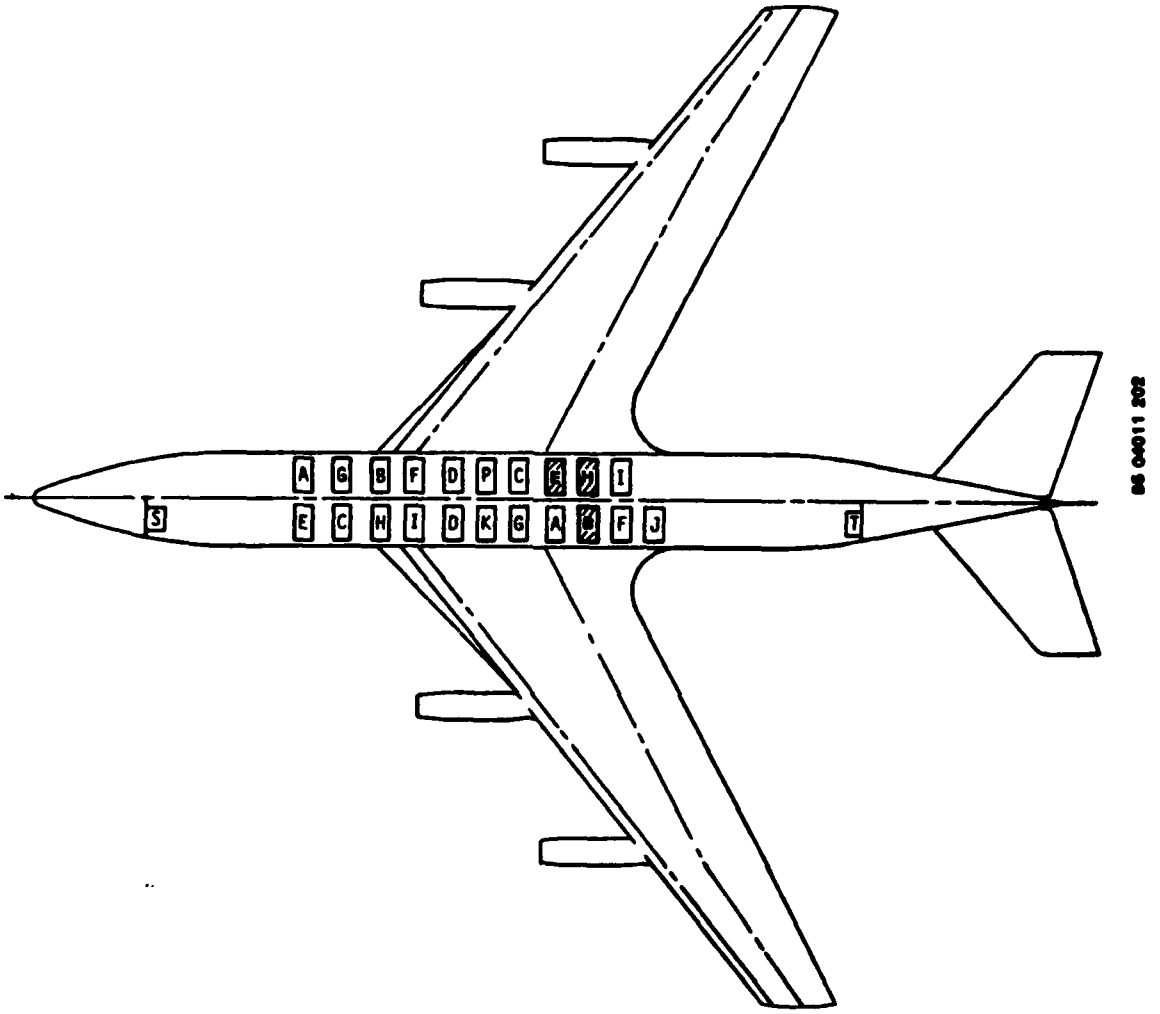

Figure 53. Locations of seats with seat pan deformation.

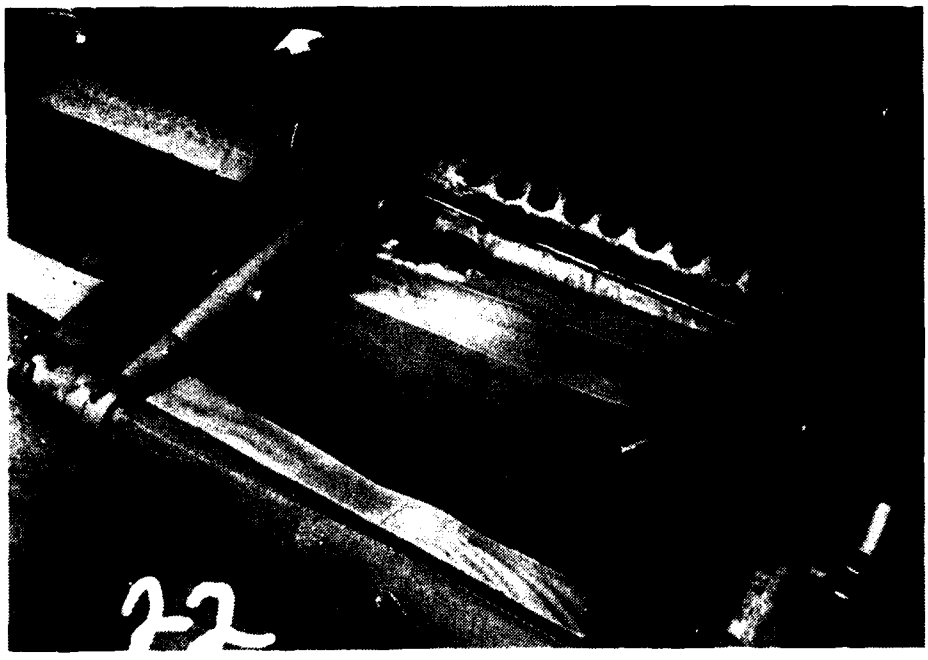

Figure 54. Seat pan deformation of seat E/R.

Figure 55. Seat pan deformation of seat H/R.

Figure 56. Seat pan deformation of seat B/L.

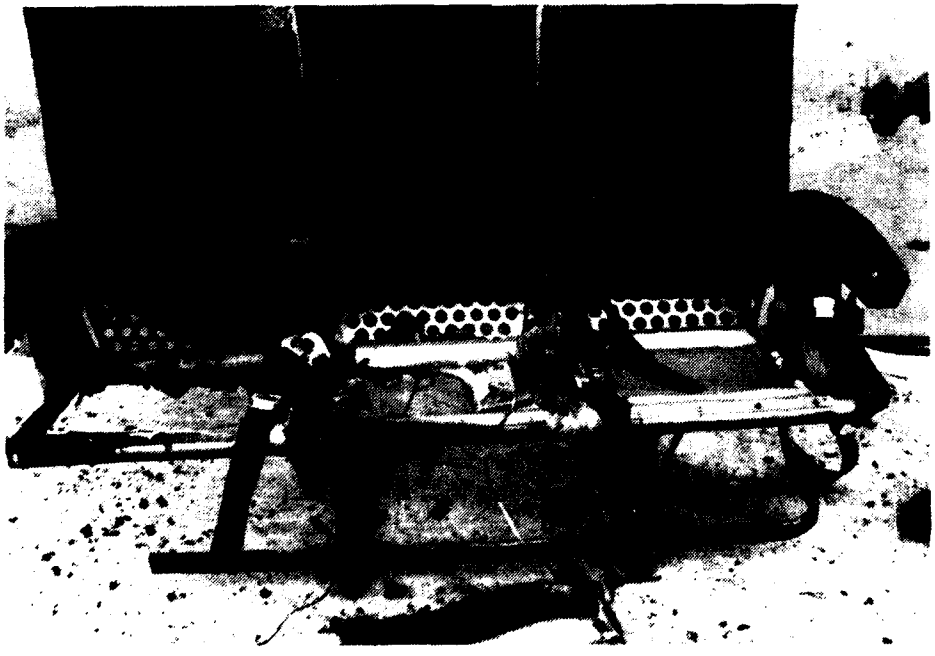

Figure 57. Damage to seat A/R.

Figure 58. Damage to seat E/L.

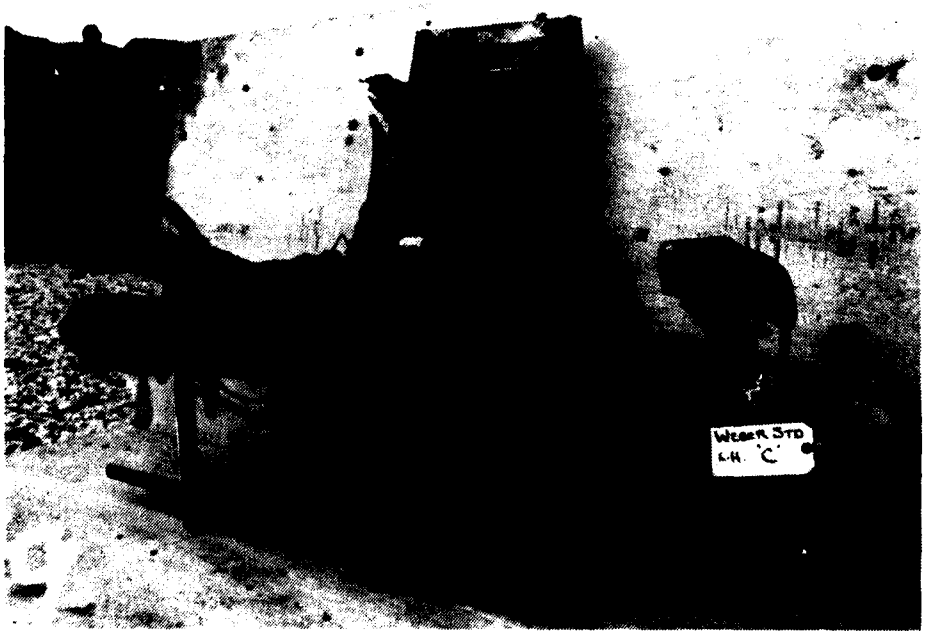

Figure 59. Damage to seat C/L.

Figure 60. Damage to seat F/R.

Figure 61. Damage to seat I/L.

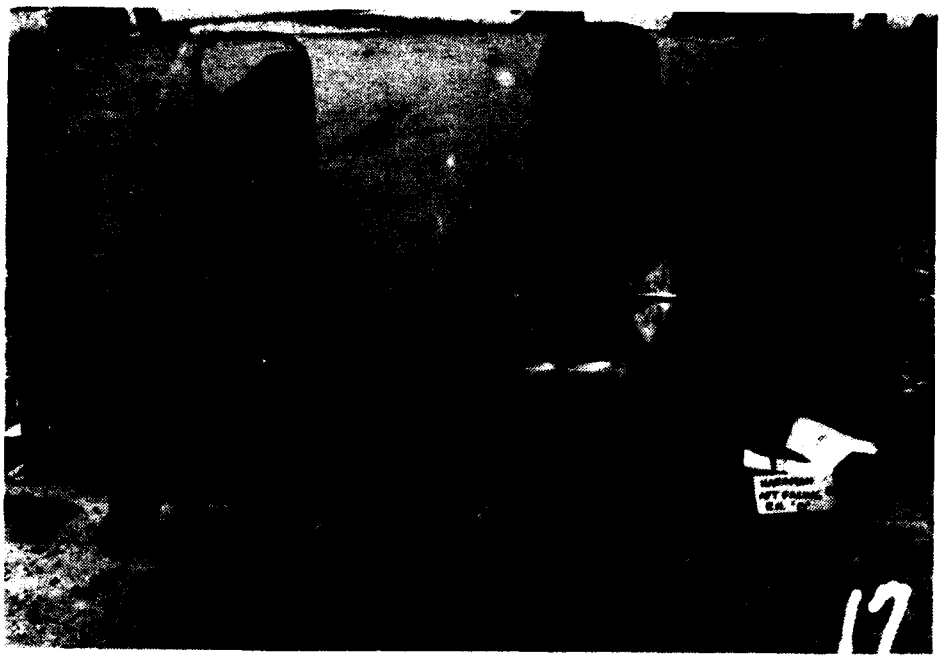

Figure 62. Damage to seat D/R.

Figure 63. Damage to seat D/L.

Figure 64. Damage to seat P/R.

Figure 65. Damage to seat K/L.

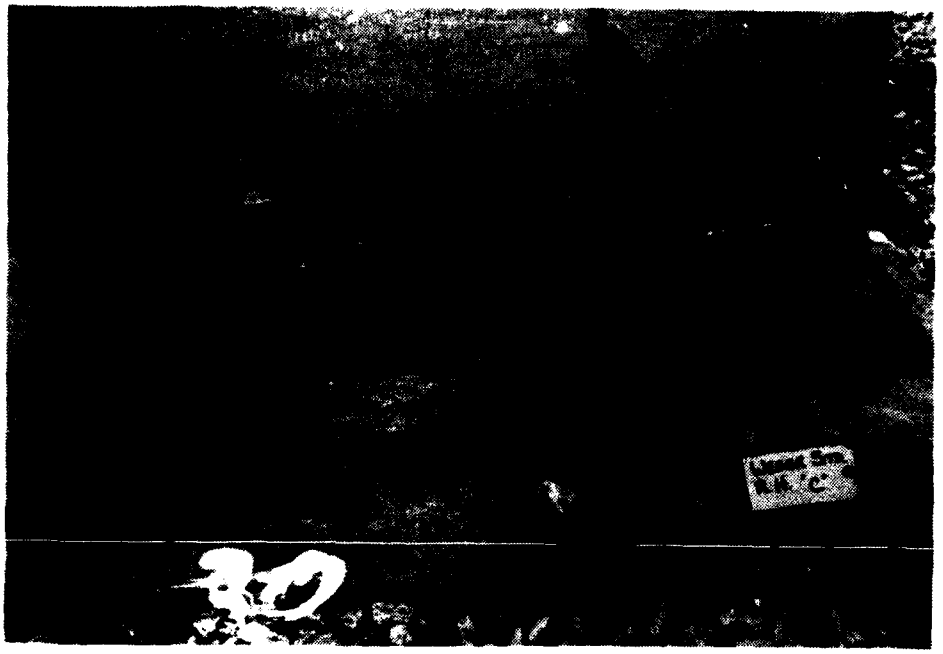

Figure 66. Damage to seat C/R.

Figure 67. Damage to seat G/L.

Figure 68. Damage to seat E/R.

Figure 69. Damage to seat H/R.

Figure 70. Damage to seat I/R.

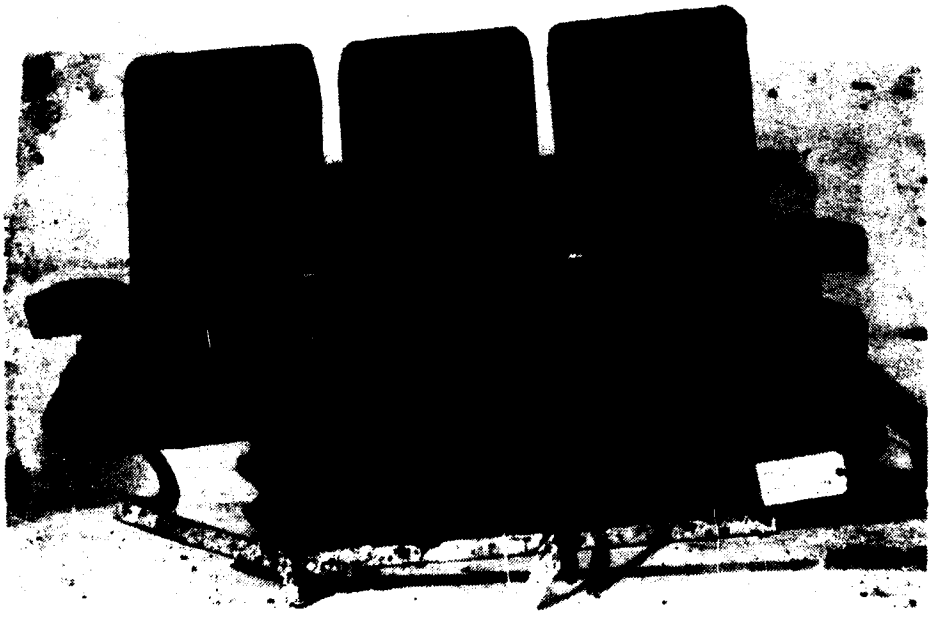

Figure 71. Damage to seat A/L.

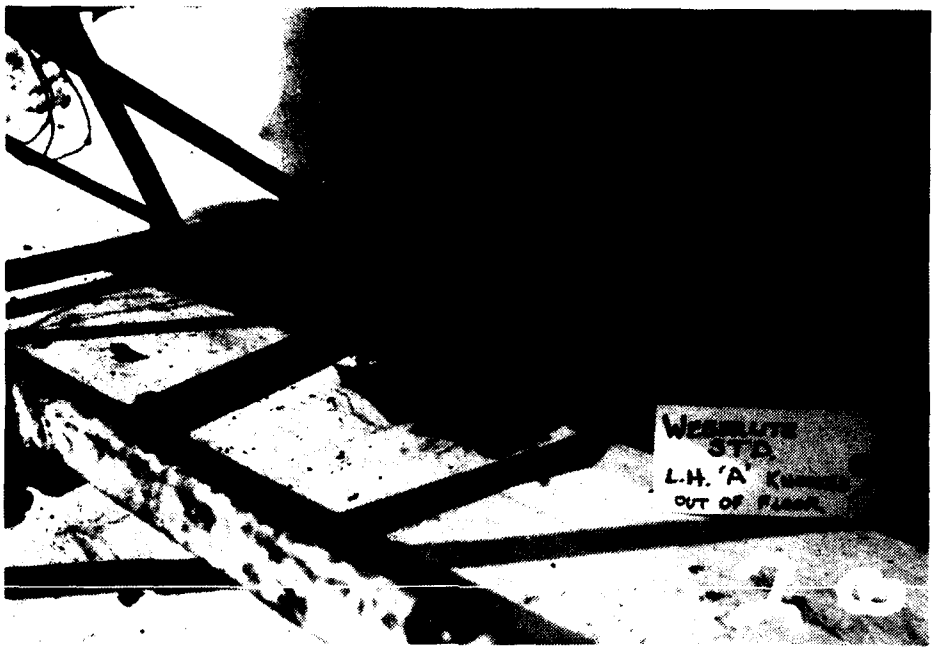

Figure 72. Floor track attached to rear outboard leg of seat A/L.

Figure 73. Damage to seat A/L baggage restraint.

Figure 74. Seat A/L front inboard track button.

Figure 75. Location of gear hub impact point beneath seat B/L.

Figure 76. Deformation of floor due to gear hub impact.

Figure 77. Buckled inboard rear leg of seat B/L.

AD-A172 245 SEAT EXPERIMENT RESULTS OF FULL-SCALE TRANSPORT AIRCRAFT CONTROLLED IMPAC. (U) RMS TECHNOLOGIES INC TREVOSE PA M R CANNON ET AL. JUL 86 TR-85413 2/3

UNCLASSIFIED DOT/FAA/TT-85/25 DTFA03-81-C-00040 F/G 1/3 NL

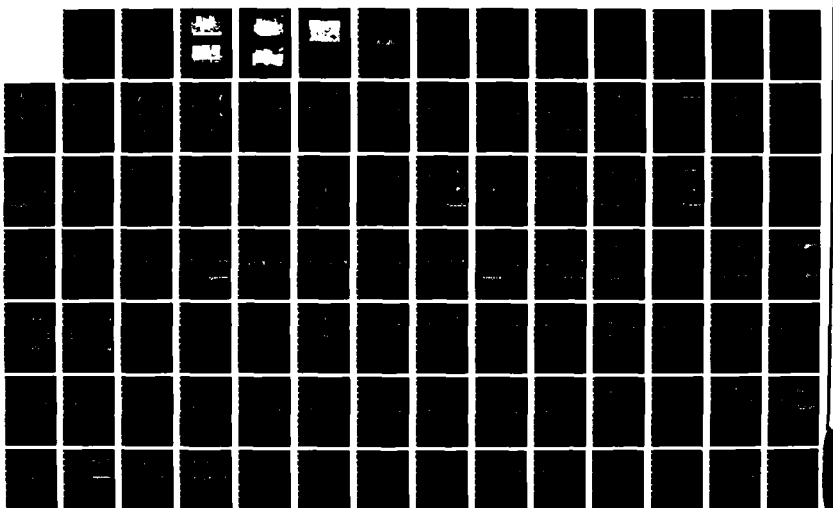

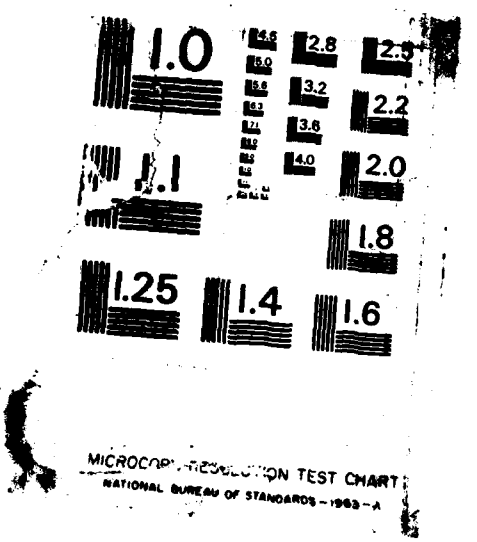
1.0
1.1
1.25
1.4
1.6
1.8
2.0
2.2
2.5
2.8
3.2
3.6
4.0
MICROCOPY RESOLUTION TEST CHART
NATIONAL BUREAU OF STANDARDS - 1963 - A

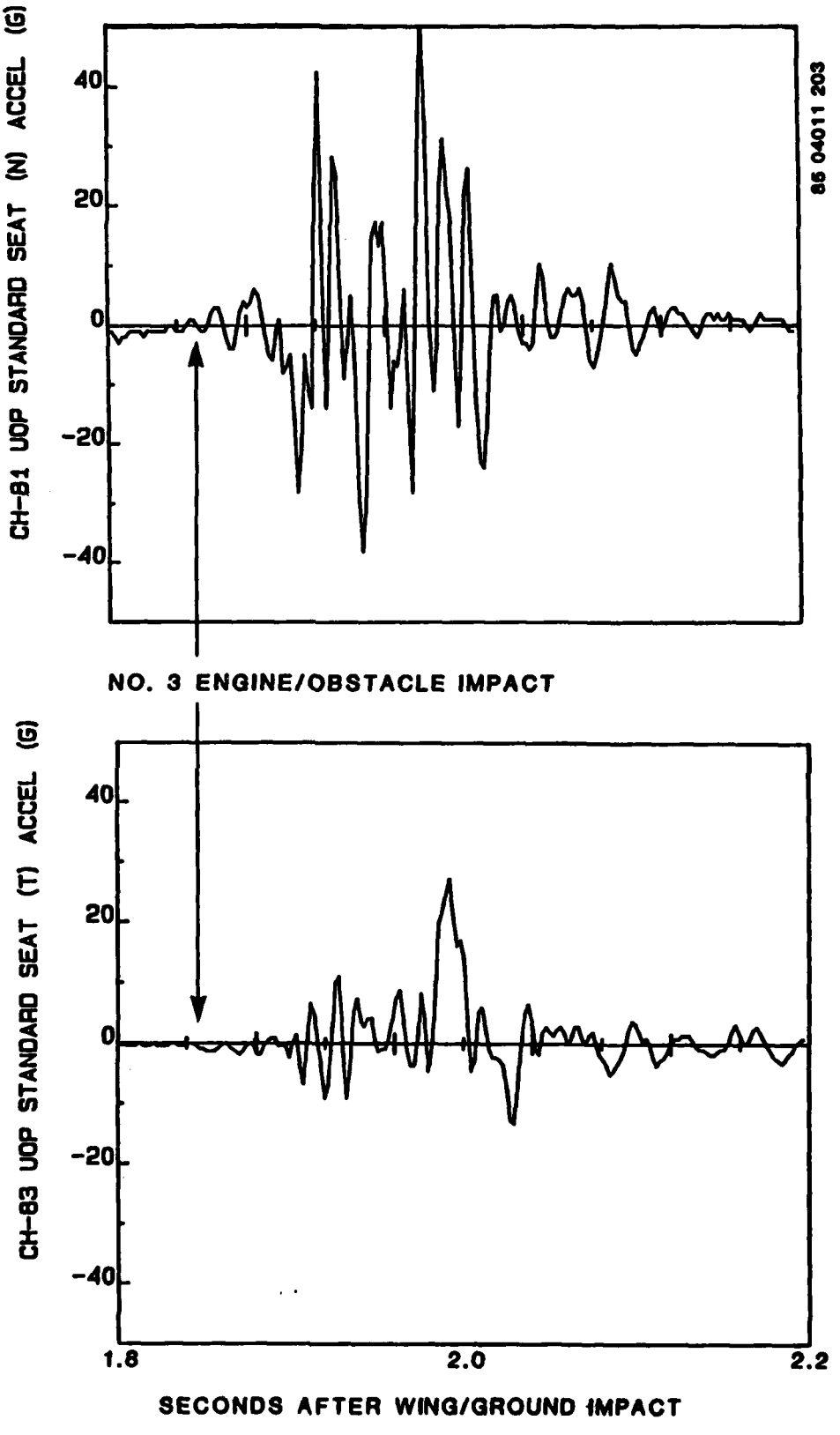

Figure 78. Seat B/L - vertical and lateral accelerations after obstacle impact.

Figure 79. Deformed front seat pan tube of seat B/L.

Figure 80. Deformed rear seat pan tube of seat B/L.

Figure 81. Damage to seat F/L.

Figure 82. Deformed legs of seat J/L.

Figure 83. Posttest position of seat J/L.

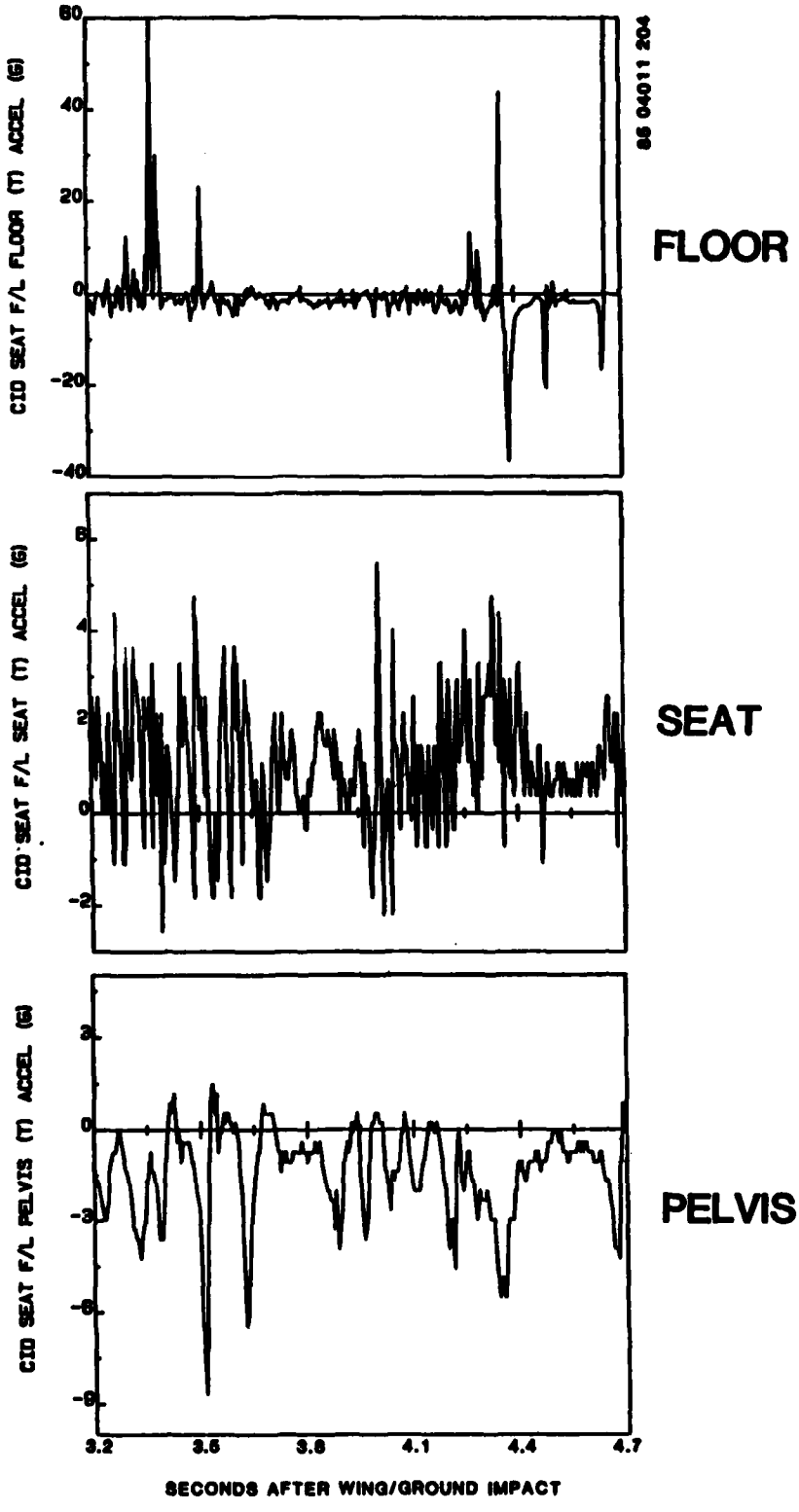

Figure 84. Seat F/L - lateral accelerations after obstacle impact.

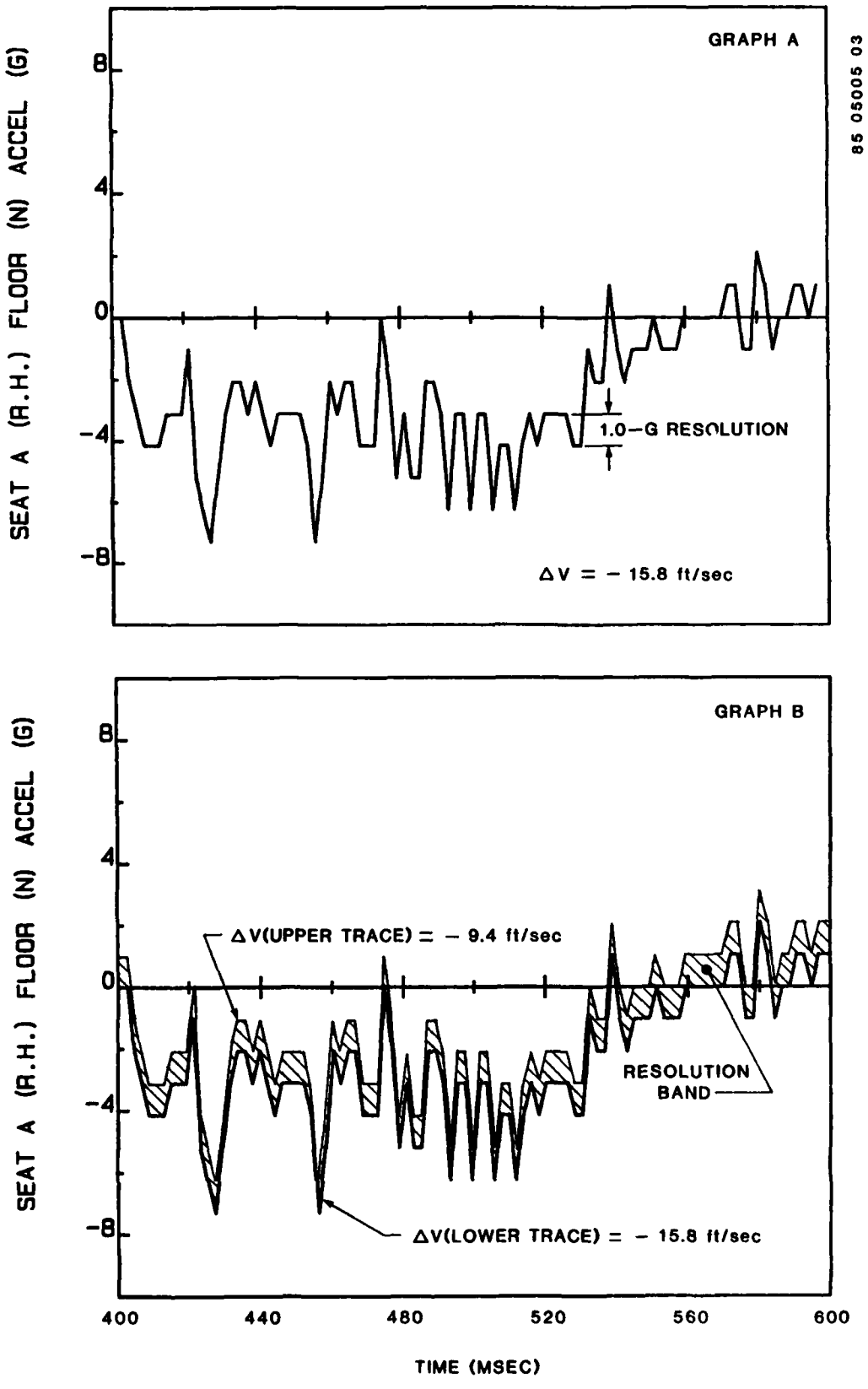

Figure 88. Example of velocity change uncertainty.

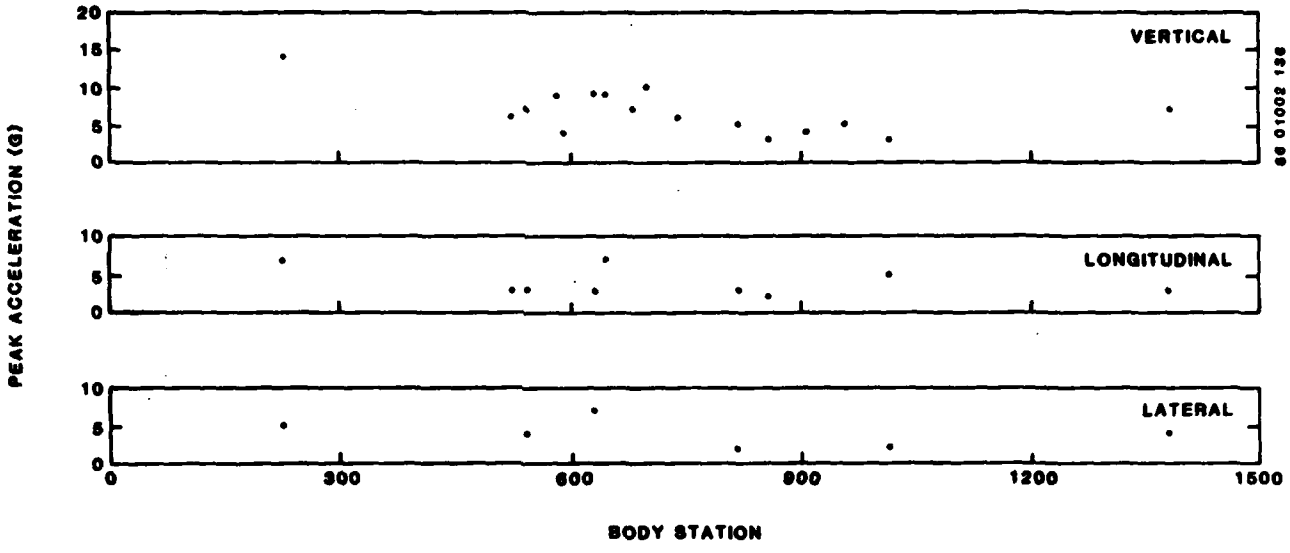

Figure 89. Plot distribution of vertical, longitudinal, and lateral floor accelerations.

APPENDIX A

FLOOR, SEAT, AND PELVIS VERTICAL ACCELERATIONS

THIS PAGE LEFT INTENTIONALLY BLANK.

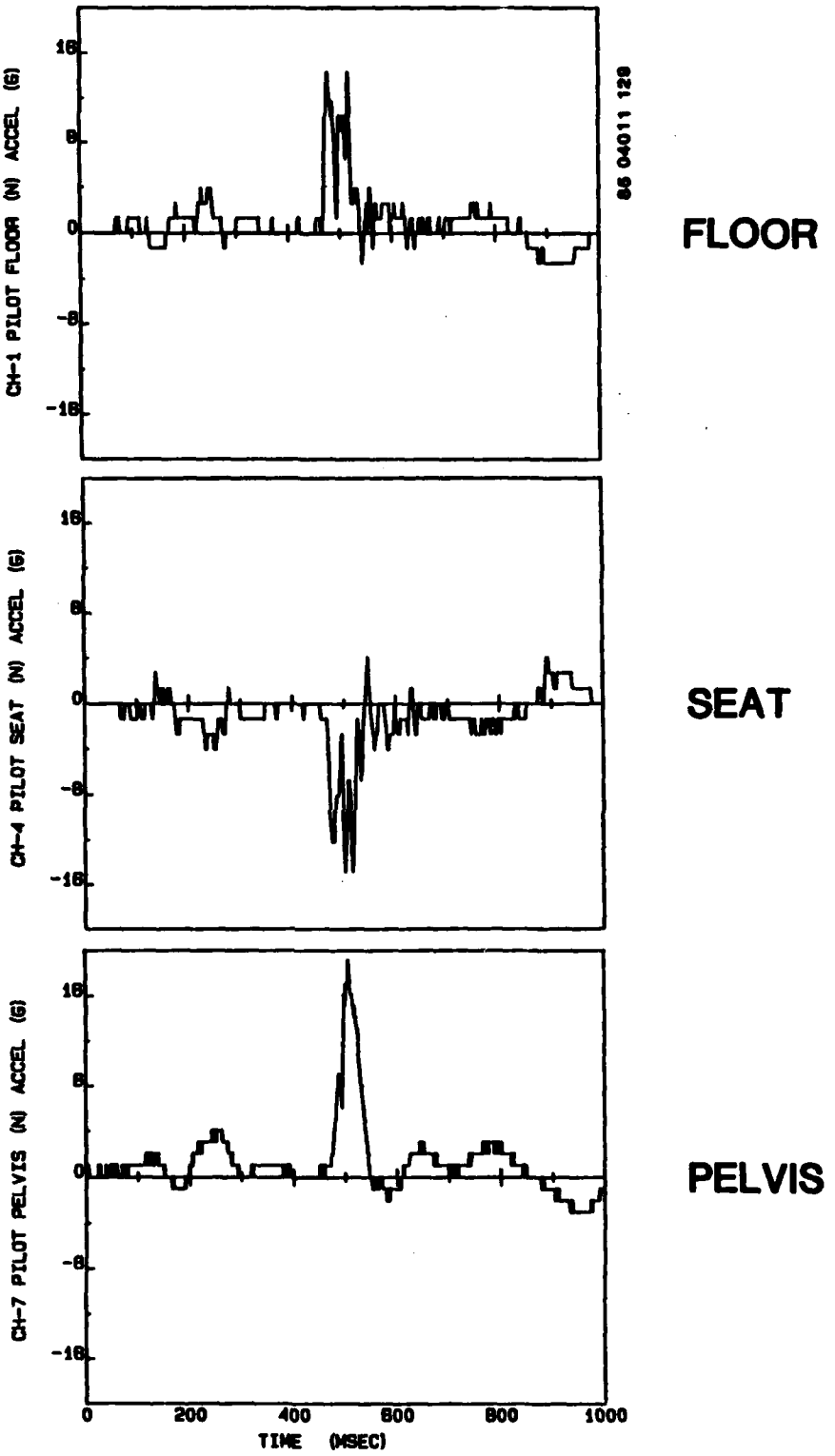

Figure A-1. Pilot seat.

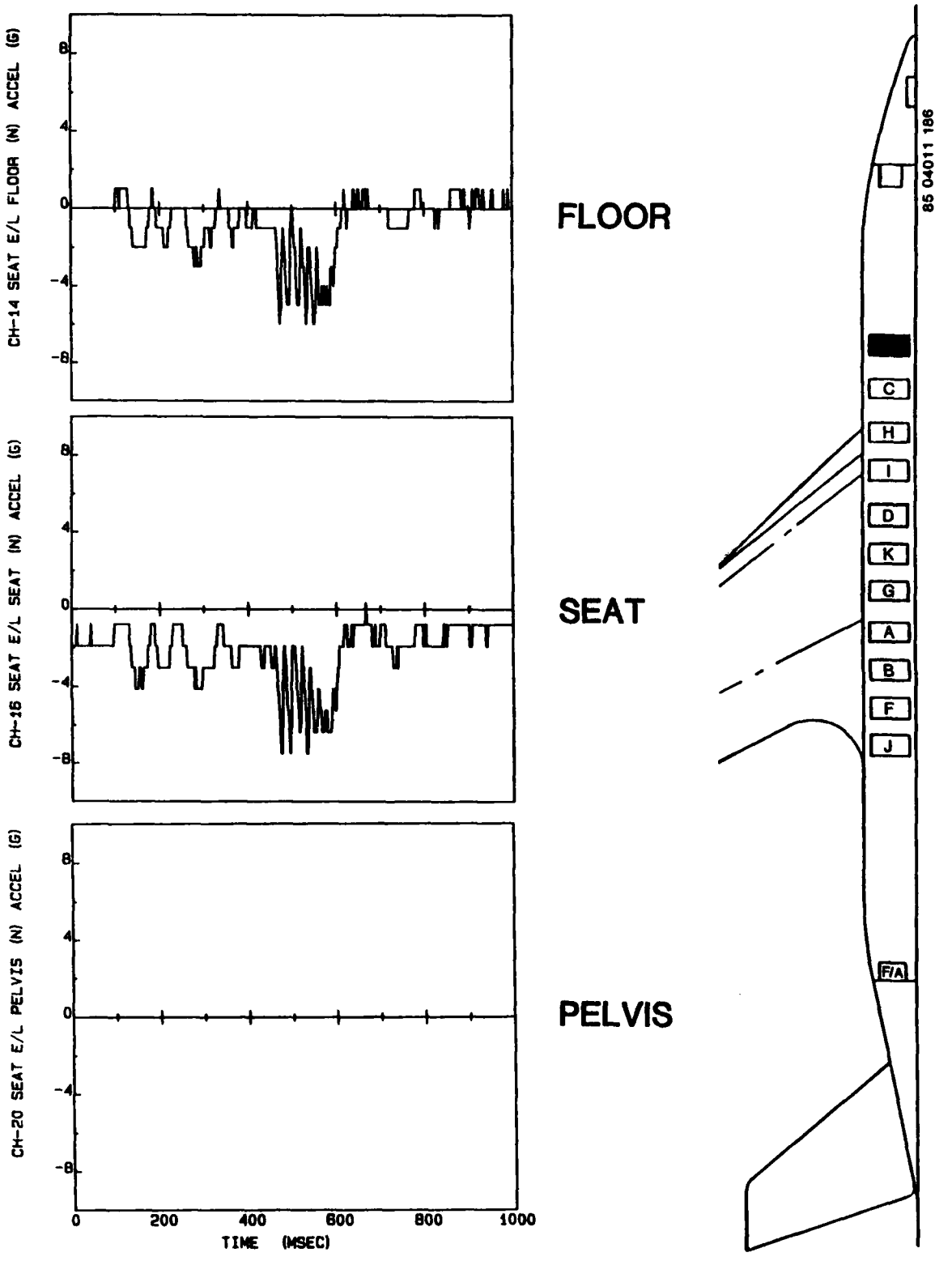

Figure A-2. Seat E/L.

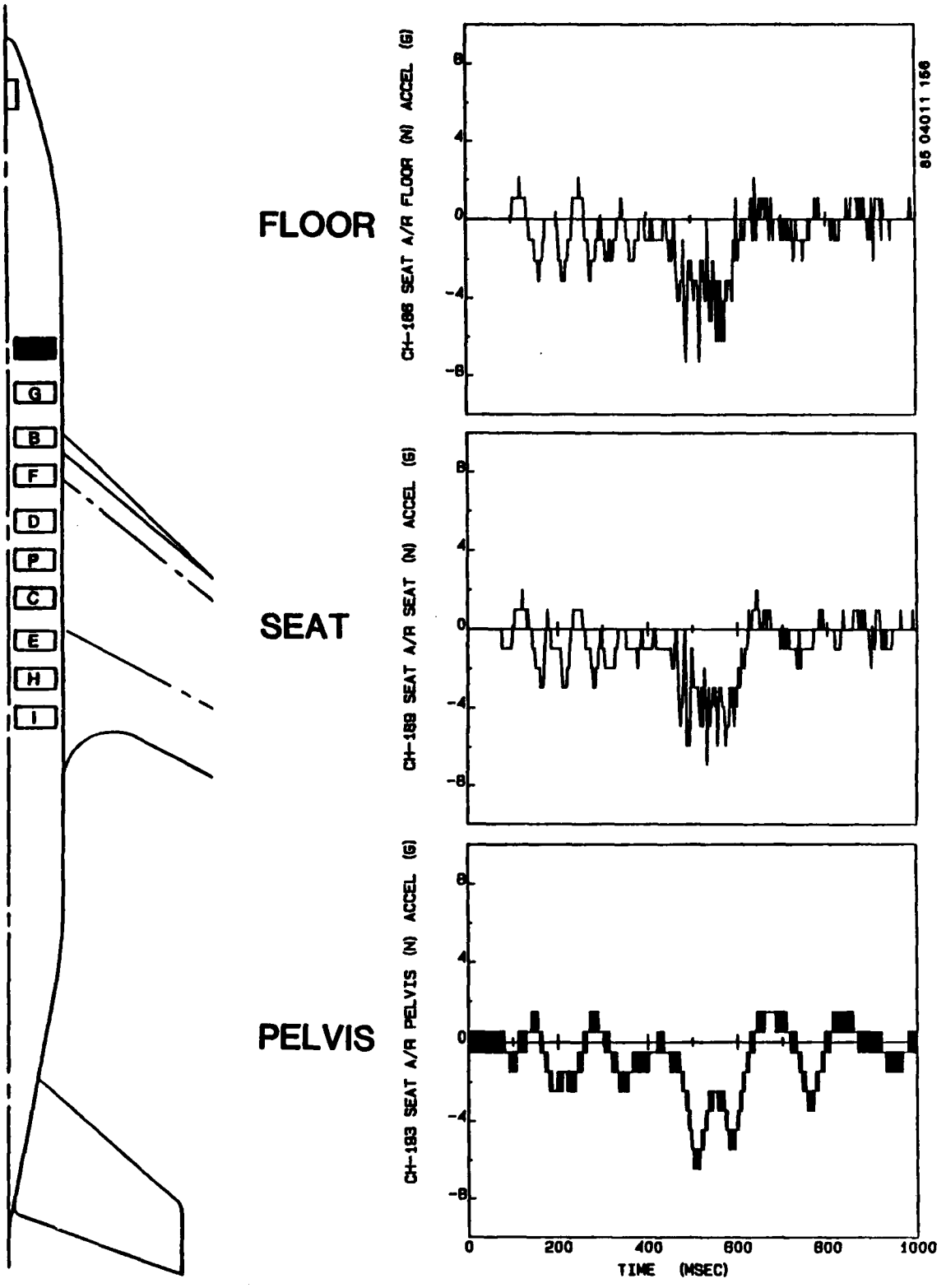

Figure A-3. Seat A/R.

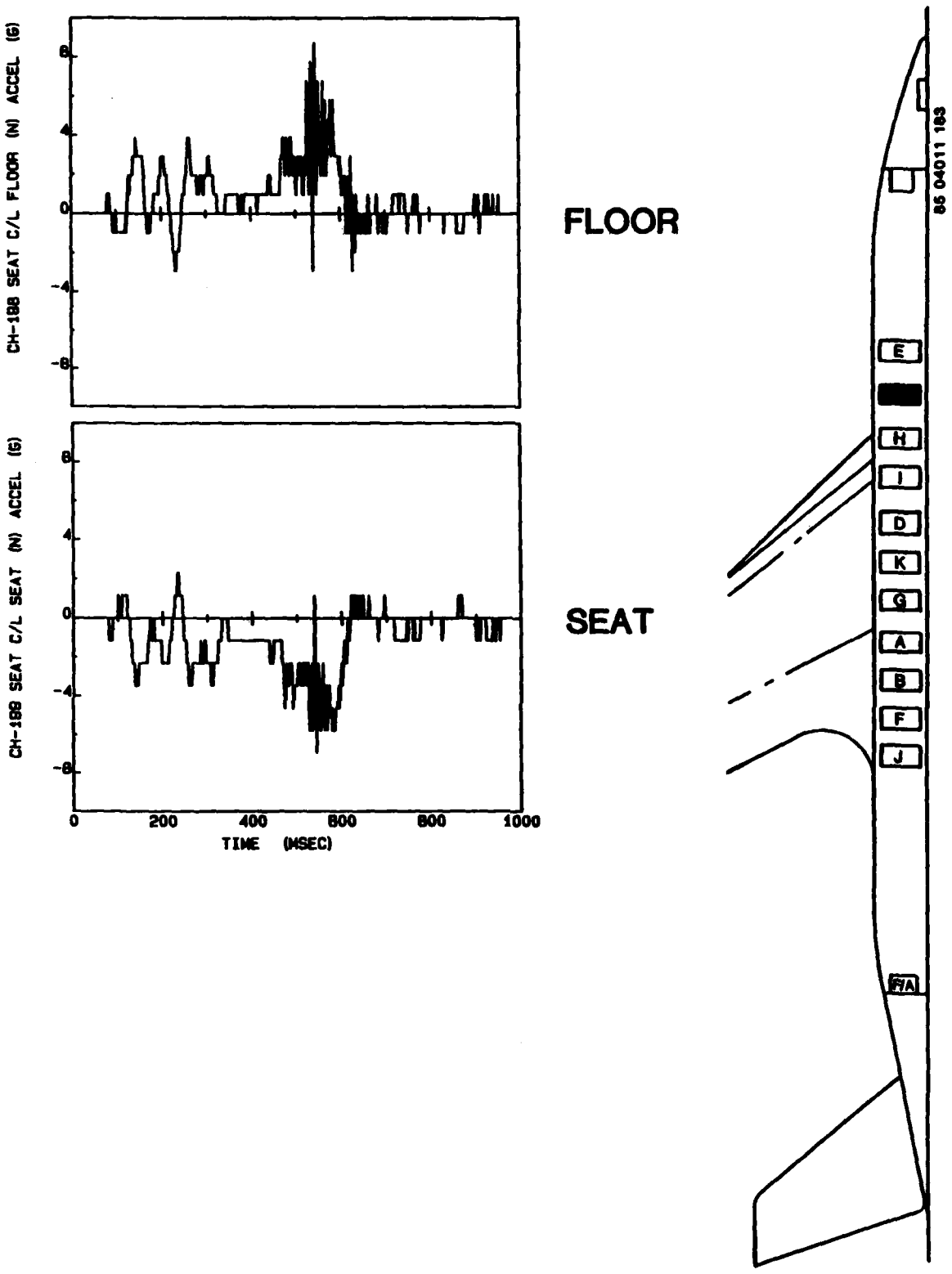

Figure A-4. Seat C/L.

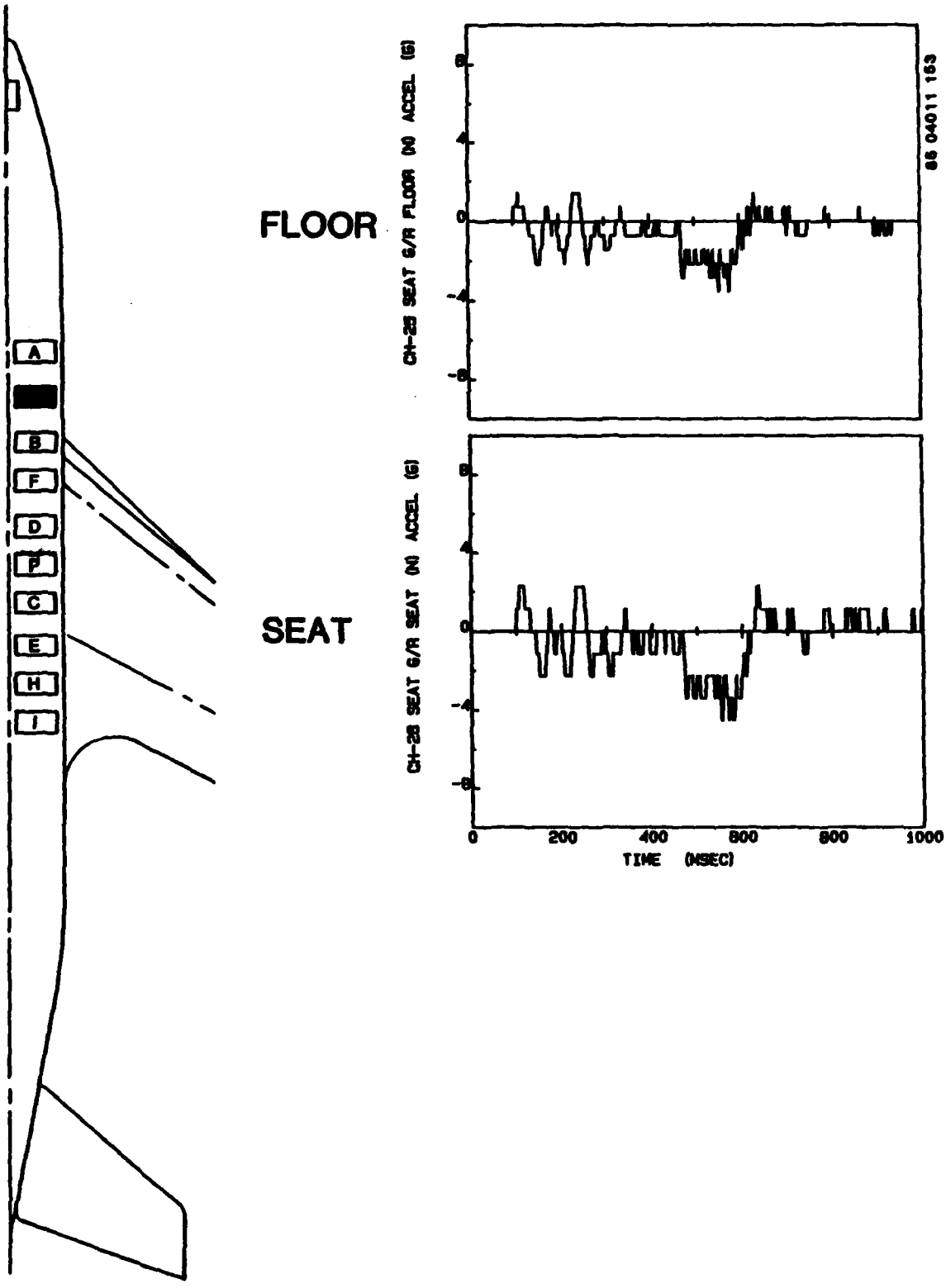

Figure A-5. Seat G/R.

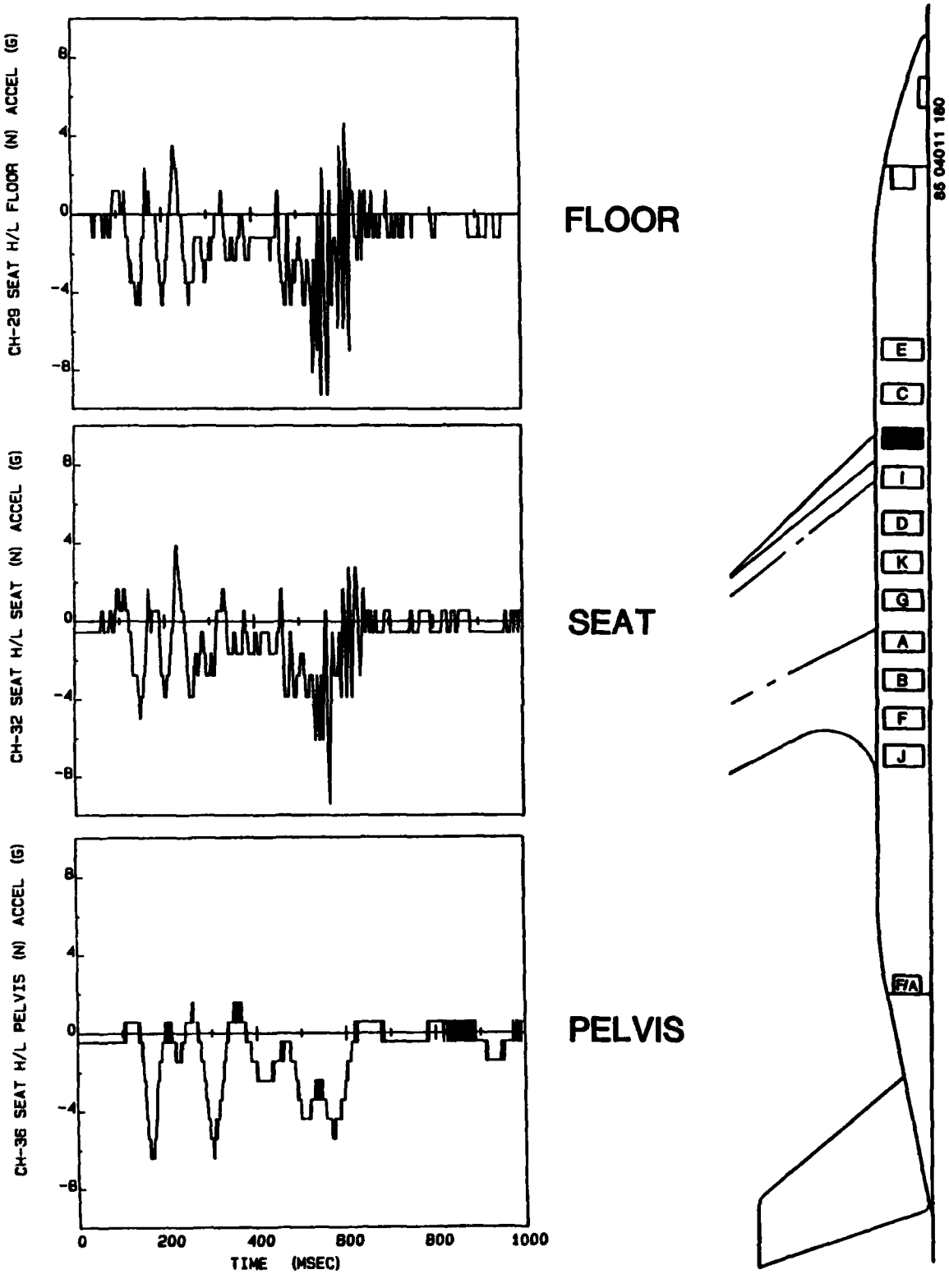

Figure A-6. Seat H/L.

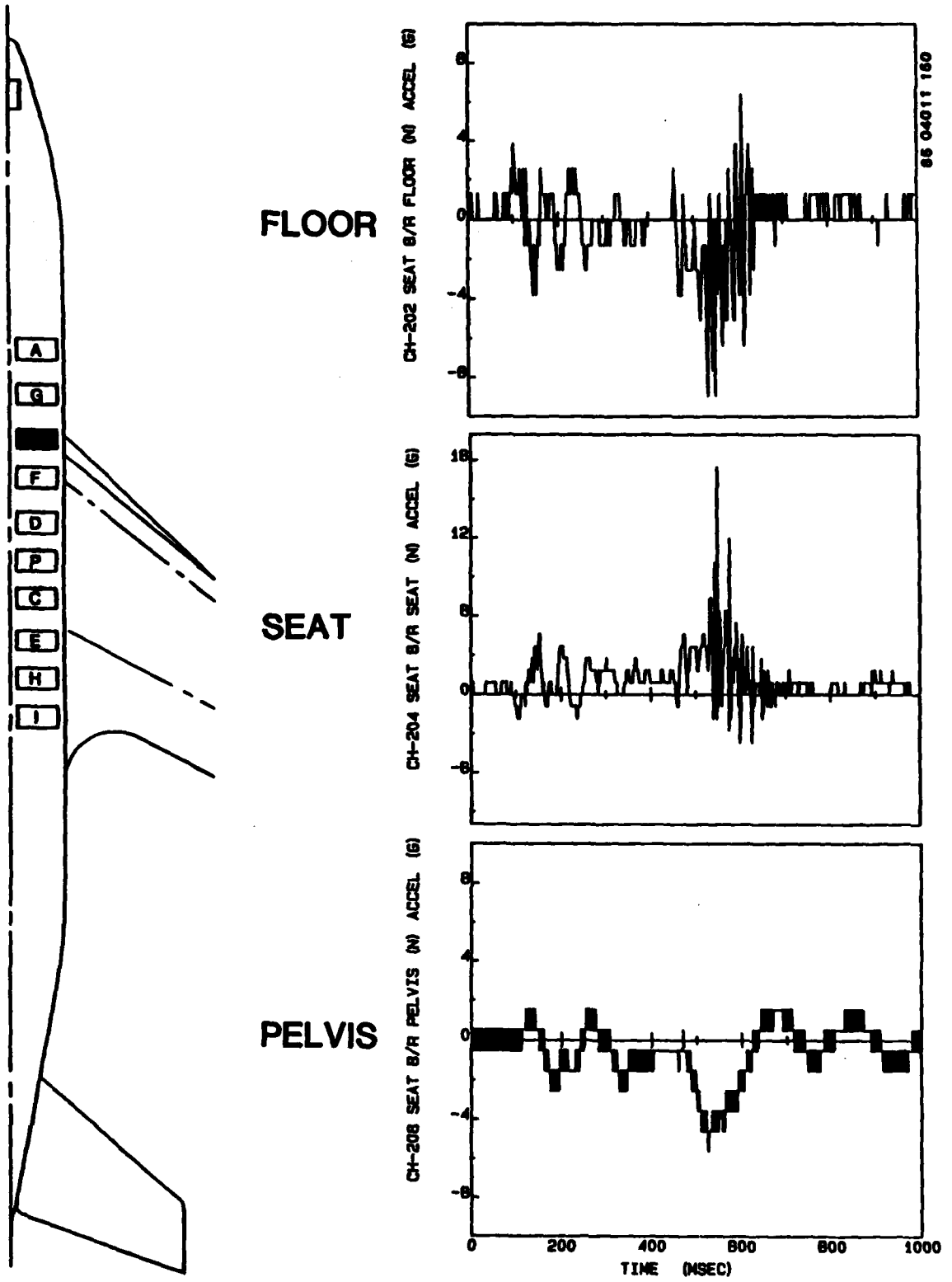

Figure A-7. Seat B/R.

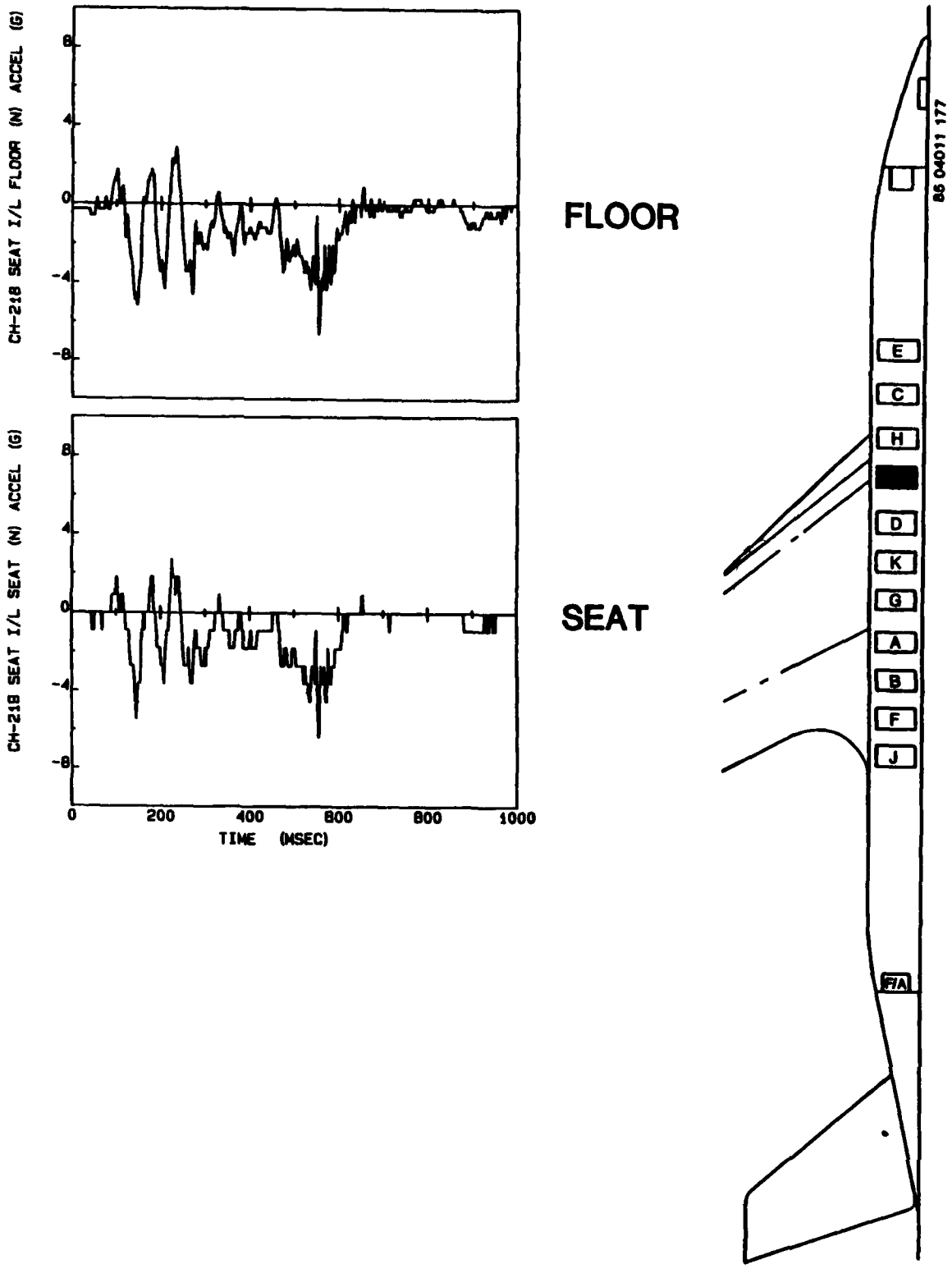

Figure A-8 Seat I/L.

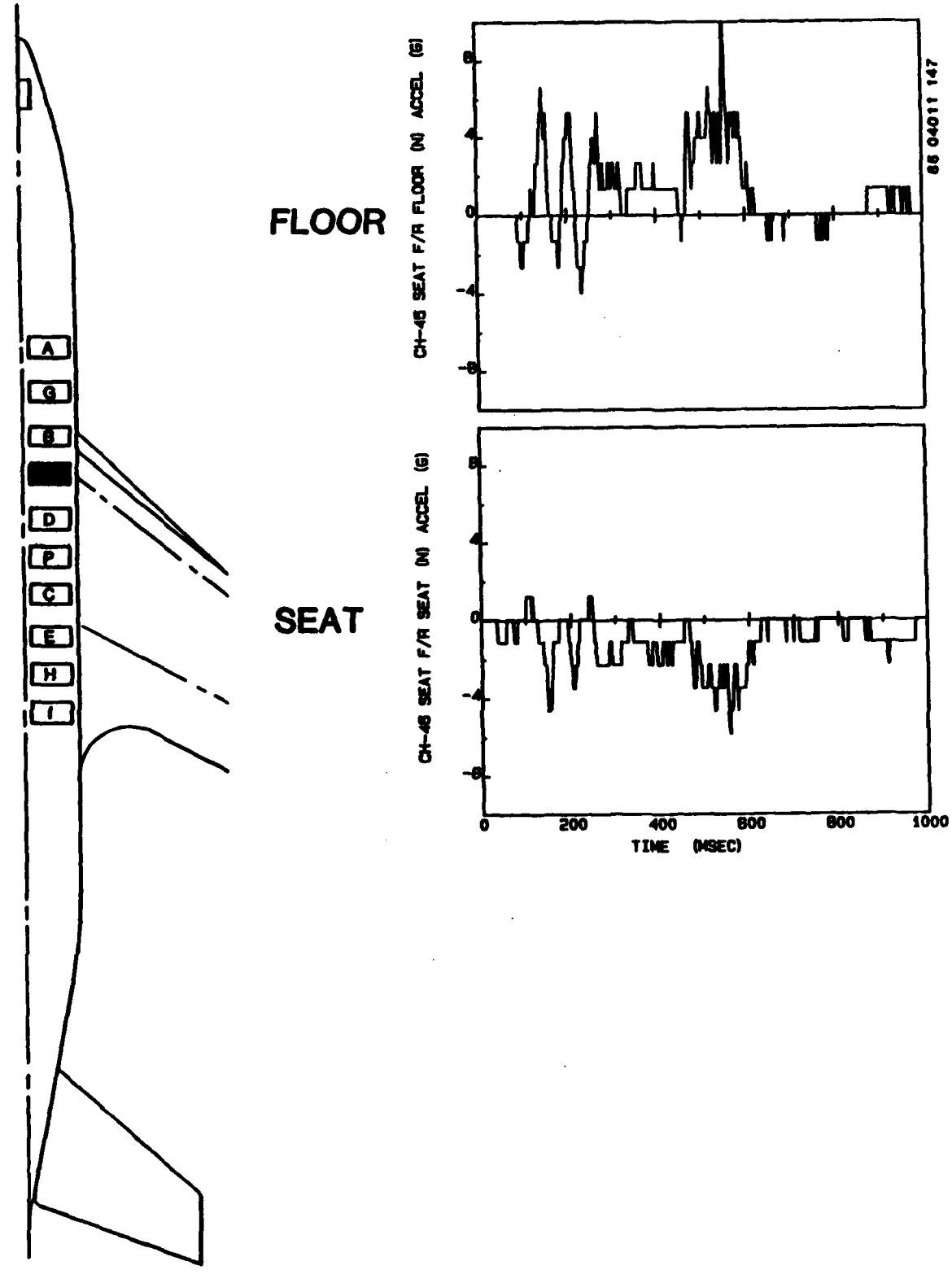

Figure A-9. Seat F/R.

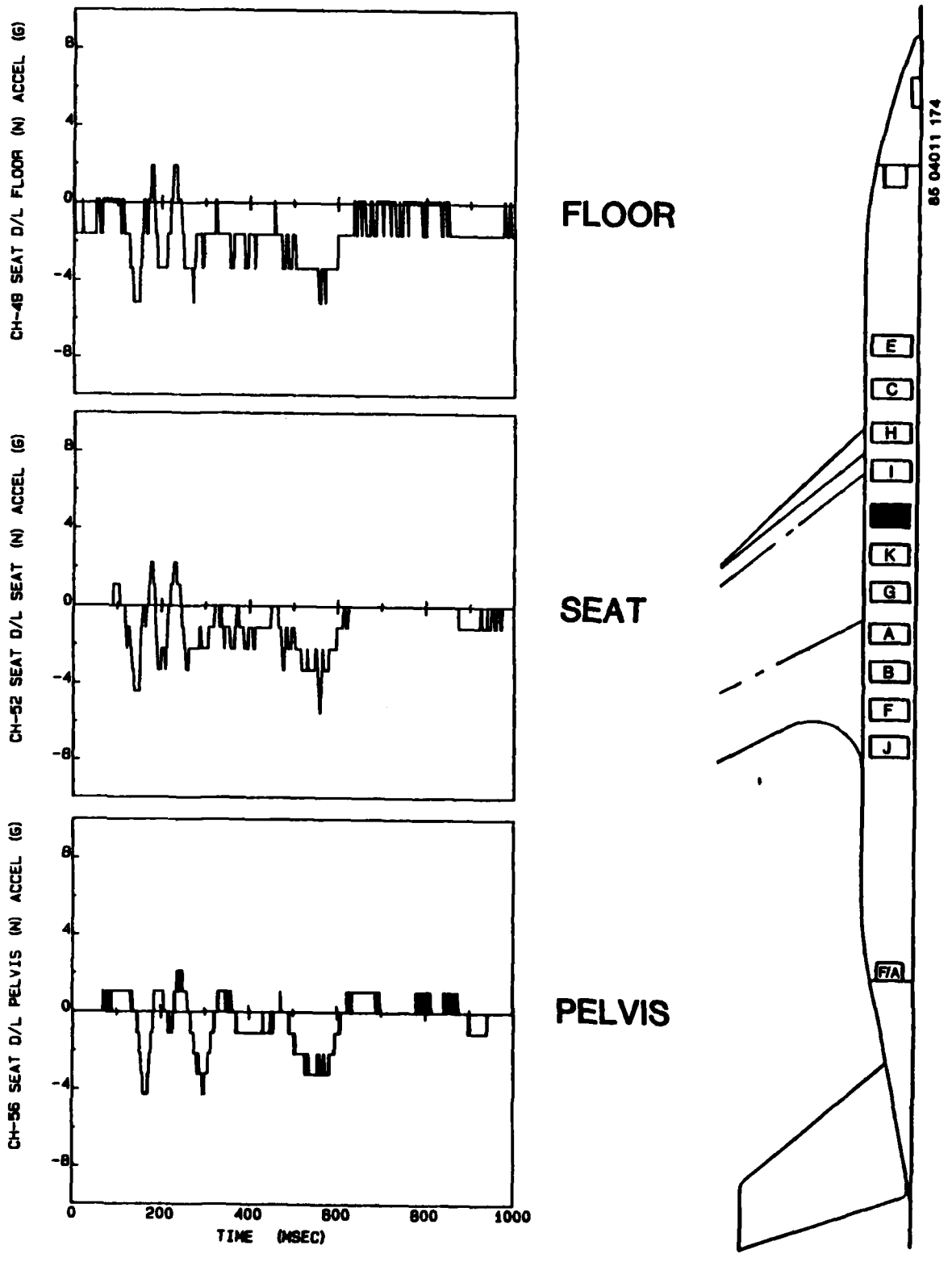

Figure A-10. Seat D/L.

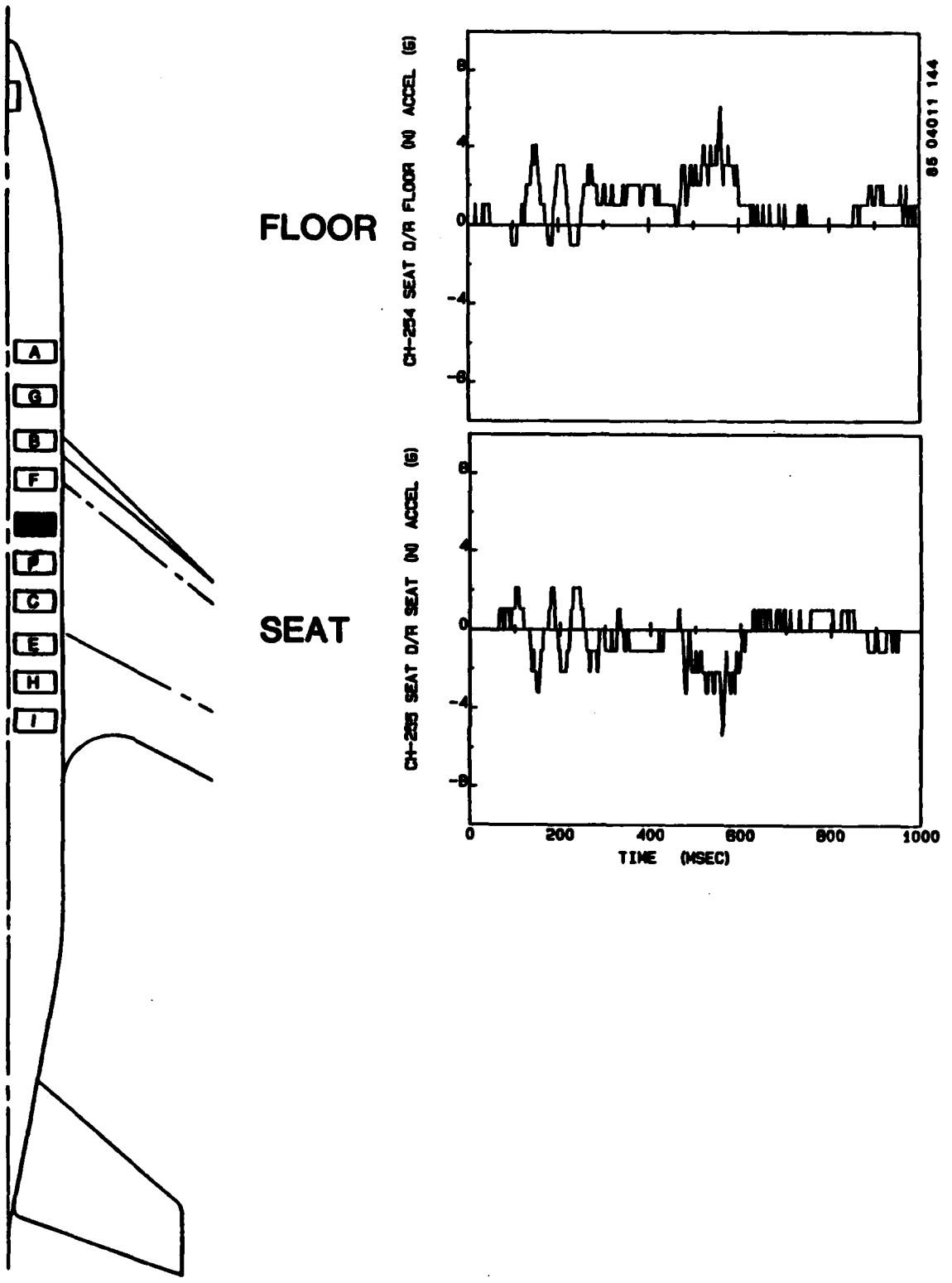

Figure A-11. Seat D/R.

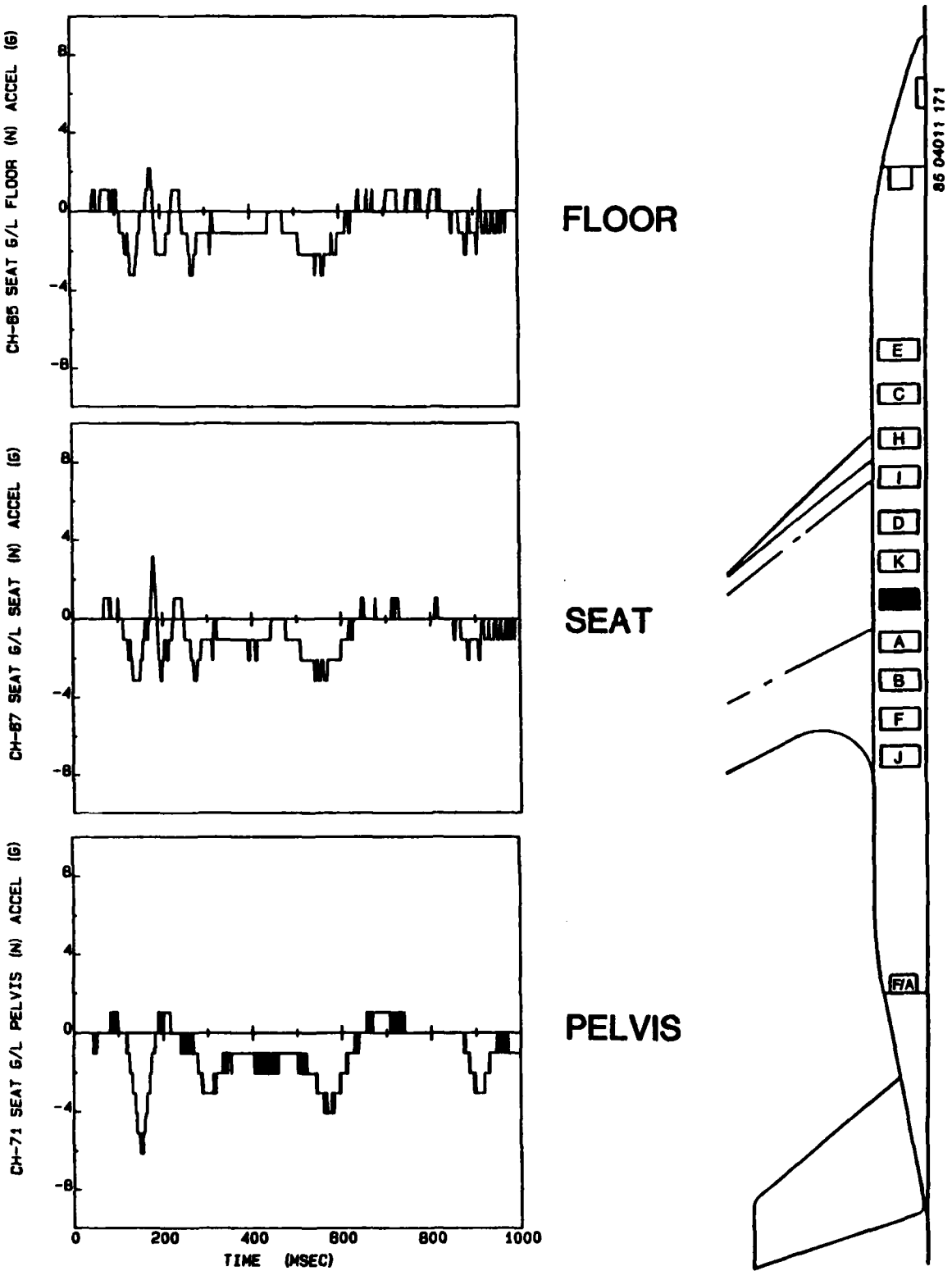

Figure A-12. Seat G/L.

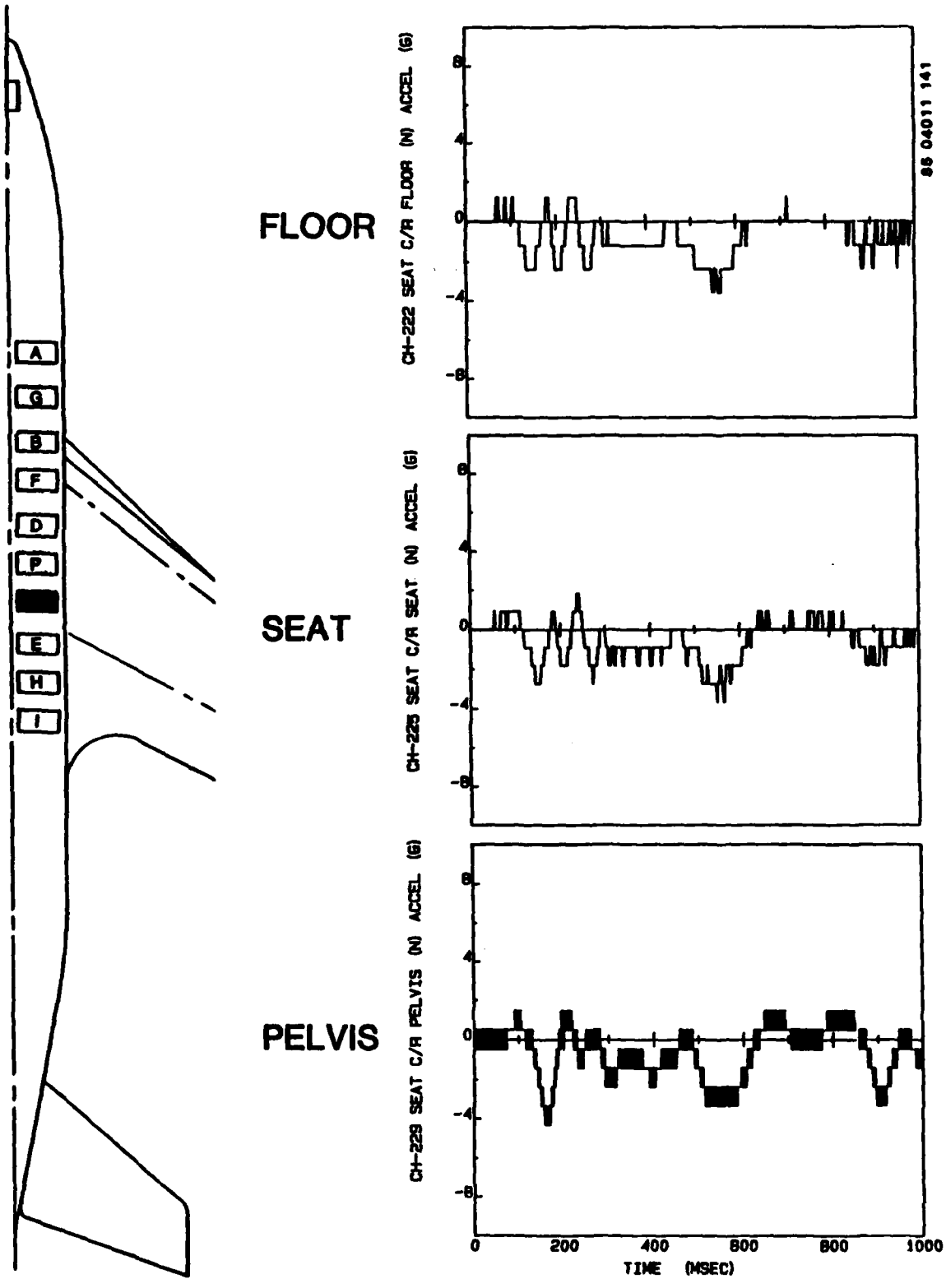

Figure A-13. Seat C/R.

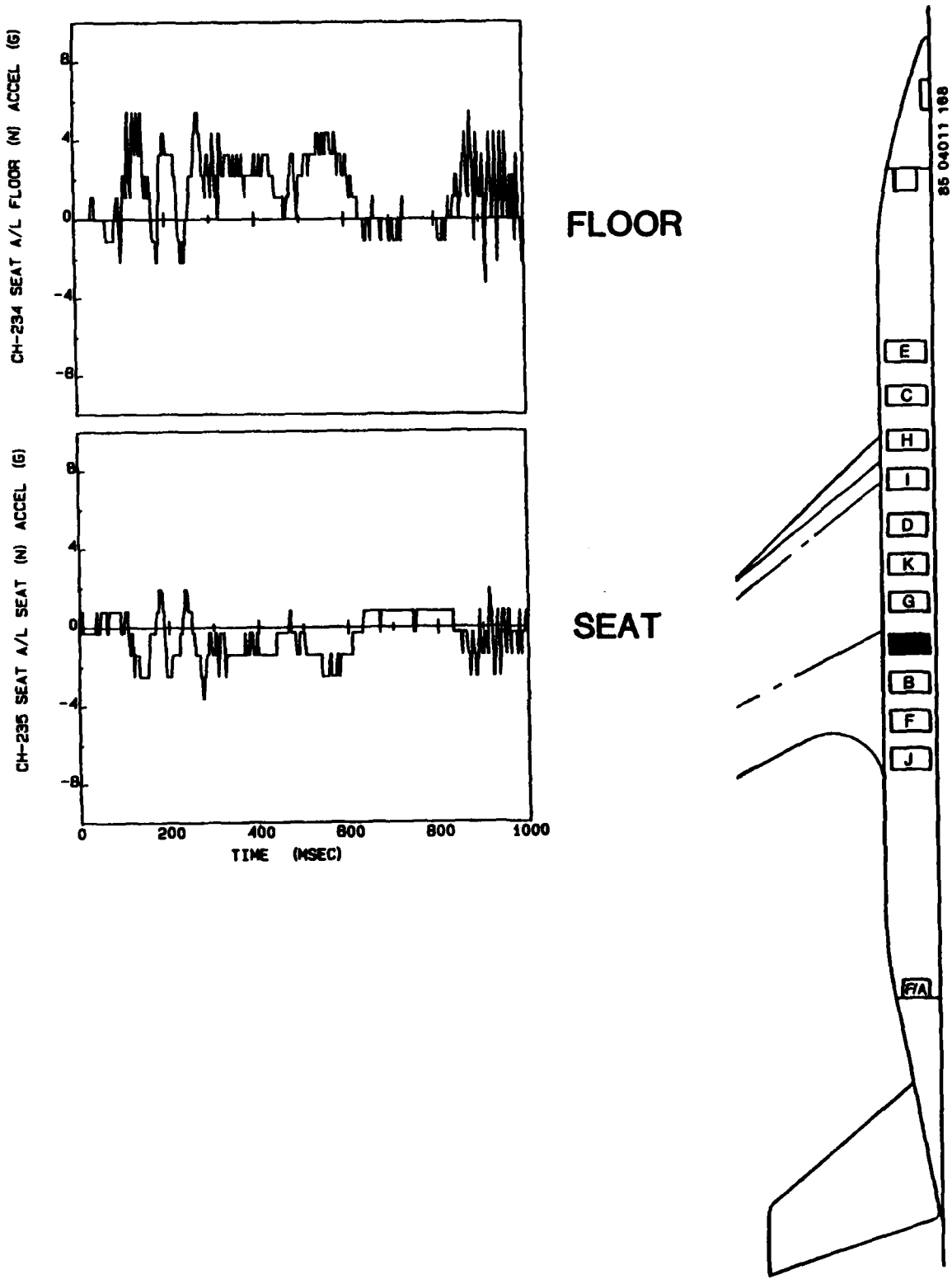

Figure A-14. Seat A/L.

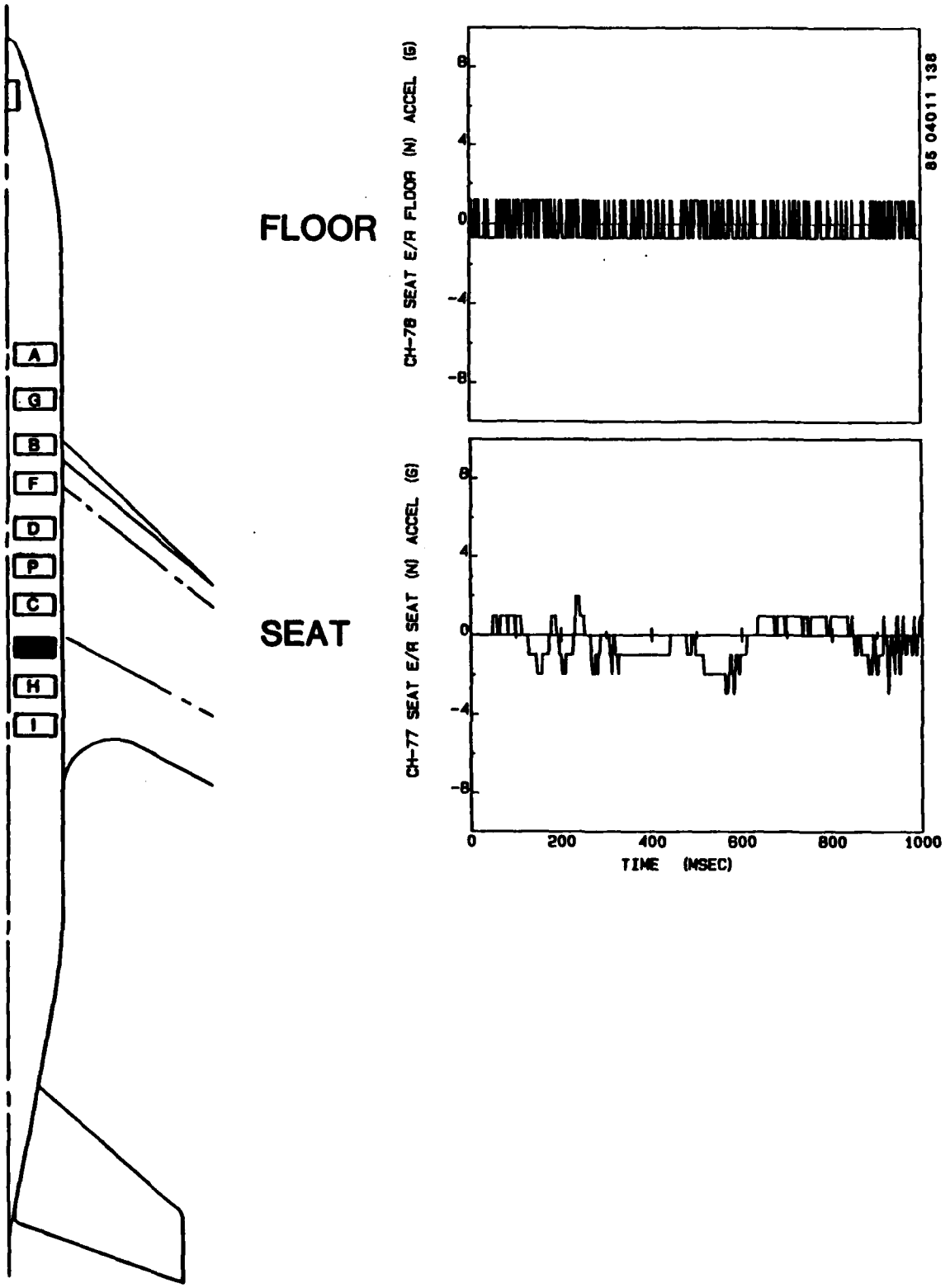

Figure A-15. Seat E/R.

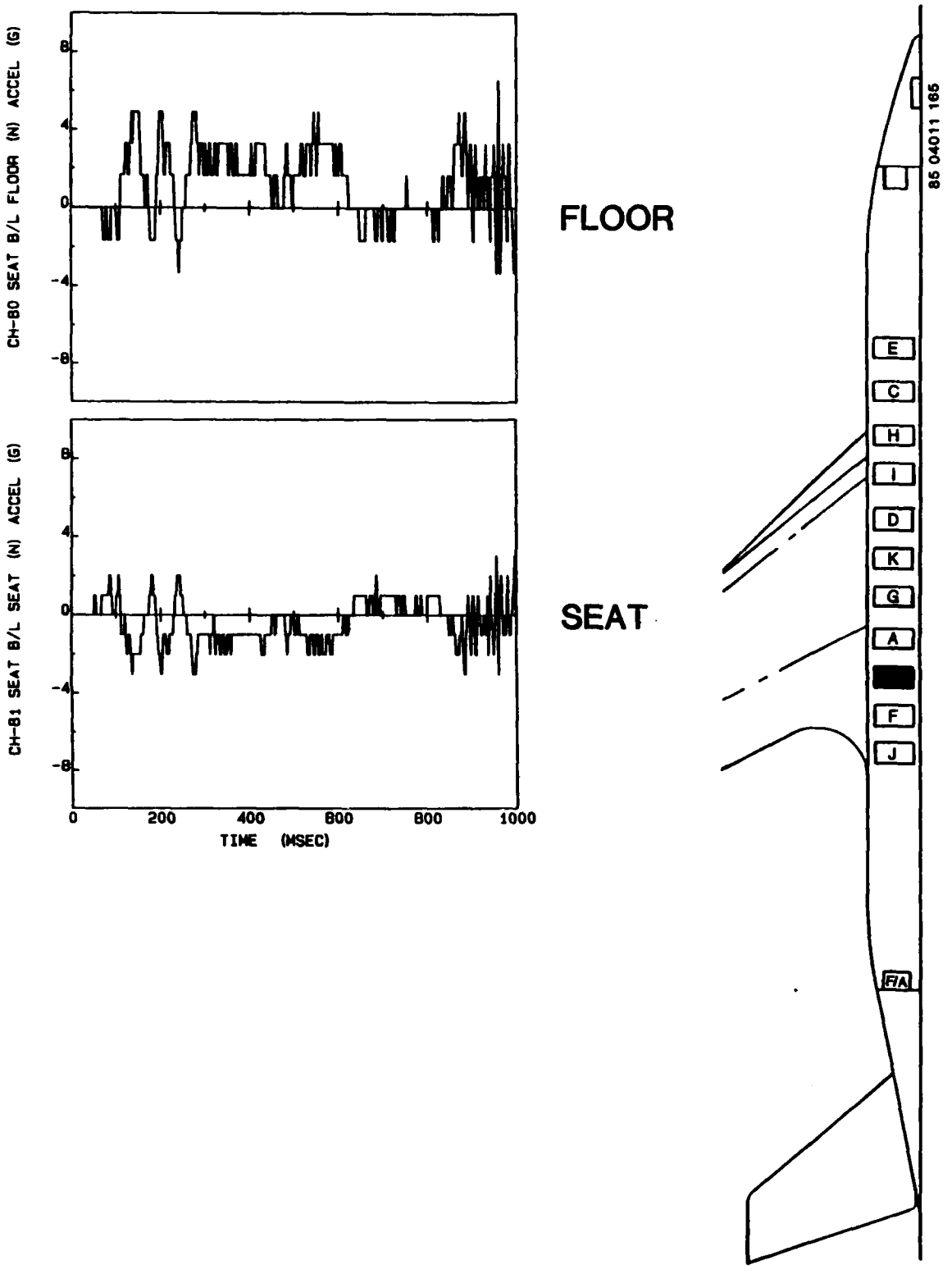

Figure A-16. Seat B/L.

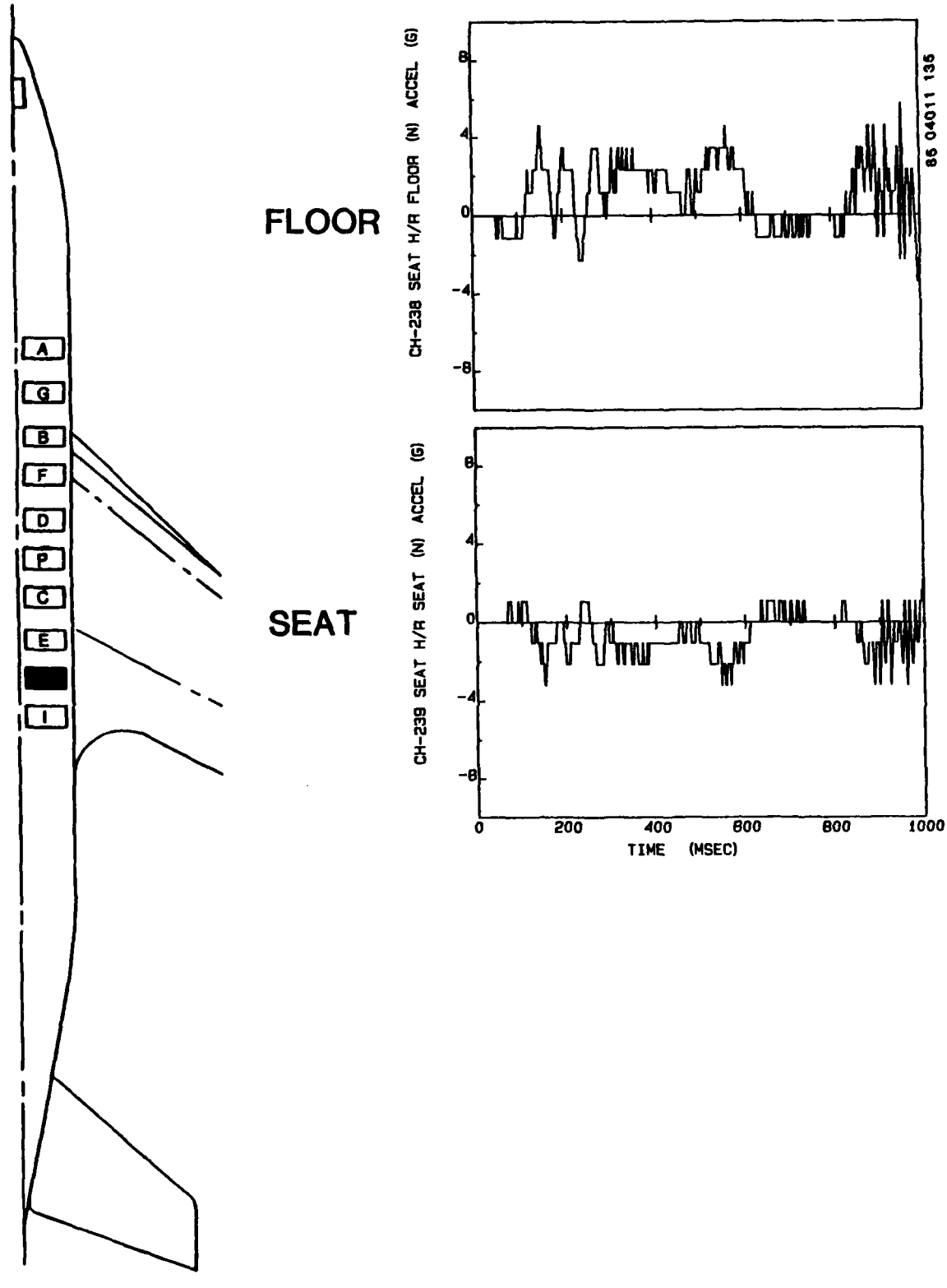

Figure A-17. Seat H/R.

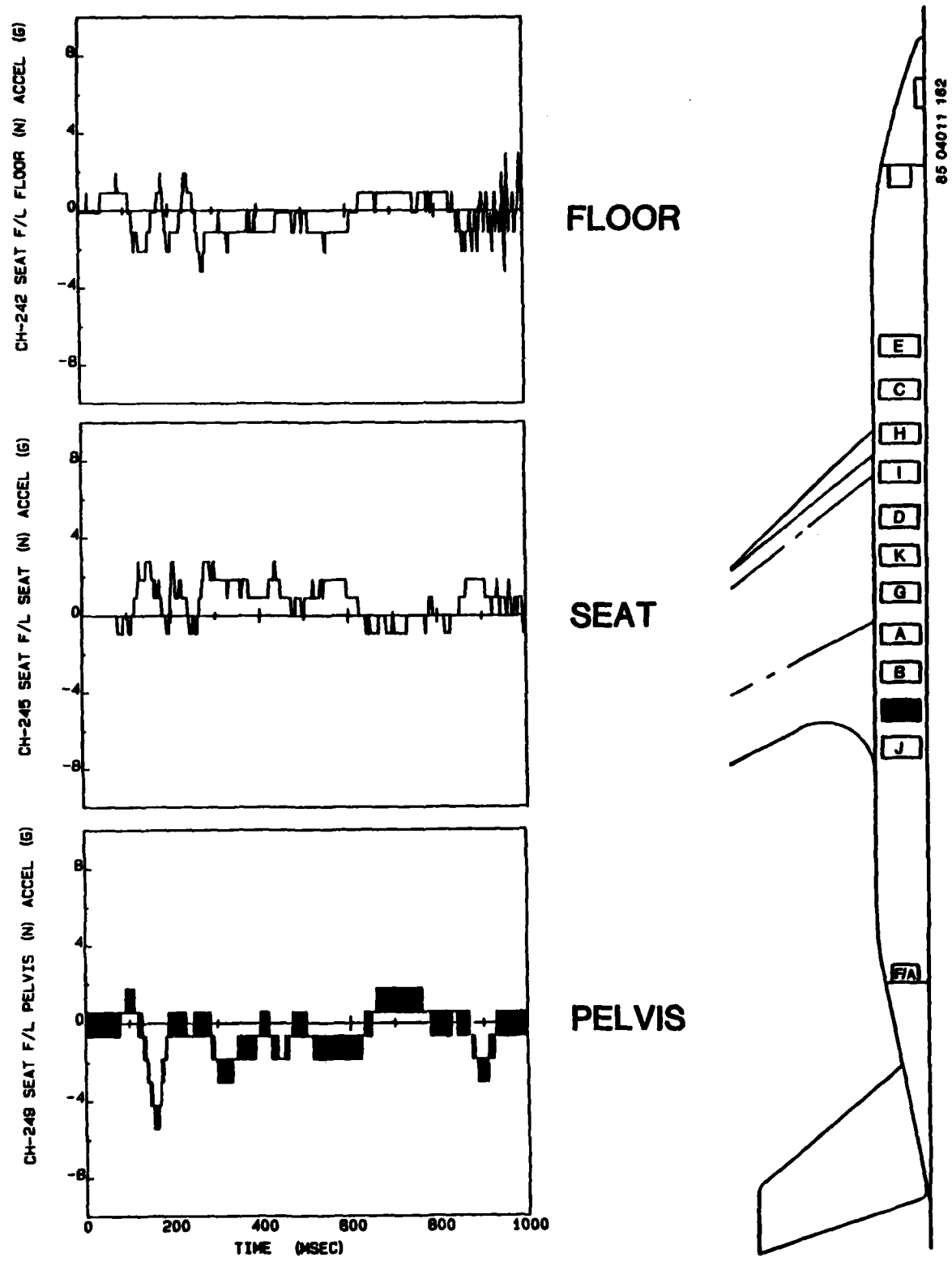

Figure A-18. Seat F/L.

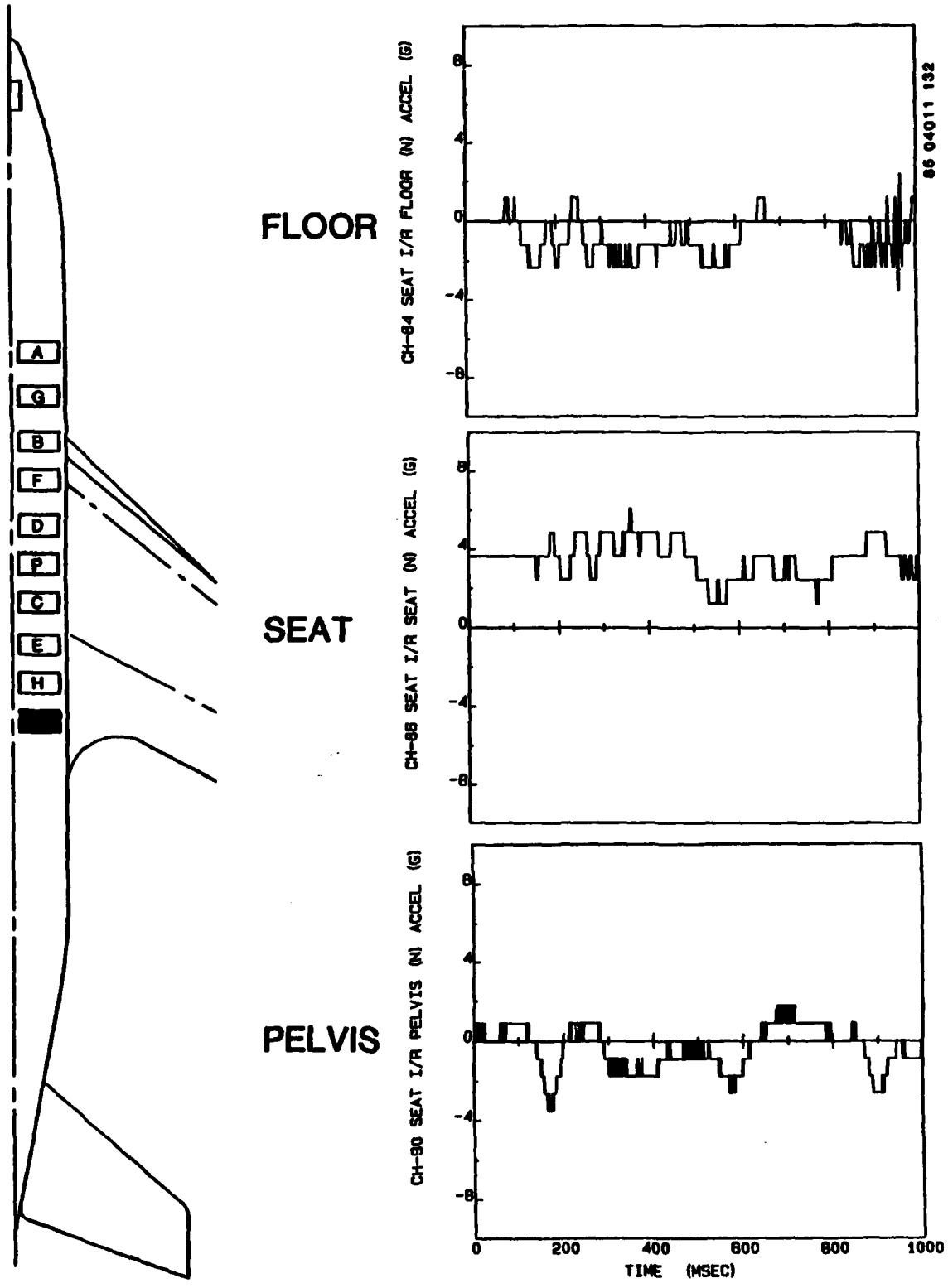

Figure A-19. Seat I/R.

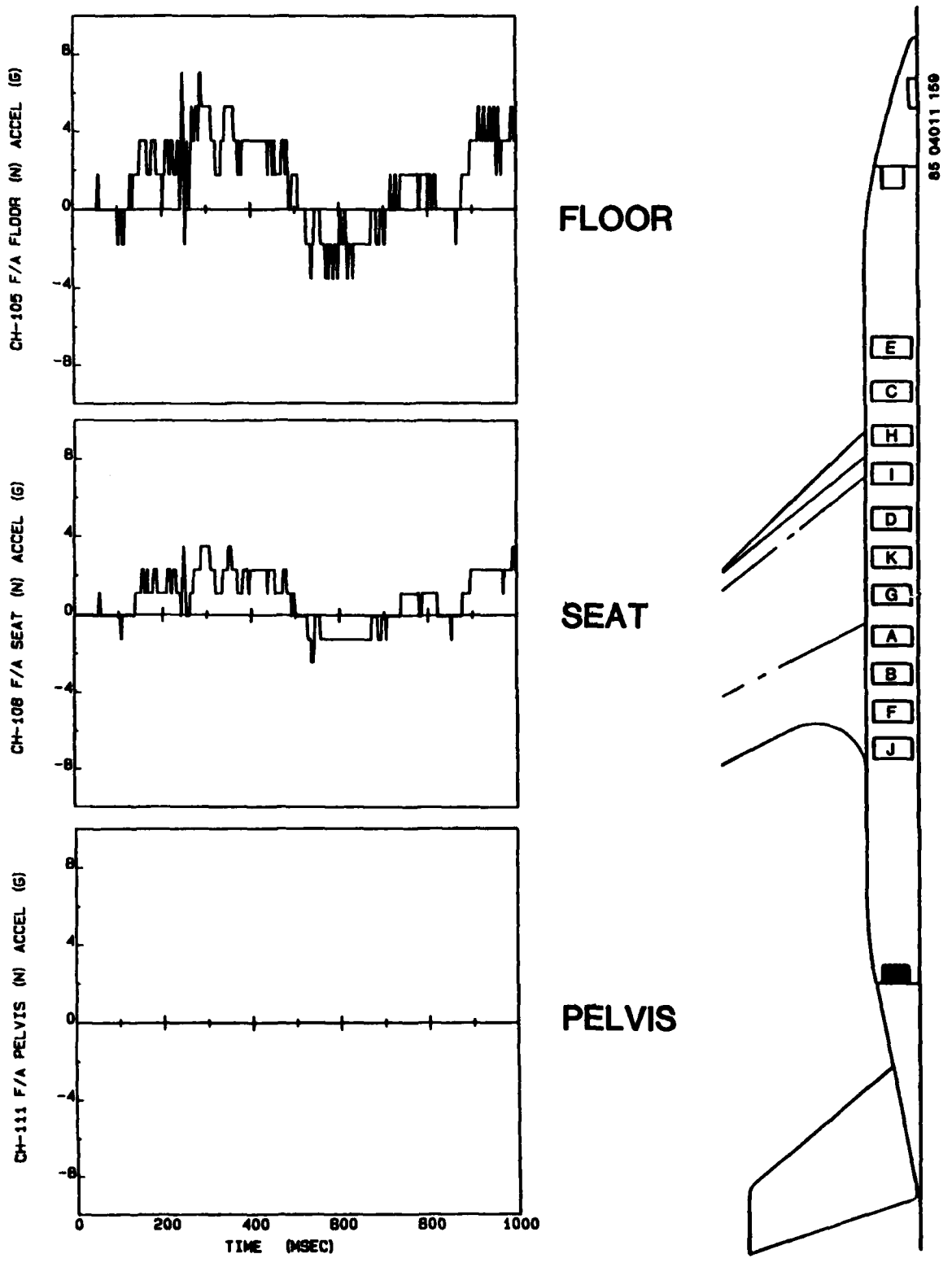

Figure A-20. Seat F/A.

APPENDIX B

FLOOR, SEAT, AND PELVIS LONGITUDINAL ACCELERATIONS

THIS PAGE LEFT INTENTIONALLY BLANK.

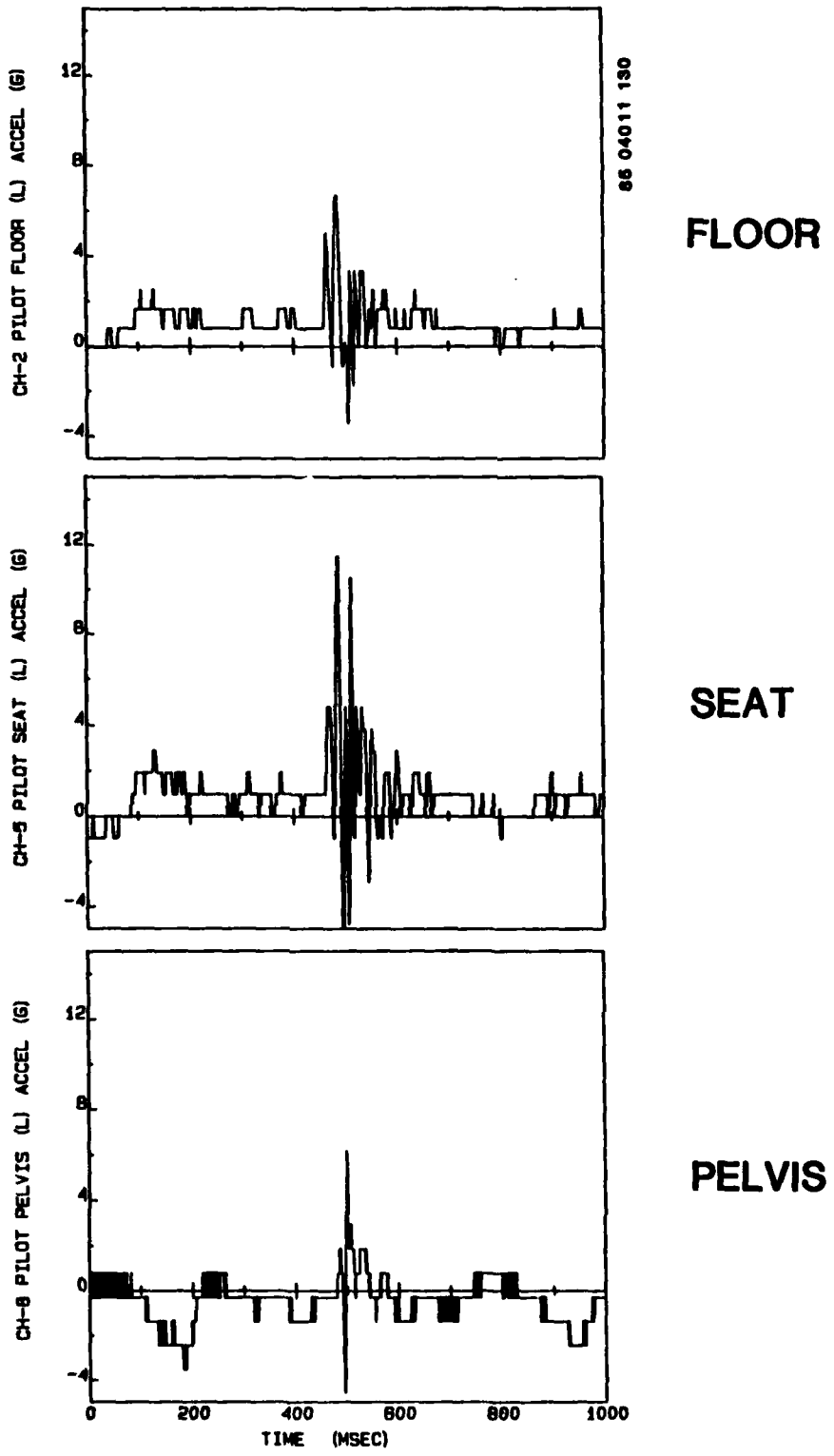

Figure B-1. Pilot seat.

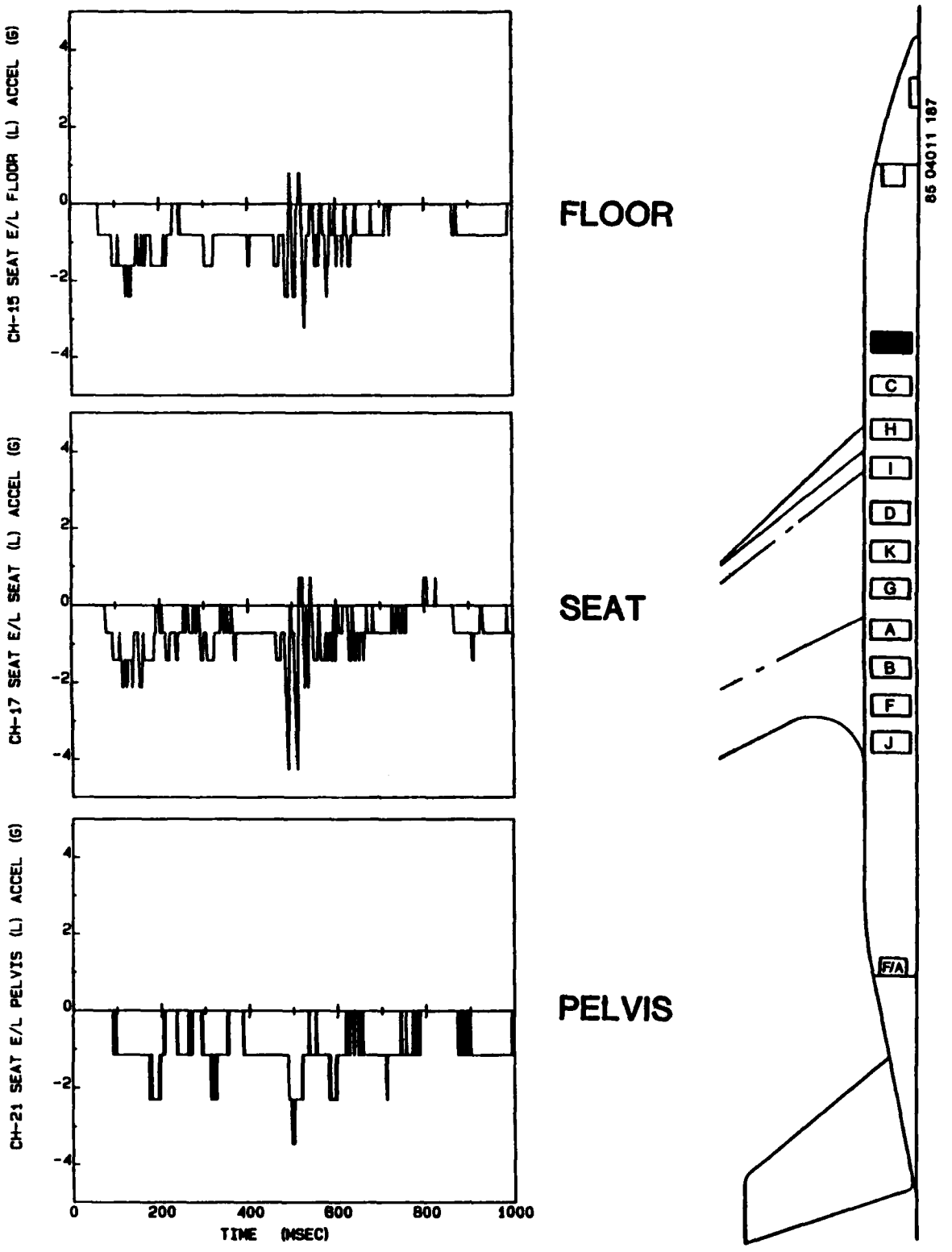

Figure B-2. Seat E/L.

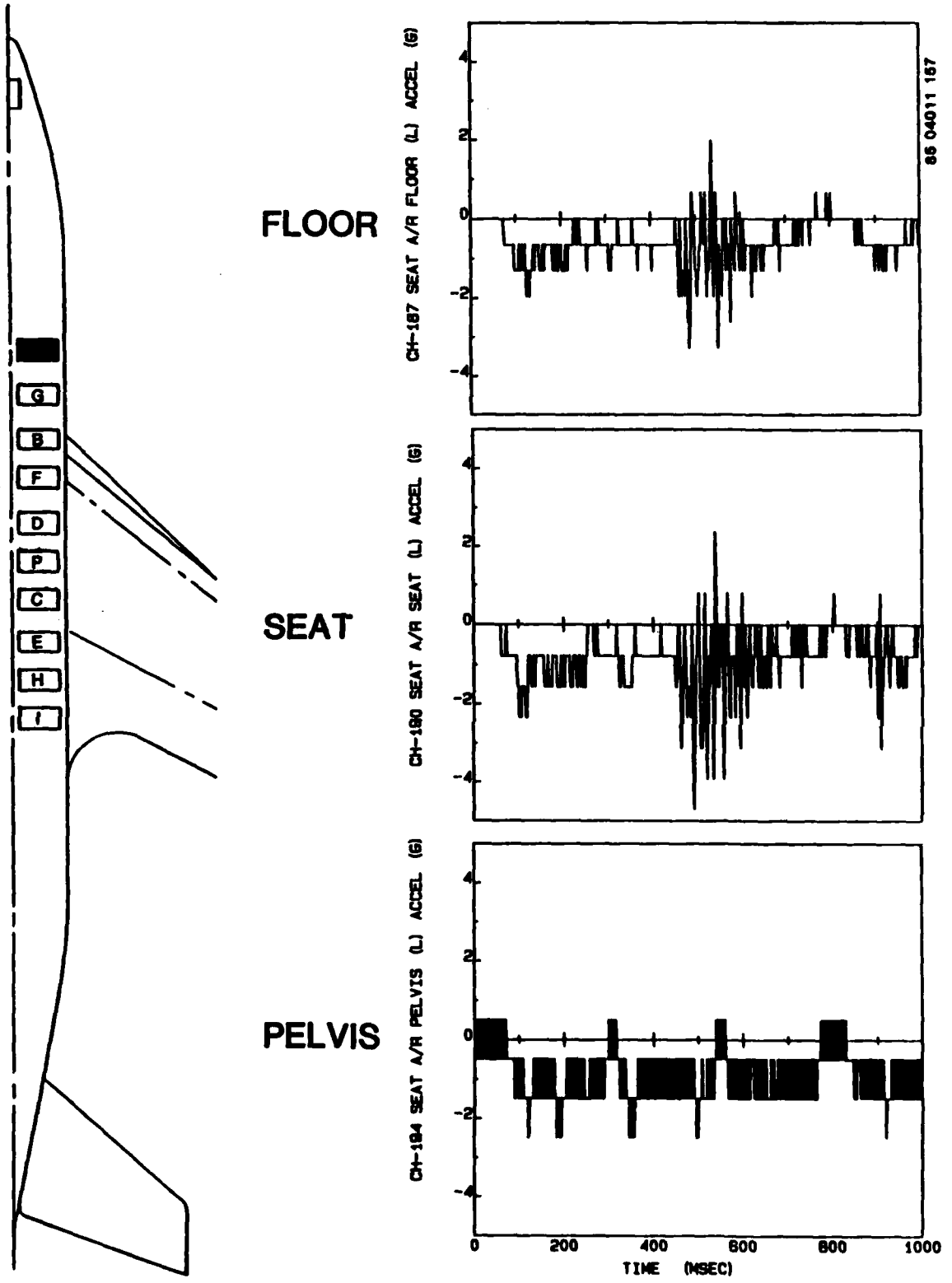

Figure B-3. Seat A/R.

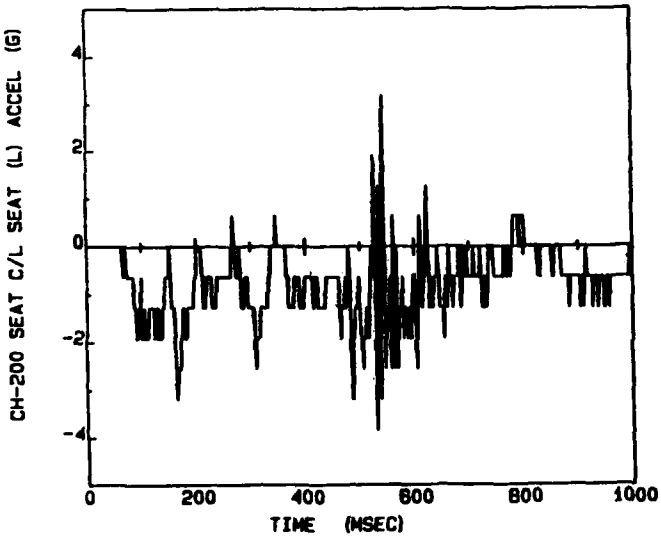

SEAT

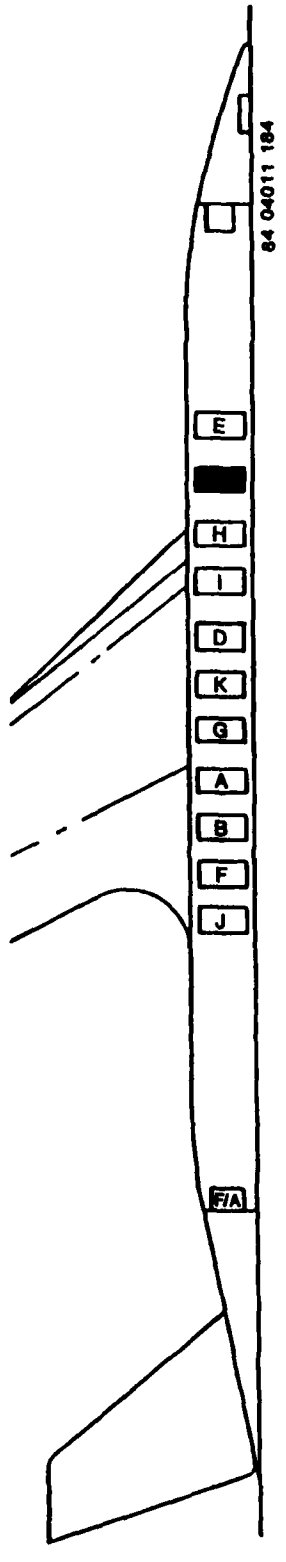

Figure B-4. Seat C/L.

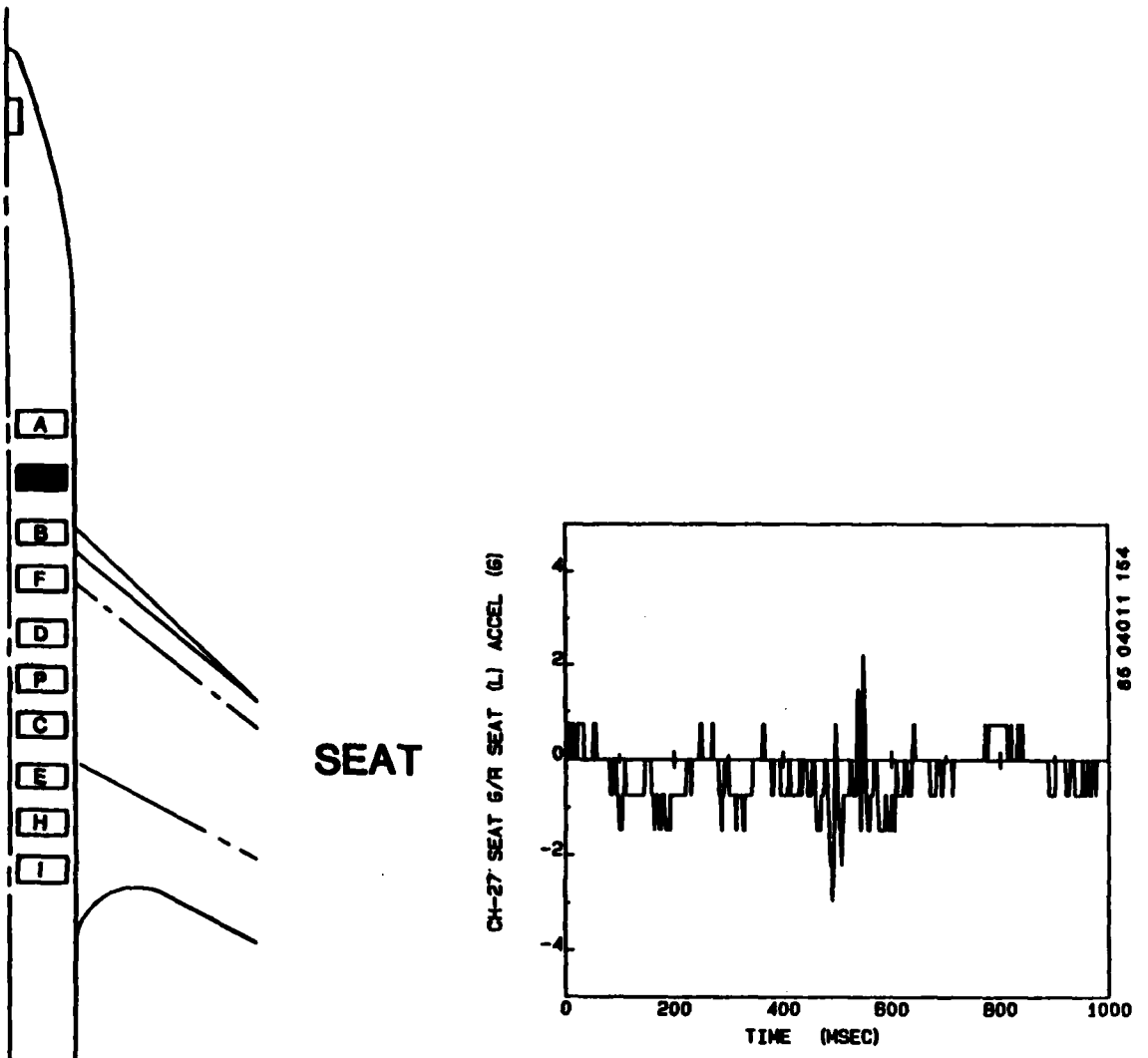

Figure B-5. Seat G/R.

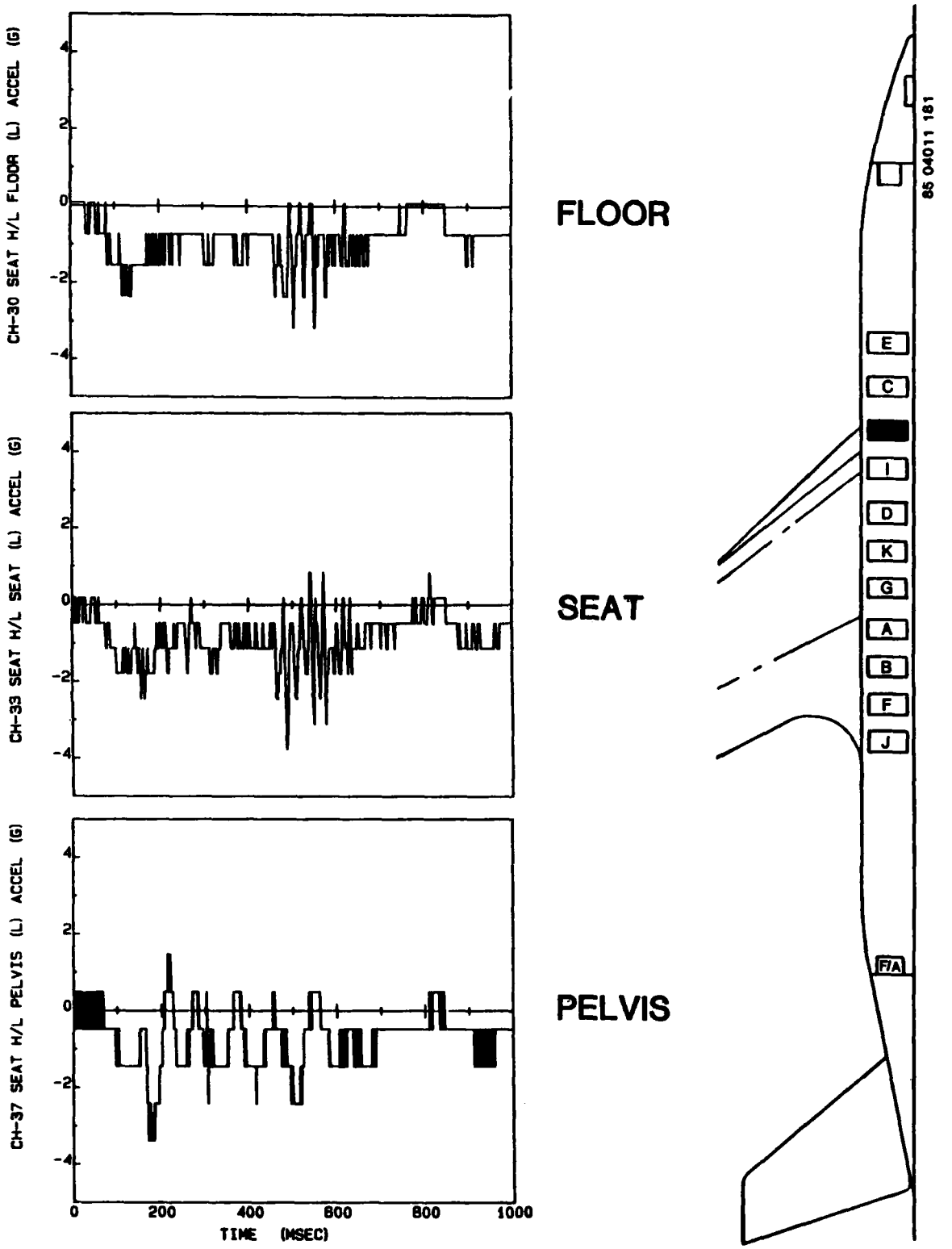

Figure B-6. Seat H/L.

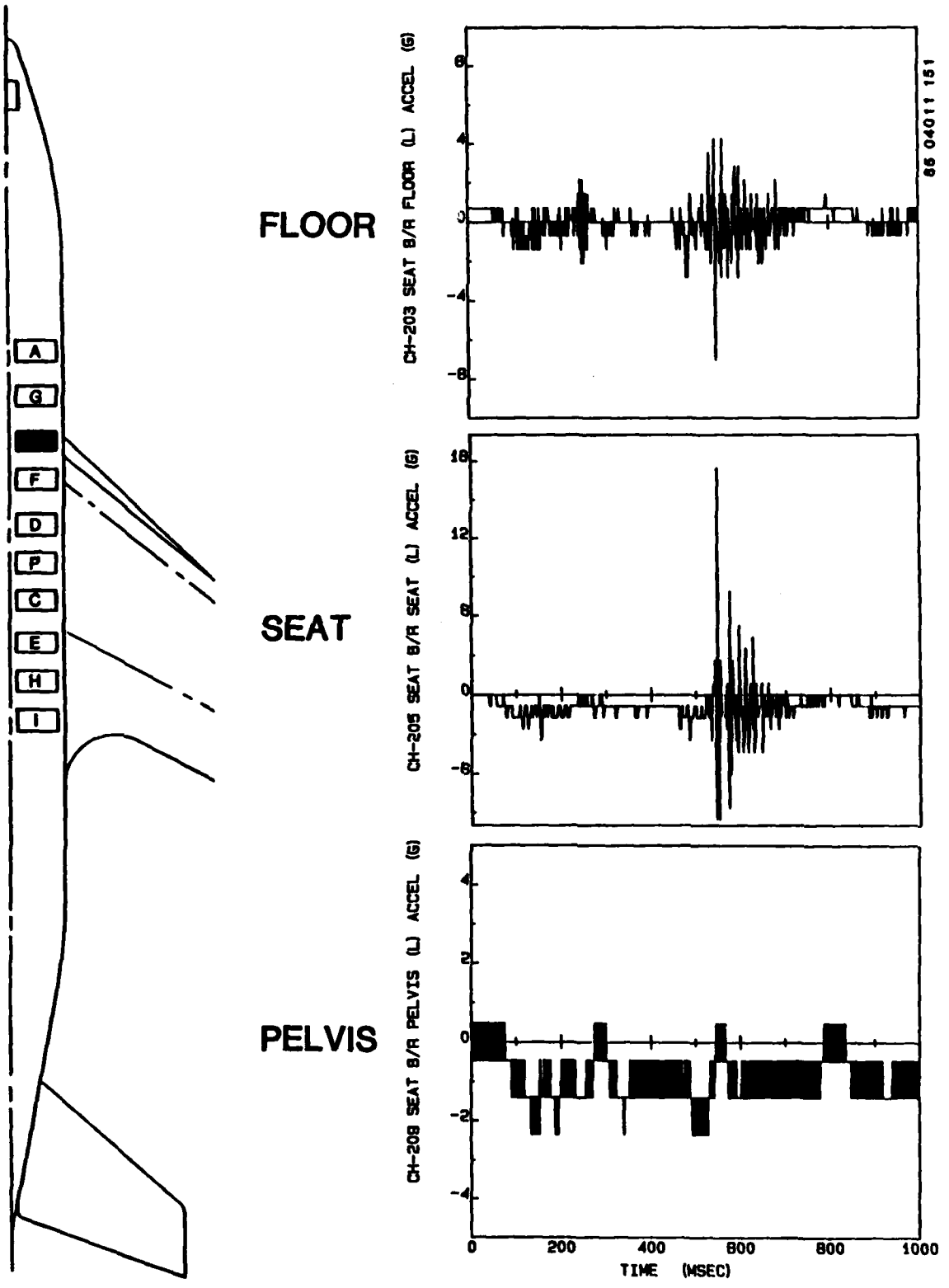

Figure B-7. Seat B/R.

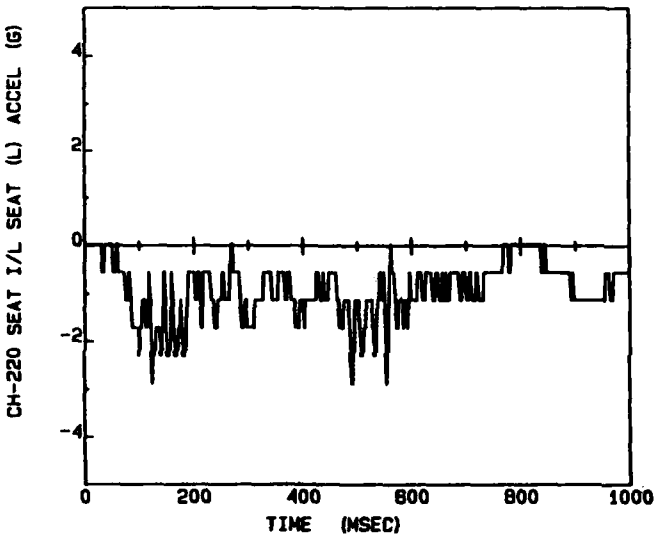

SEAT

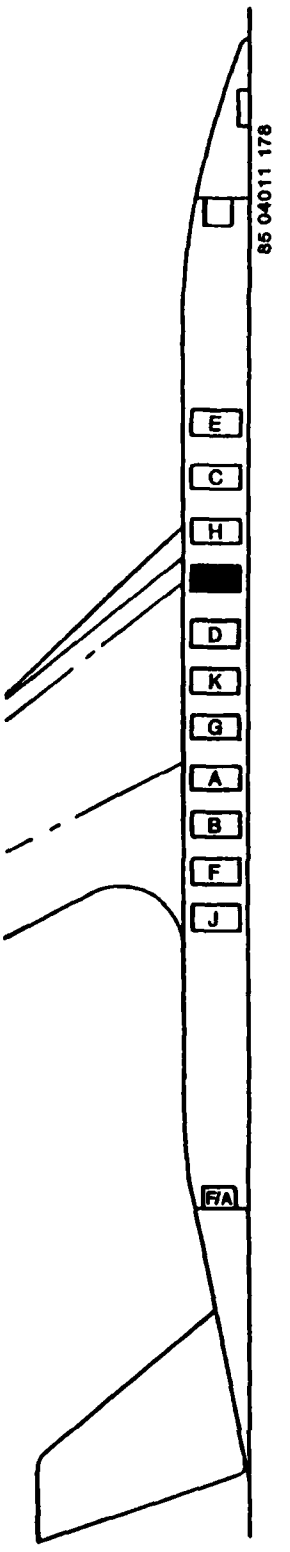

Figure B-8. Seat I/L.

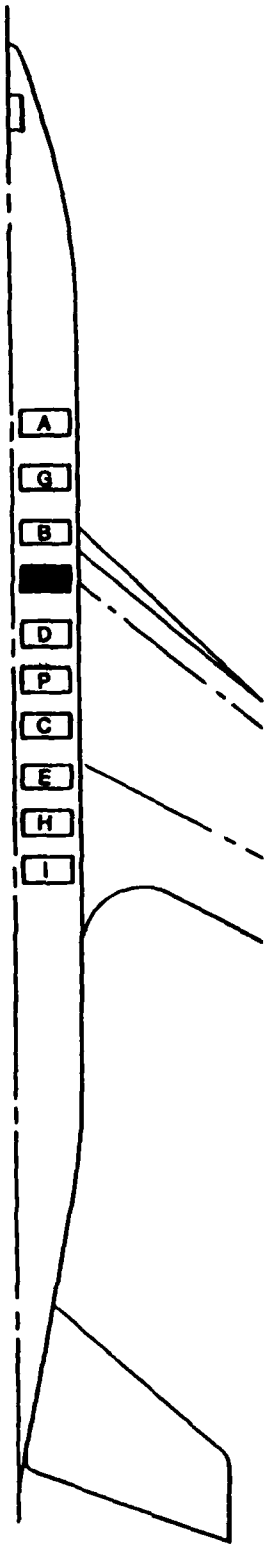

SEAT

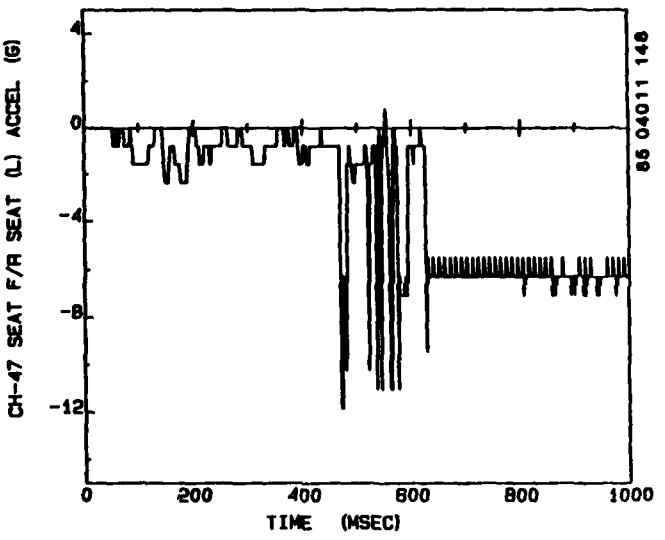

Figure B-9. Seat F/R.

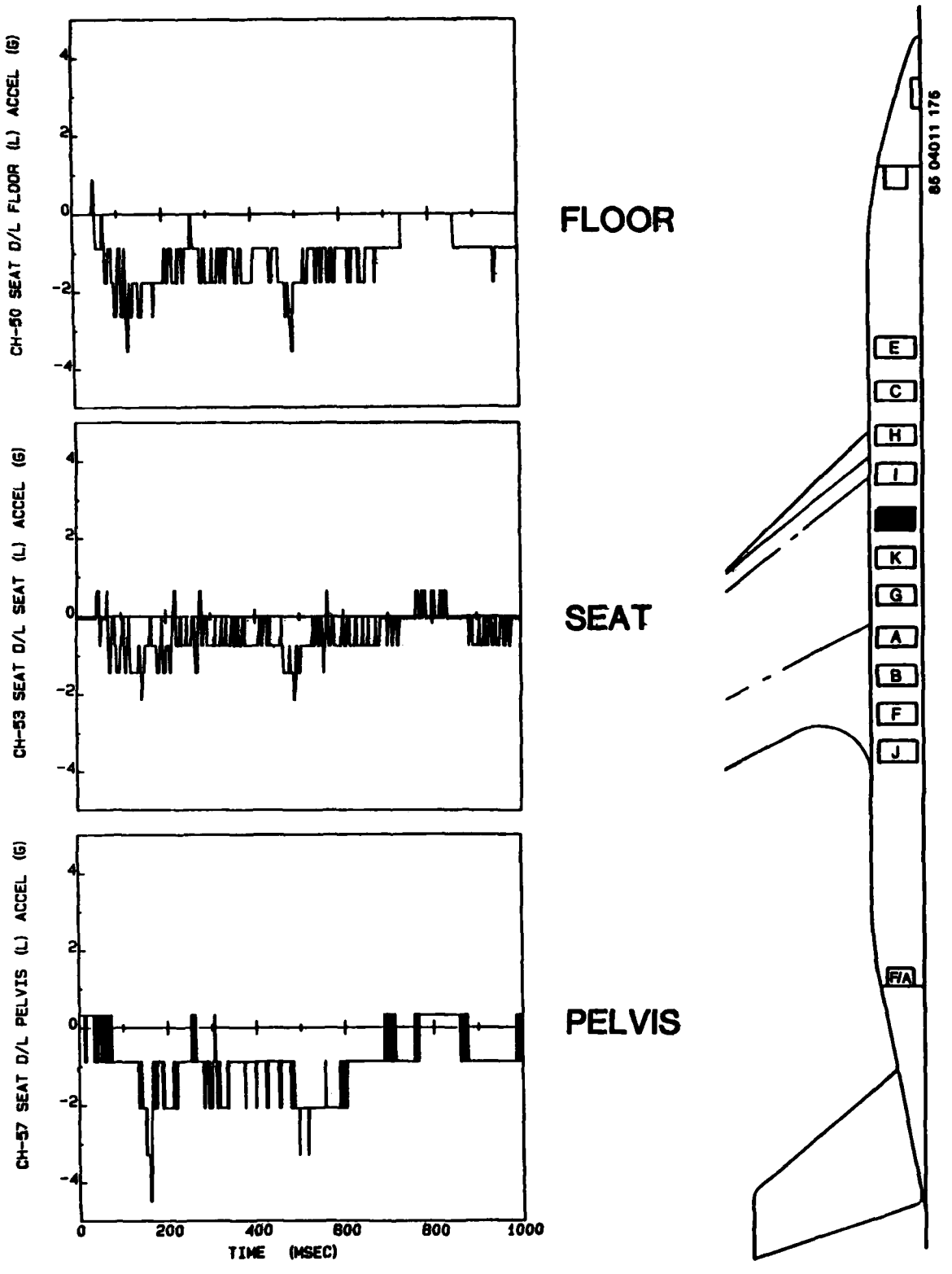

Figure B-10. Seat D/L.

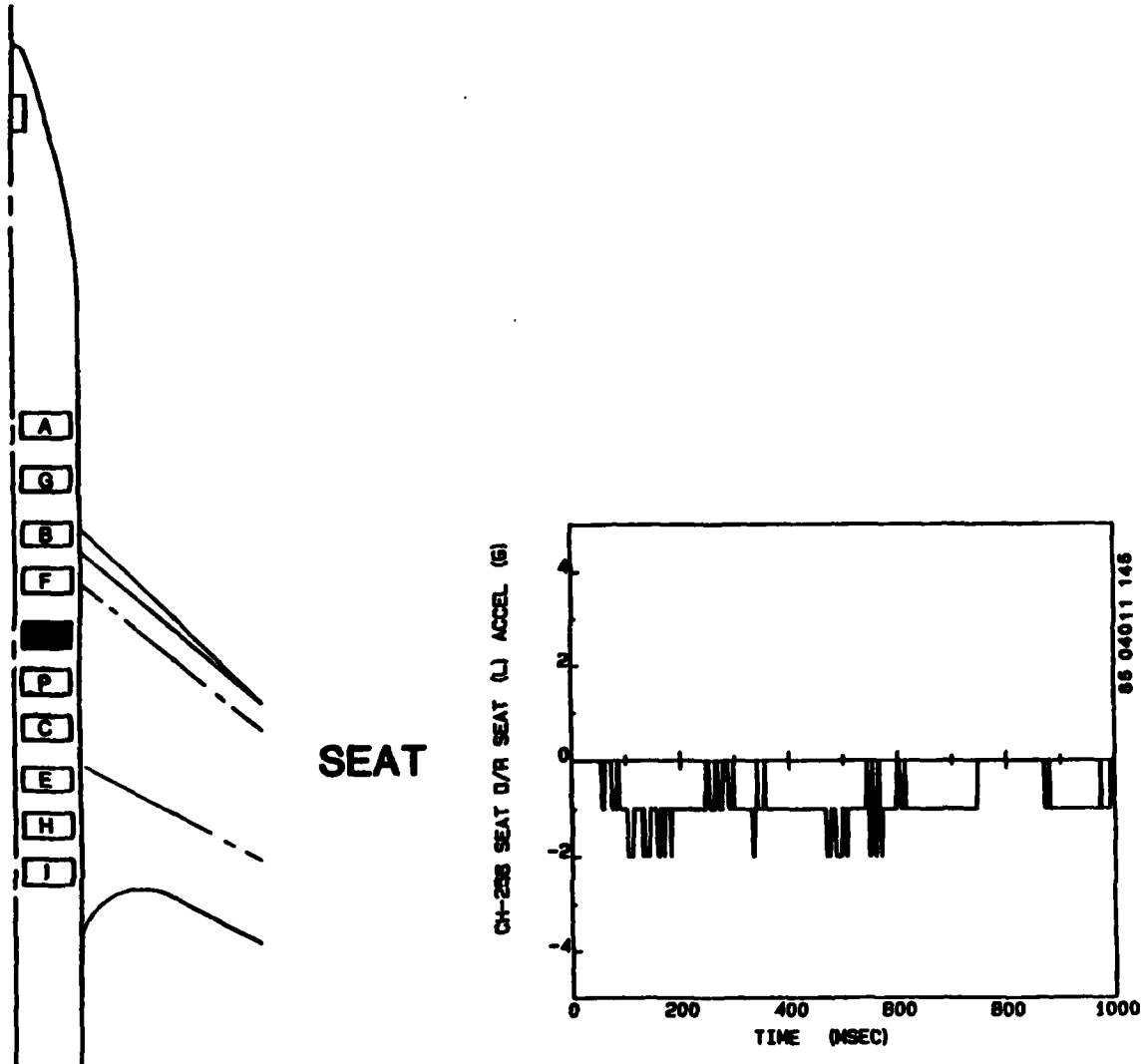

Figure B-11. Seat D/R.

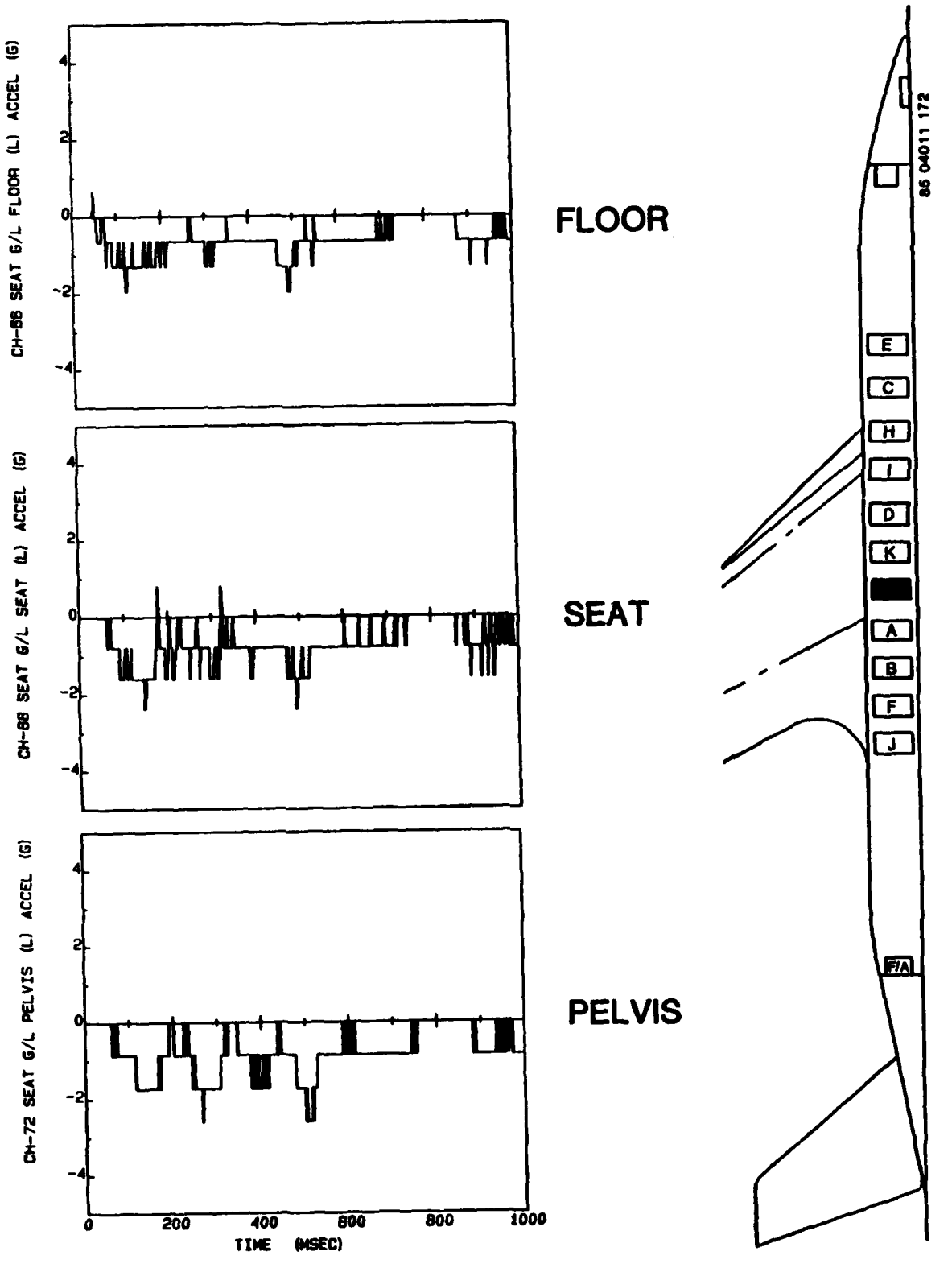

Figure B-12. Seat G/L.

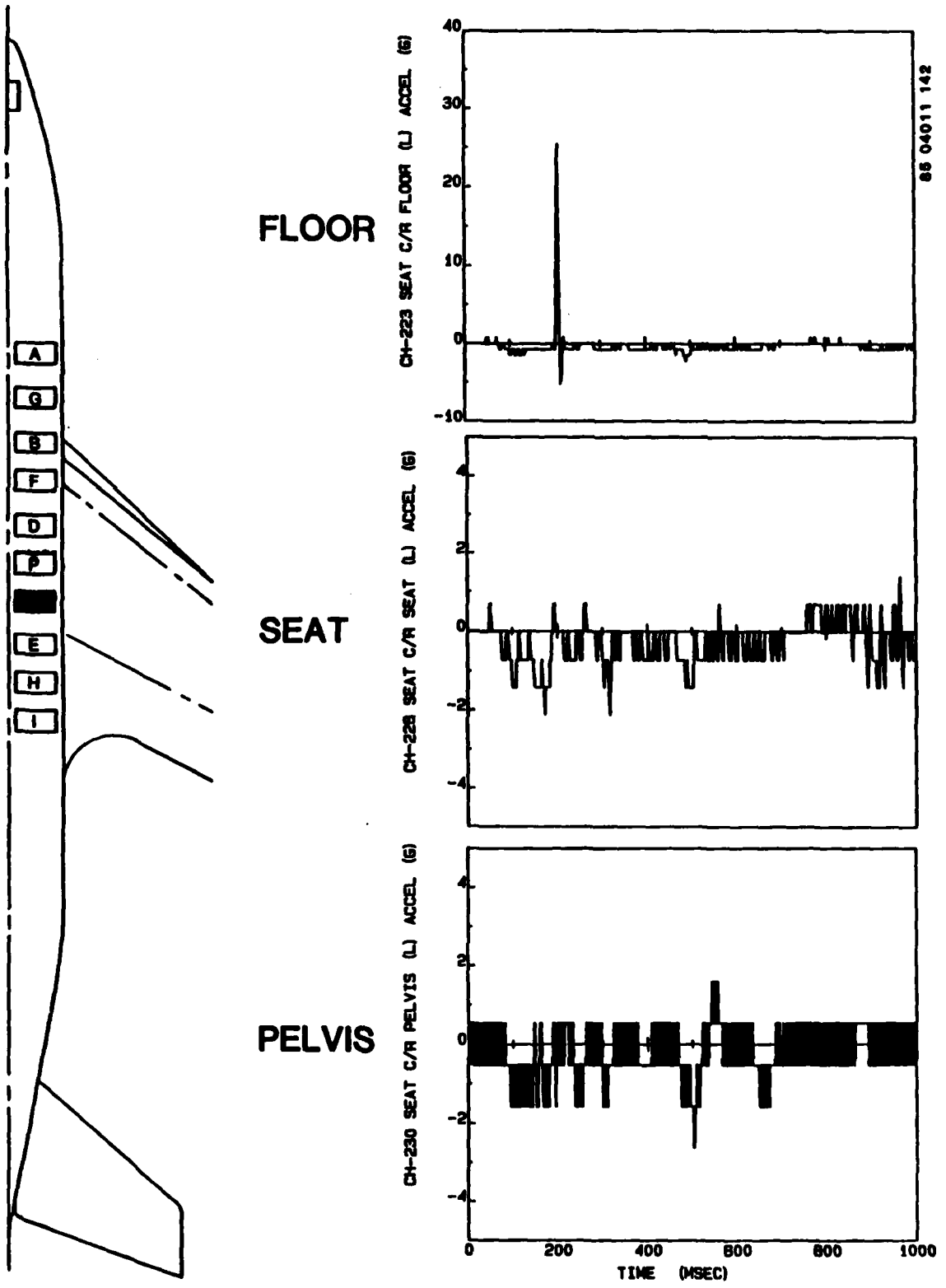

Figure B-13. Seat C/R.

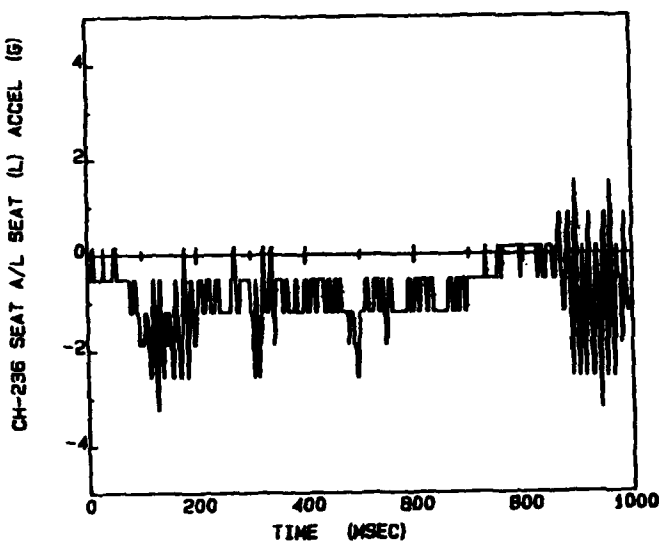

SEAT

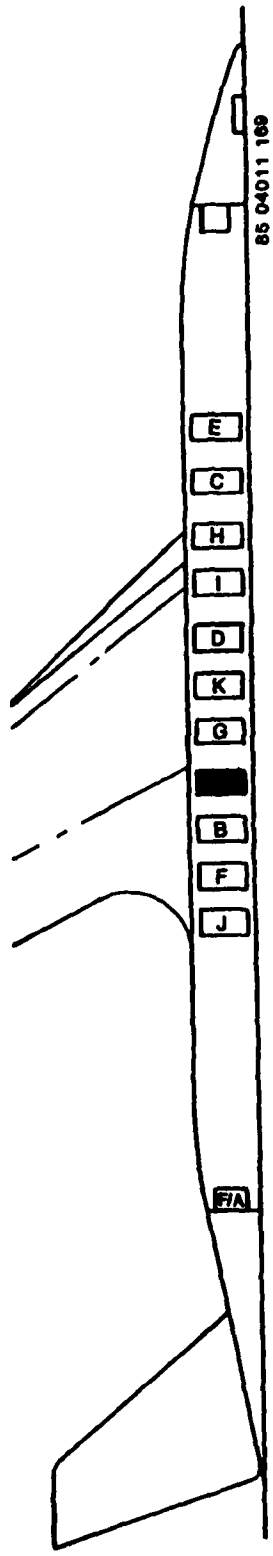

Figure B-14. Seat A/L.

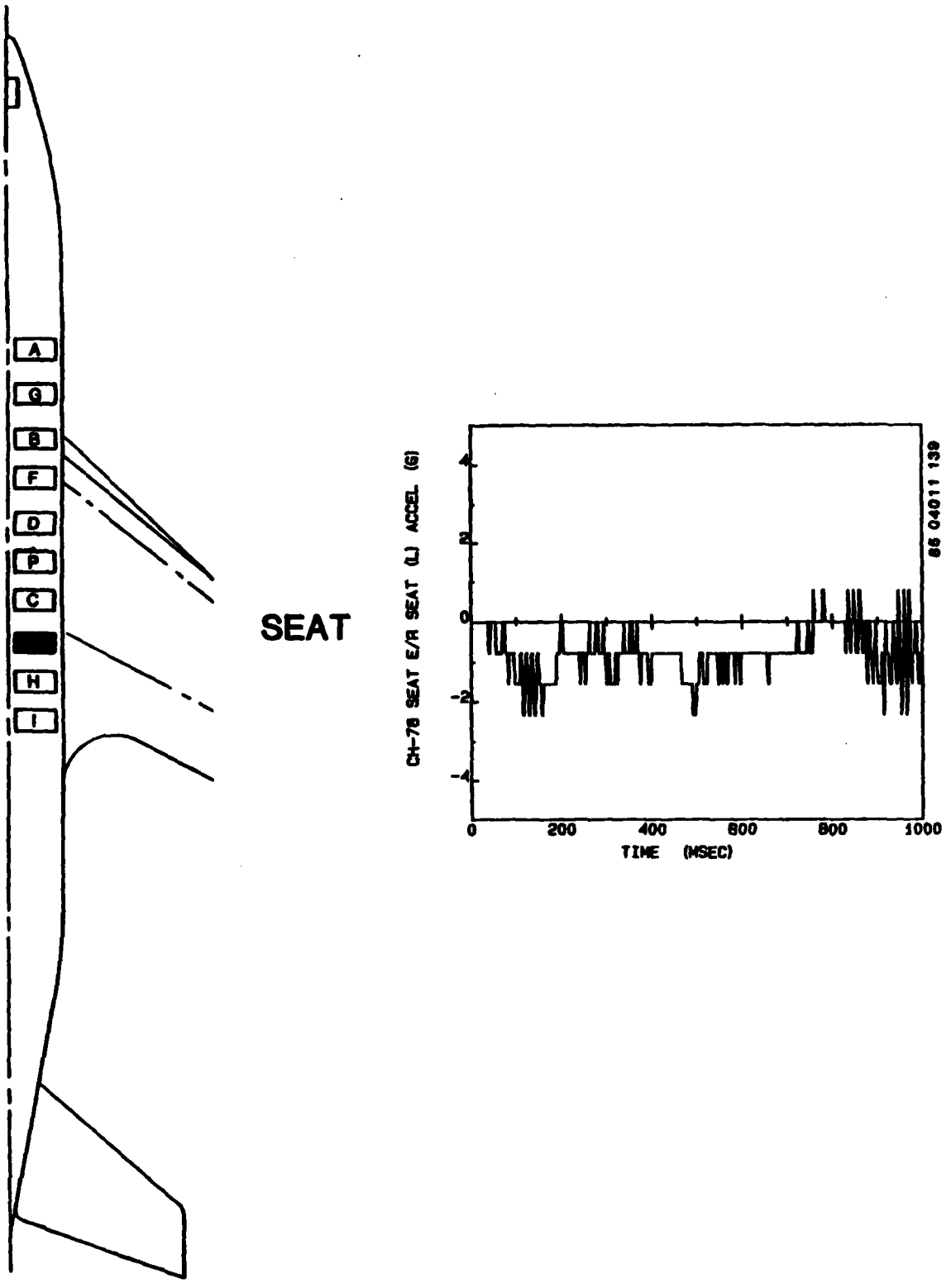

Figure B-15. Seat E/R.

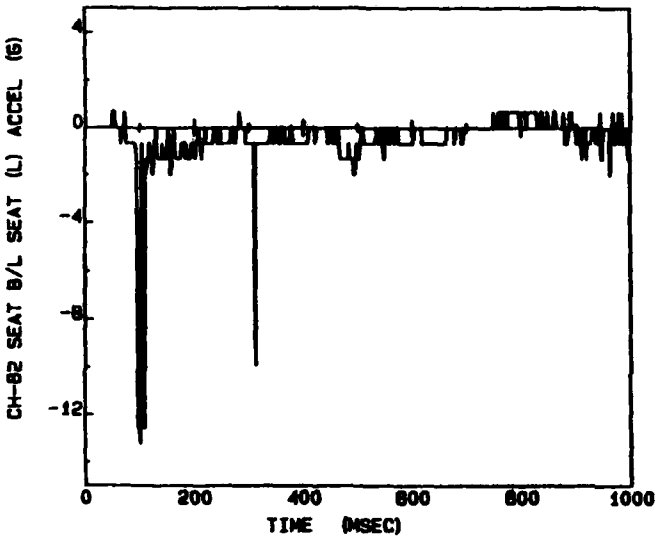

SEAT

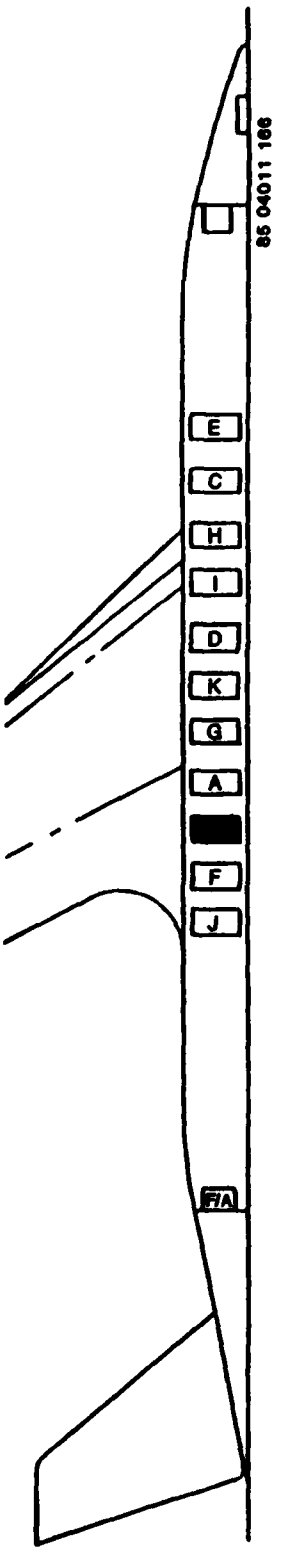

Figure B-16. Seat B/L.

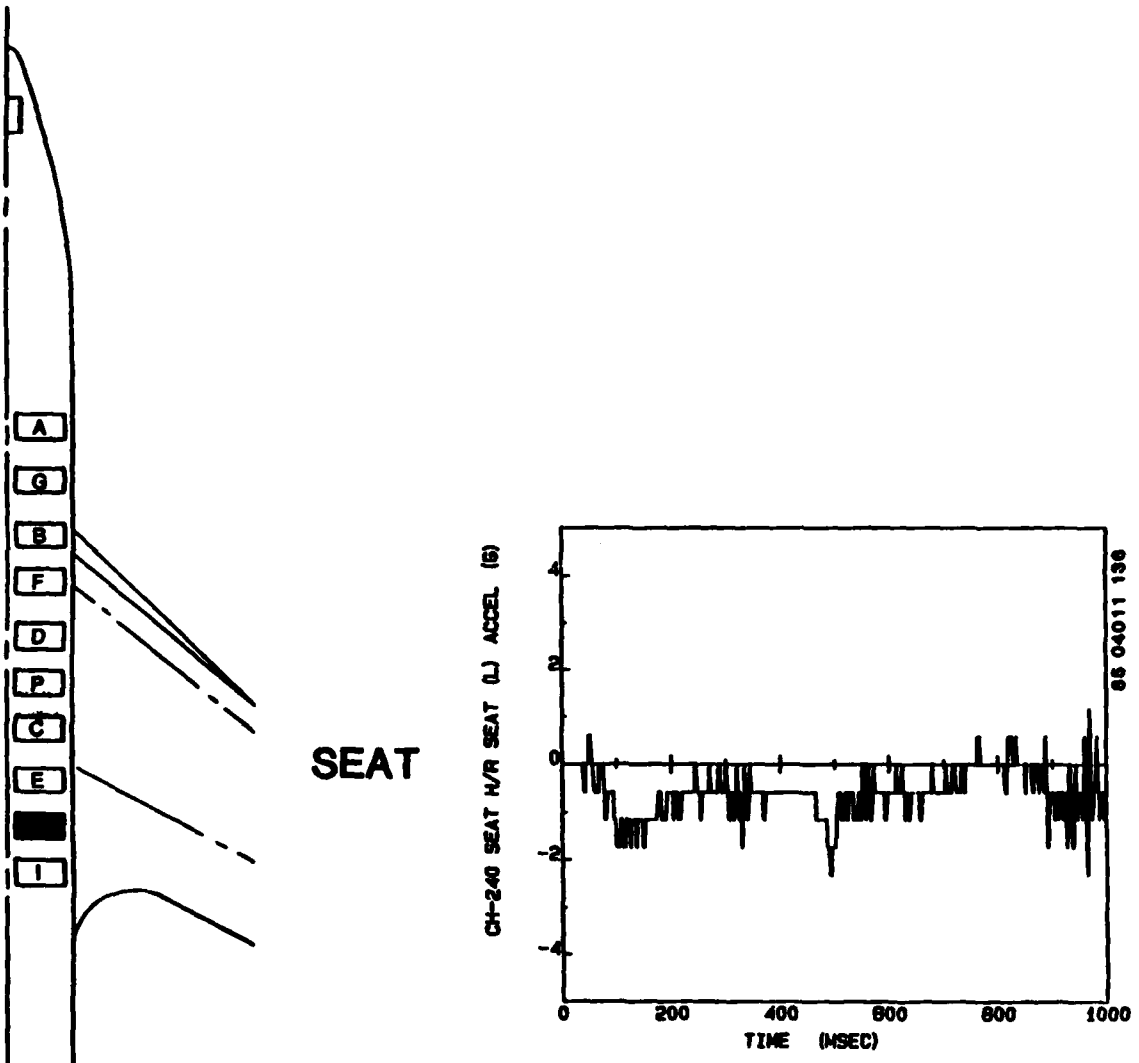

Figure B-17. Seat H/R.

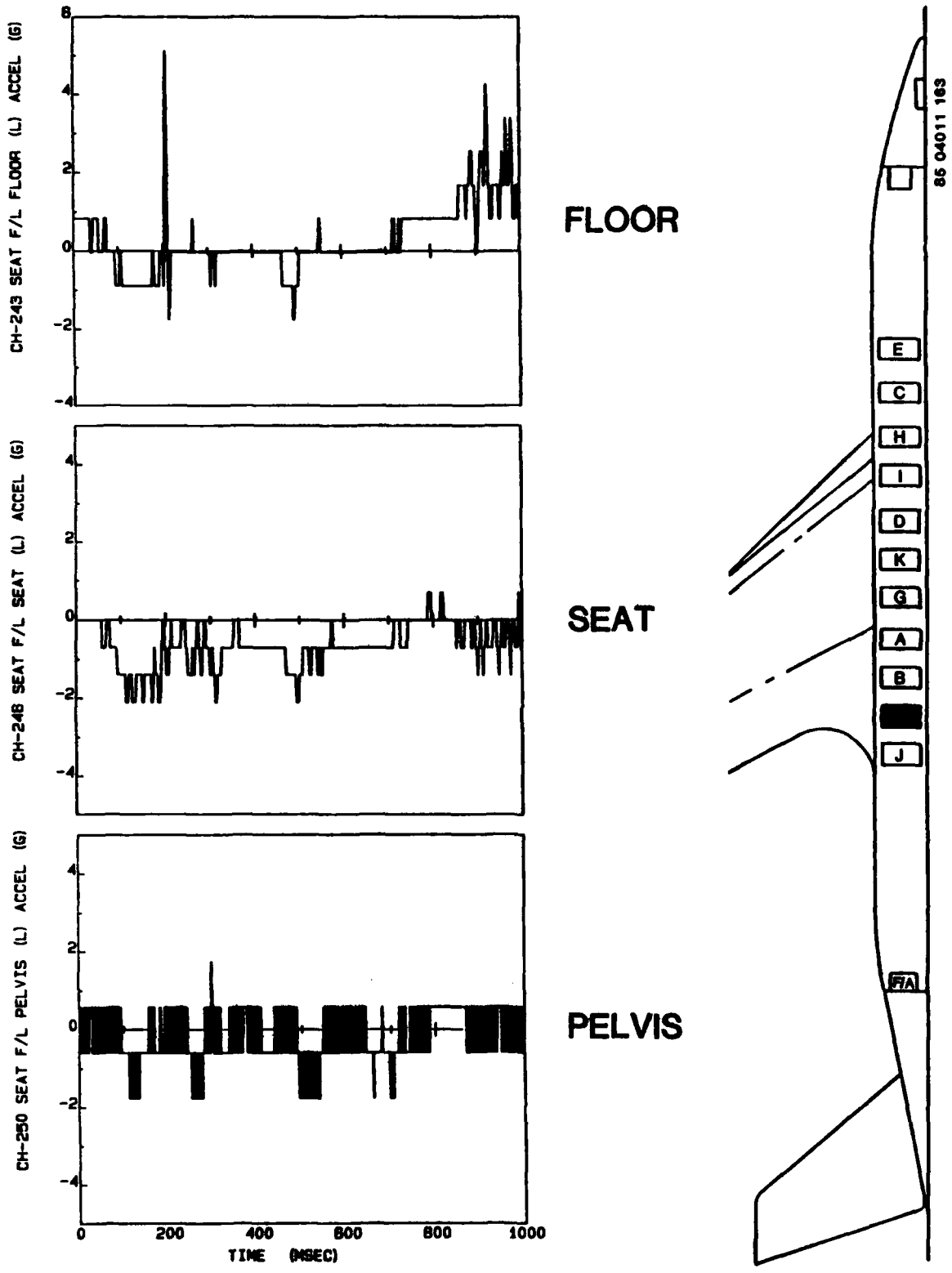

Figure B-18. Seat F/L.

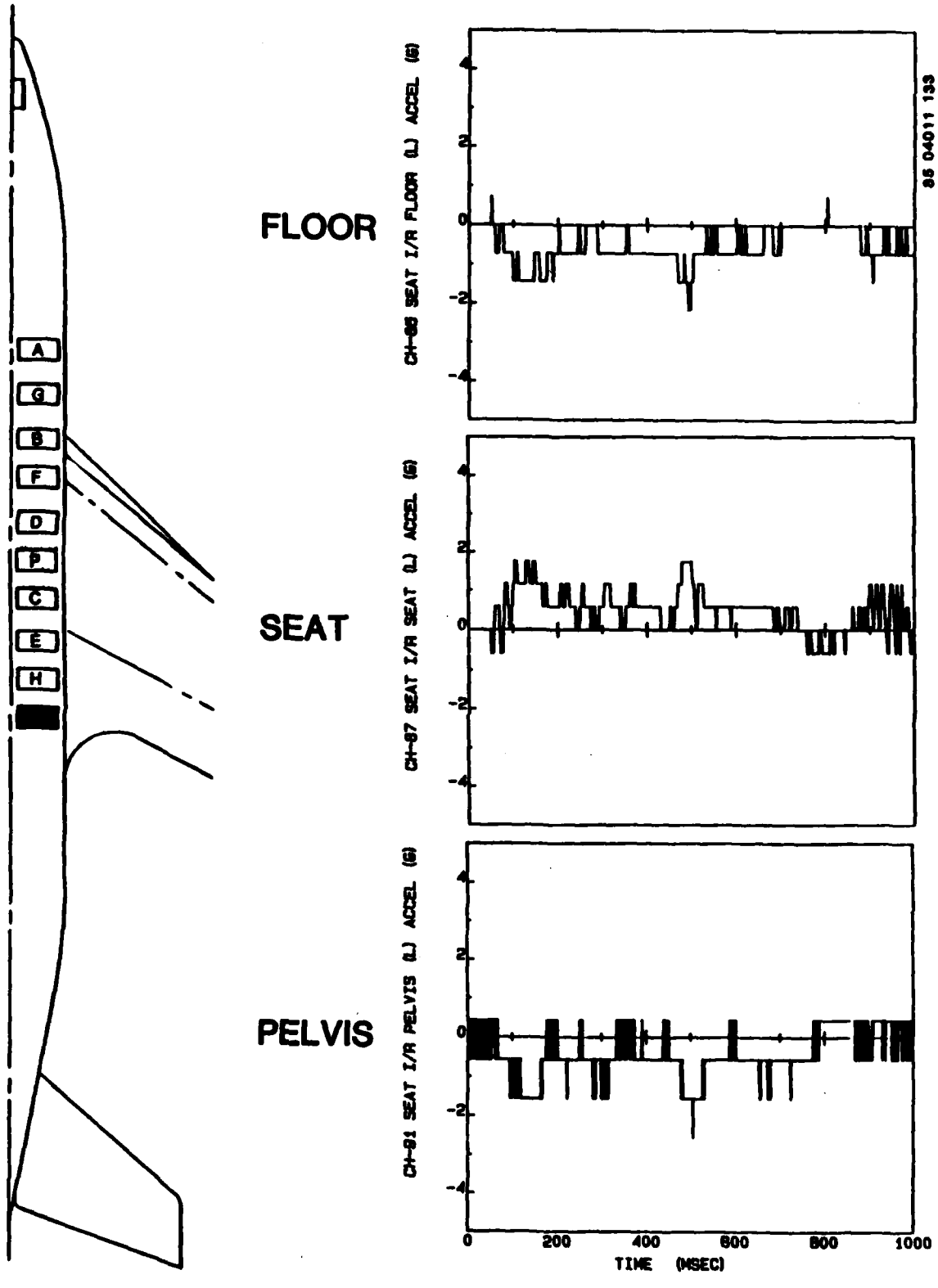

Figure B-19. Seat I/R.

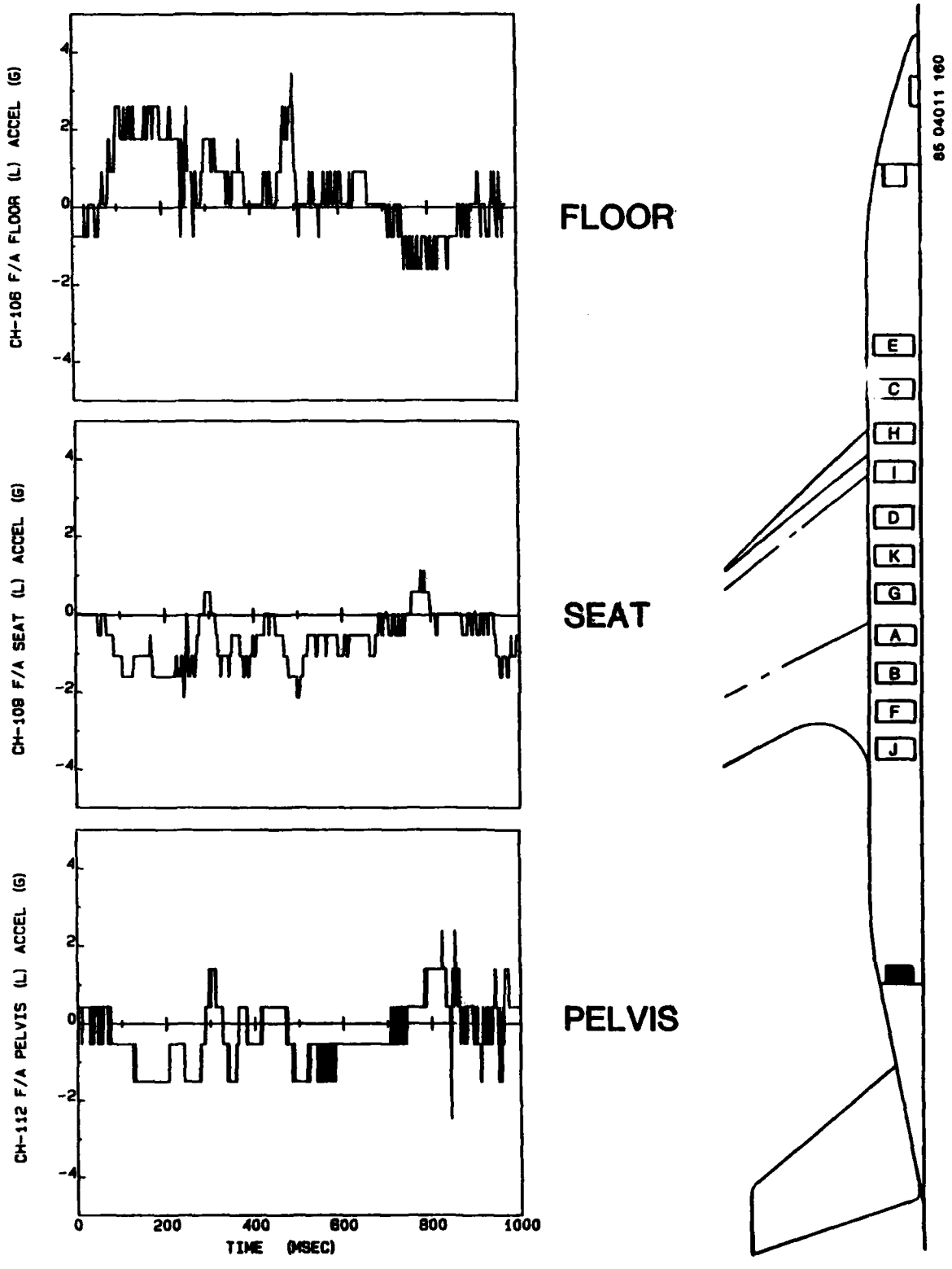

Figure B-20. Seat F/A.

THIS PAGE LEFT INTENTIONALLY BLANK.

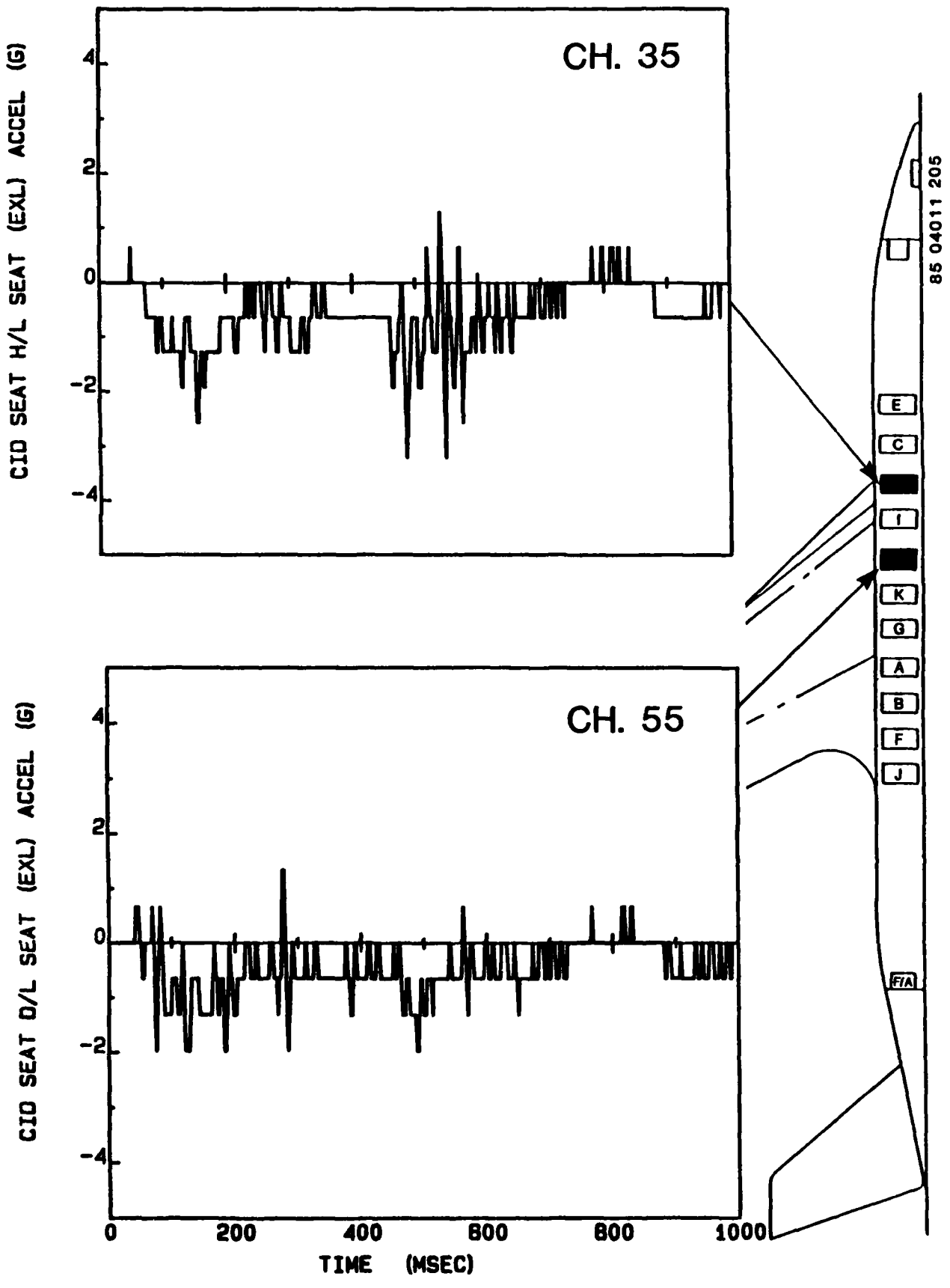

Figure B-21. Outboard seat accelerometers.

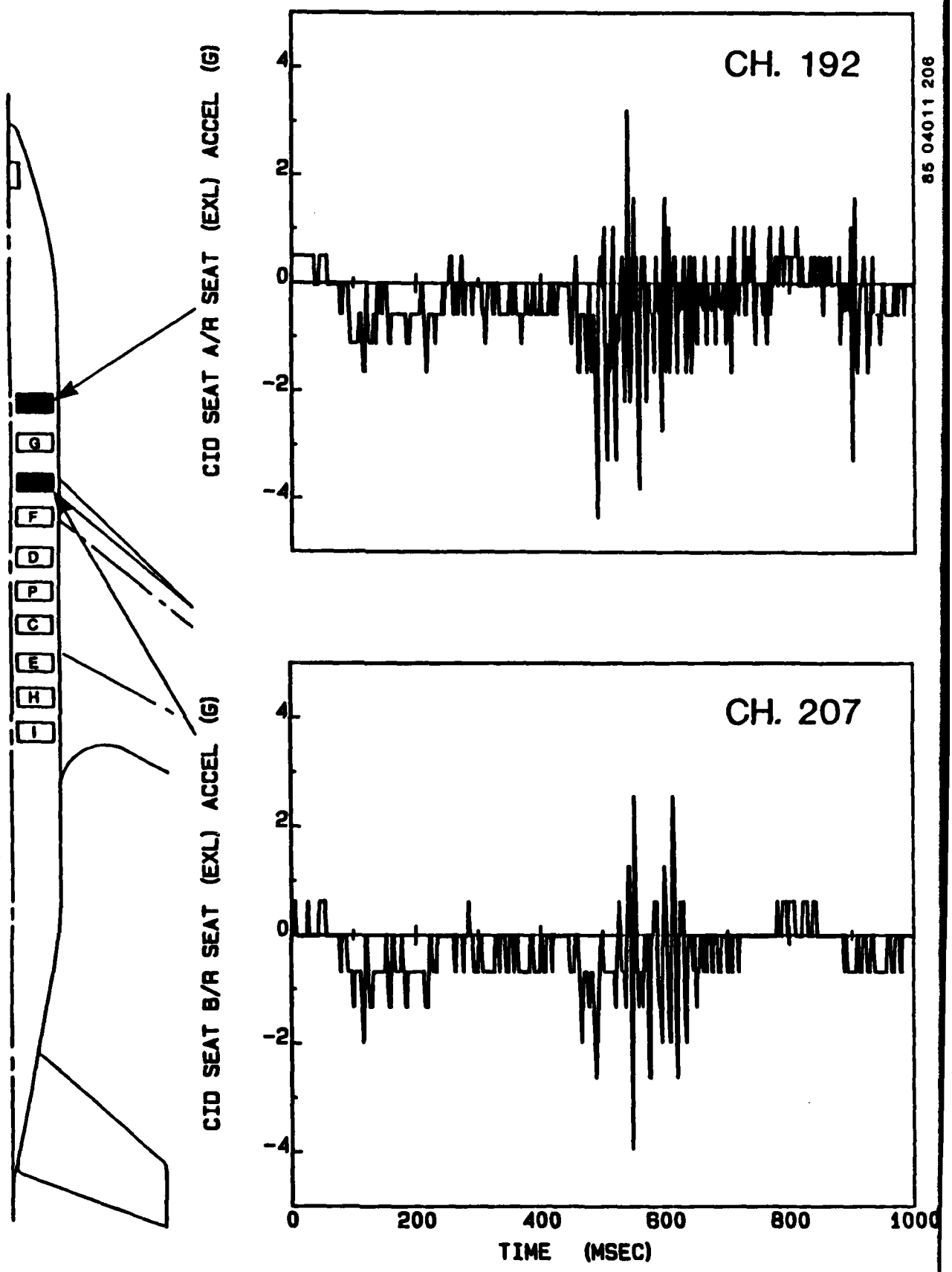

Figure B-22. Outboard seat accelerometers.

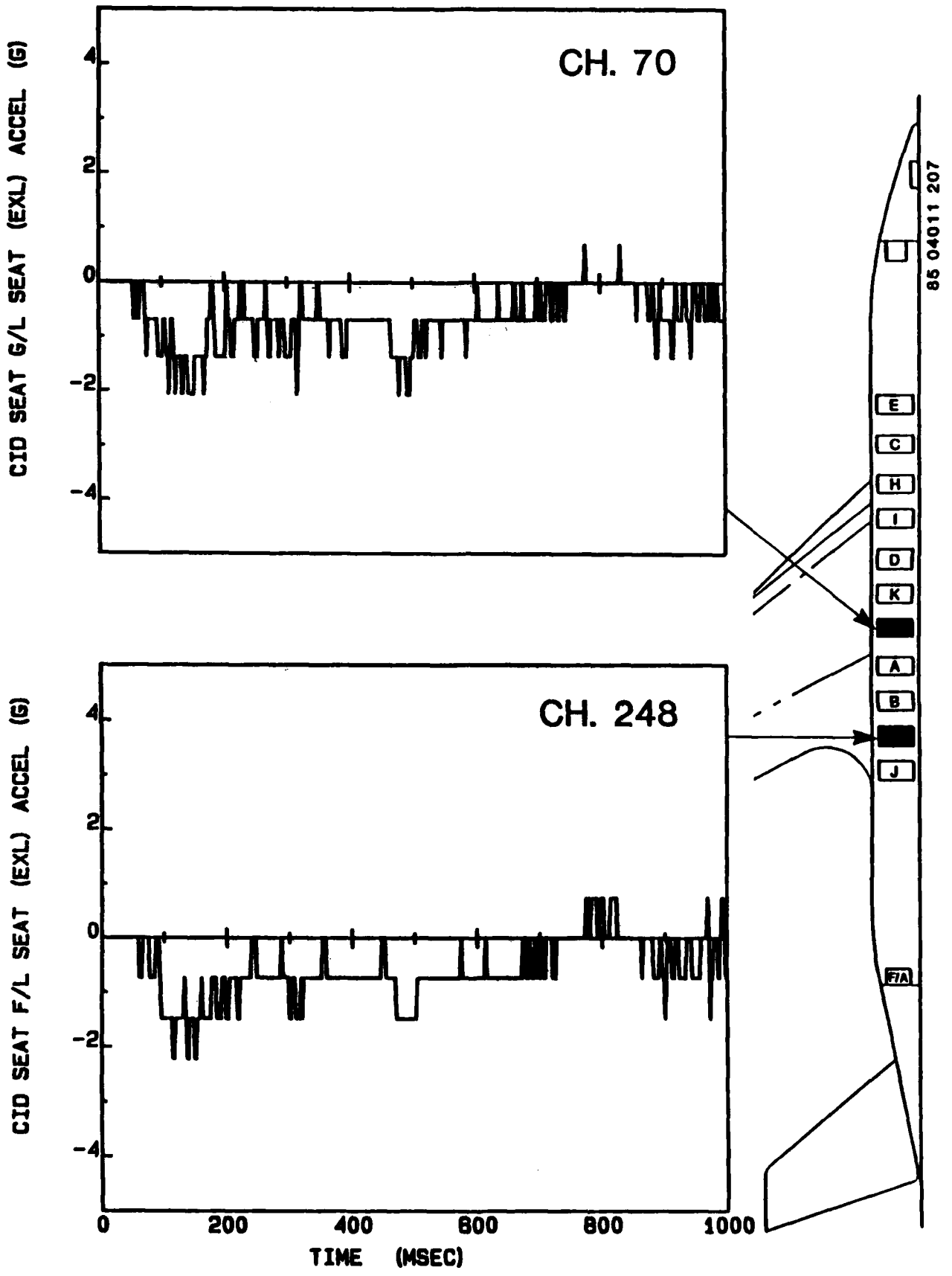

Figure B-23. Outboard seat accelerometers.

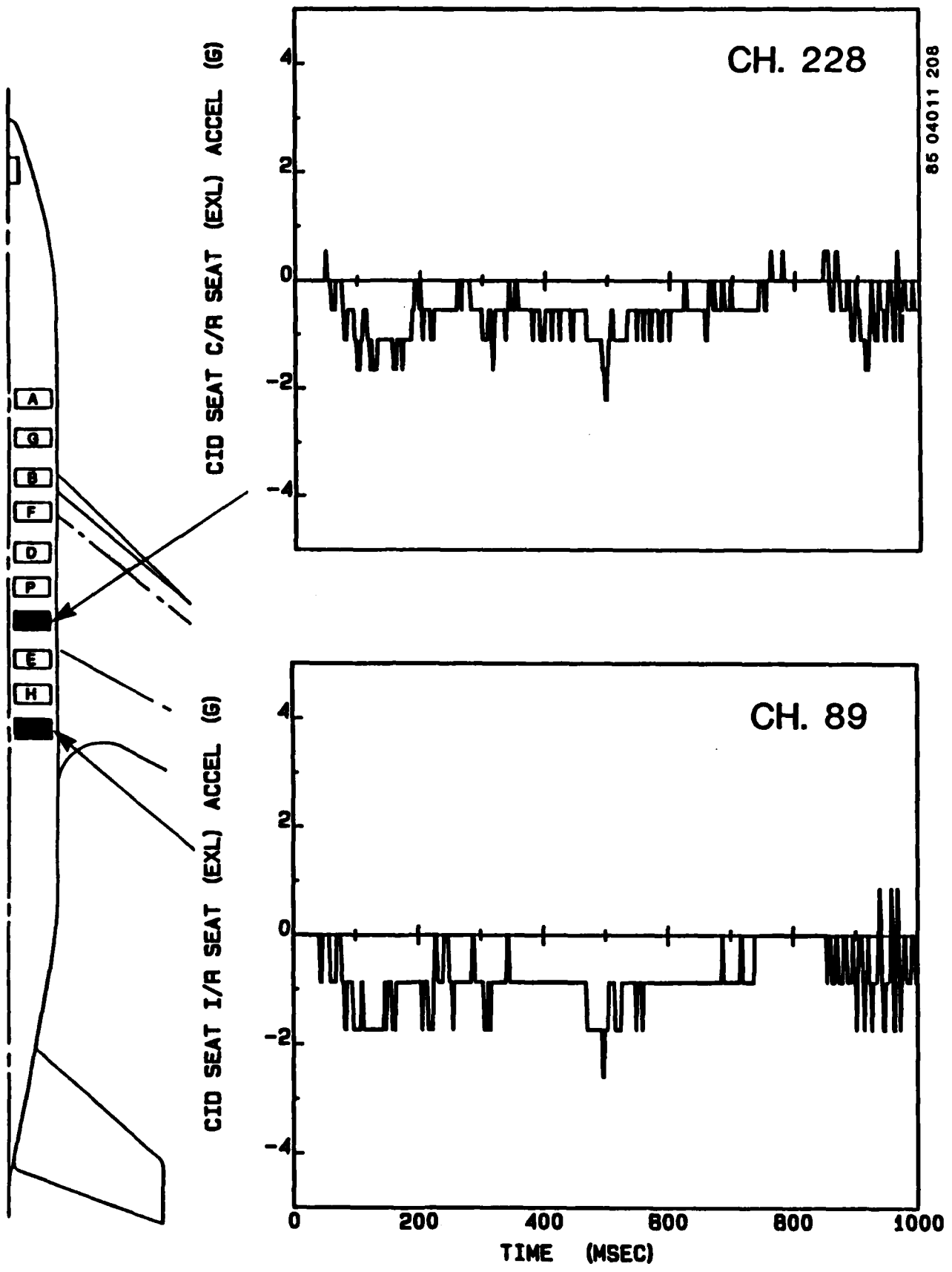

Figure B-24. Outboard seat accelerometers.

THIS PAGE LEFT INTENTIONALLY BLANK.

APPENDIX C

FLOOR, SEAT, AND PELVIS LATERAL ACCELERATIONS

THIS PAGE LEFT INTENTIONALLY BLANK.

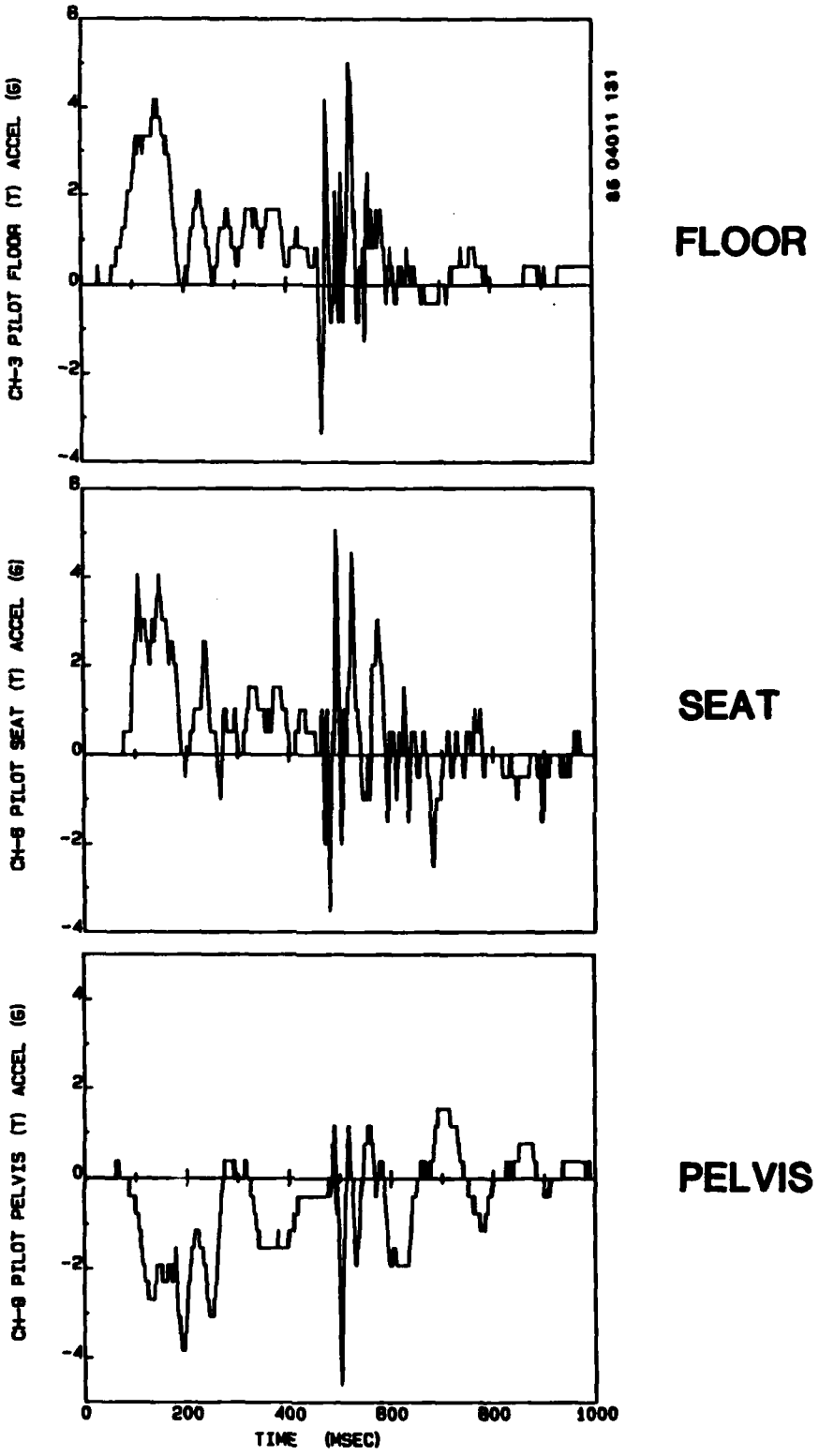

Figure C-1. Pilot seat.

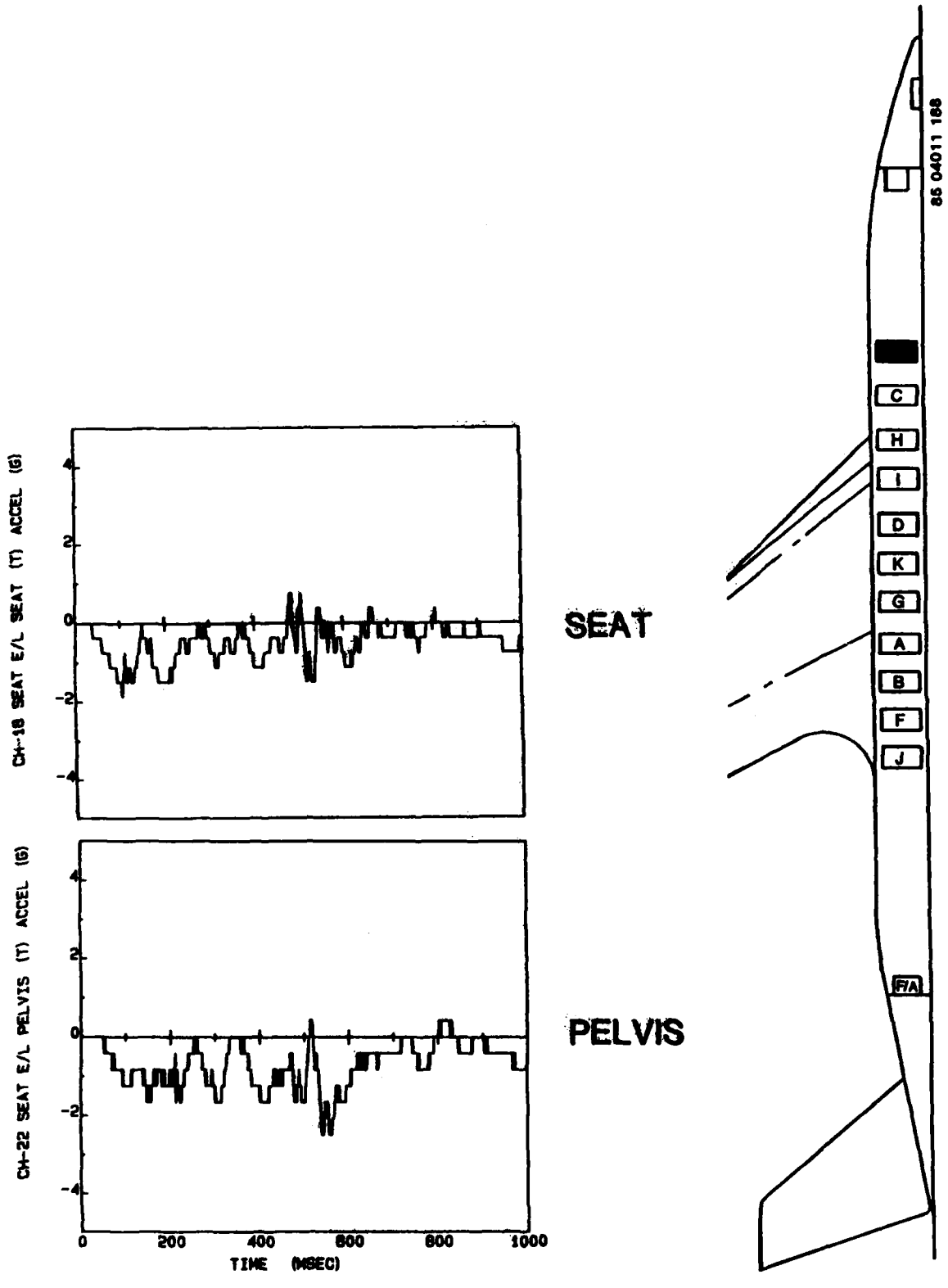

Figure C-2. Seat E/L.

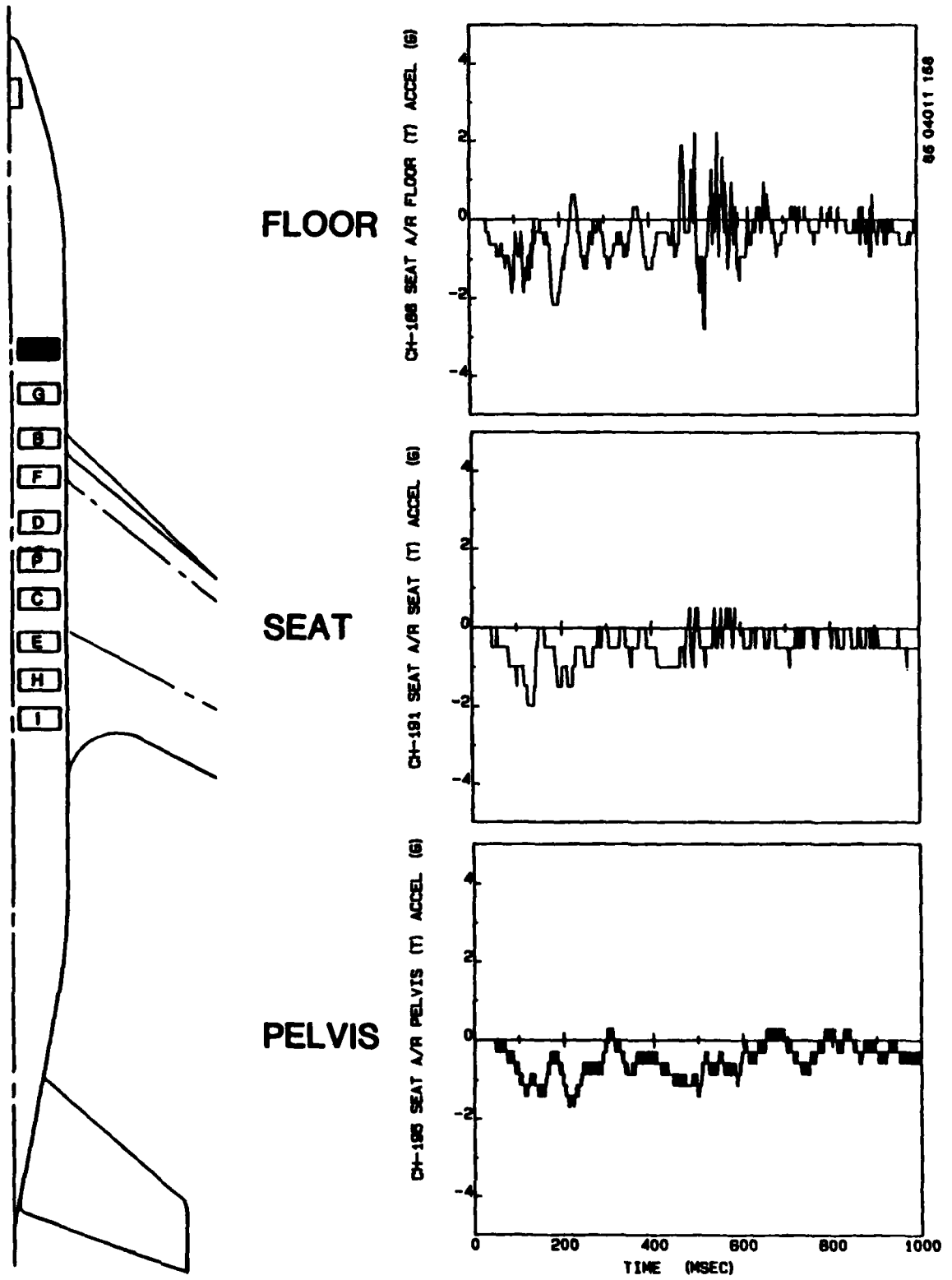

Figure C-3. Seat A/R.

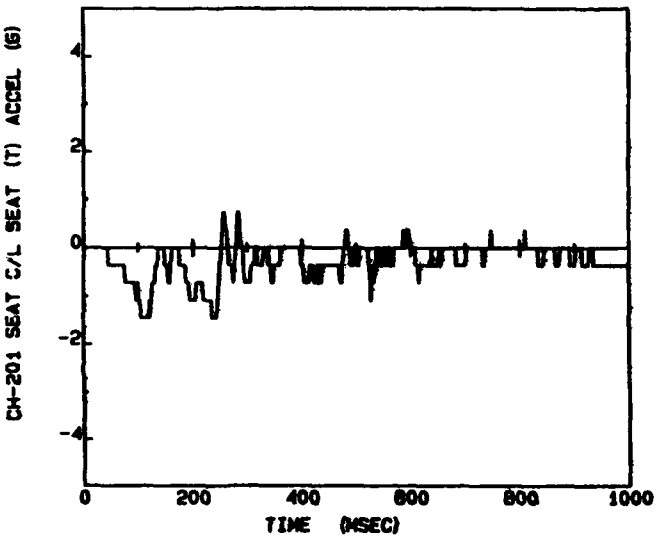

SEAT

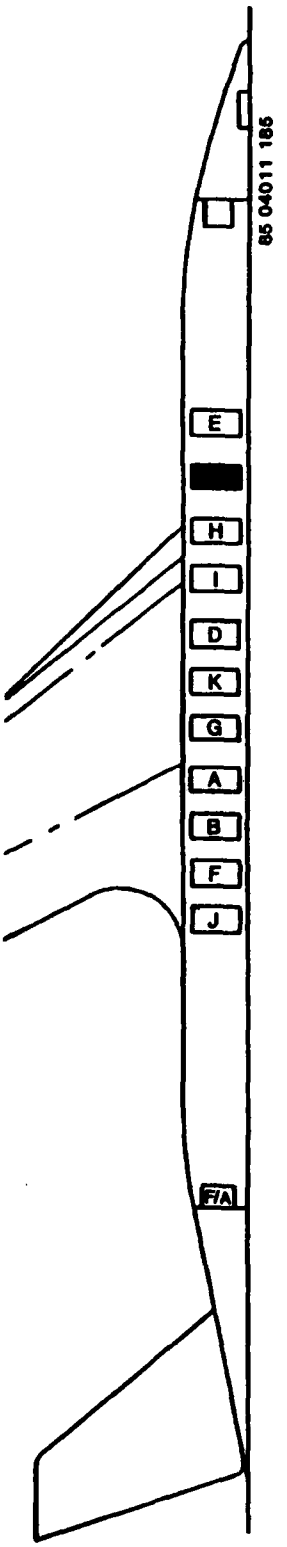

Figure C-4. Seat C/L.

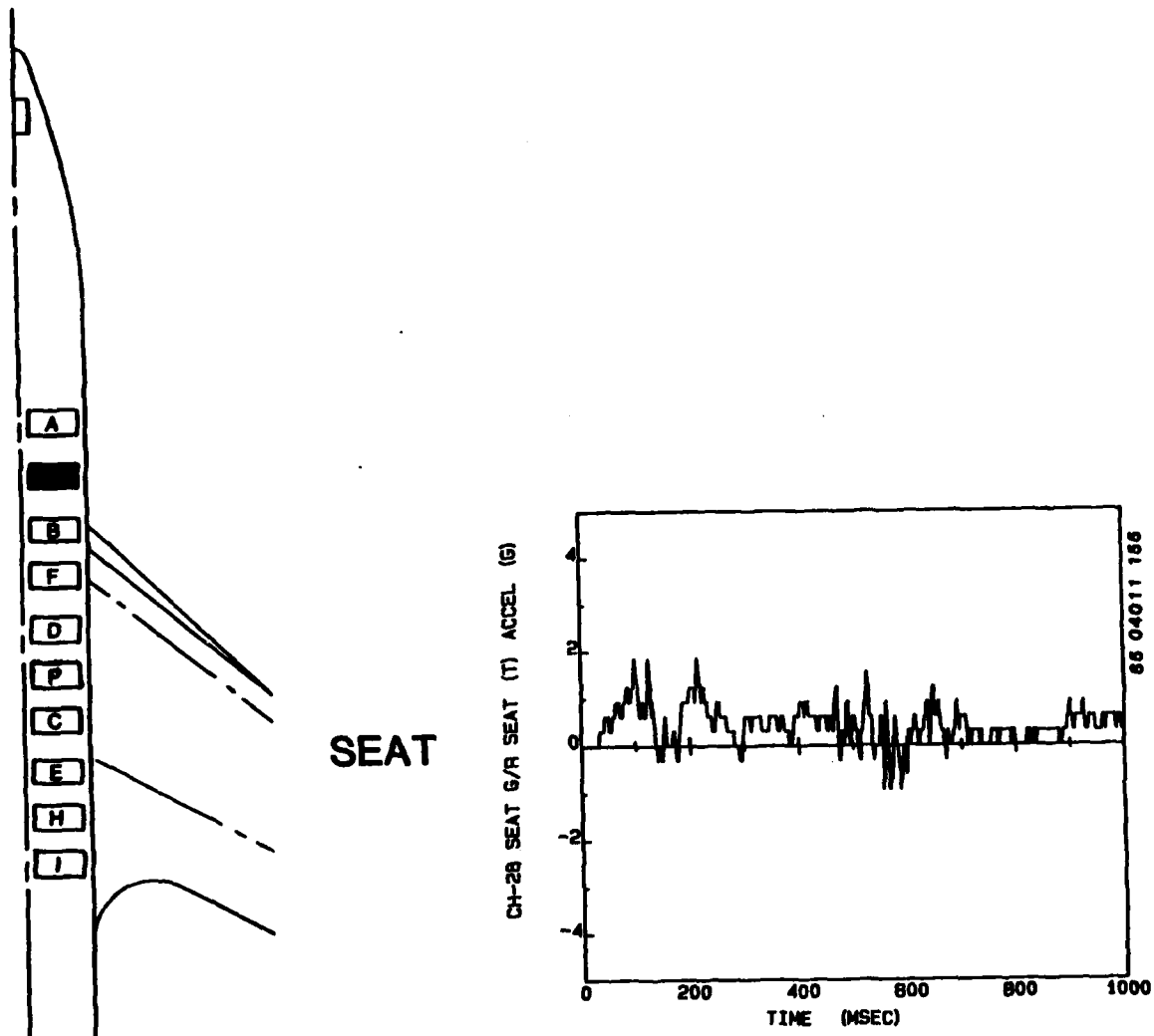

Figure C-5. Seat G/R.

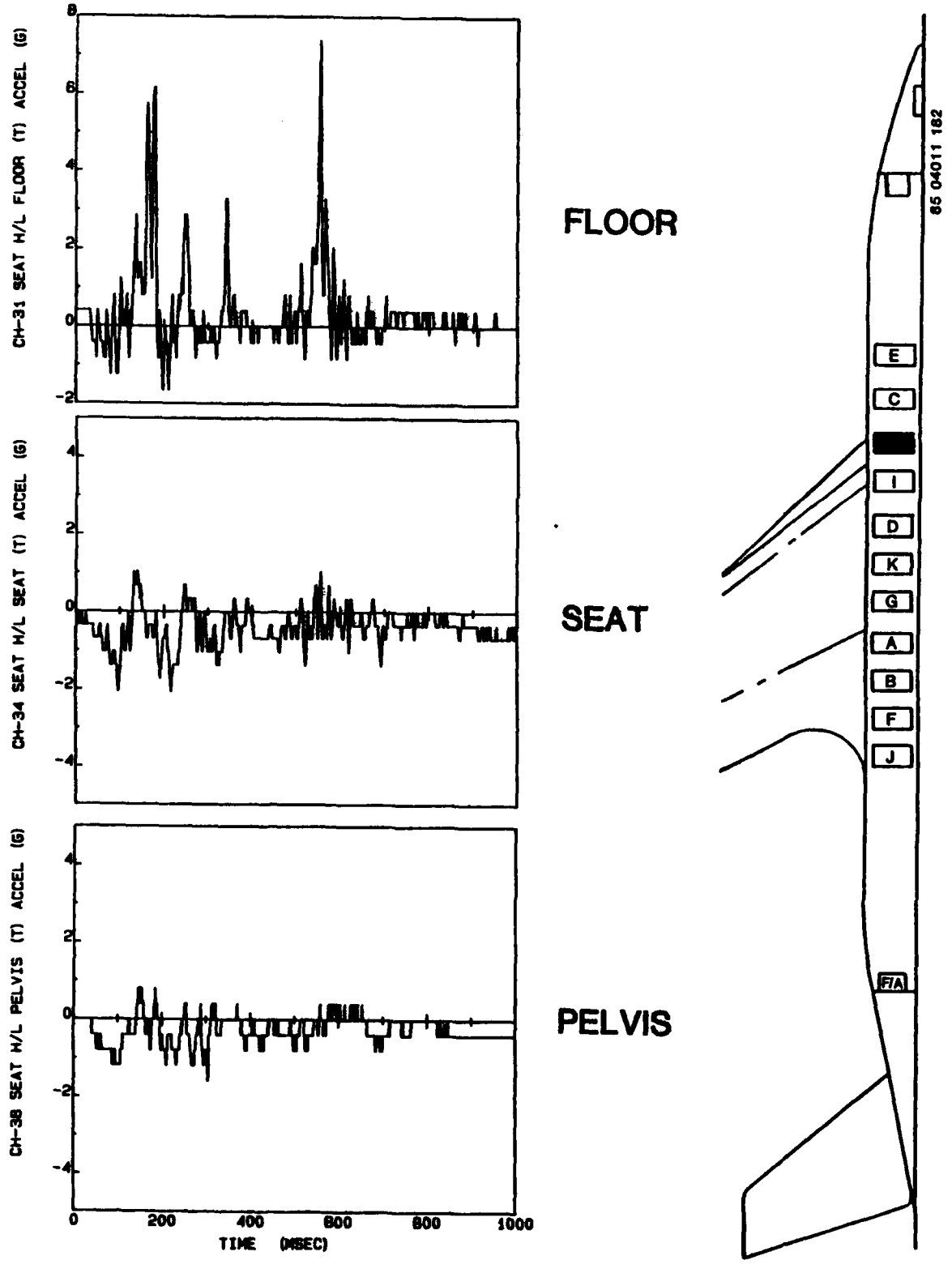

Figure C-6. Seat H/L.

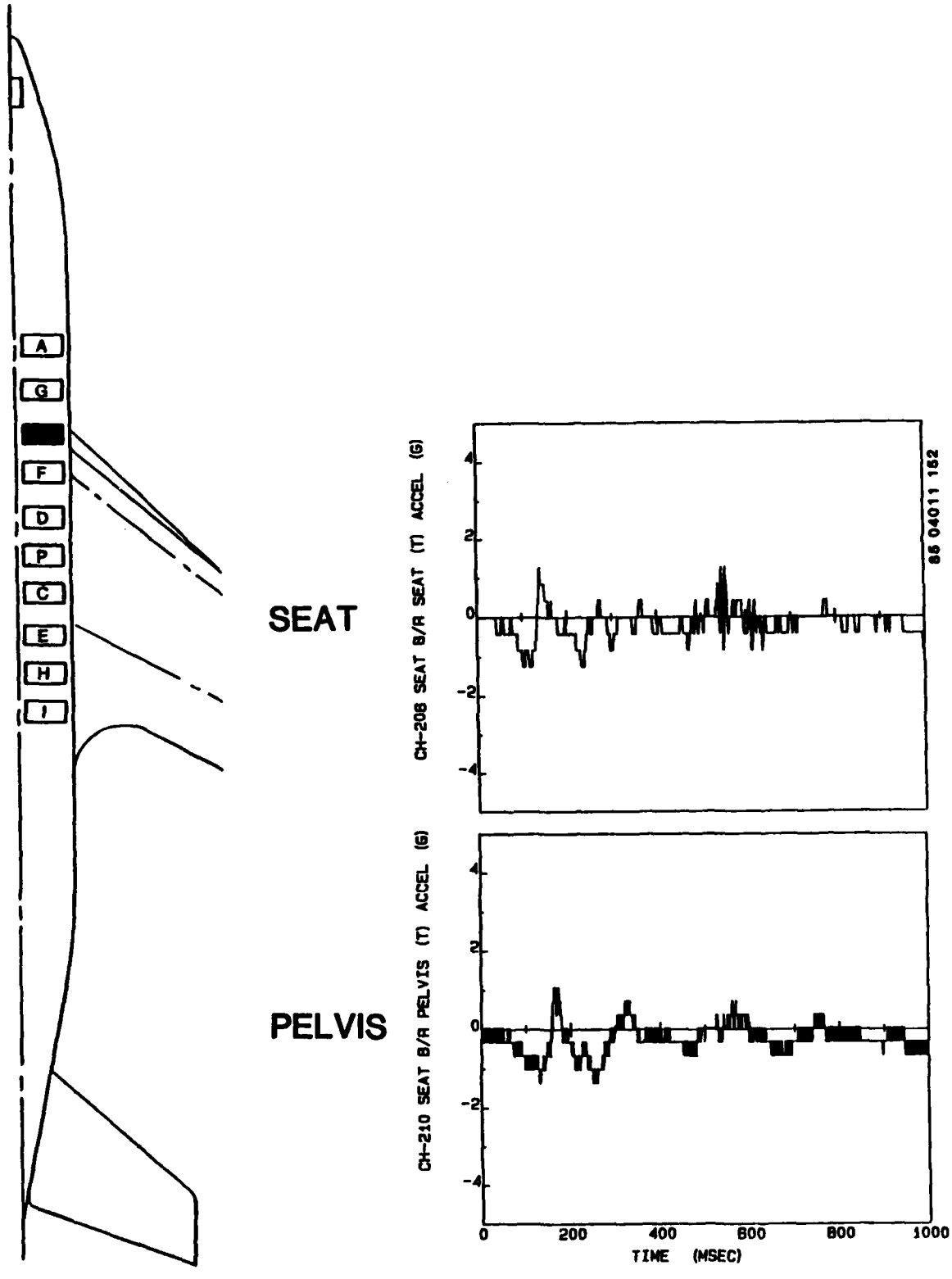

Figure C-7. Seat B/R.

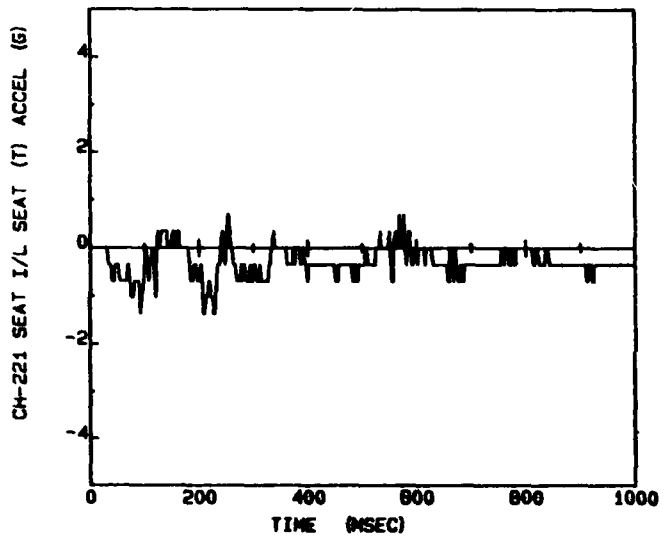

SEAT

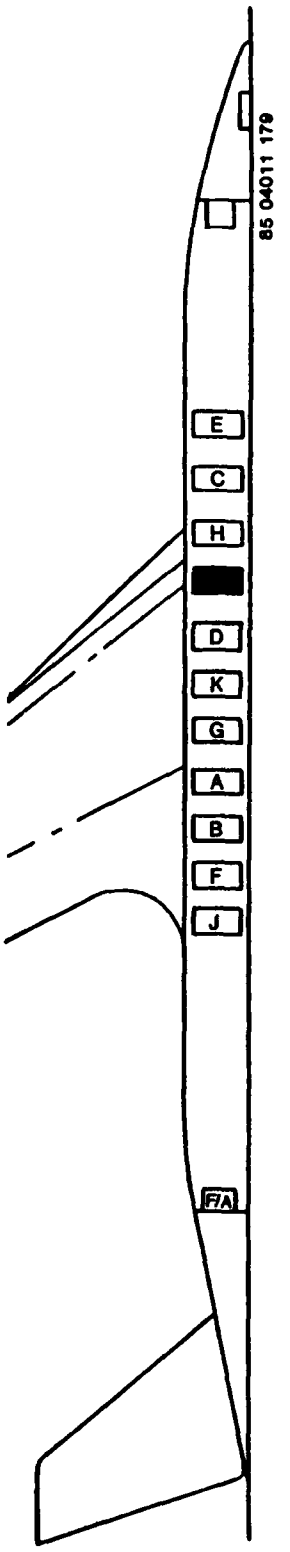

Figure C-8. Seat I/L.

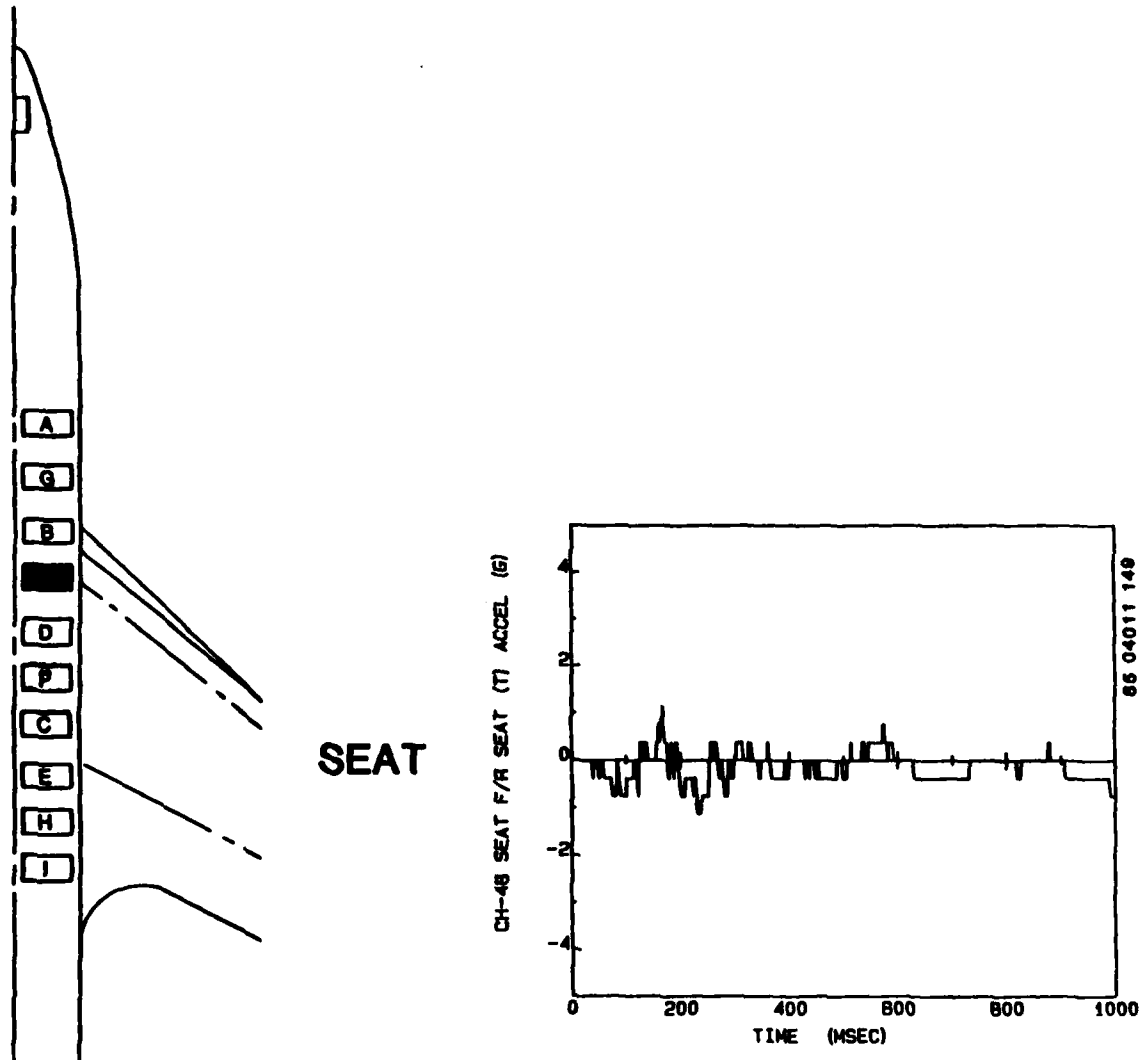

Figure C-9. Seat F/R.

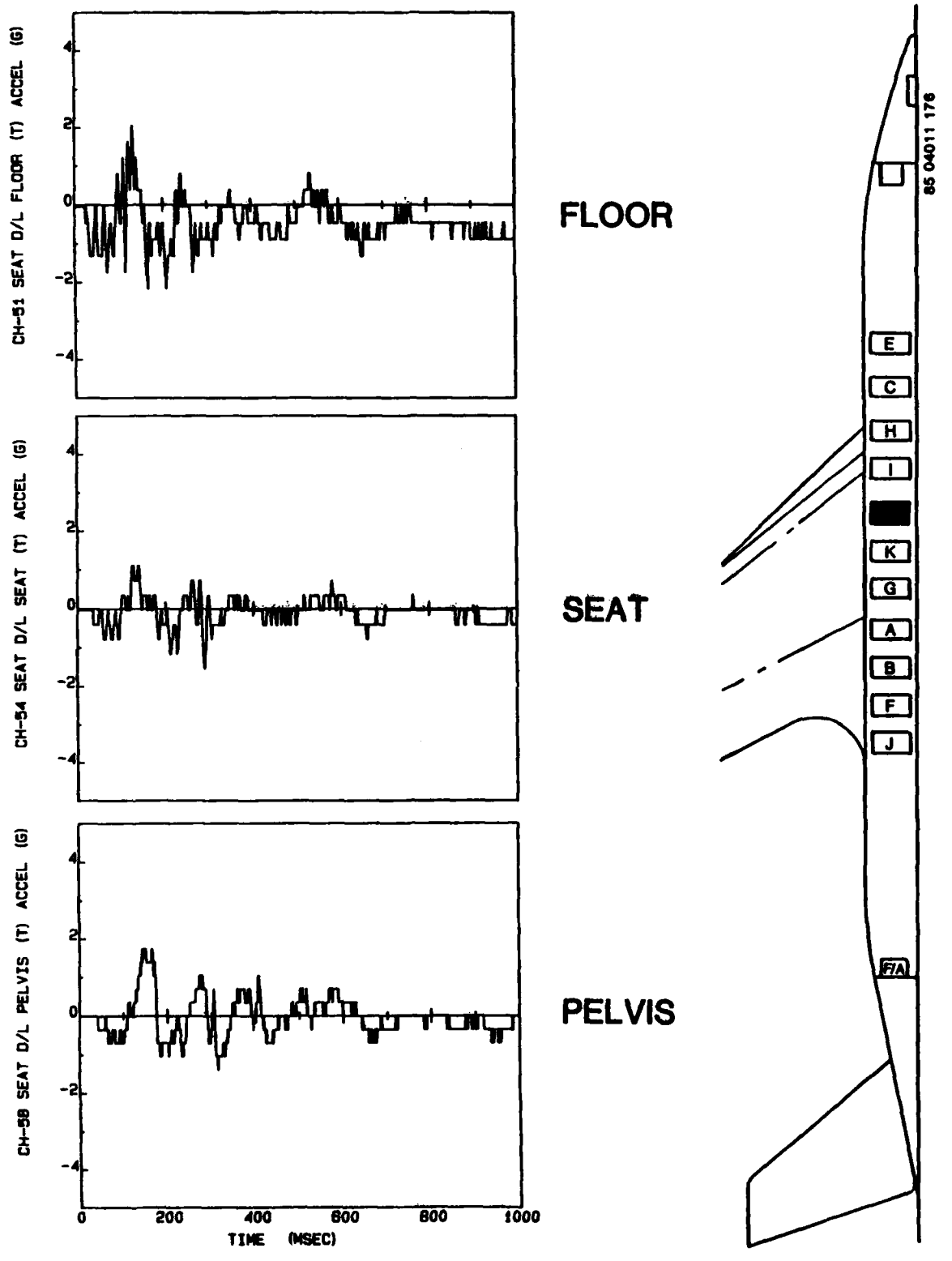

Figure C-10. Seat D/L.

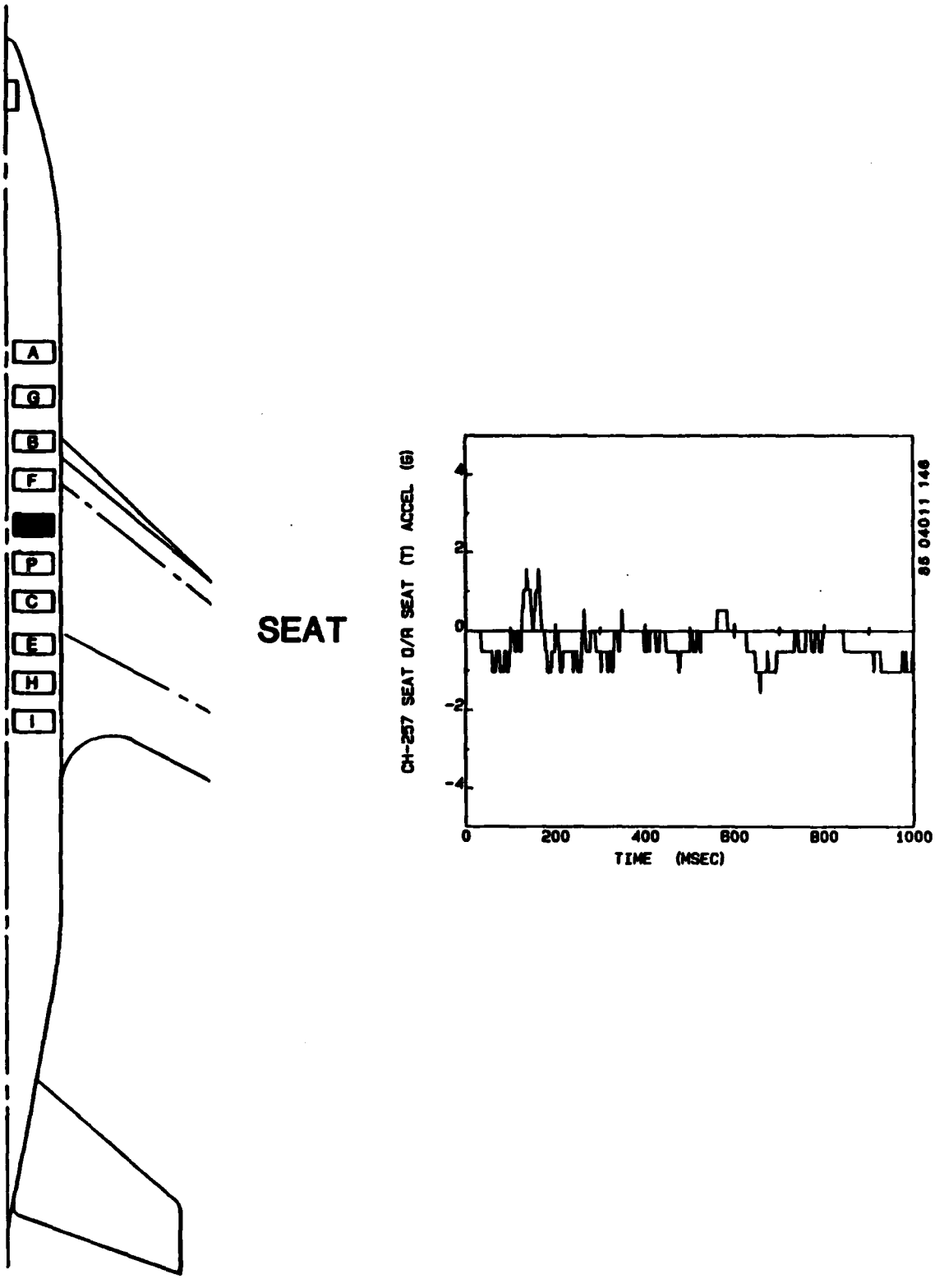

Figure C-11. Seat D/R.

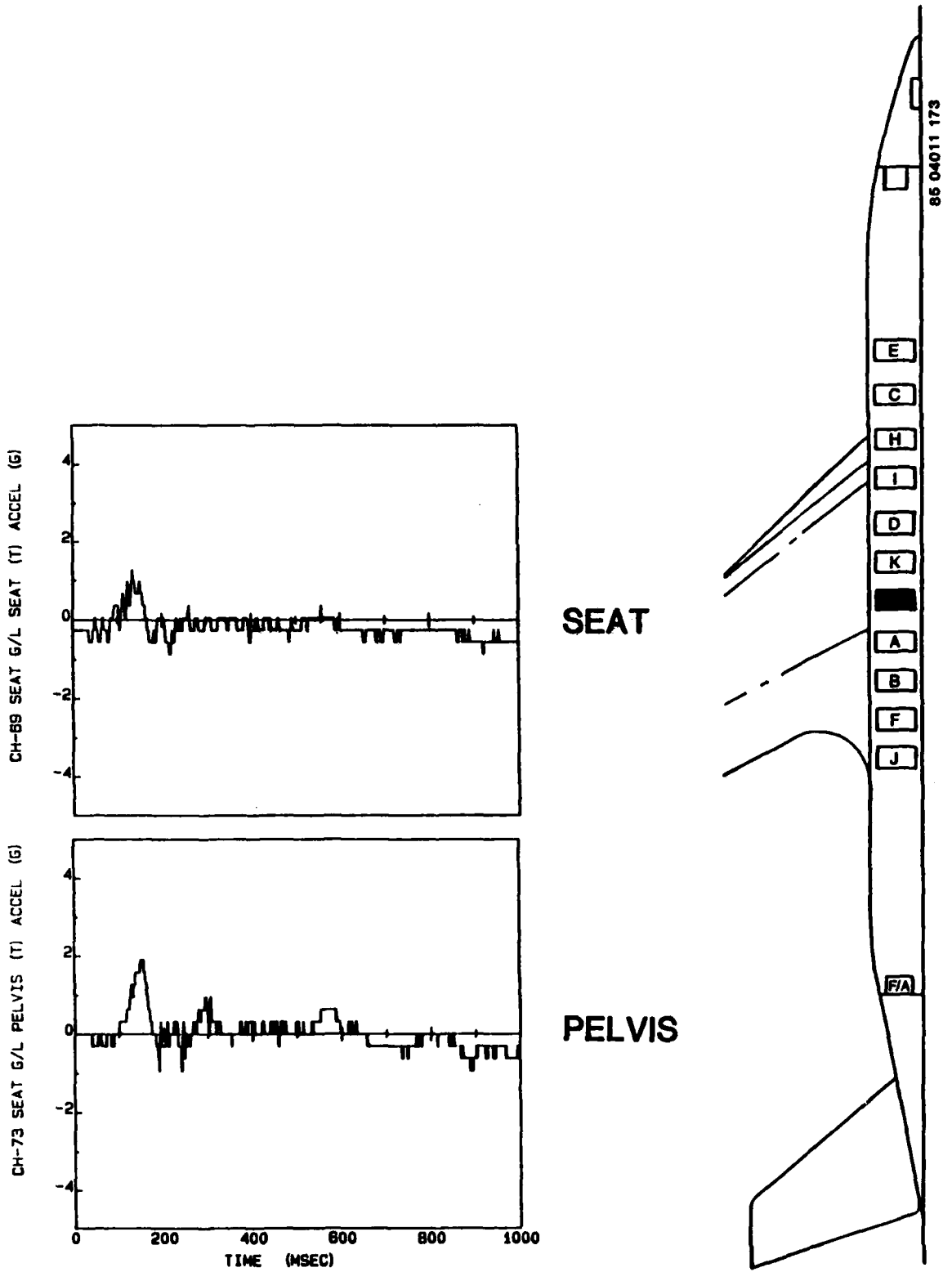

Figure C-12. Seat G/L.

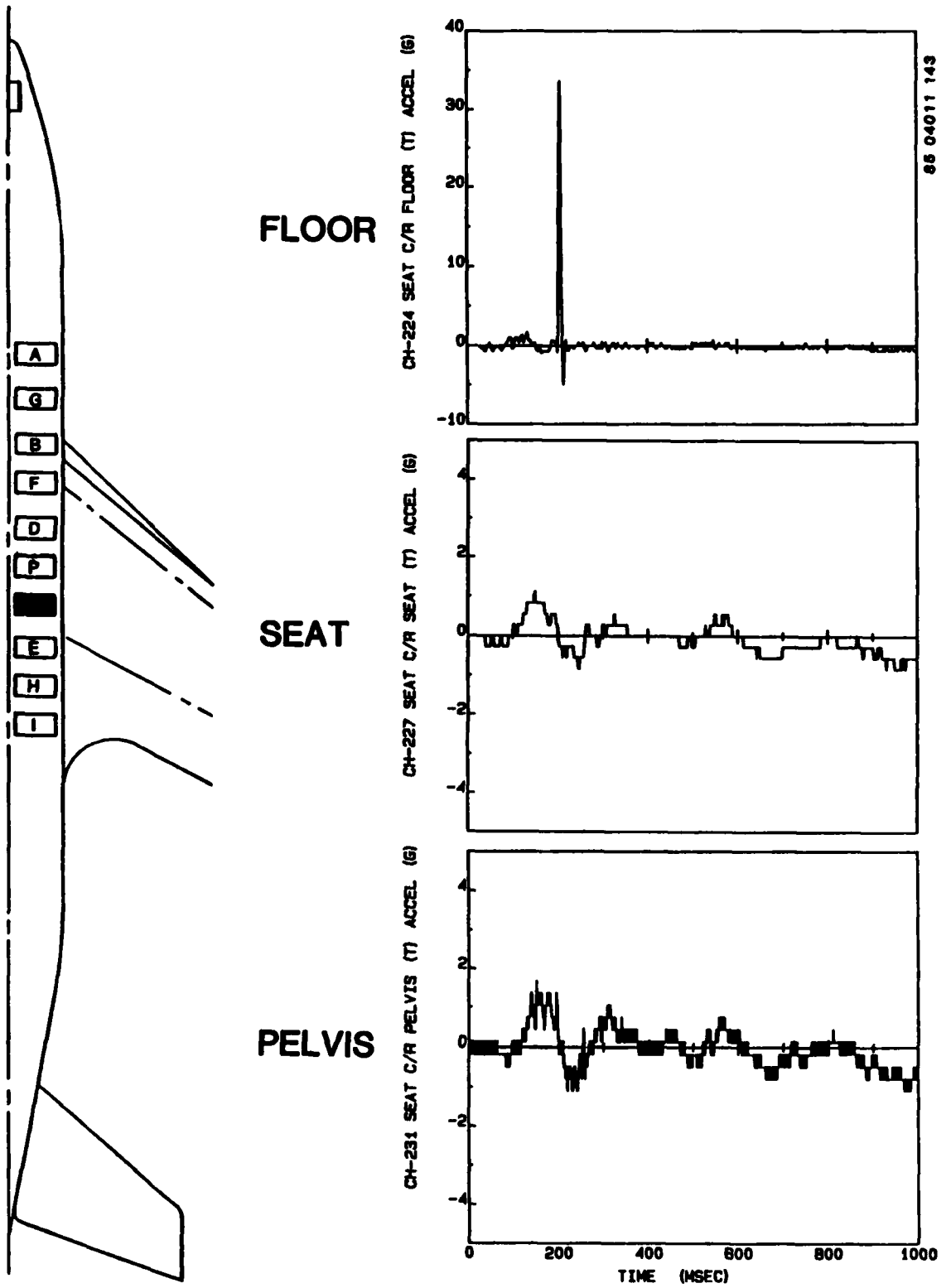

Figure C-13. Seat C/R.

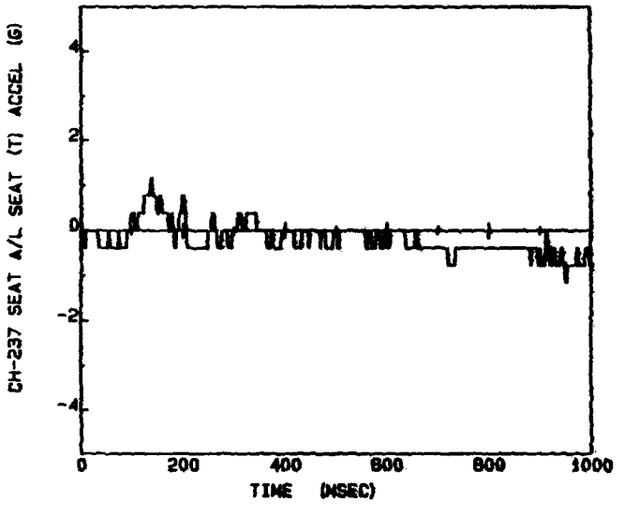

SEAT

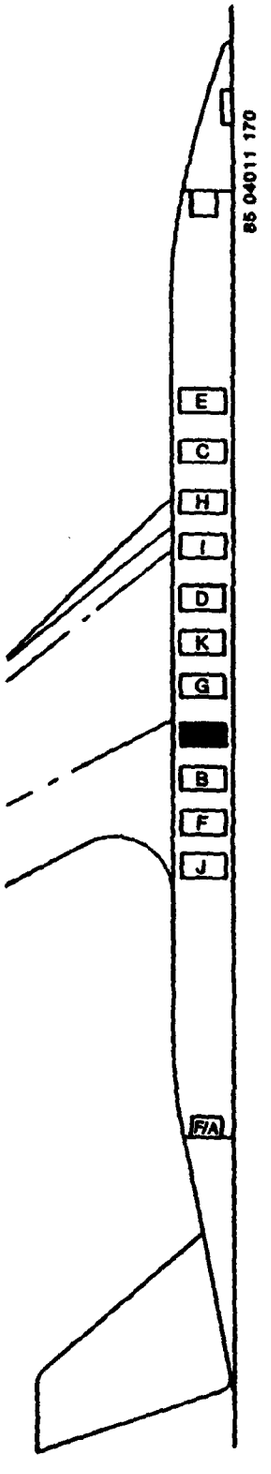

Figure C-14. Seat A/L.

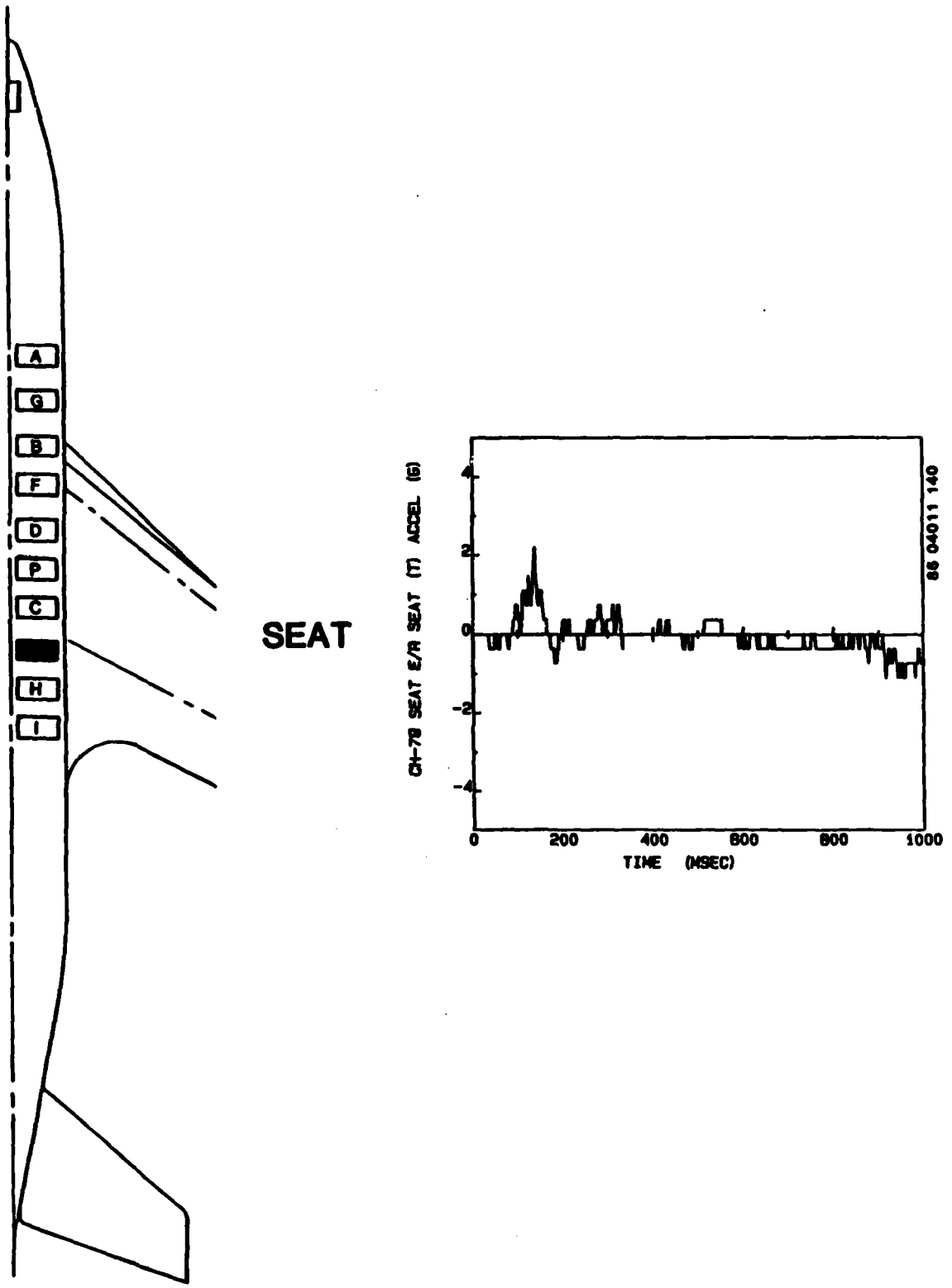

Figure C-15. Seat E/R.

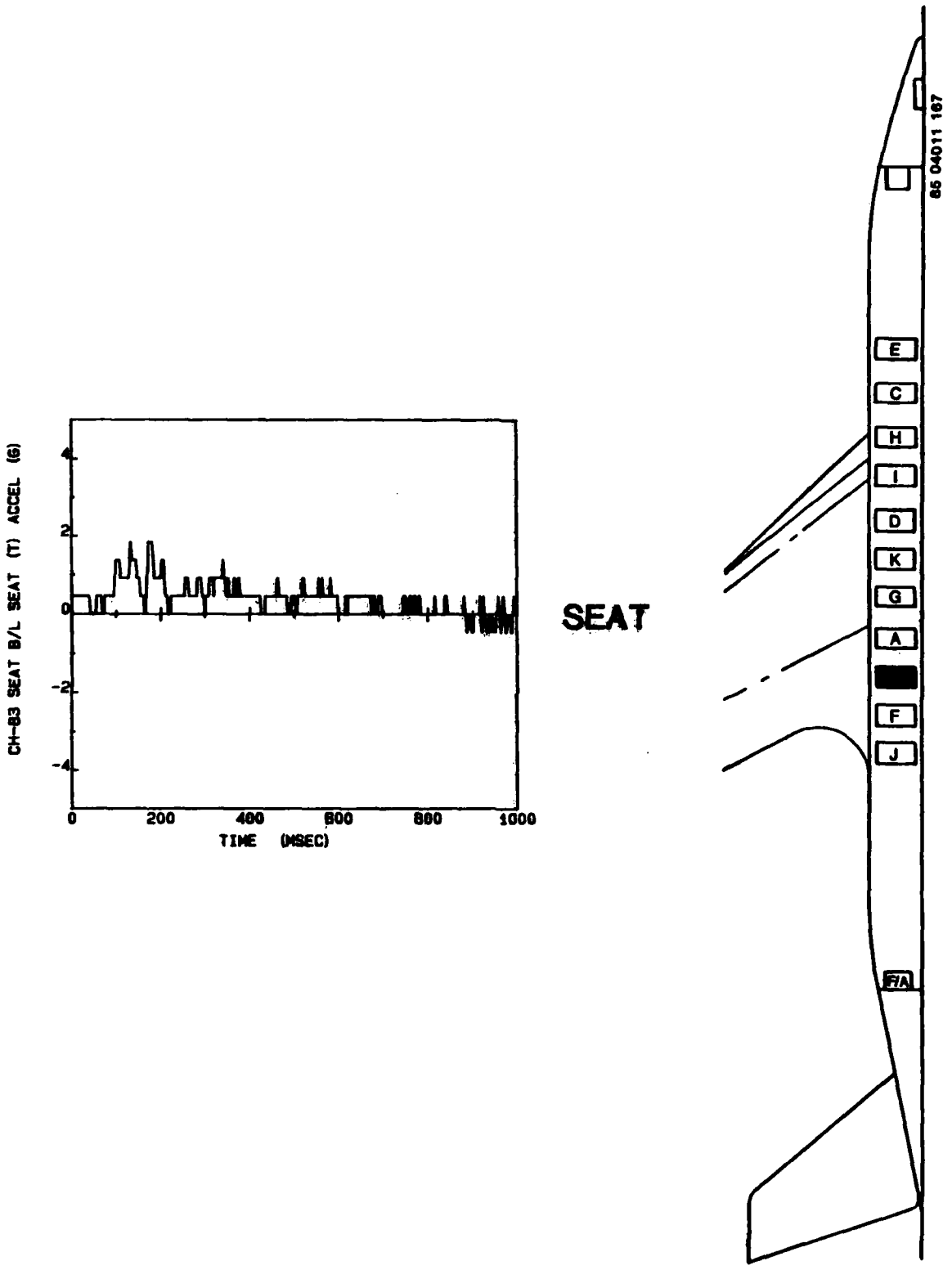

Figure C-16. Seat B/L.

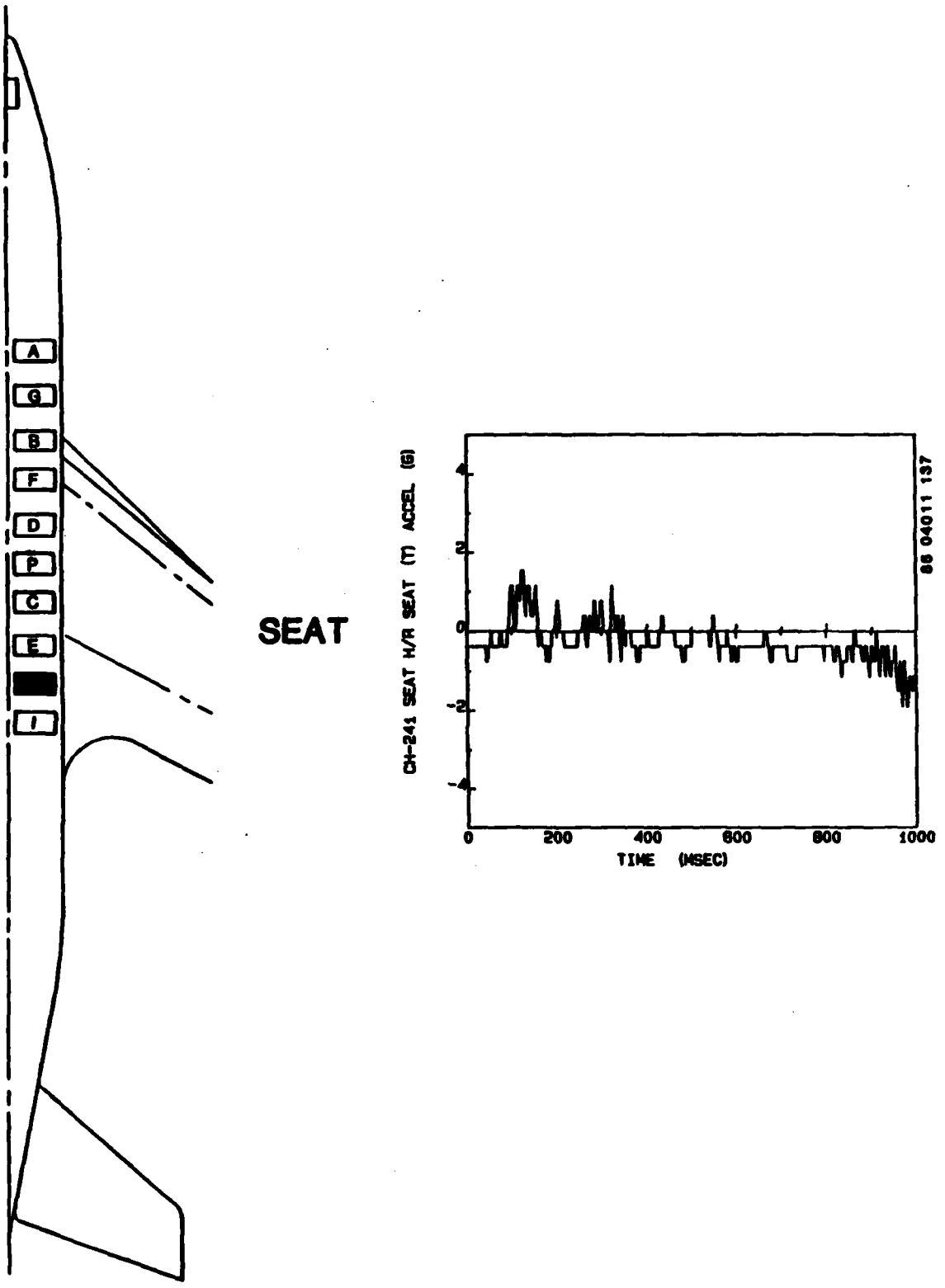

Figure C-17. Seat H/R.

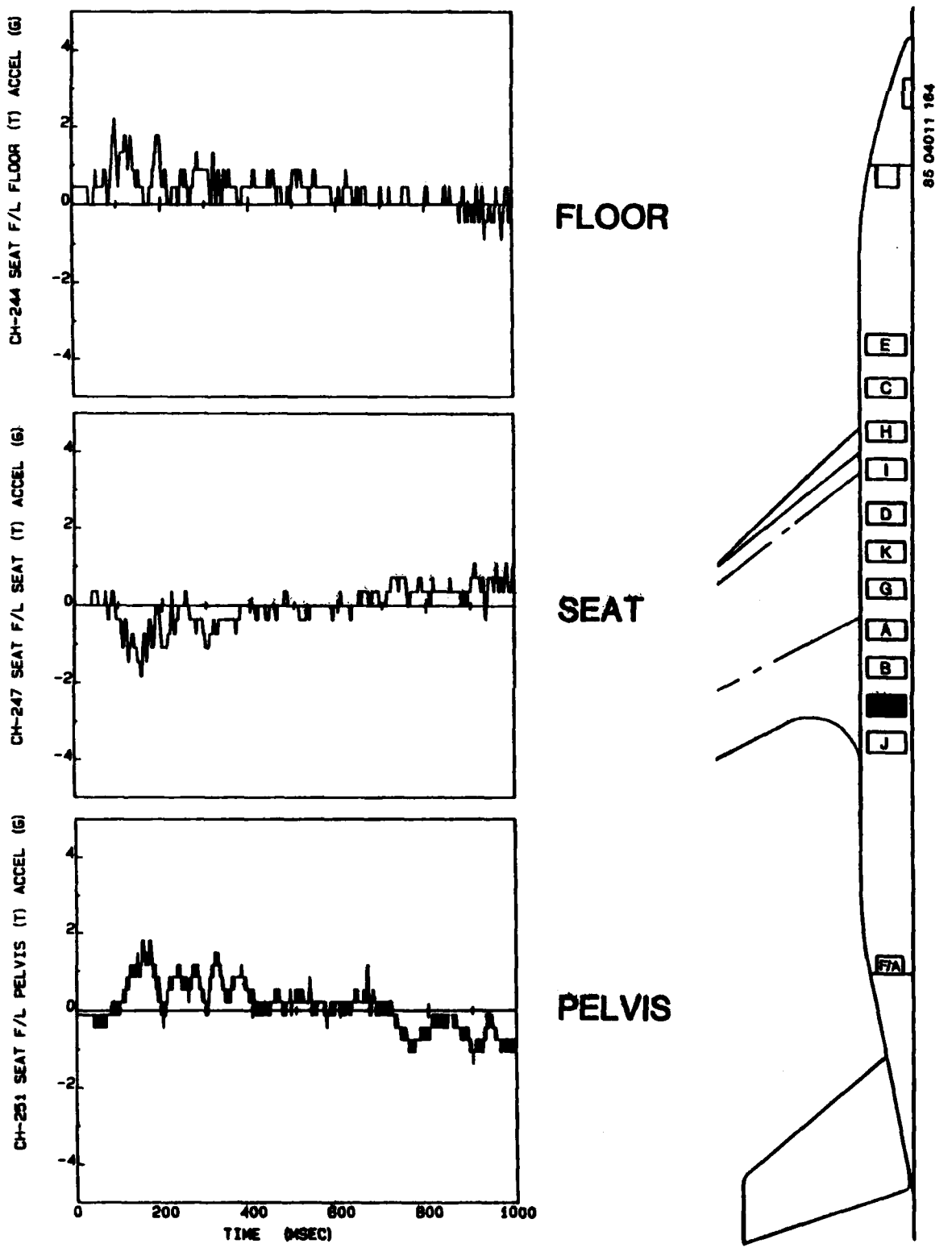

Figure C-18. Seat F/L.

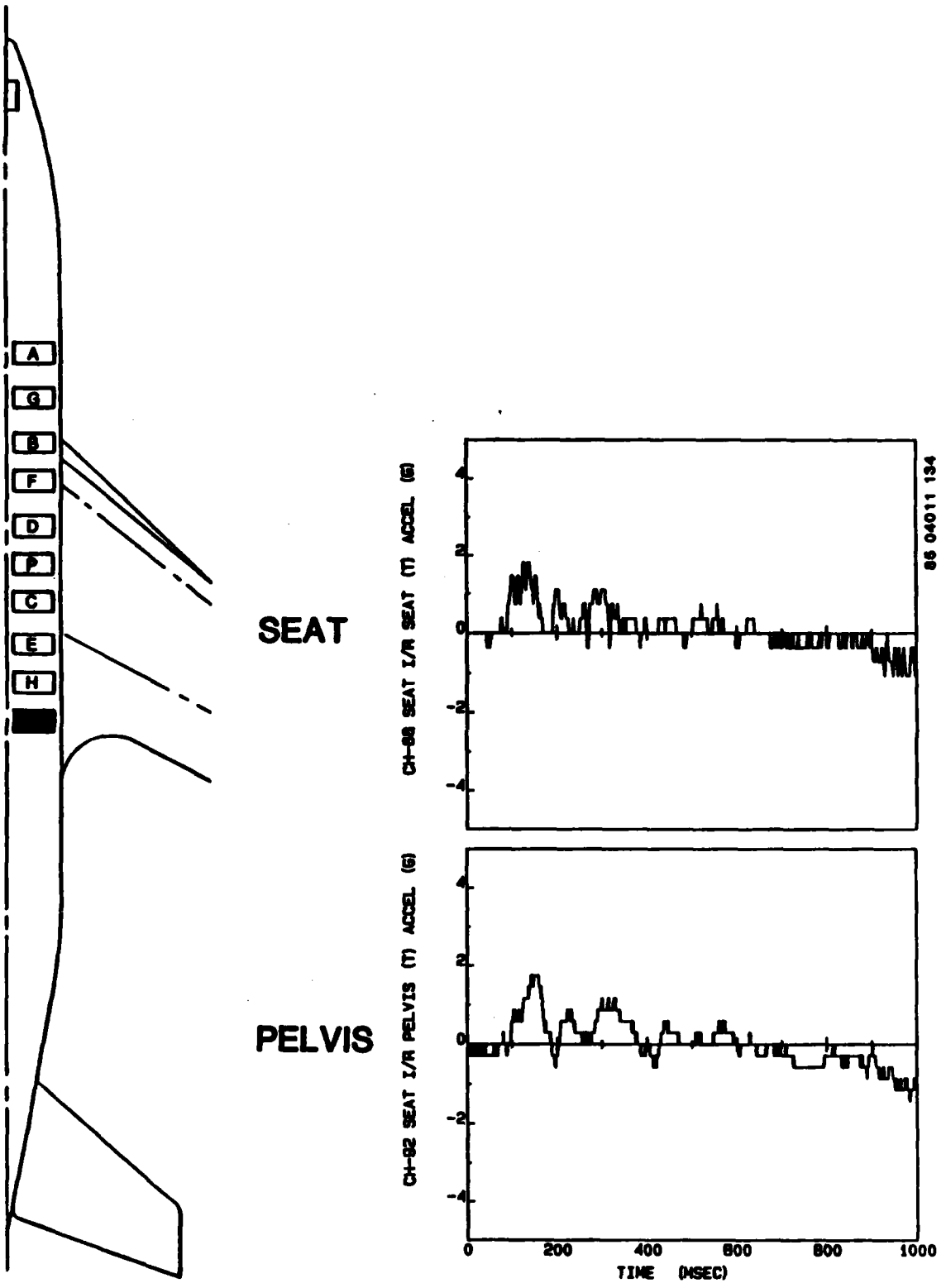

Figure C-19. Seat I/R.

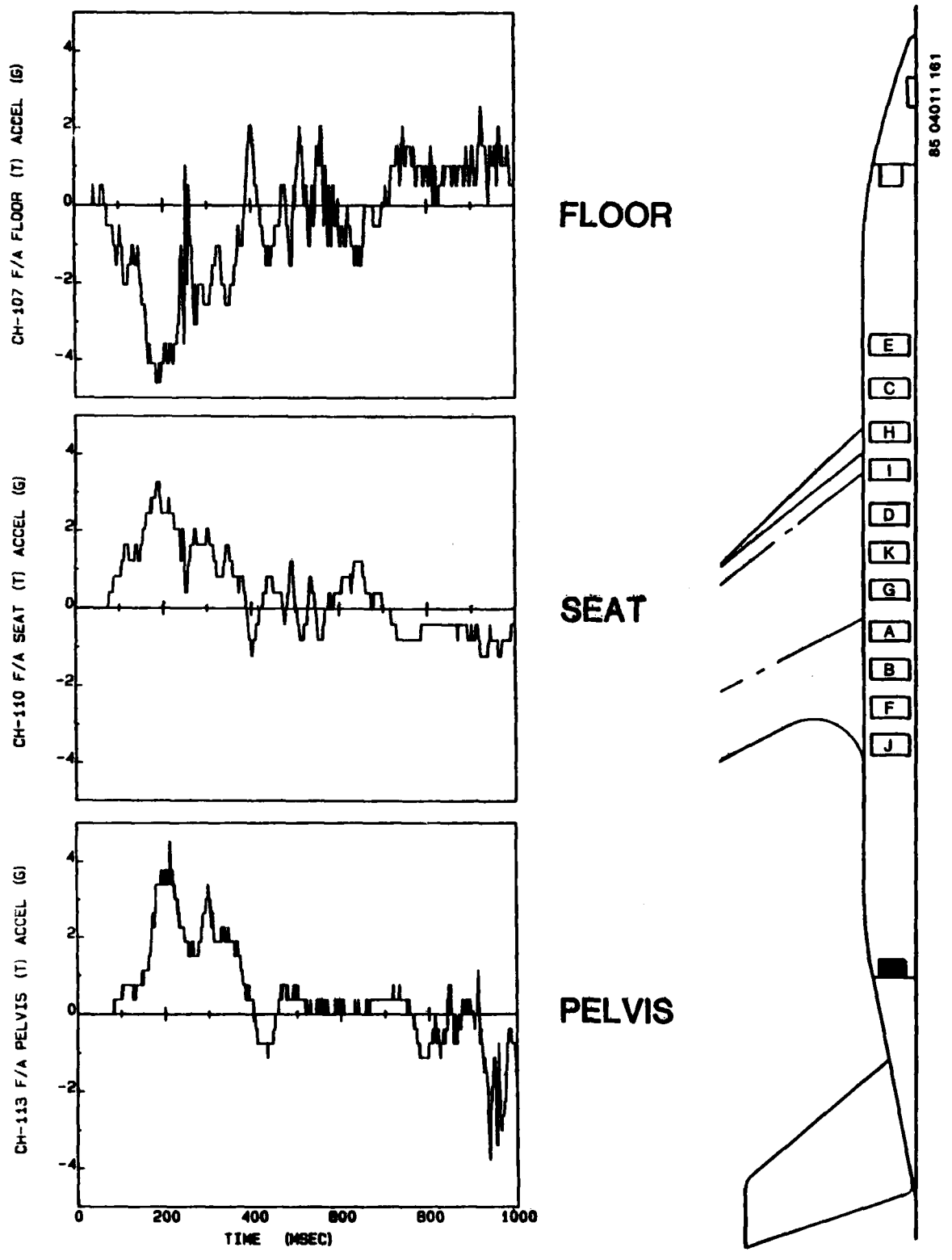

Figure C-20. Seat F/A.

APPENDIX D

HEAD AND CHEST ACCELERATIONS

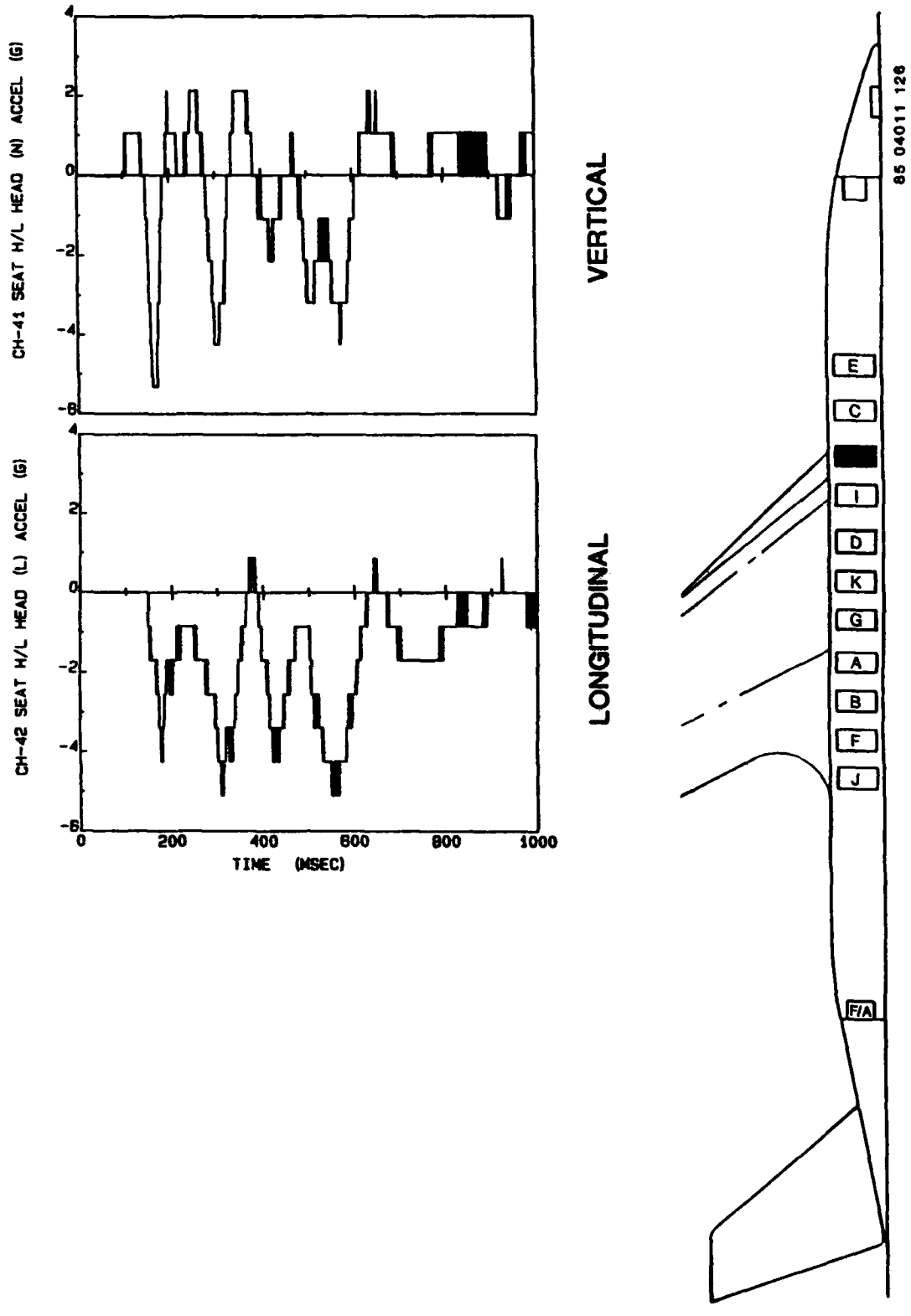

Figure D-1. Seat H/L - head.

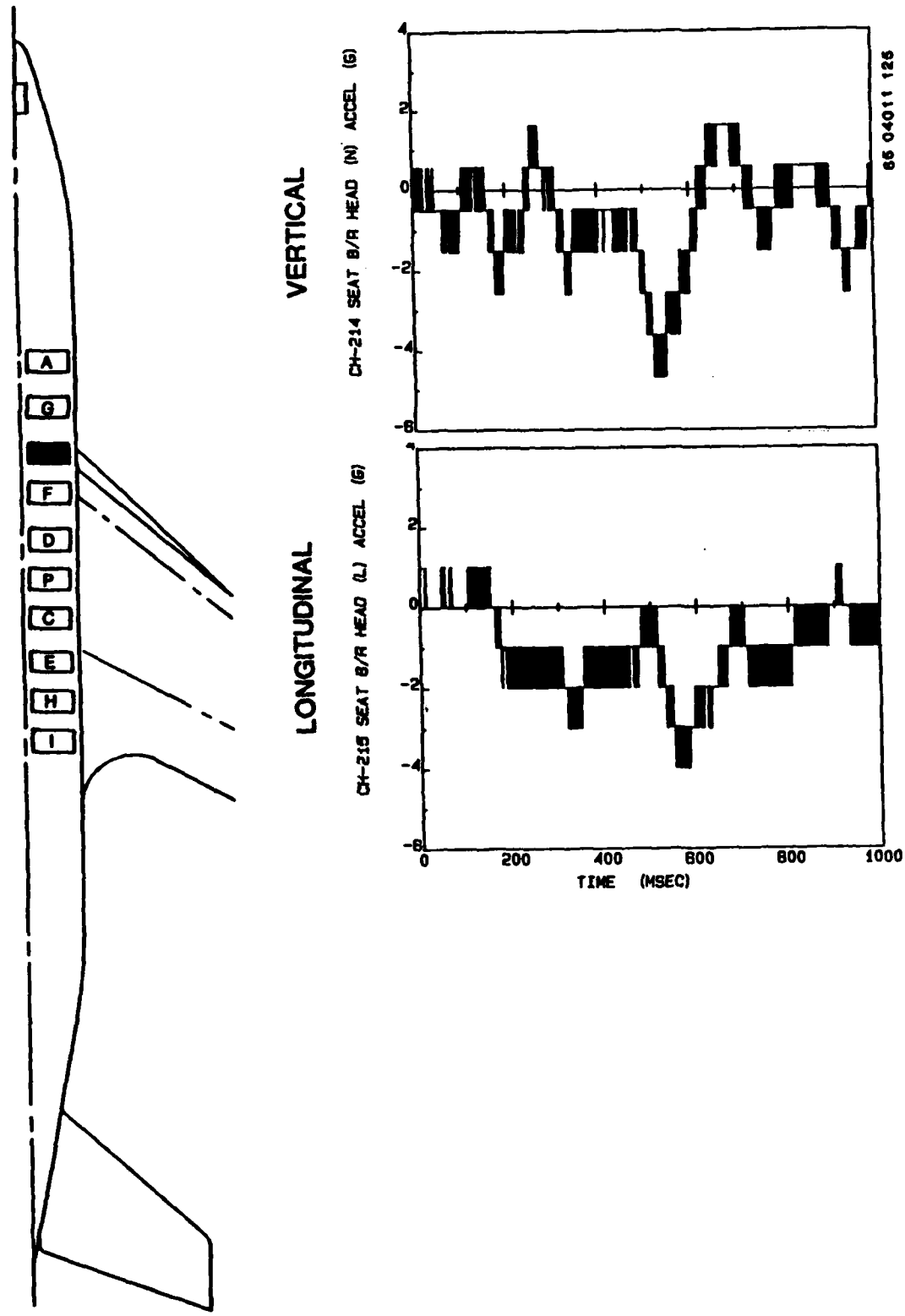

Figure D-2. Seat B/R - head.

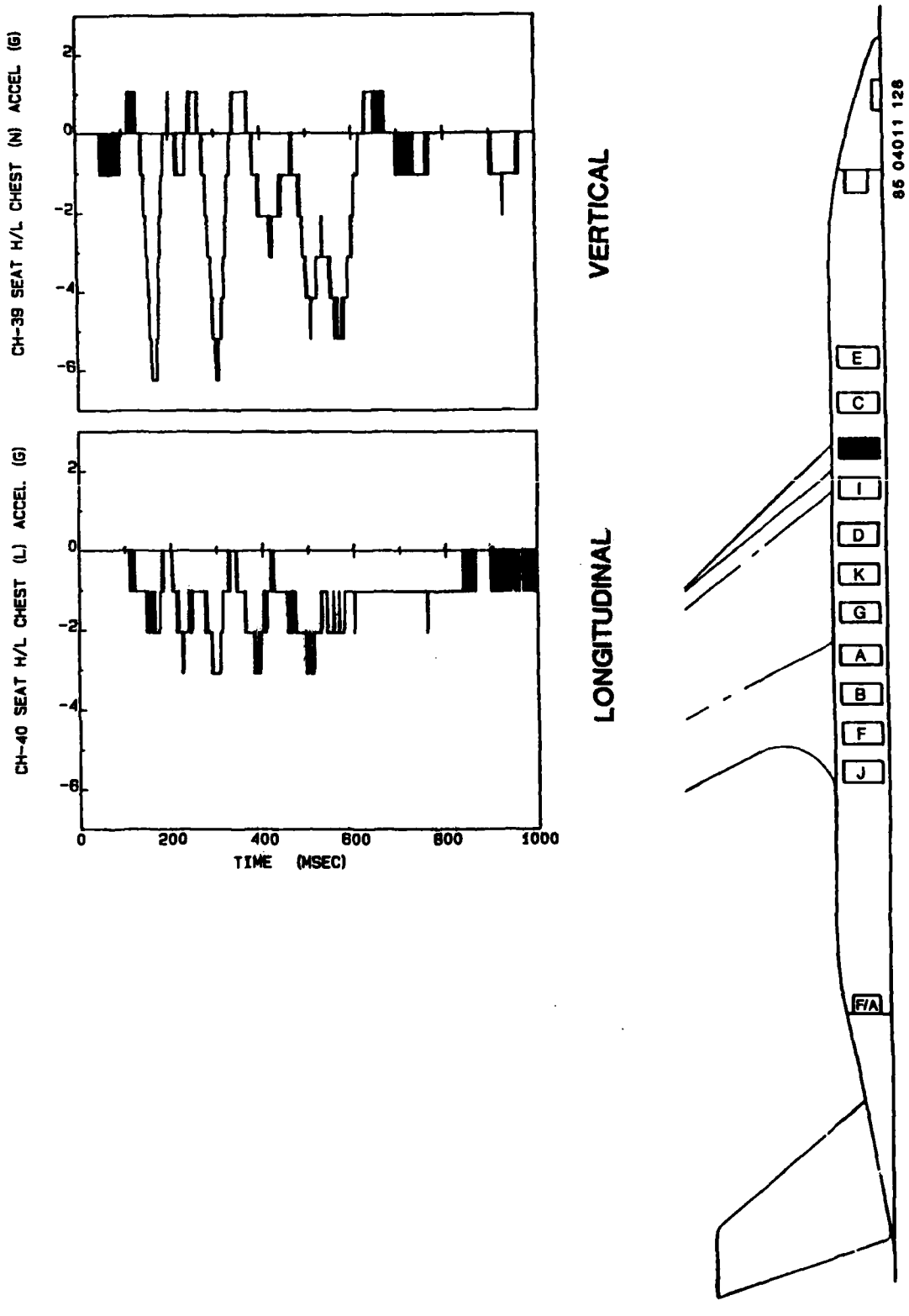

Figure D-3. Seat H/L - chest.

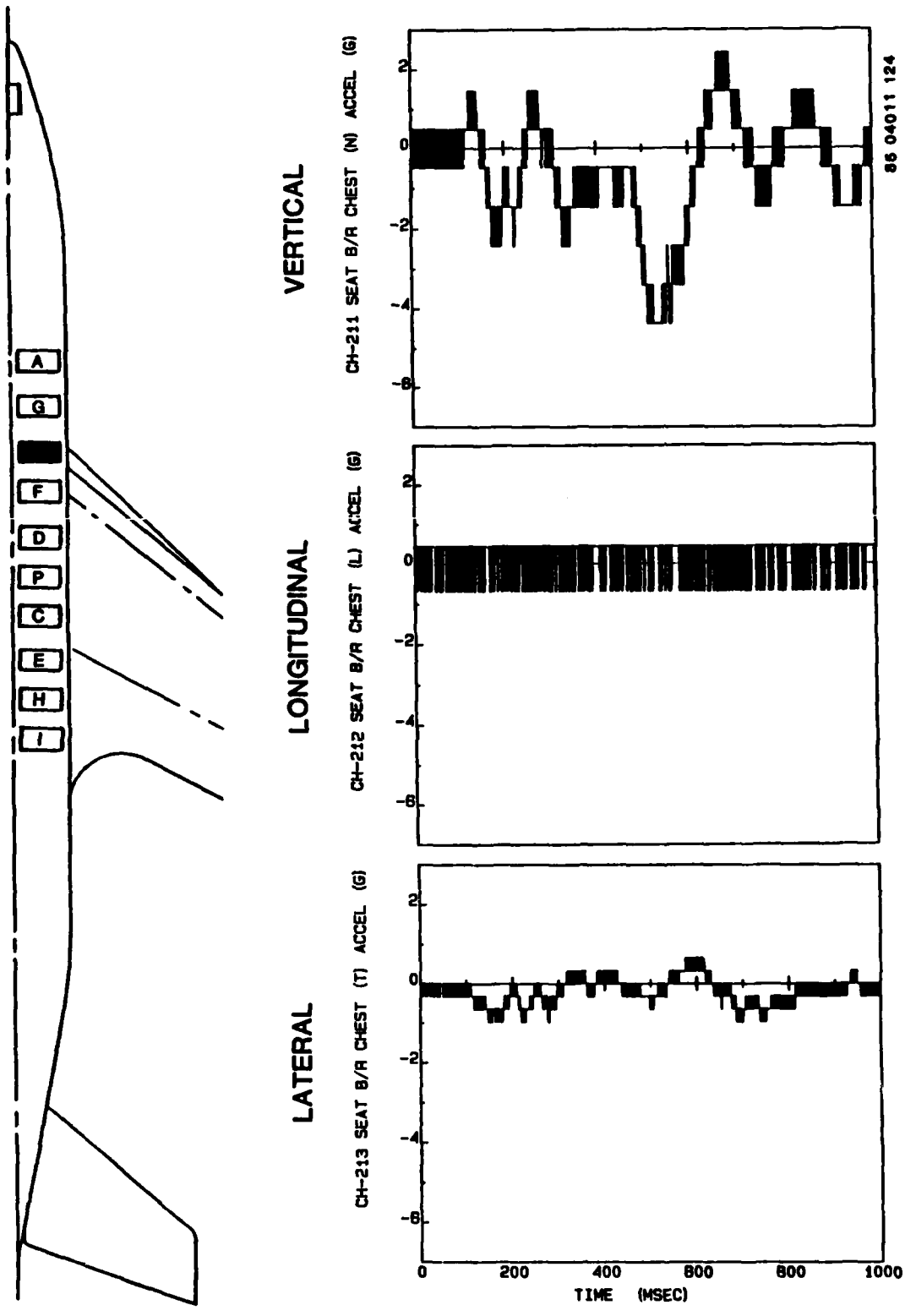

Figure D-4. Seat B/R - chest.

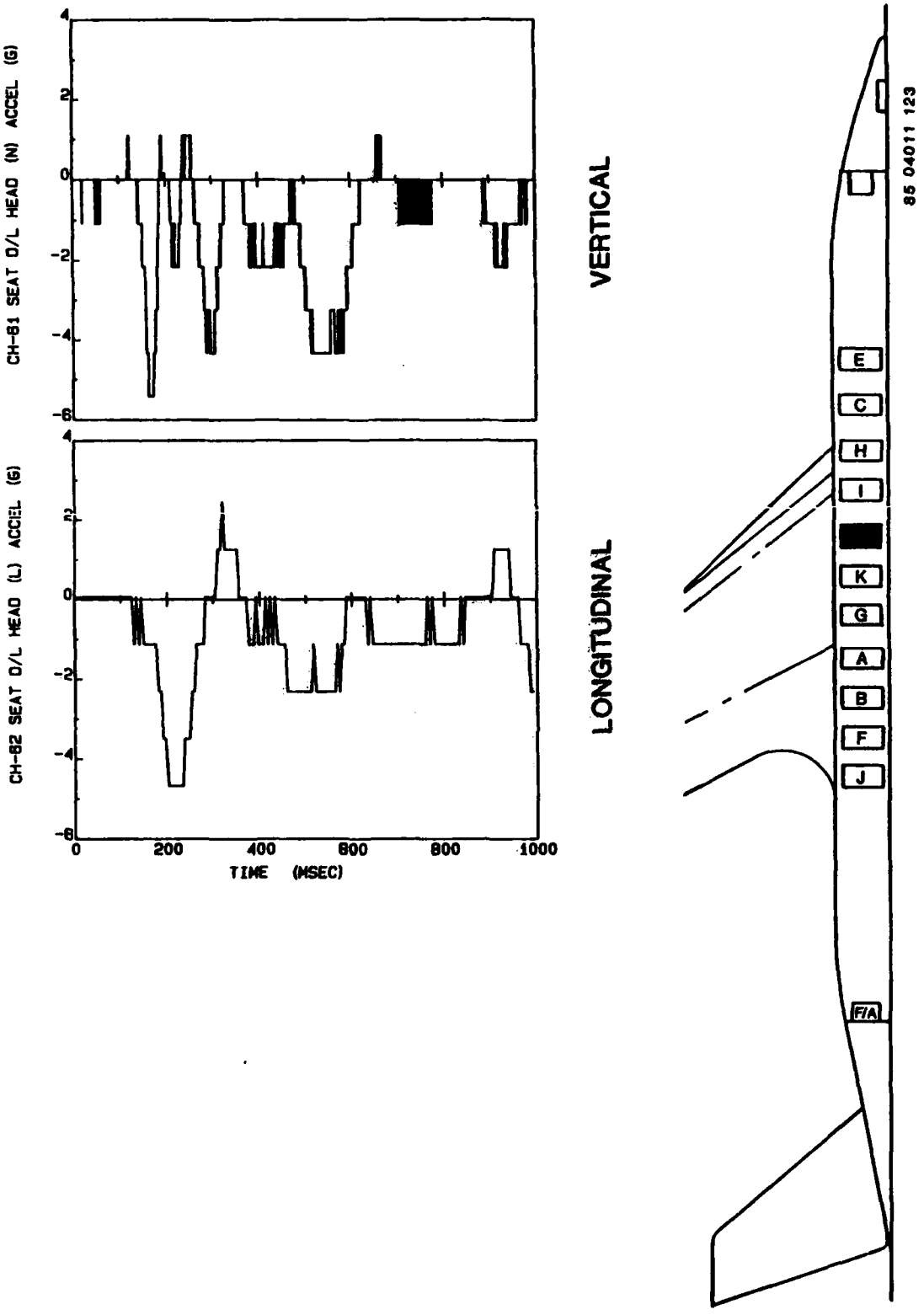

Figure D-5. Seat D/L - head.

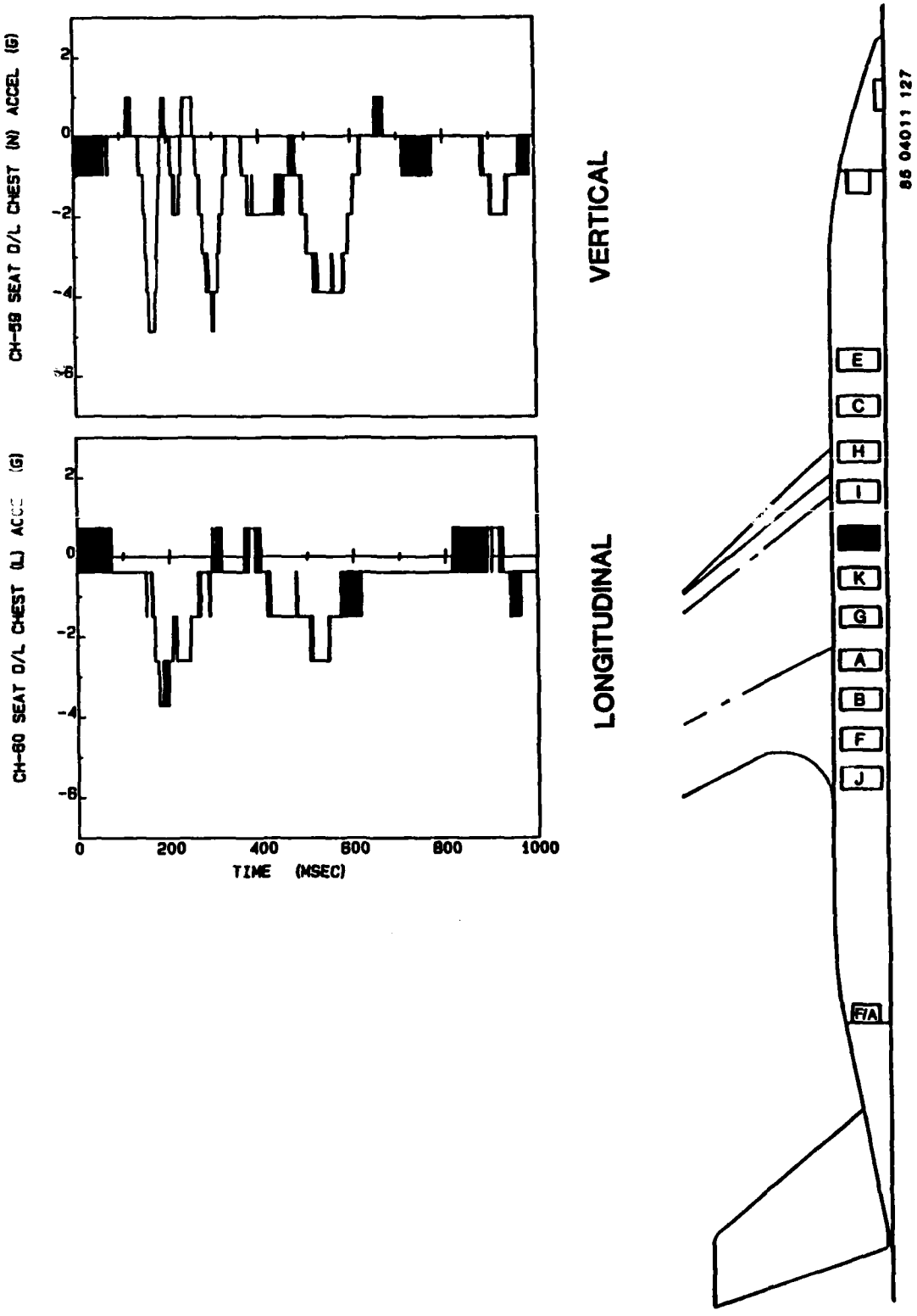

Figure D-6. Seat D/L - chest.

THIS PAGE LEFT INTENTIONALLY BLANK.

APPENDIX E

LAP BELT LOADS

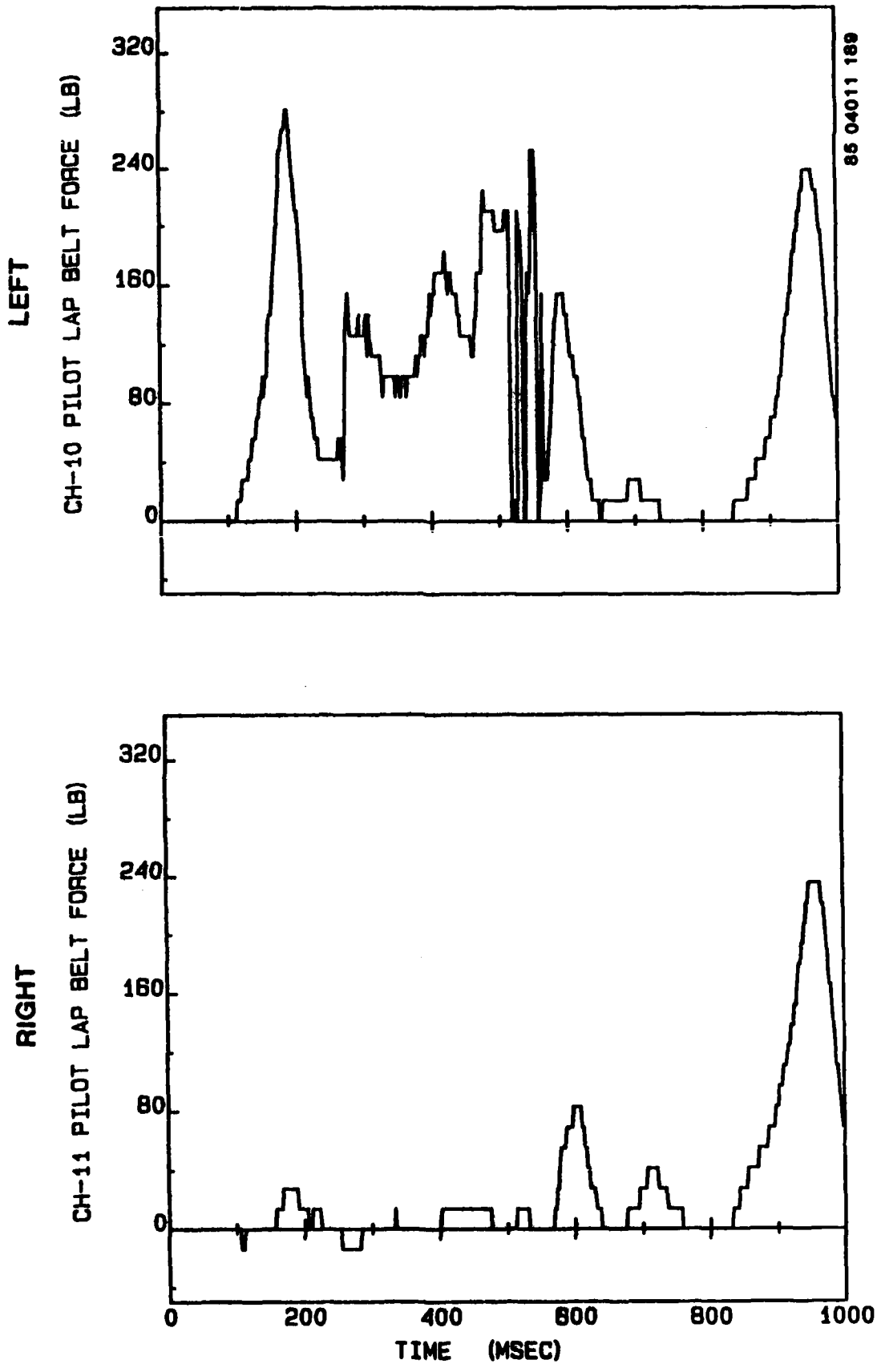

Figure E-1. Pilot seat.

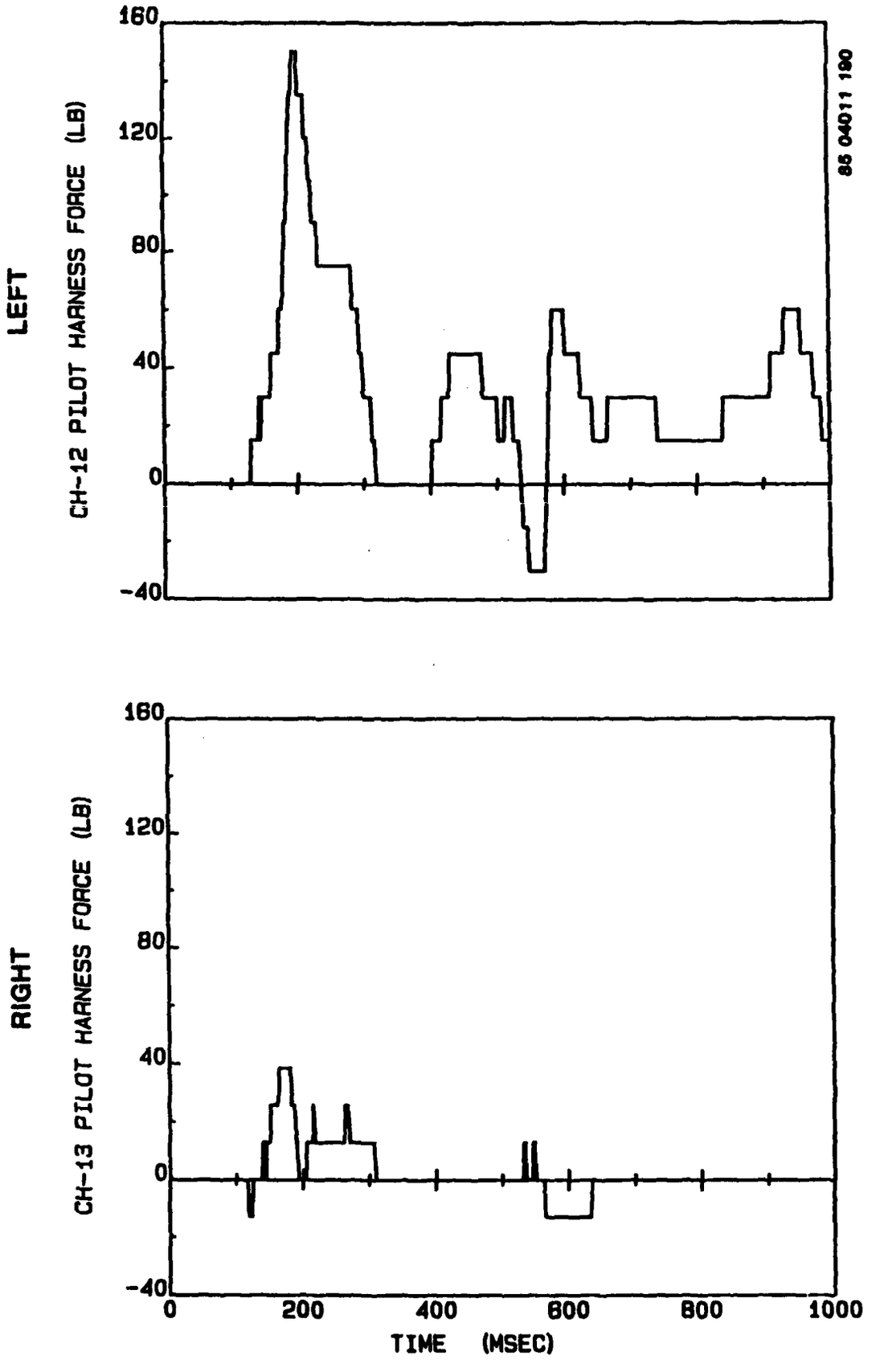

Figure E-2. Pilot seat - harness.

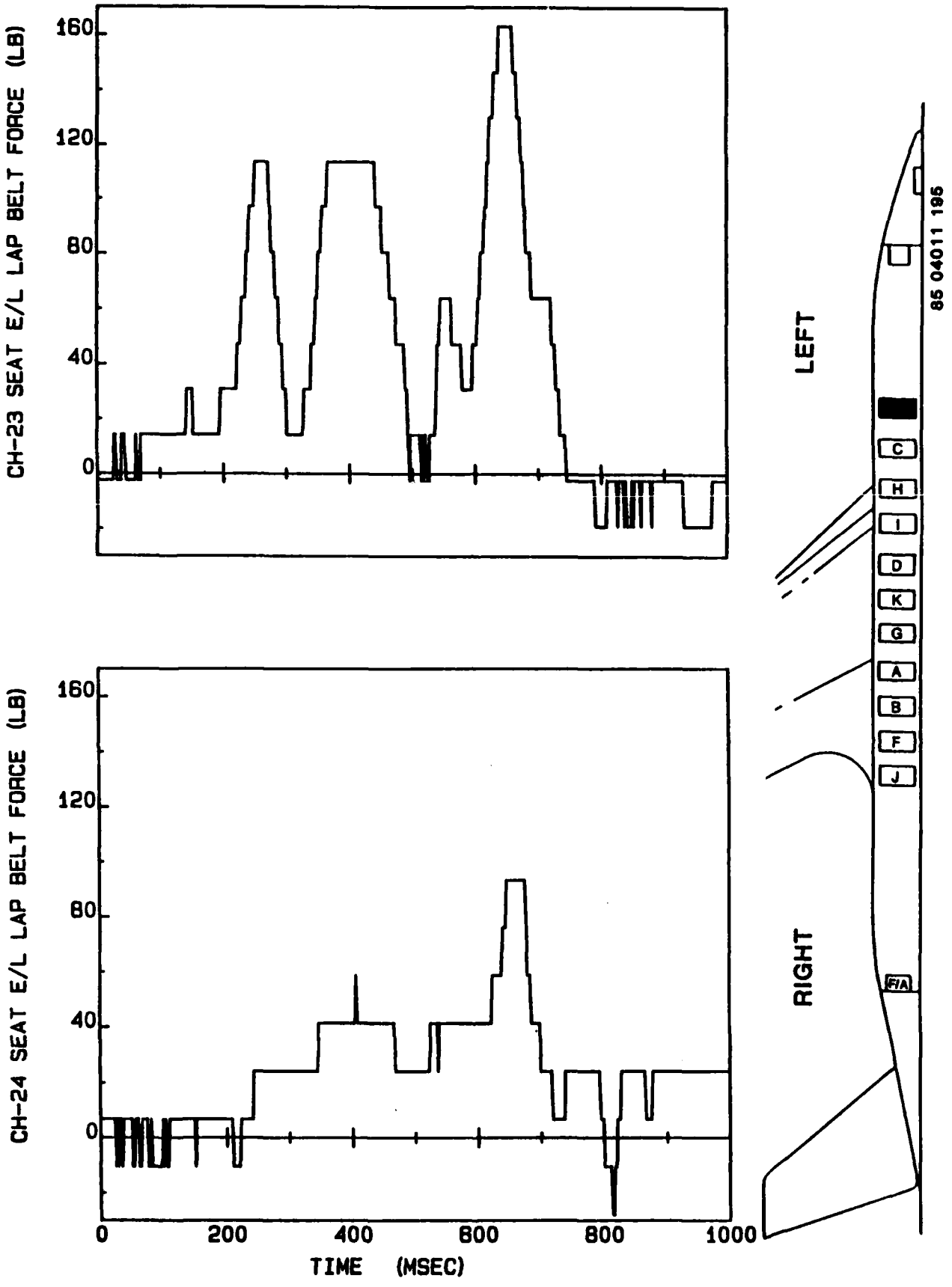

Figure E-3. Seat E/L.

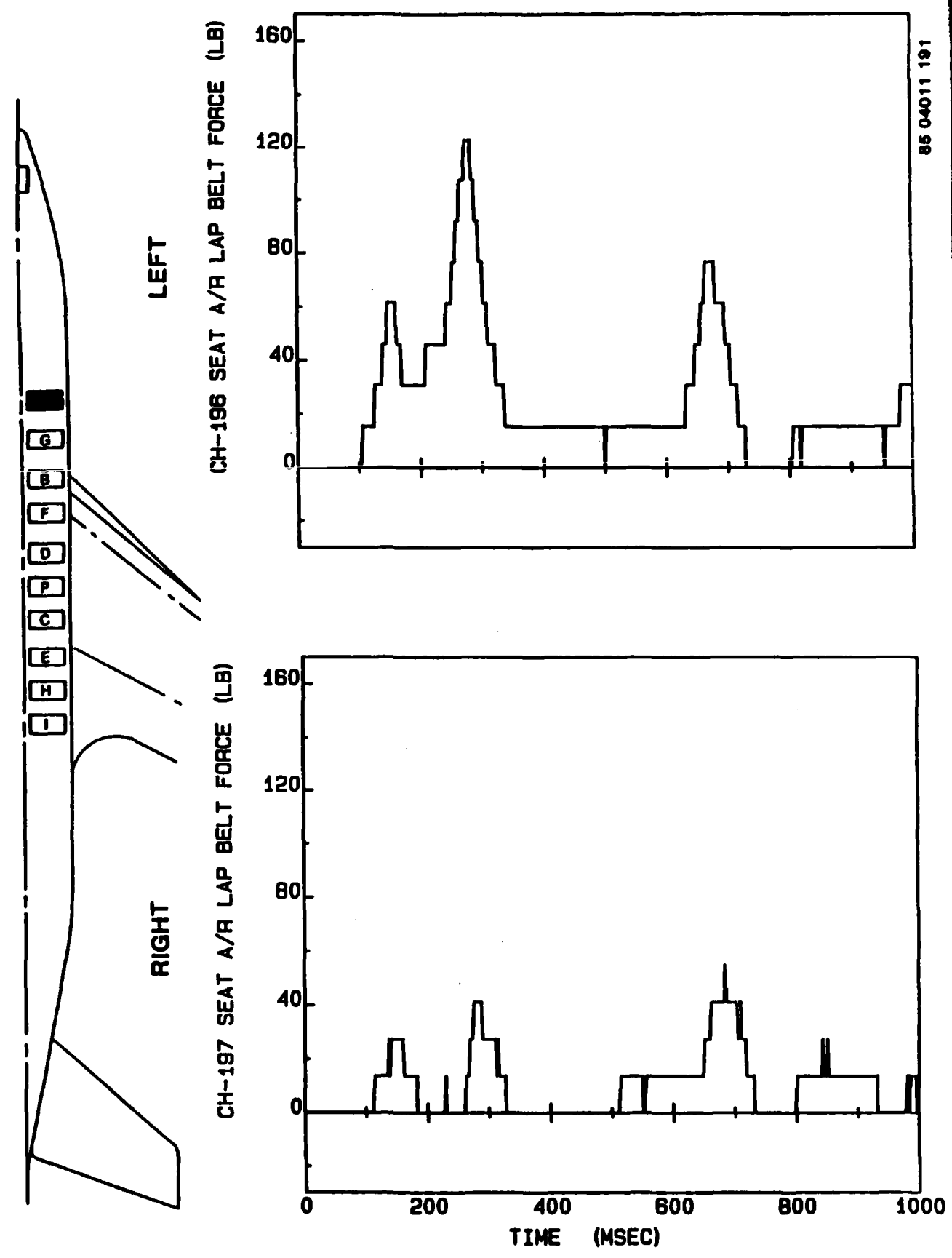

Figure E-4. Seat A/R.

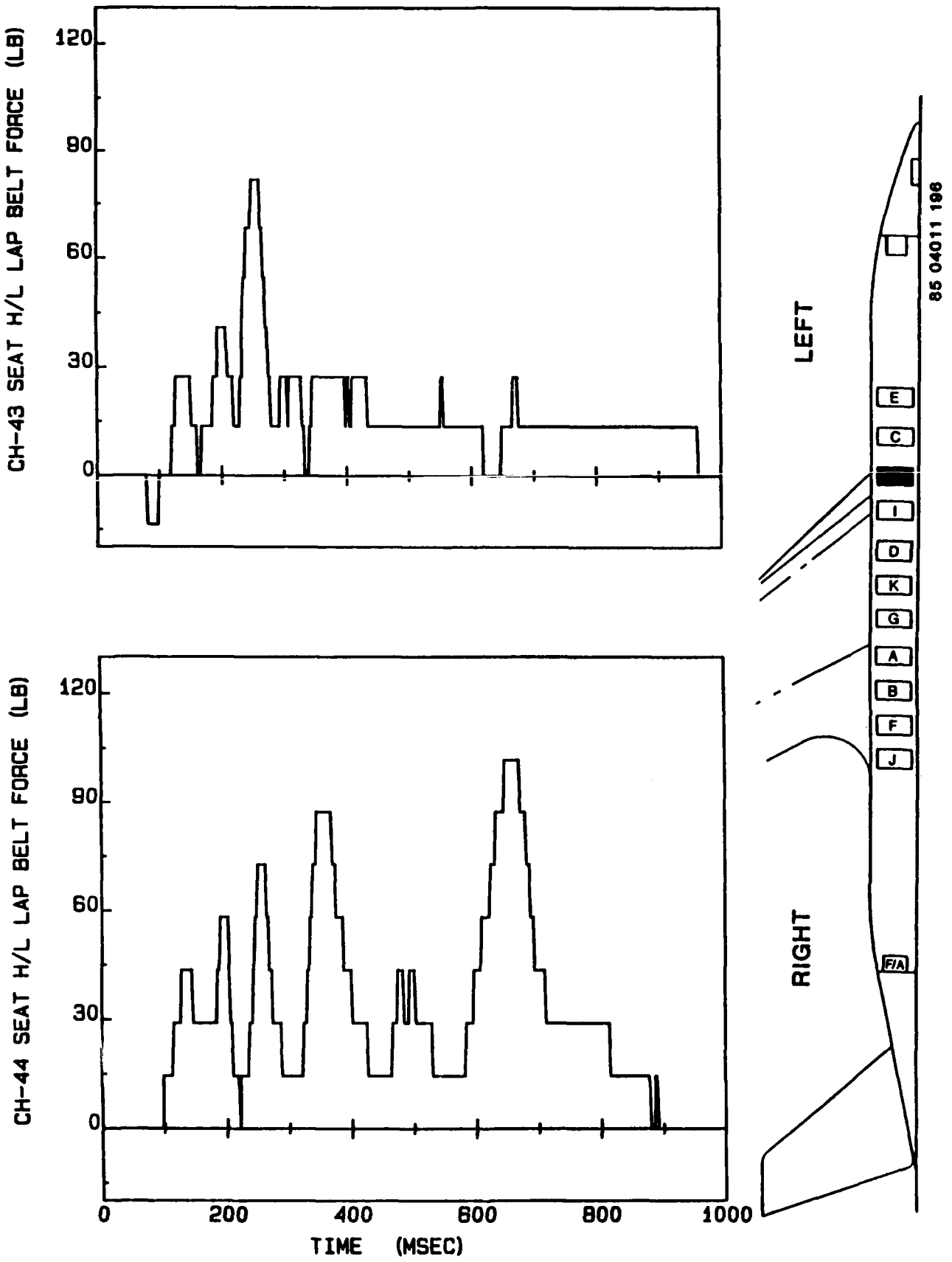

Figure E-5. Seat H/L.

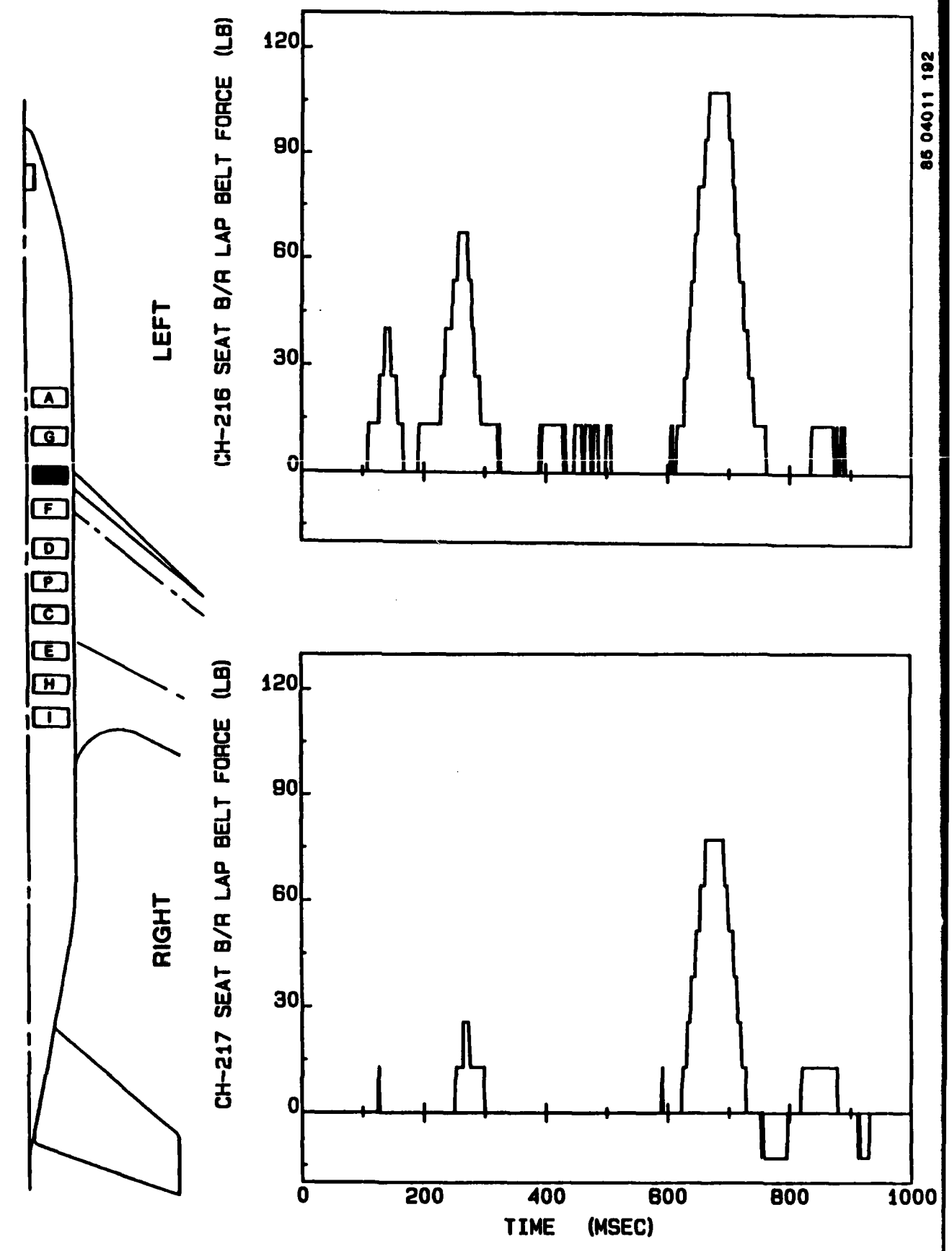

Figure E-6. Seat B/R.

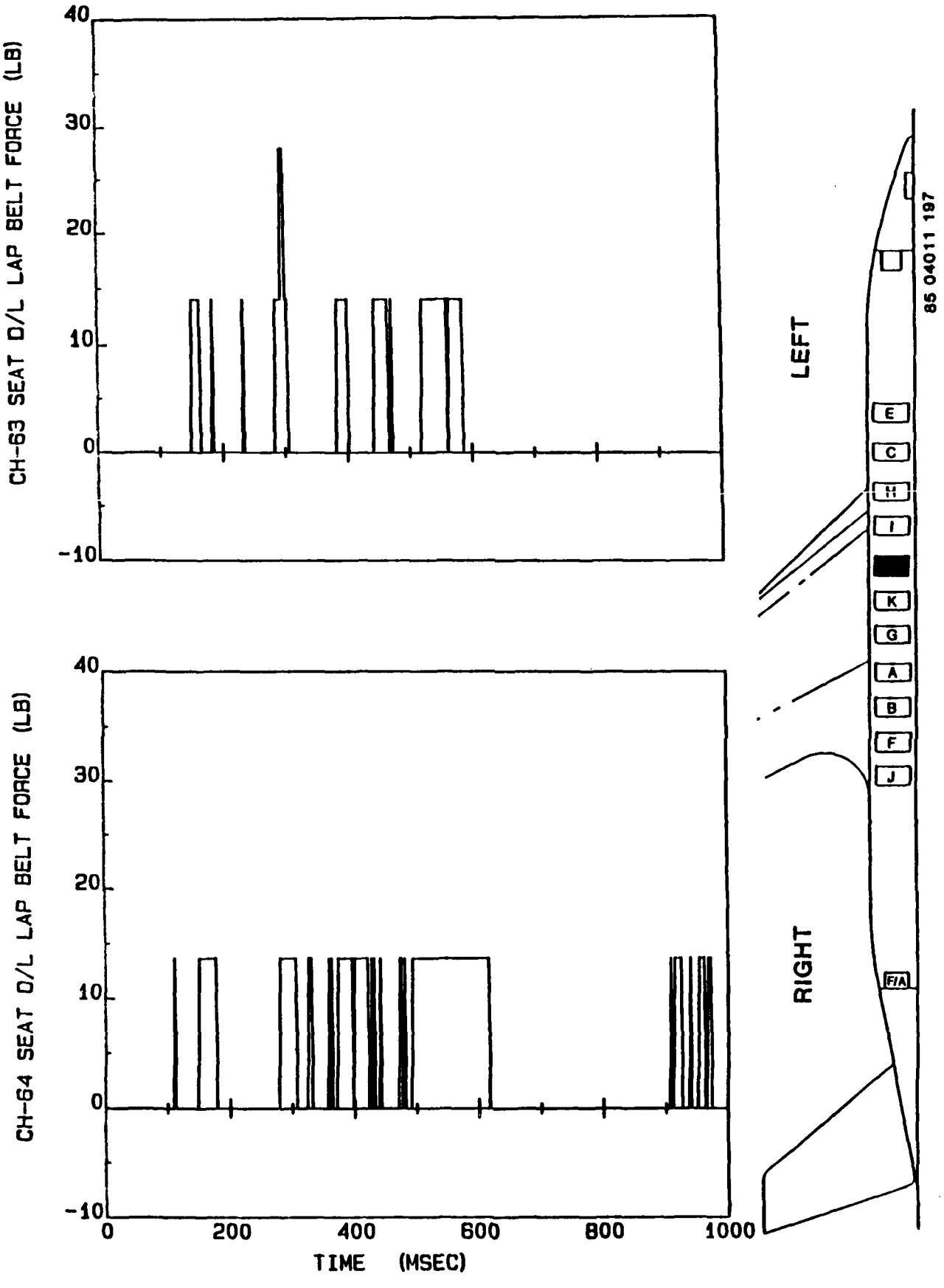

Figure E-7. Seat D/L.

THIS PAGE LEFT INTENTIONALLY BLANK.

AD-A172 245 SEAT EXPERIMENT RESULTS OF FULL-SCALE TRANSPORT AIRCRAFT CONTROLLED IMPAC (U) RMS TECHNOLOGIES INC TREVOSE PA M R CANNON ET AL JUL 86 TR-85413 3/3

UNCLASSIFIED DOT/FAA/TT-85/25 DTFA03-81-C-00040 F/G 1/3 NL

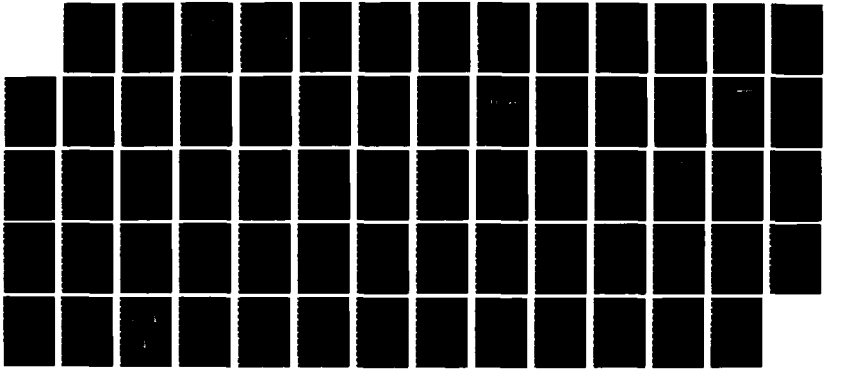

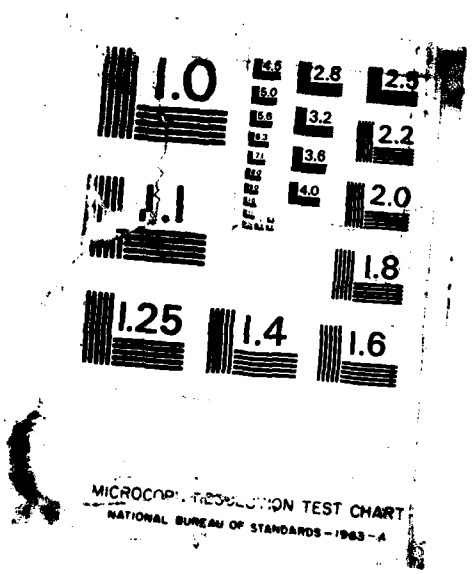
1.0
1.1
1.25
1.4
1.6
1.8
2.0
2.2
2.5
2.8
3.2
3.6
4.0
4.5
5.0
5.6
6.3
7.1
MICROCOPY RESOLUTION TEST CHART
NATIONAL BUREAU OF STANDARDS - 1963 - A

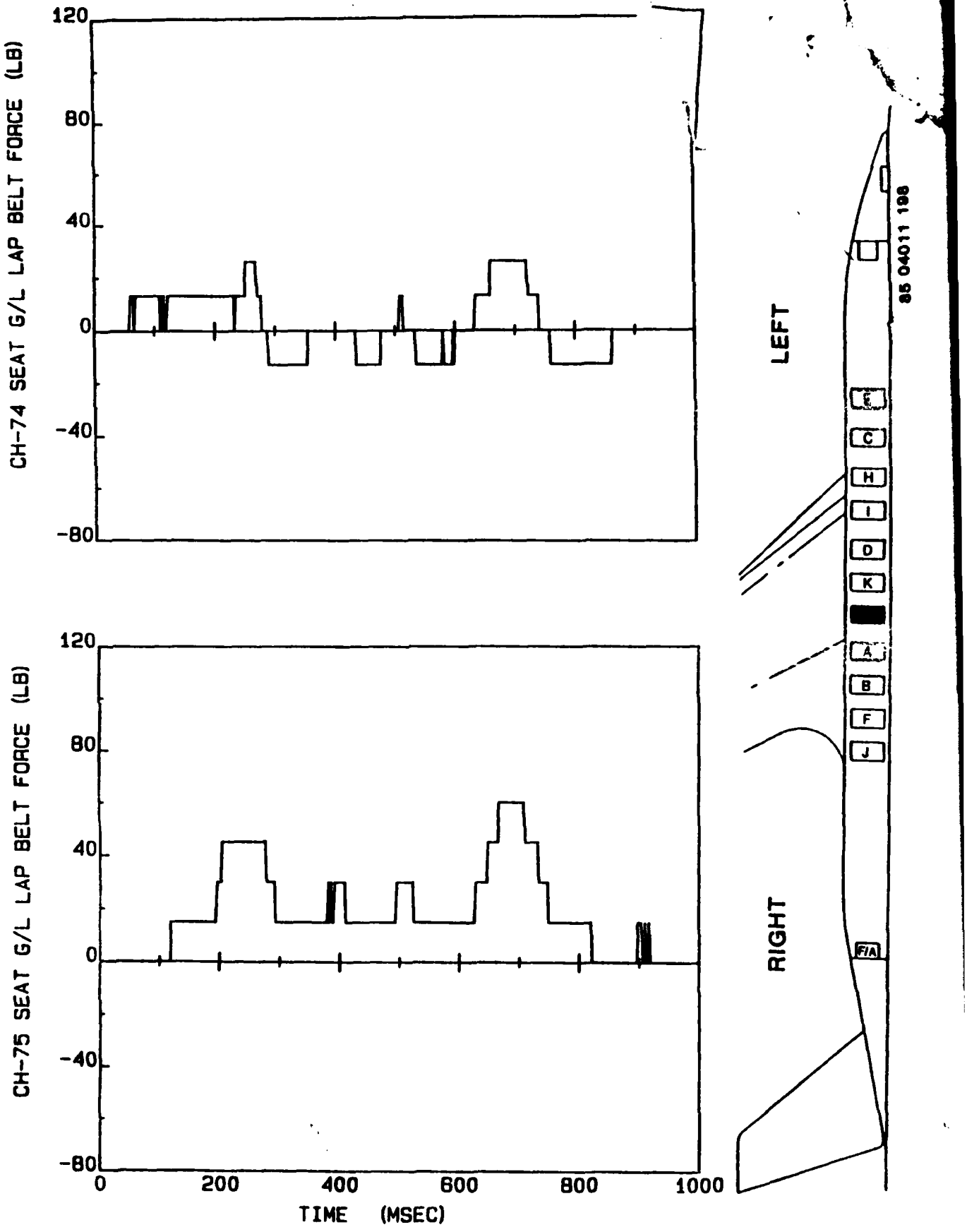

Figure E-8. Seat G/L.

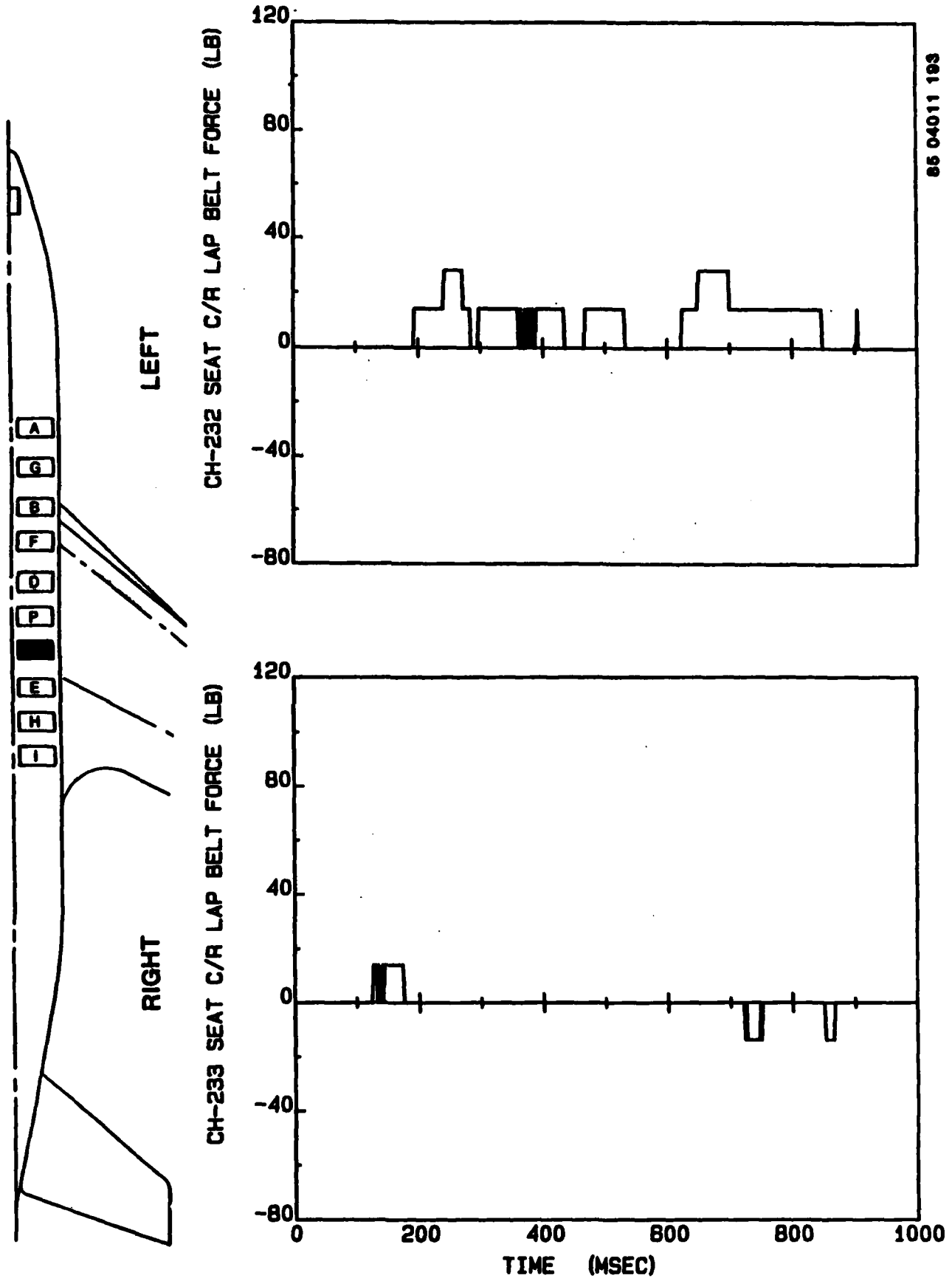

Figure E-9. Seat C/R.

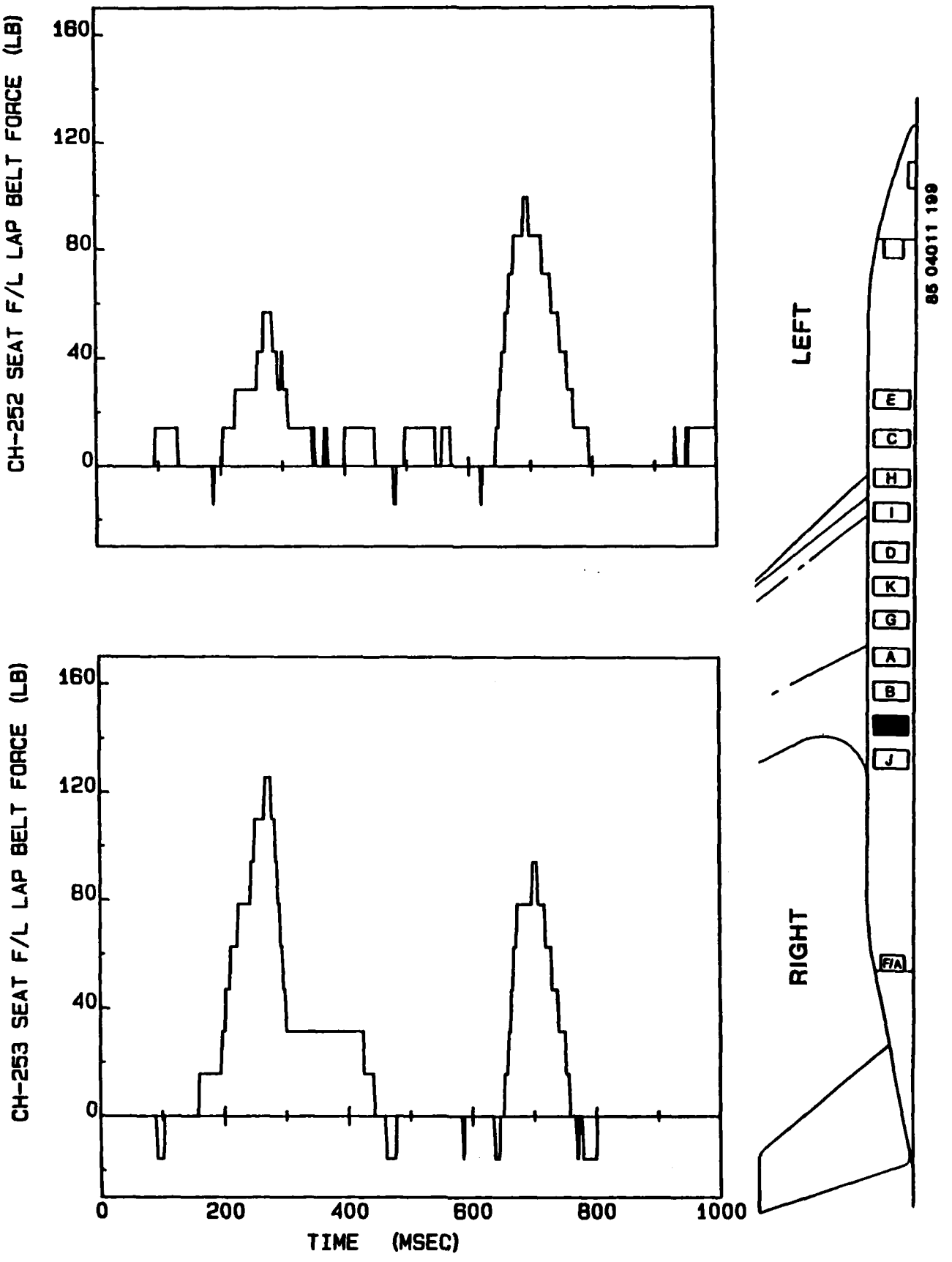

Figure E-10. Seat F/L.

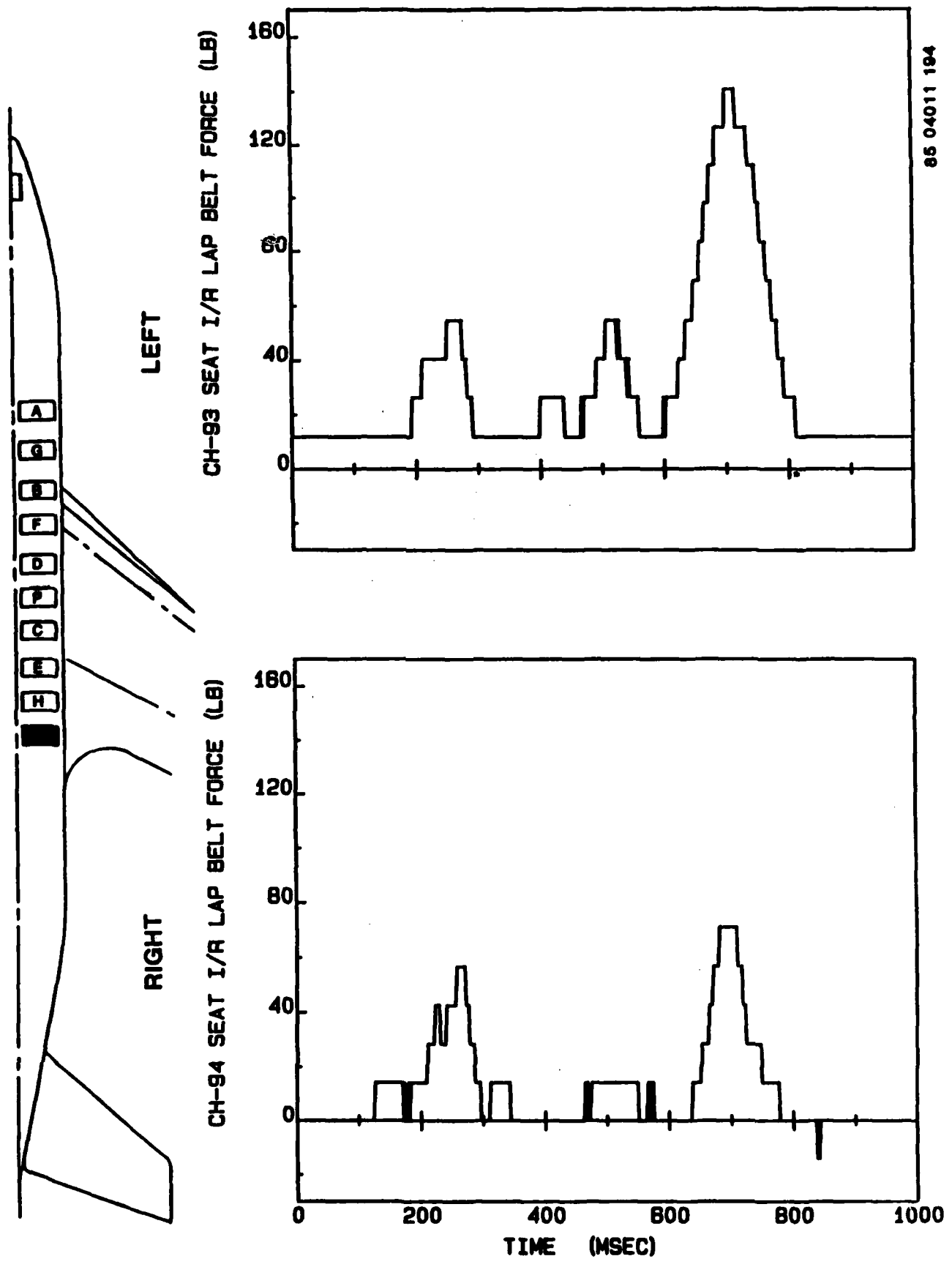

Figure E-11. Seat I/R.

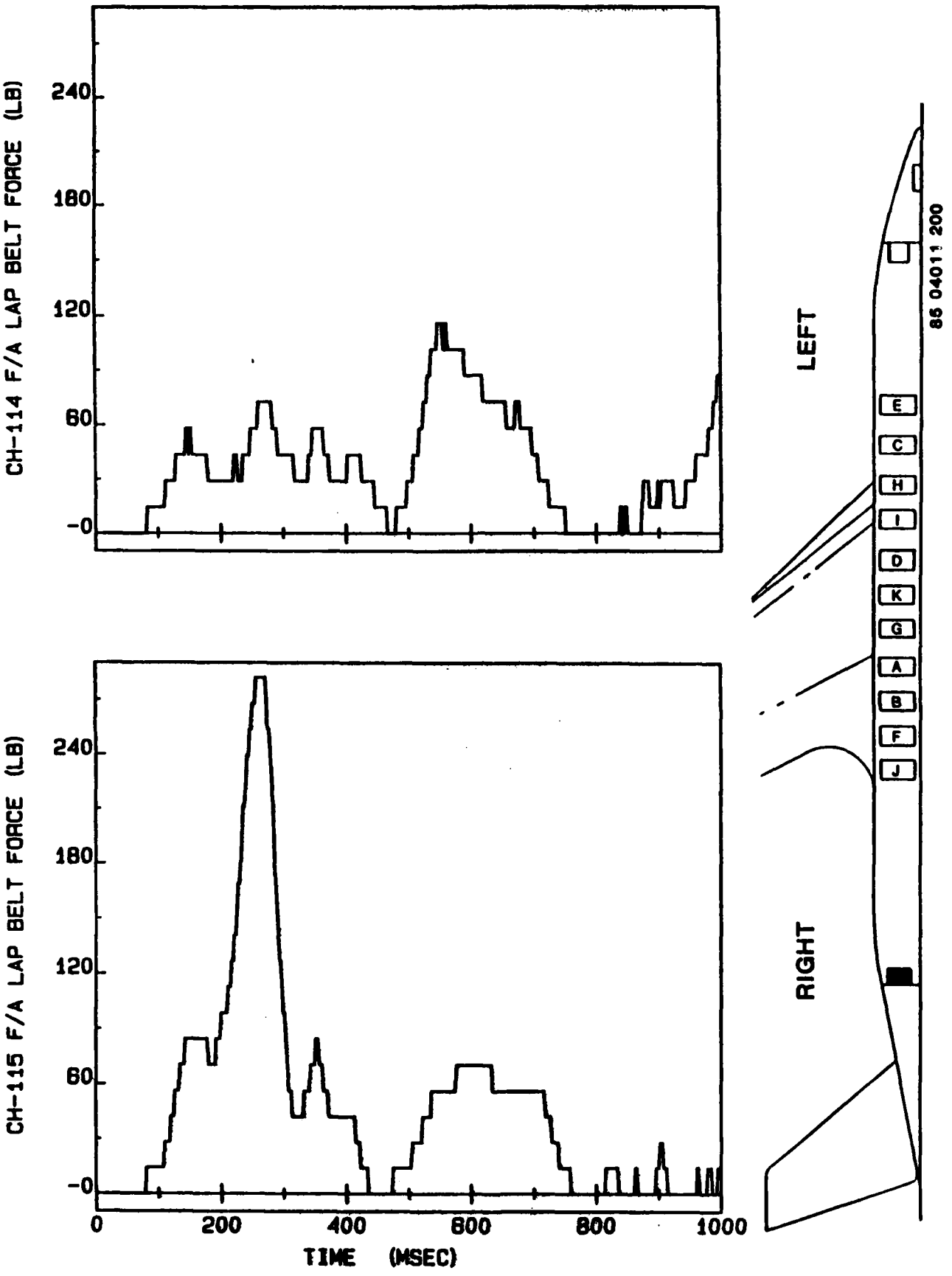

Figure E-12. Seat F/A.

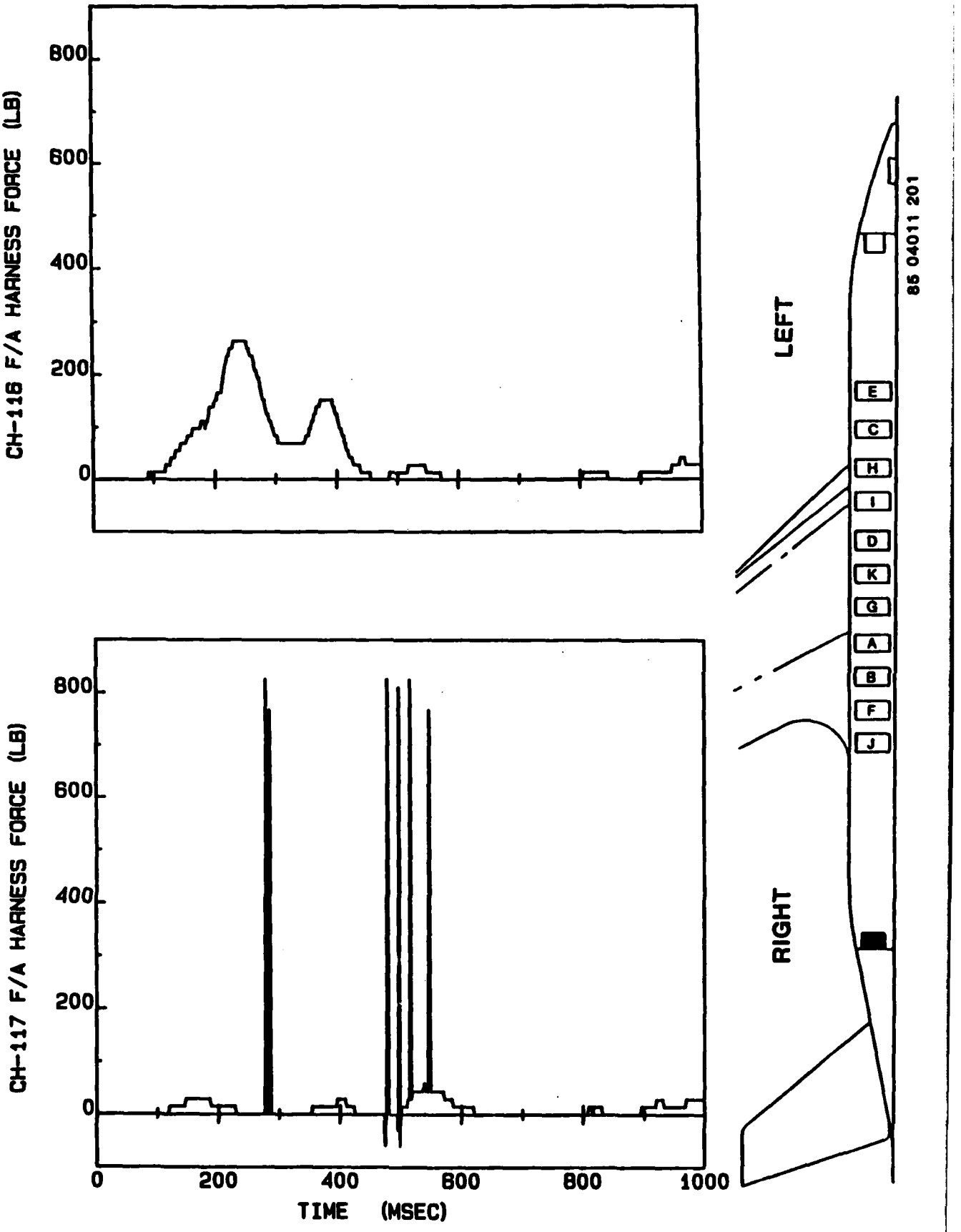

Figure E-13. Seat F/A - harness.

APPENDIX F

PROGRAM SOM-TA COMPUTER SIMULATIONS

1.0 INTRODUCTION

This appendix describes the computer modeling of two transport aircraft seats and their occupants in the Controlled Impact Demonstration (CID) crash test of a Boeing 720 aircraft, using Program SOM-TA (Seat Occupant Model - Transport Aircraft). Program SOM-TA was developed under the Federal Aviation Administration (FAA) sponsorship and permits simulation of a double- or triple-occupant seat, with up to three occupants, and includes other features appropriate for the transport seat environment. A brief description of Program SOM-TA is presented in Section 2.0 of this appendix.

The seats modeled were a Weberlite 4000 seat and a modified UOP 901 seat located in the right front and the left rear of the aircraft, respectively. These seats were chosen after careful review of the test data and seat design features indicated these aircraft locations as being the most suitable for SOM-TA simulation. Modeling of the occupants and seat structures is described in detail in Section 3.0 of this appendix.

The results of the computer simulation were compared with the available test data. After satisfactory correlation between available test data and SOM-TA simulations was obtained, the simulations were used to predict data not available from the test. The results of the computer simulations are presented in Section 4.0 of this appendix.

2.0 DESCRIPTION OF PROGRAM SOM-TA

Program SOM-TA (Seat/Occupant Model - Transport Aircraft) was developed for use in evaluating the crashworthiness of transport seats and restraint systems. It combines a three-dimensional dynamic model of the human body with a finite element model of the seat structure. The program allows simulation of one, two, or three passengers, of the same or different sizes. It is intended to provide the design engineer a tool with which he can analyze the structural elements of the seat as well as evaluate the dynamic response for the occupants during a crash.

The occupant model, shown in figure F-1, consists of 12 masses that represent the upper and lower torso, the arms, and legs. An optional model of the human body includes beam elements in the spine and neck, but is restricted to two-dimensional motion.

External forces are applied to the occupant by the cushions, floors, and restraint system. An interface between the occupant and seat is provided by the seat bottom cushion, back cushion, and an optional headrest. The restraint system can consist of a lap belt alone or can be combined with a single shoulder belt over either shoulder, or a double-strap shoulder harness. Each component of the restraint systems can be attached to either the seat or the aircraft structure.

For two standard occupants, a 50th-percentile human male and a 50th-percentile (Part 572), anthropomorphic dummy, all dimensions and inertial

properties required for simulation are stored within the program. For other percentile occupants, characteristics must be provided as input.

The seat structure is modeled using the finite element method of analysis, selected because it is not dependent on previous testing, and it has the flexibility to deal with a wide range of design concepts. Program SOM-TA seat analysis uses three-dimensional beam elements. It has the capability to model large displacements, nonlinear material behavior, local buckling, and various end release conditions for beam elements.

The digital computer program based on the occupant and seat models described previously has been written entirely in FORTRAN to ensure a high degree of compatibility with various computer systems. During its development, the program was run on IBM and Digital computer systems. Output data include occupant segment positions, velocities, and accelerations; restraint systems and cushion forces; injury criteria; and details of contact between the occupant and the seat in front. Seat output includes model displacements, element stresses, and forces at the points of attachment to the aircraft structure.

3.0 MODELING OF OCCUPANTS AND SEAT STRUCTURE

The seats modeled were a Weberlite 4000 seat and a modified UOP 901 seat. These seats were chosen after careful review of the CID test data, seat design features, and relative location in the aircraft. The location of both seats in the aircraft is shown in figure F-2. The Weberlite 4000 seat was located in position "A/R" in the right front of the aircraft. The modified UOP 901 seat was located in position "F/L" in the left rear of the aircraft.

3.1 OCCUPANT MODELING

The occupants in both seats were modeled using the properties of a 50th-percentile (Part 572) anthropomorphic dummy, for which all properties required for simulation are stored within the program. The plots of occupants seated in the Weberlite 4000 seat (Seat A/R) are shown in figures F-3 and F-4.

The seat pan cushion properties and occupant buttocks compliances are modeled using an exponential force-deflection relationship, shown in figure F-5. The lap belts were modeled using the properites for nylon webbing (figure F-6).

3.2 SEAT STRUCTURE MODELING

The seat structure of both seats was modeled using Program SOM-TA finite element analysis capability. SOM-TA has the capability to model large displacements, nonlinear material behavior, local buckling, and various end release conditions for beam elements.

3.2.1 Weberlite 4000 Seat Model

The finite element model of the Weberlite 4000 seat, shown in figure F-7, consists of 33 beam elements and 24 nodes. The seat is primarily of tubular construction. The beam elements used to model the seat structure included six

cross-section types of various shapes and two material properties corresponding to 4130 steel and 2024-T3 aluminum. Beam end release codes were also used to model moment and shear release at the required nodes.

The interface between the seat track fittings and the tracks were modeled using the appropriate boundary condition codes at these locations. The Weberlite 4000 seat track fitting design is typical of production transport seats. The rear fittings have two studs and a locking mechanism, and the front fittings have a single stud and no locking mechanism. These fittings were modeled using the following boundary conditions.

	Longitudinal Force	Transverse Force	Vertical Force	Pitch Moment	Roll Moment	Yaw Moment
Front Fittings	No	Yes	Yes	Yes	Yes	No
Rear Fittings	Yes	Yes	Yes	Yes	Yes	Yes

3.2.2 Modified UOP 901 Seat Model

The UOP 901 seat modeled was a modified version of the standard production design. The production design was modified to include a compressive energy absorber as shown in figure F-8. The seat track fittings were also replaced by track fittings of Simula Inc. design (figure F-9). These fittings were locked in both the front and rear legs and also provided moment release about the pitch and roll axes.

The finite element model of the modified UOP 901 seat, shown in figure F-10, consists of 41 beam elements and 32 nodes. The beam elements used to model the structure included eight cross-section types of various shapes and two material properties corresponding to 4130 steel and 2024-T3 aluminmum. Beam end release codes were also used to model the moment and shear releases at the required nodes.

The modified track fittings were modeled by the following boundary conditions:

	Longitudinal Force	Transverse Force	Vertical Force	Pitch Moment	Roll Moment	Yaw Moment
All Fittings	Yes	Yes	Yes	No	No	Yes

3.3 SIMULATION TIME INTERVAL

The time interval of primary interest was limited to 0 to 2 sec, corresponding to wing and fuselage ground impact, but not the impact with the wing cutting obstacles. The acceleration data in this time interval was carefully

reviewed and the simulation was limited to subintervals of the largest floor accelerations. This approach provided the best opportunity for correlation of test data with the simulations. The simulation time interval for the Weberlite 4000 seat (Seat A/R) was 300-700 msec, and for the modified UOP 901 seat (Seat F/L) 100-350 and 900-1050 msec.

The measured floor accelerations in the CID were approximated by a series of straight lines through up to 120 points for input to Program SOM-TA. Appropriate conversions in the signs of the accelerations were made to account for the different coordinate systems used in Program SOM-TA and for the CID data acquisition system. The two coordinate systems are shown in figure F-11. Forward direction is positive in both coordinate systems; however, vertical and lateral directions are reversed.

4.0 RESULTS OF THE COMPUTER SIMULATIONS

The results of the Program SOM-TA computer simulations were first compared with the available test data. After satisfactory correlation between the available test data and Program SOM-TA simulations was obtained, simulations were used to predict data not available from the CID.

For the Weberlite 4000 and modified UOP 901 seats, available test data included the following:

- Floor accelerations
- Center occupant pelvis accelerations
- Center occupant lap belt loads.

Program SOM-TA computes a number of indices that provide some indication of probability of injury. These include the Head and Chest Severity Index (SI), and the Dynamic Response Index (DRI) for the spine. A tolerable SI value of 1000 is accepted for frontal impact of the head, and a value of 1500 for distributed, or noncontact acceleration. DRI values of less than 20 are generally considered to cause no spinal injuries. All injury criteria were computed for both seats simulated.

4.1 WEBERLITE 4000 SEAT (A/R) SIMULATIONS

The floor accelerations in longitudinal (X), transverse (Y), and normal (Z) directions for the time interval (300-700 msec) simulated are shown in figure F-12. The sign convention used for these accelerations corresponds to the aircraft coordinate system as described in Section 3.3 of this appendix.

The center occupant pelvis accelerations predicted by Program SOM-TA simulations and measured in CID are presented in figure F-13. The pelvis accelerations predicted by Program SOM-TA, particularly in the vertical direction, have the same shape and peak values as the test data except for a phase shift. This level of correlation with the measured test data is typical of Program SOM-TA simulations. The acceleration data for the center occupant chest and head are not available from the CID data. The predicted accelerations for Program SOM-TA simulation of the center occupant chest and head are

presented in figures F-14 and F-15, respectively. The sign convention used for these accelerations corresponds to the coordinate system used in the Program SOM-TA as described in Section 3.3 of this appendix.

The center occupant lap belt loads measured in CID and predicted by Program SOM-TA simulations are presented in figure F-16. Measured lap belt loads are low in comparison to those predicted by Program SOM-TA. However, as shown in figure F-16, Program SOM-TA simulations of transport seat tests conducted in a laboratory environment correlate well with measured lap belt loads in the 500-1000 lb range.

The lap belt loads and acceleration data for the left and right occcupants are not available from the CID. The predicted accelerations and lap belt loads for these occupants are shown in figures F-16 through F-22.

The injury criteria computed for the center occupant in the Weberlite 4000 Seat (A/R) were very low. The maximum severity indices for the chest and head were 4.43 and 3.52, respectively. These are well below allowable SI of 1000. The DRI computed was 7.3, less than the allowable DRI of 20.

The plots of the occupant response at various times during the simulation are shown in figures F-23 and F-24. The occupant motion predicted by Program SOM-TA is very similar to the film footage from the cameras onboard the CID (B-720) aircraft.

Program SOM-TA simulations of the Weberlite 4000 seat (A/R) indicate that the impact did not produce any significant seat deformations. The internal loads predicted for the beam elements used to model the seat structure were all below those that will cause structural failures.

4.2 MODIFIED UOP 901 SEAT (F/L) SIMULATIONS

The floor accelerations in longitudinal (X), transverse (Y), and normal (Z) directions for the time intervals simulated (100-350 and 900-1050 msec) are shown in figure F-25. The sign convention used for these accelerations corresponds to the aircraft coordinate systems as described in Section 3.3 of this appendix.

The center occupant pelvis accelerations measured in CID and predicted by Program SOM-TA simulations are presented in figure F-26. The acceleration data for the center occupant head and chest are not available from the CID data. The predicted accelerations from Program SOM-TA simulations for the center occupant chest and head are presented in figures F-27 and F-28. The acceleration data for the left and right occupants are not available from the CID. The predicted accelerations for these occupants are shown in figures F-29 through F-34. The sign convention for the accelerations in figures F-27 through F-34 corresponds to the coordinate system used in Program SOM-TA as described in Section 3.3 of this appendix.

The injury criteria computed for the center occupant in the modified UOP 901 seat (F/L) were very low. The maximum severity indices for the chest and head were 2.67 and 3.61, respectively. These are well below the allowable SI of 1000. The DRI computed was 3.9, less than the allowable DRI of 20.

The plots of the occupant response at various times during the simulations are shown in figures F-35 and F-36. The occupant motion predicted by Program SOM-TA is very similar to the film footage from the cameras onboard the CID (B-720) aircraft.

Program SOM-TA simulations of the modified UOP 901 seat (F/C) and the CID test data indicate that the impact did not produce any significant seat deformations. The internal loads for the beam elements used to model the seat structure were all below those that will cause any structural failures.

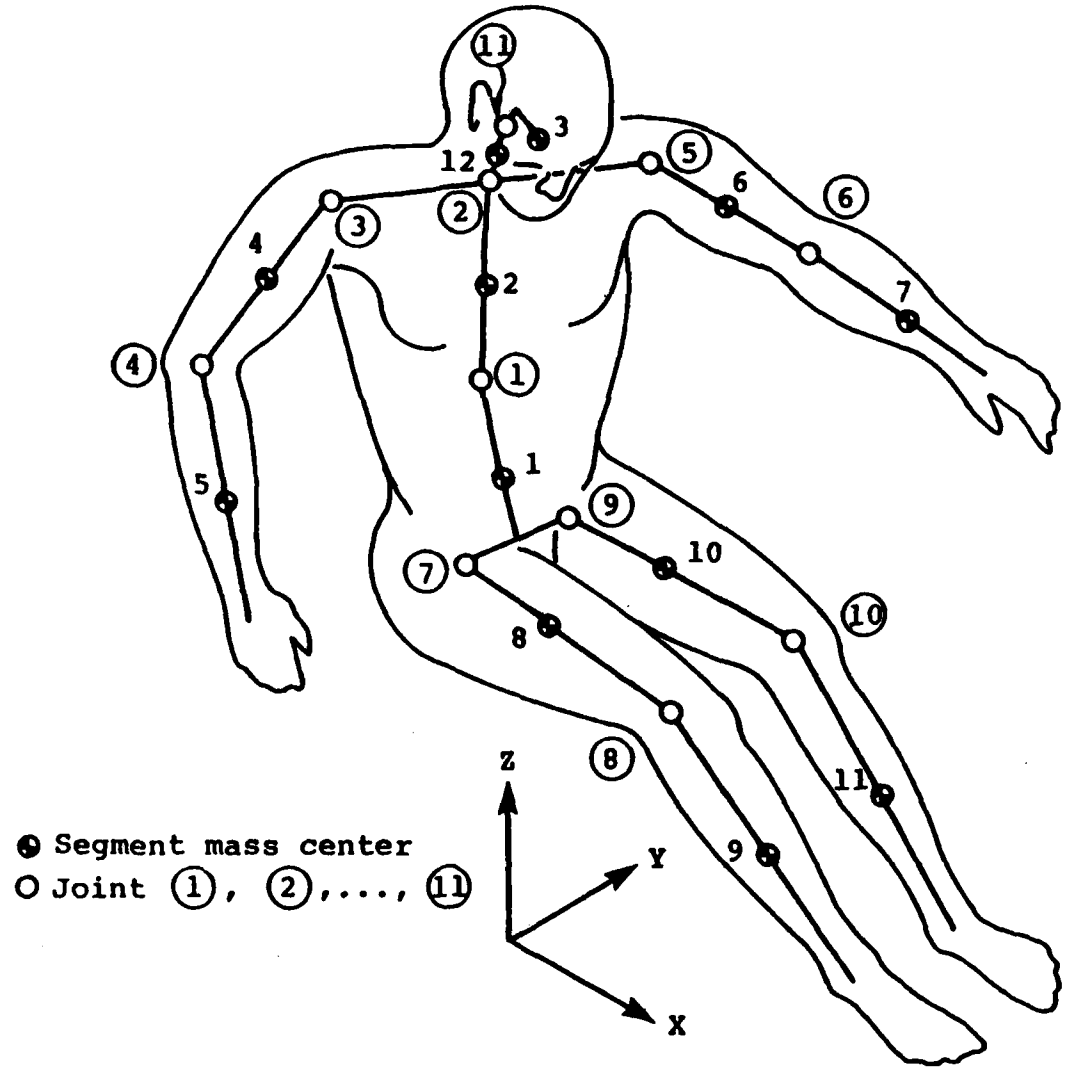

Figure F-1. Program SOM-TA three-dimensional occupant model.

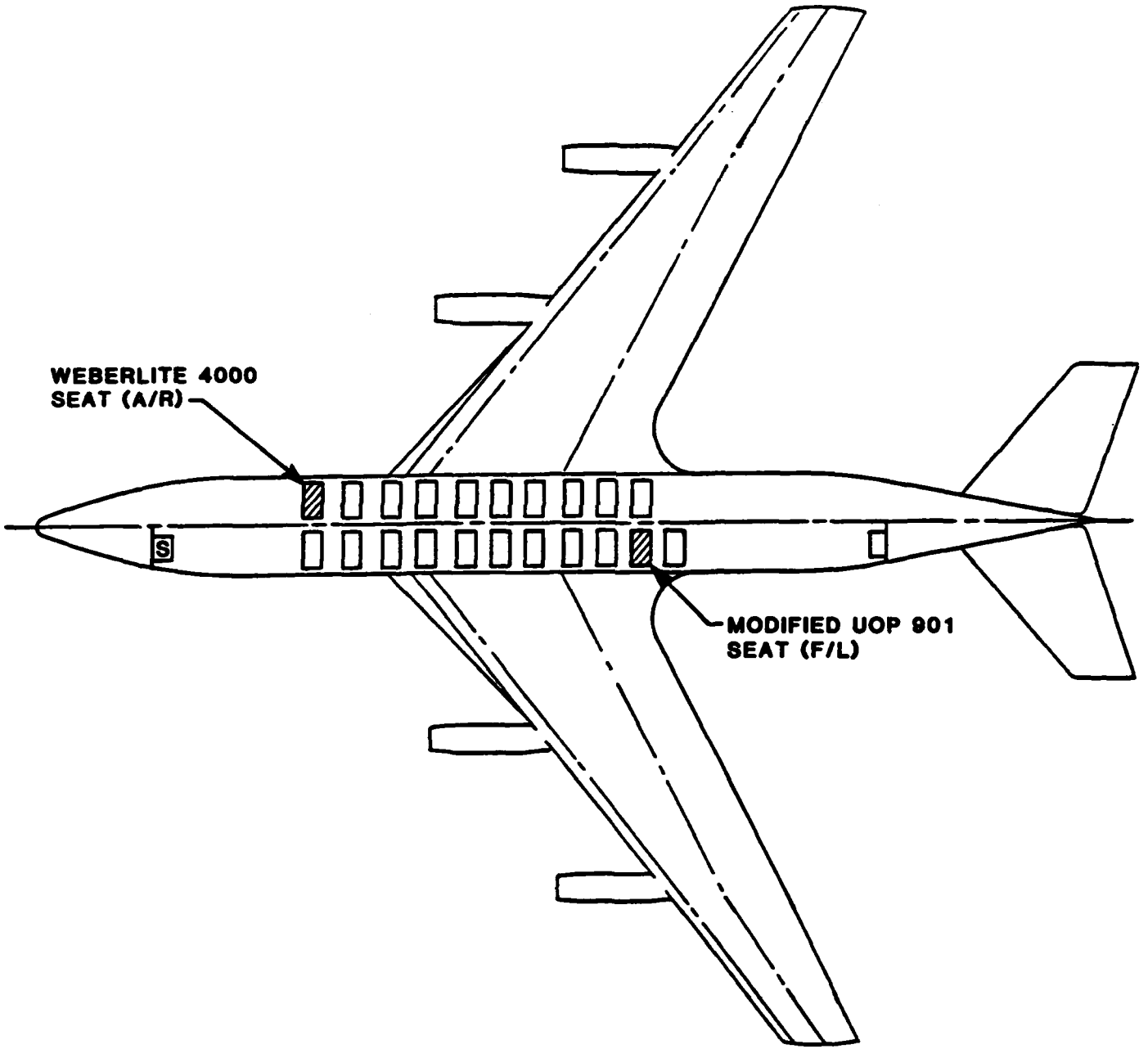

Figure F-2. Locations of the Weberlite 4000 seat (A/R) and the modified UOP 901 seat (F/L) in the CID B-720 aircraft.

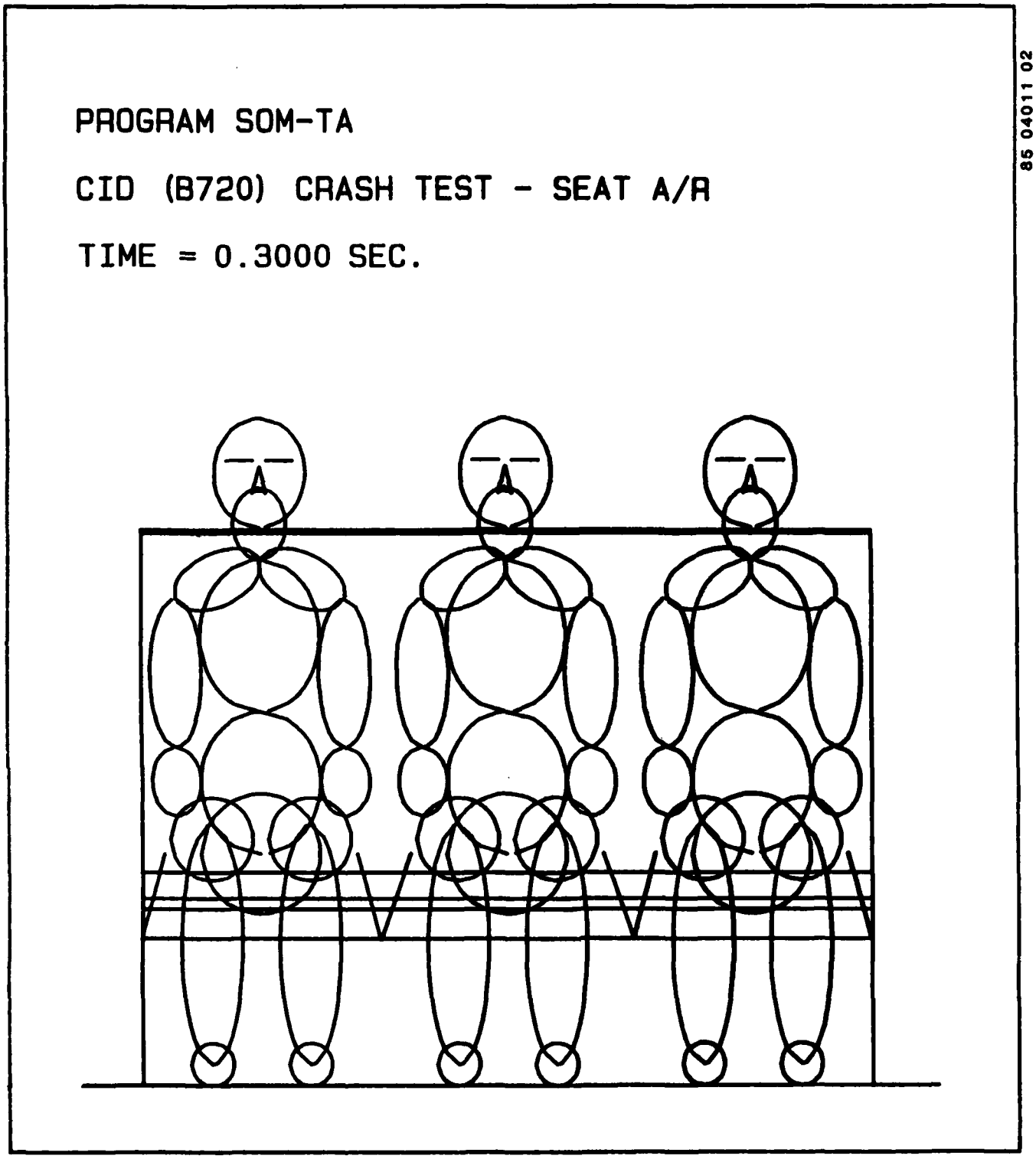

Figure F-3. Weberlite 4000 seat (A/R) occupant model plots (front view).

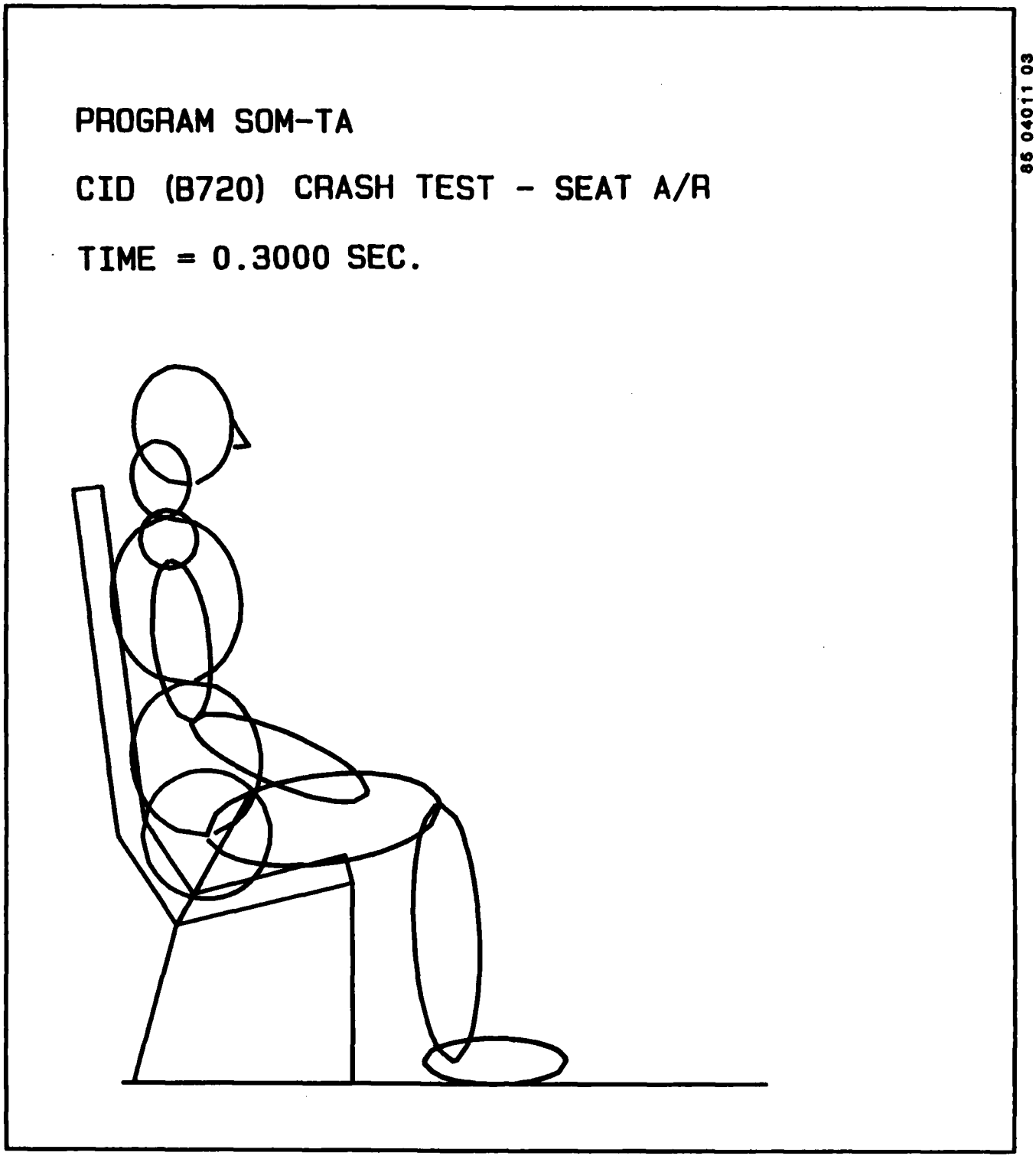

Figure F-4. Weberlite 4000 seat (A/R) occupant model plots (side view).

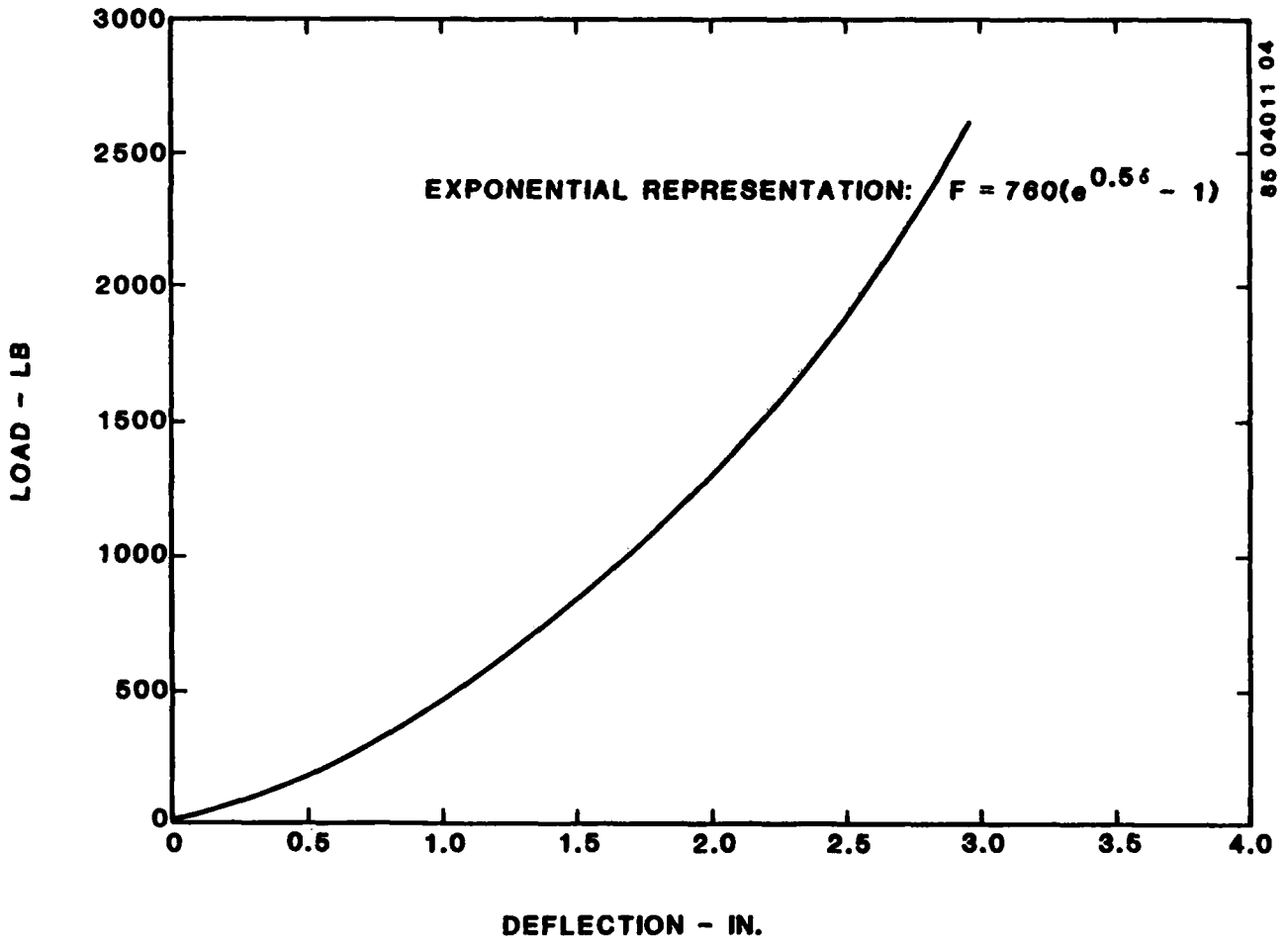

Figure F-5. Load-deflection curve for the seat cushions and dummy buttocks and pelvis.

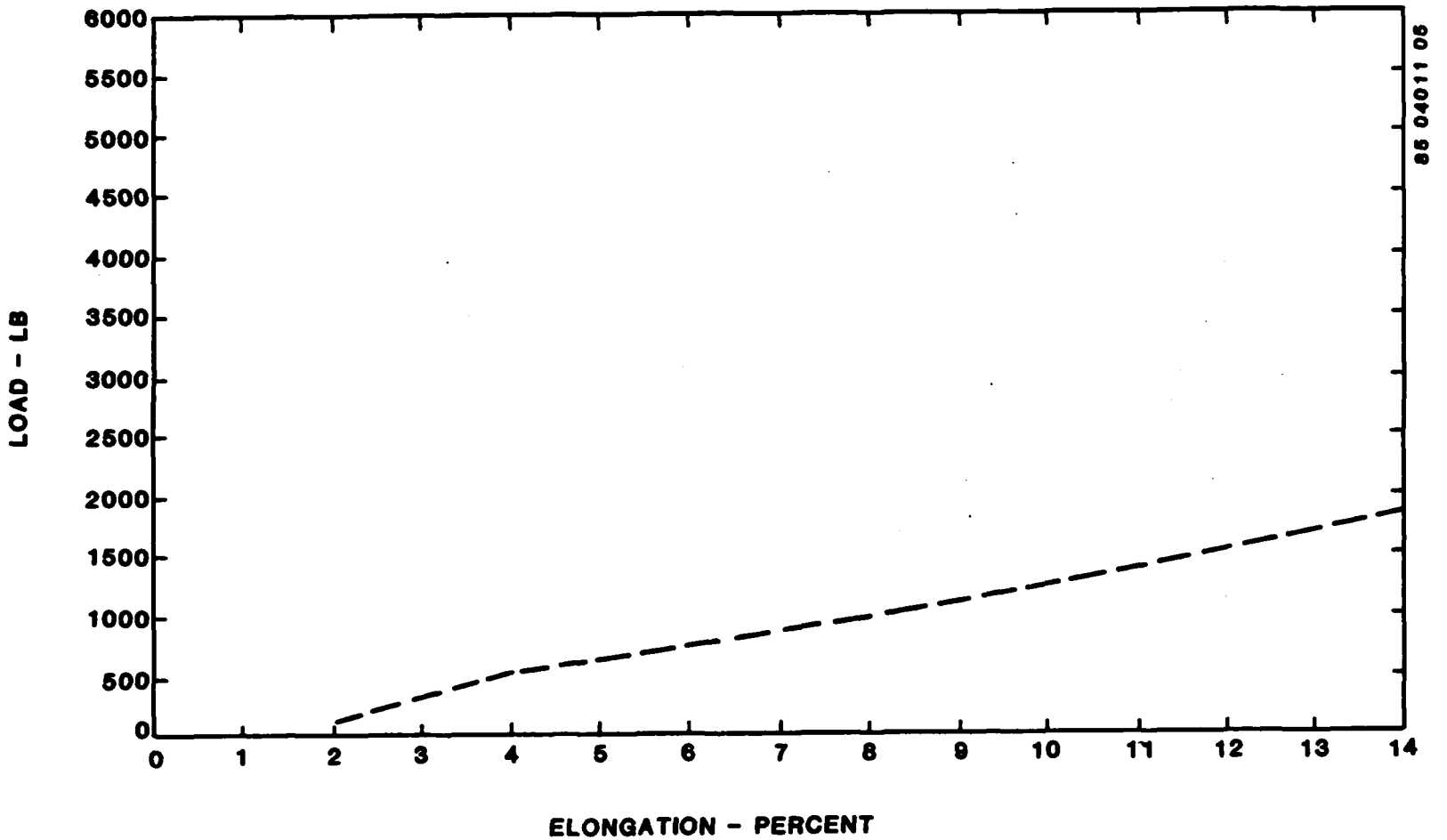

Figure F-6. Load-elongation characteristics for the lap belt nylon webbing.

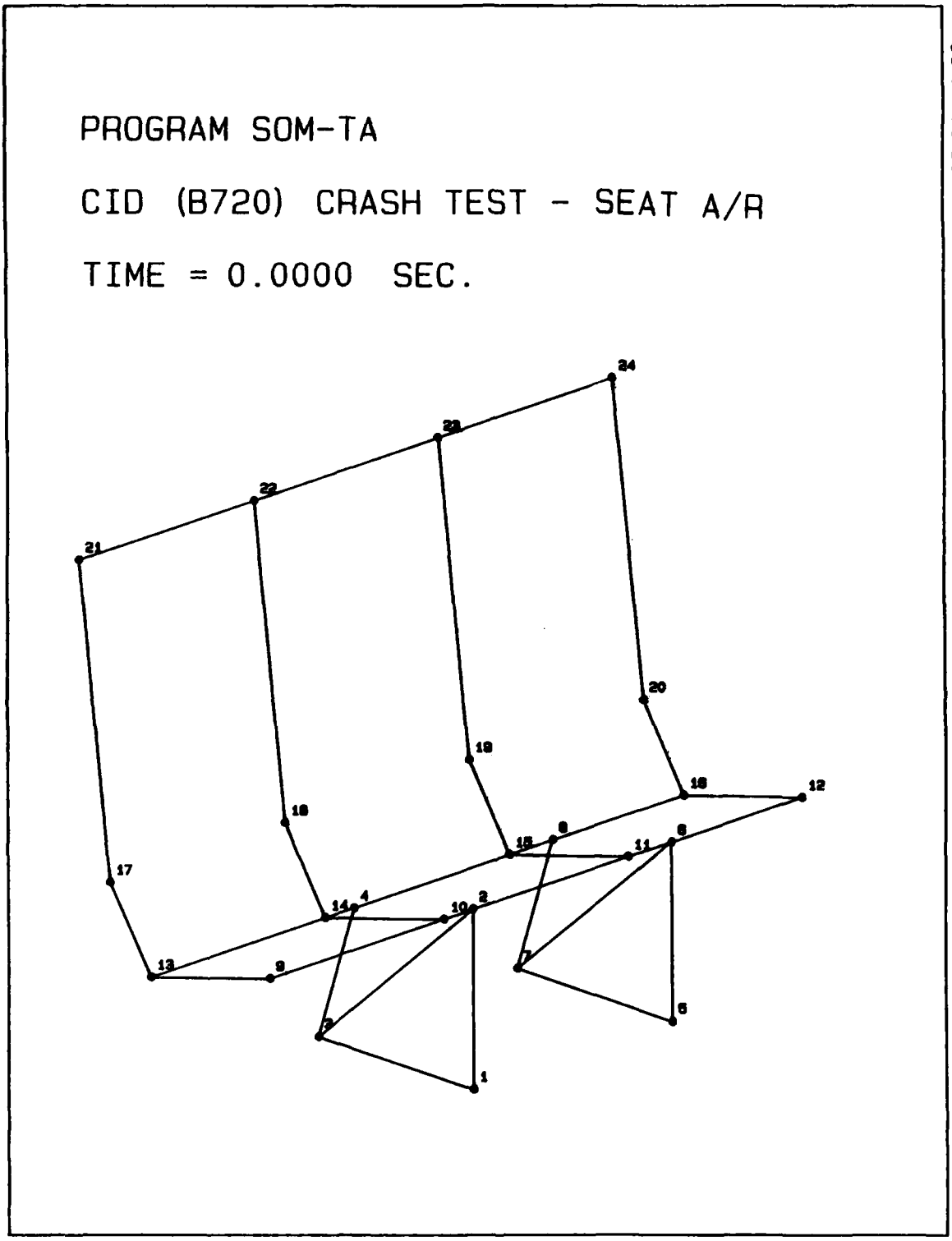

Figure F-7. Weberlite 4000 seat (A/R) finite element model.

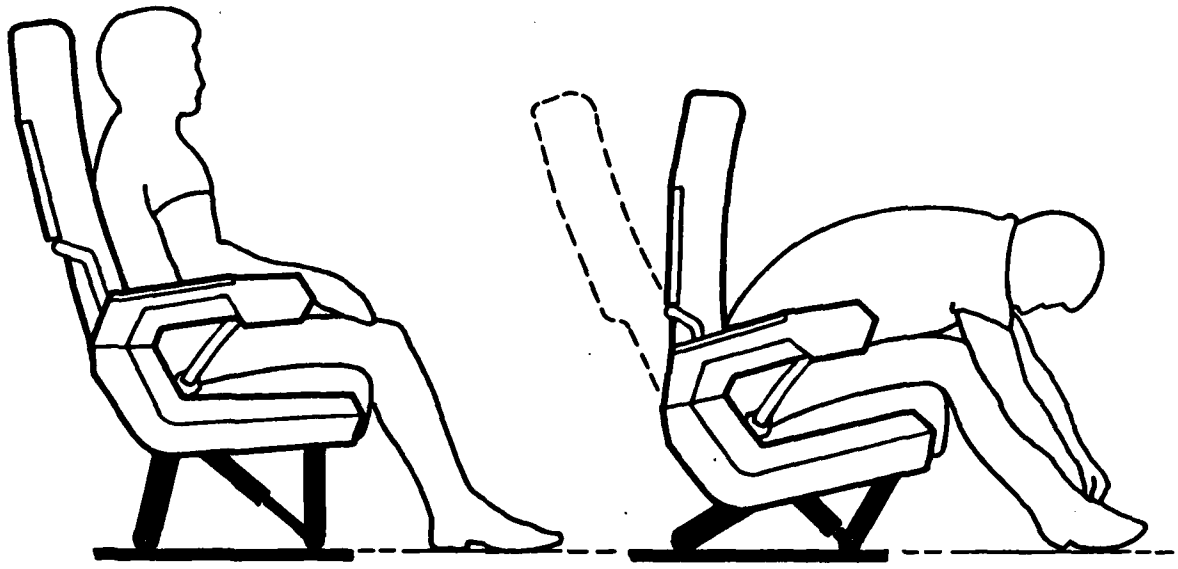

84 01004 36

Figure F-8. Modified UOP 901 seat (F/L) before and after stroking of the diagonal compressive energy absorbers.

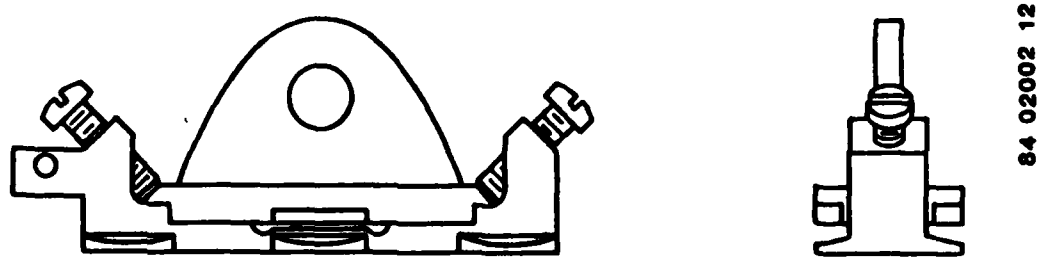

84 02002 12

Figure F-9. Simula Inc. track fitting design used on the modified UOP 901 seat (F/L).

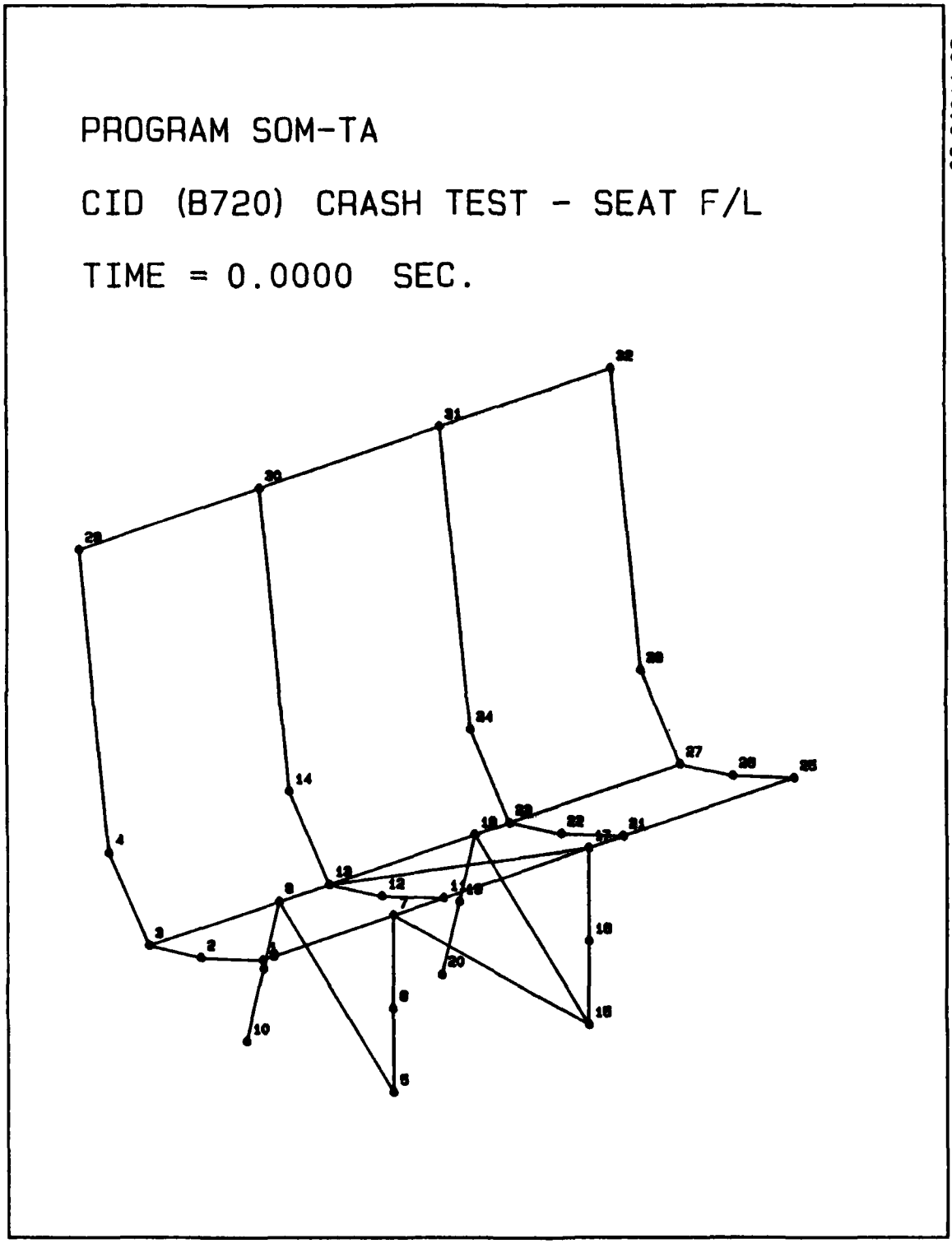

Figure F-10. Modified UOP 901 seat (F/L) finite element model.

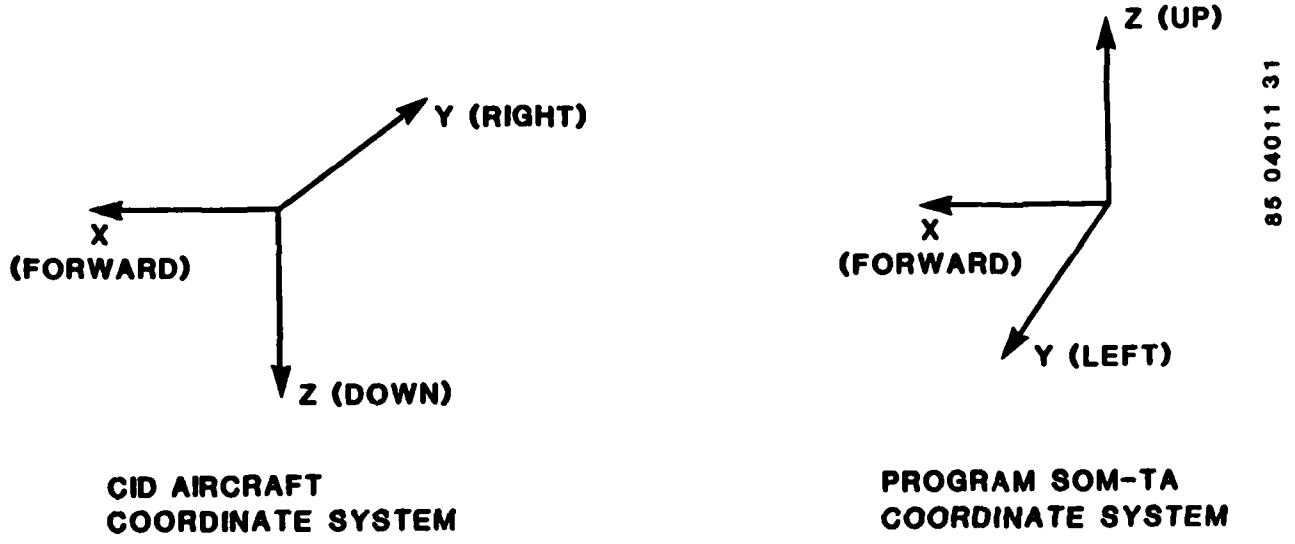

Figure F-11. The coordinate systems used in Program SOM-TA and CID data acquisition system.

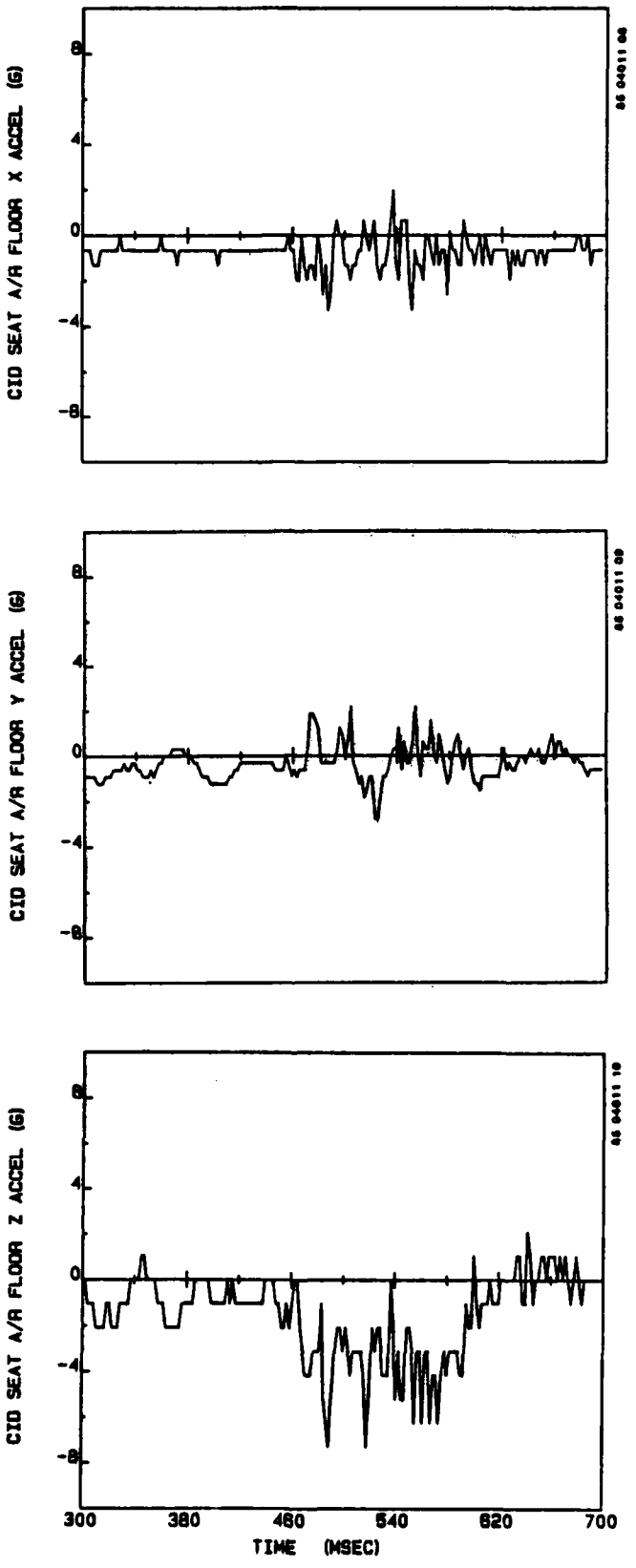

Figure F-12. Weberlite 4000 seat (A/R) floor accelerations.

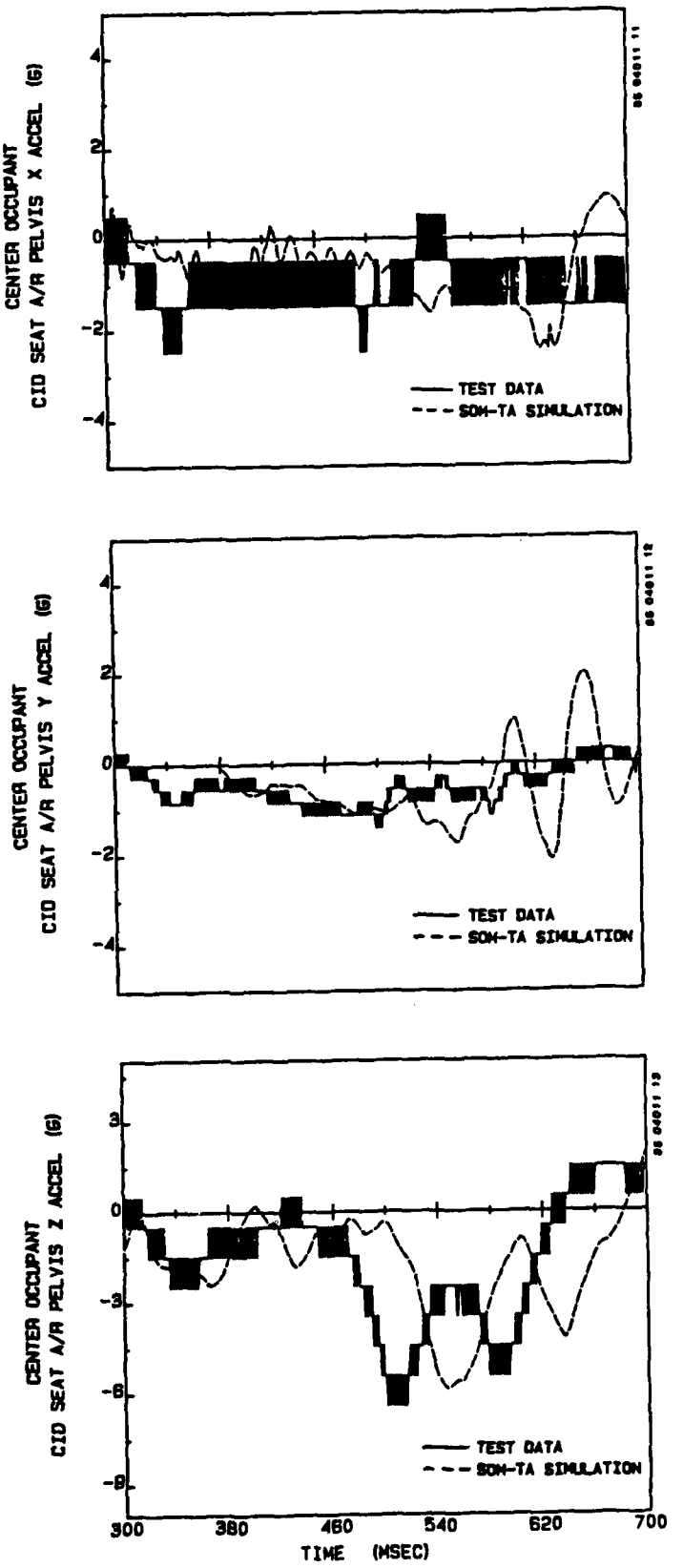

Figure F-13. Weberlite 4000 seat (A/R) center occupant pelvis accelerations.

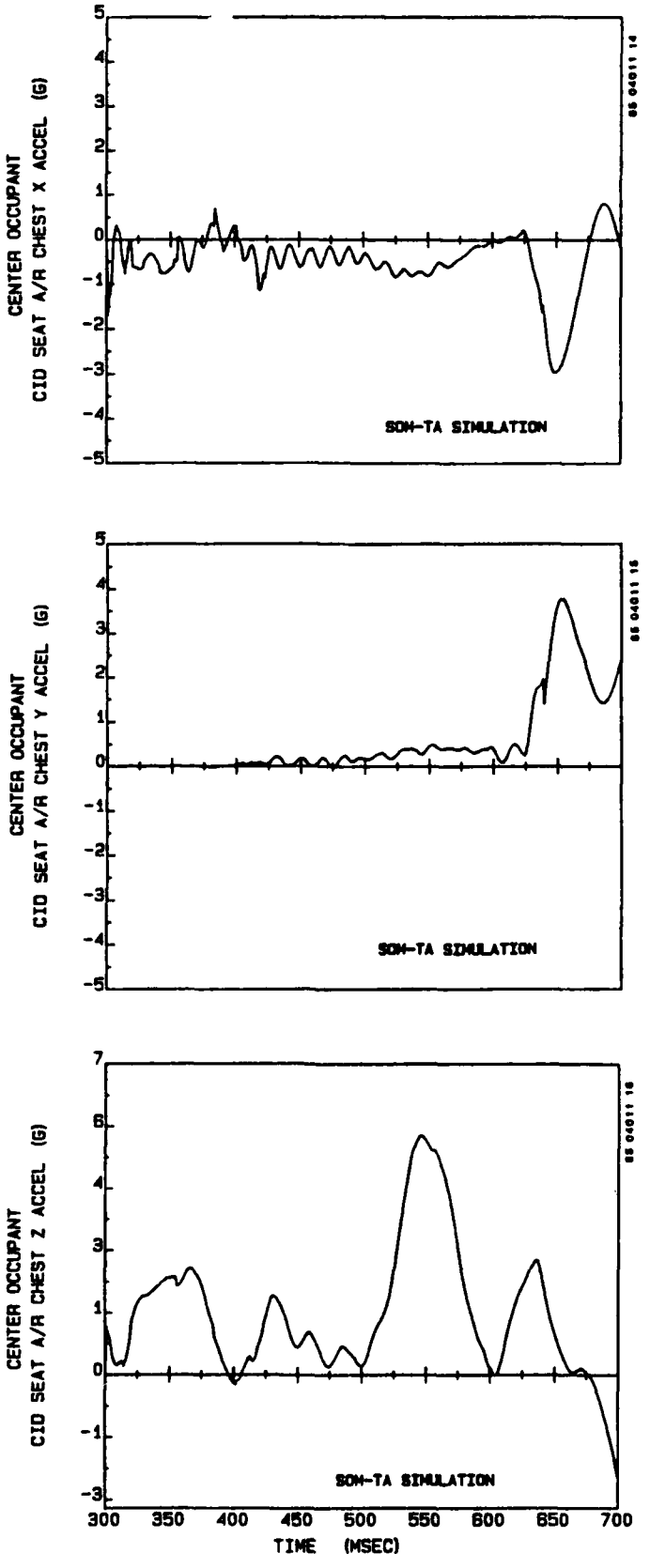

Figure F-14. Weberlite 4000 seat (A/R) center occupant chest accelerations.

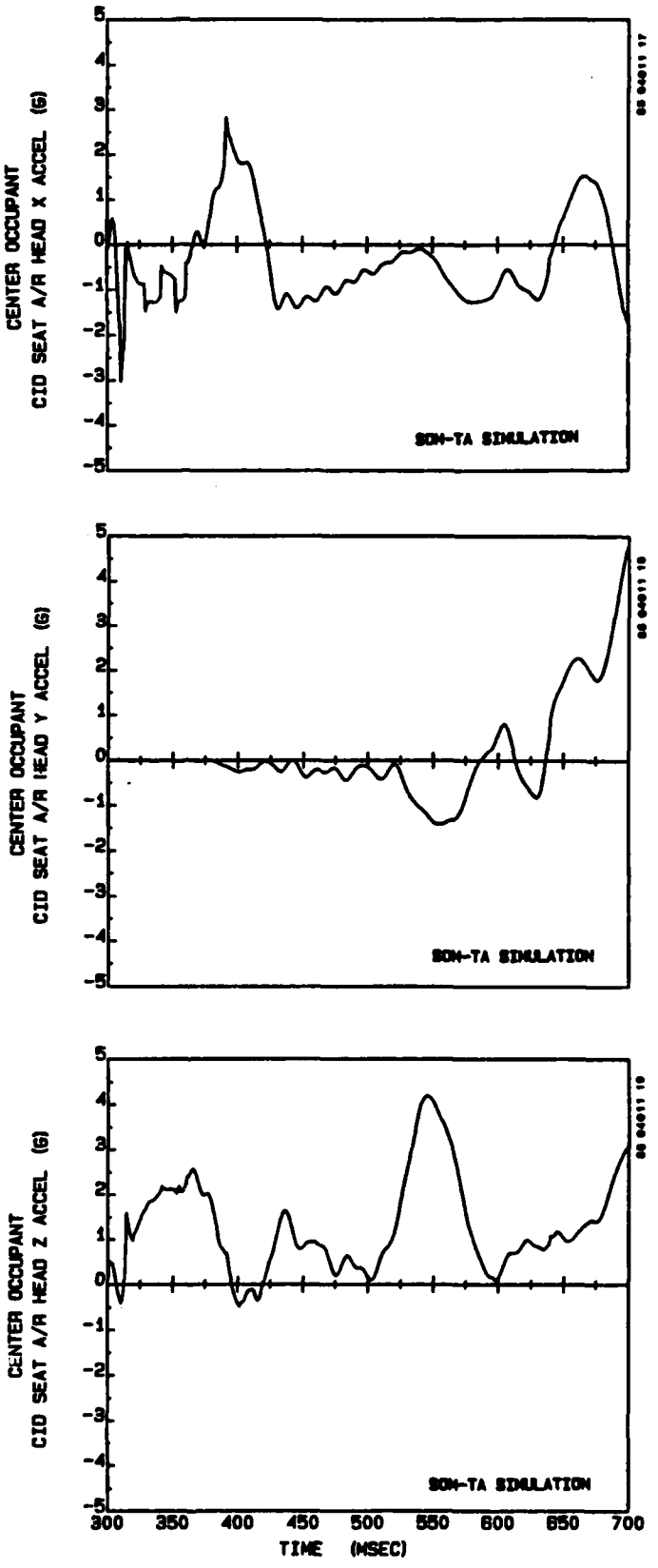

Figure F-15. Weberlite 4000 seat (A/R) center occupant head accelerations.

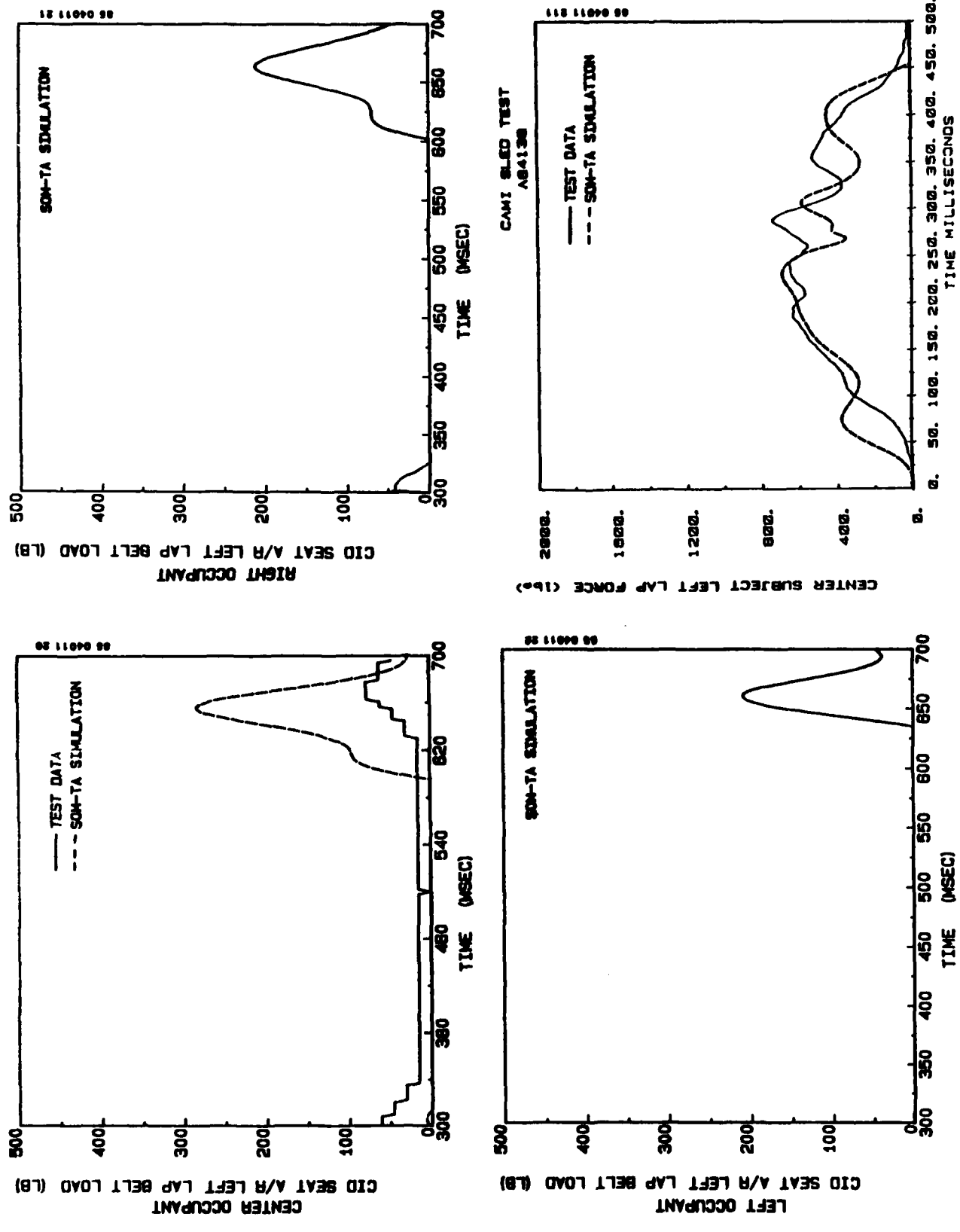

Figure F-16. CID Weberlite 4000 seat (A/R) and CAMI sled test A84138 (UOP 901 Seat) lap belt loads.

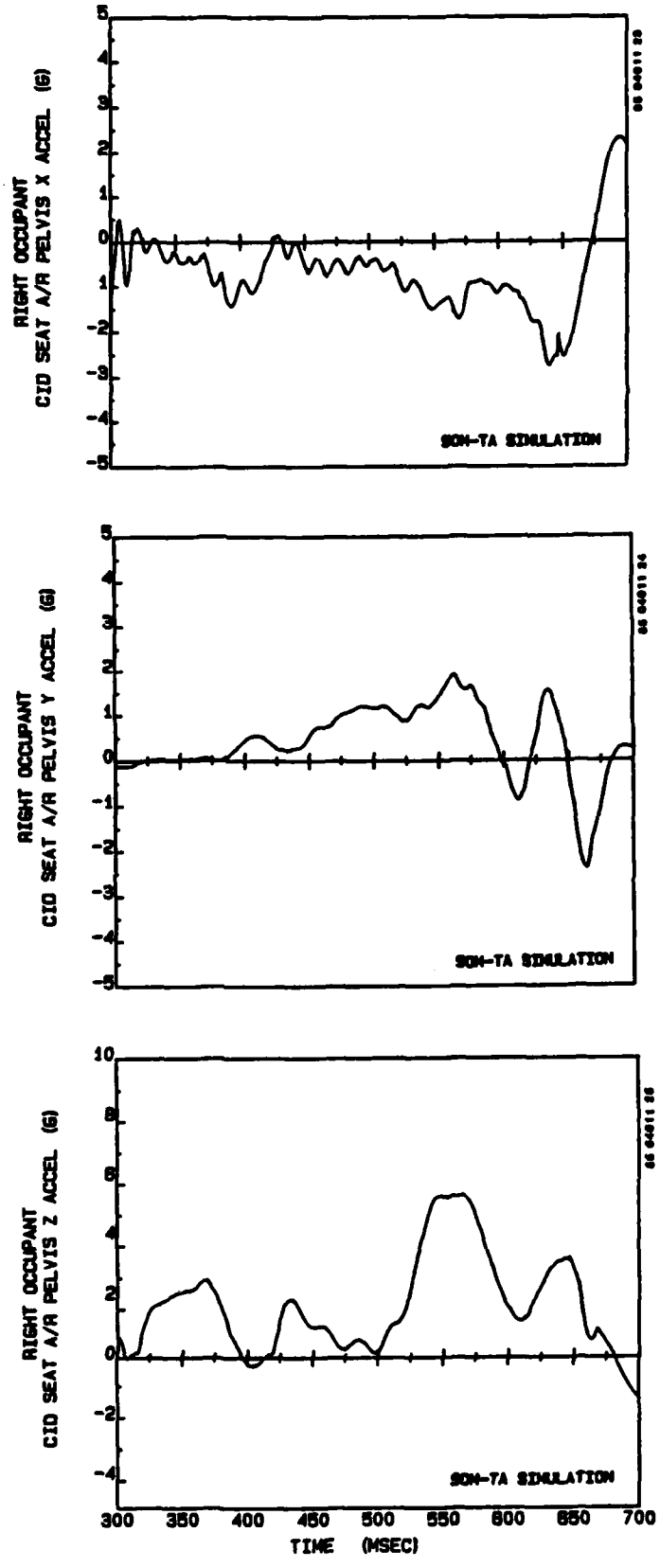

Figure F-17. Weberlite 4000 seat (A/R) right occupant pelvis accelerations.

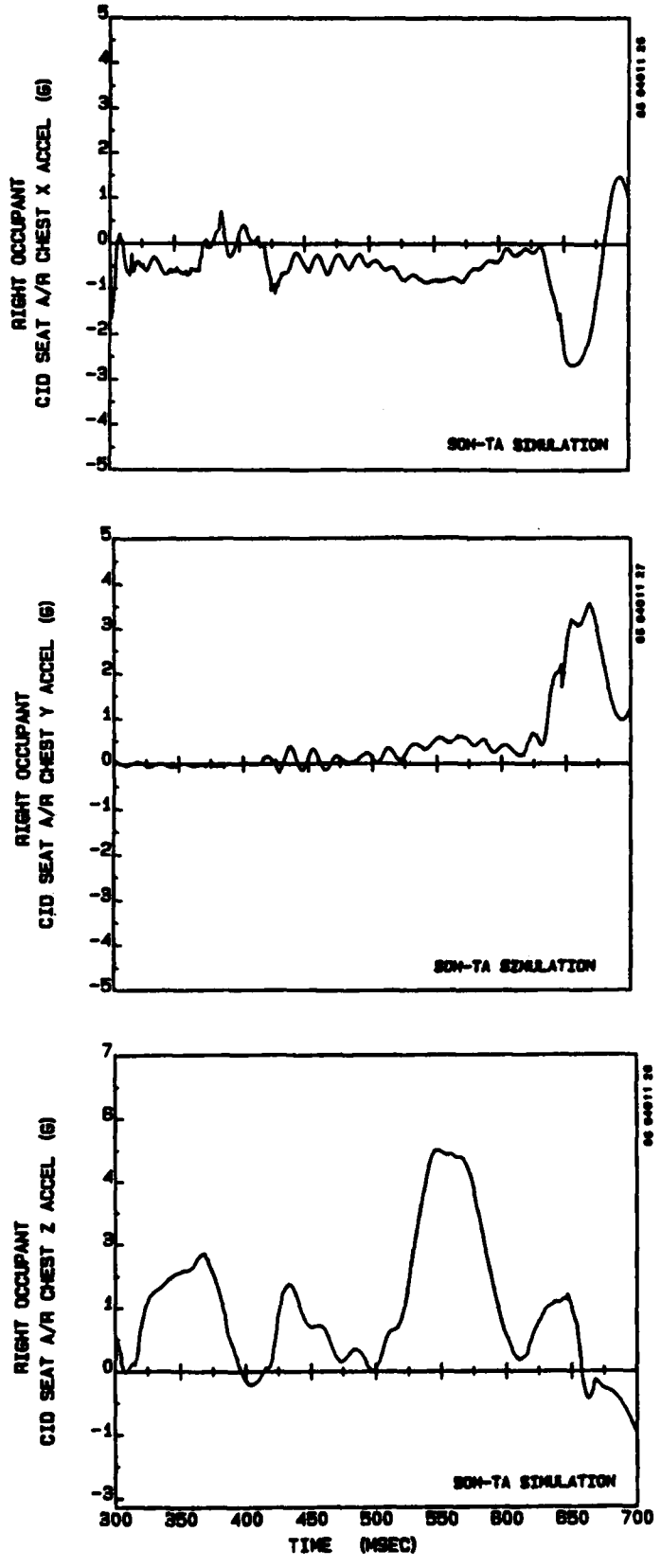

Figure F-18. Weberlite 4000 seat (A/R) right occupant chest accelerations.

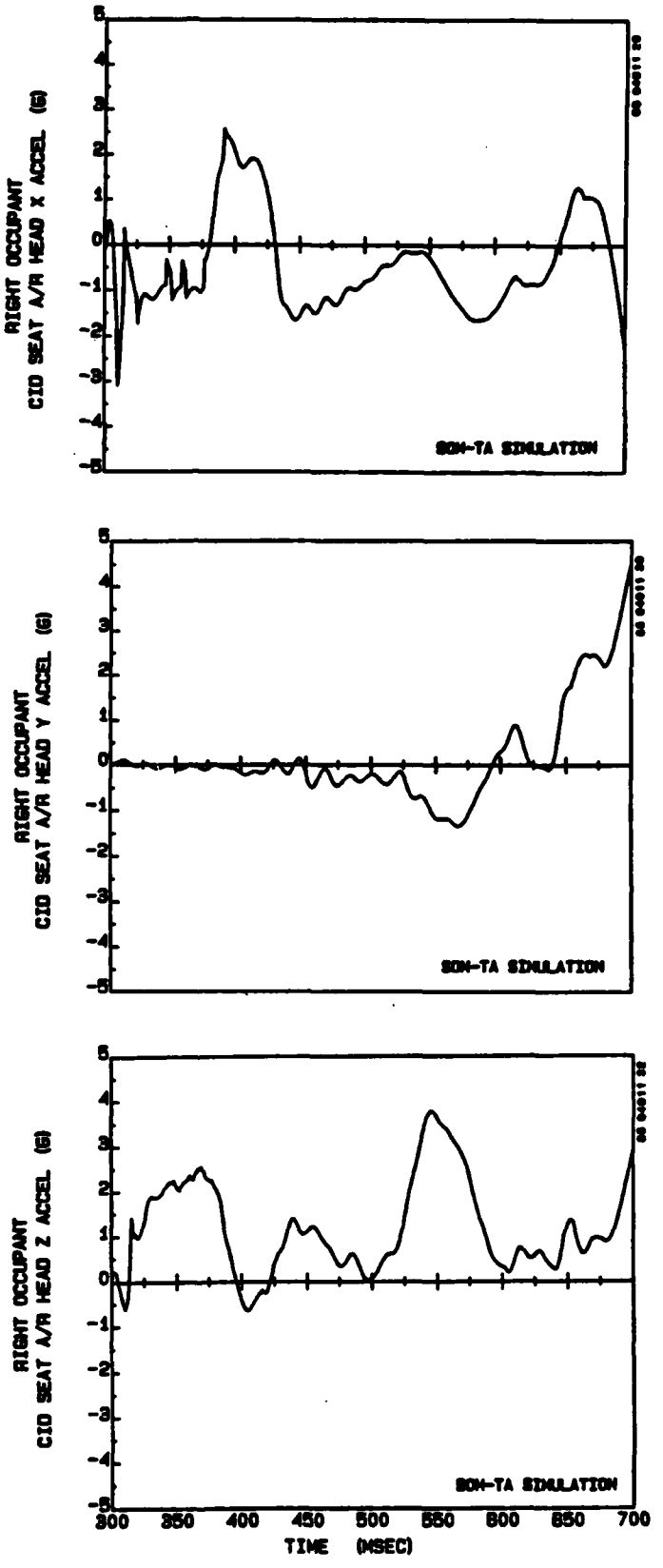

Figure F-19. Weberlite 4000 seat (A/R) right occupant head accelerations.

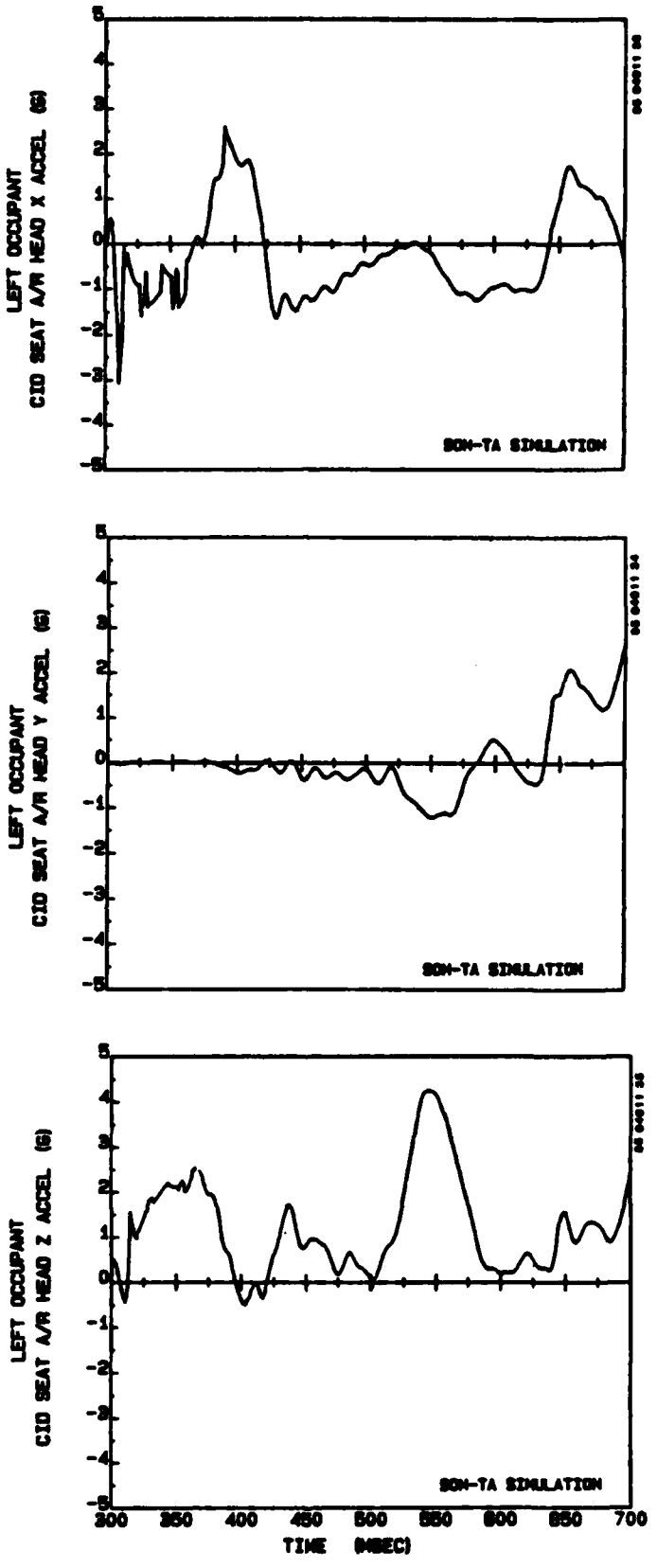

Figure F-20. Weberlite 4000 seat (A/R) left occupant pelvis accelerations.

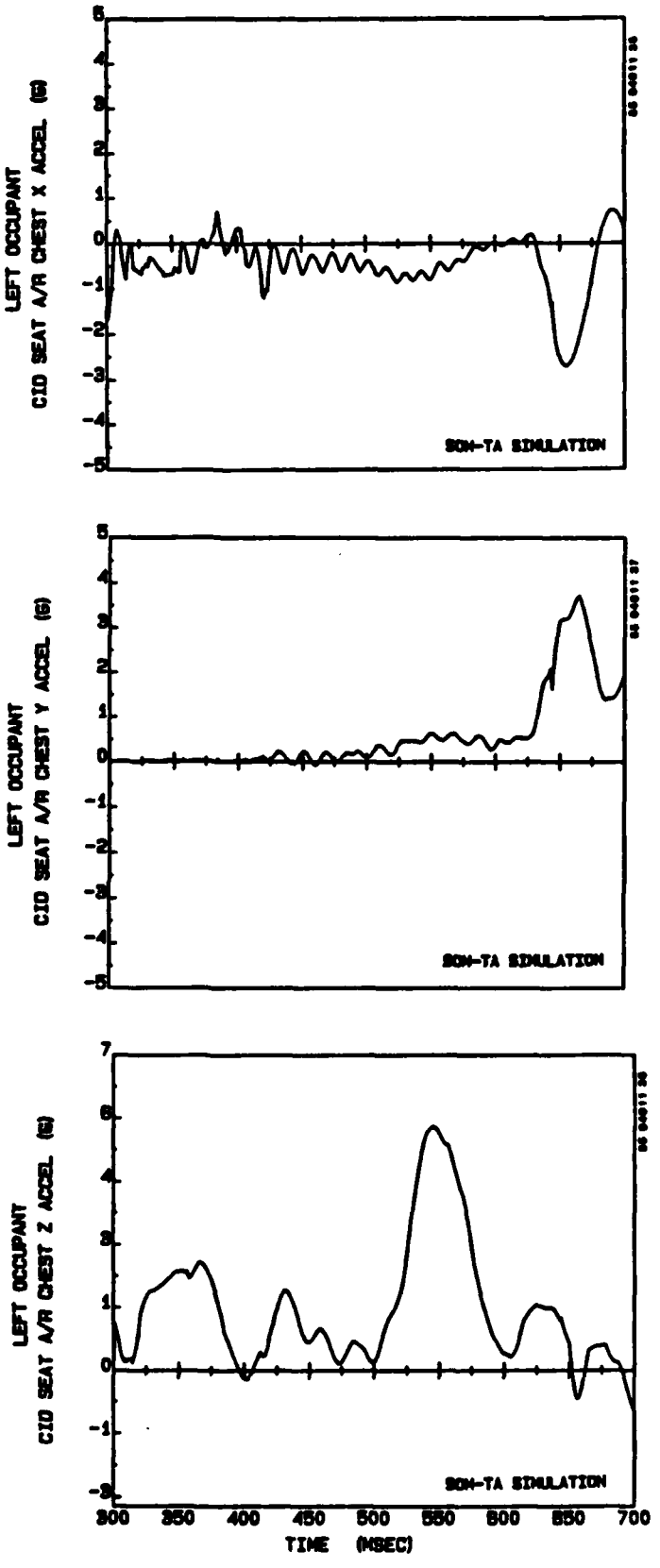

Figure F-21. Weberlite 4000 seat (A/R) left occupant chest accelerations.

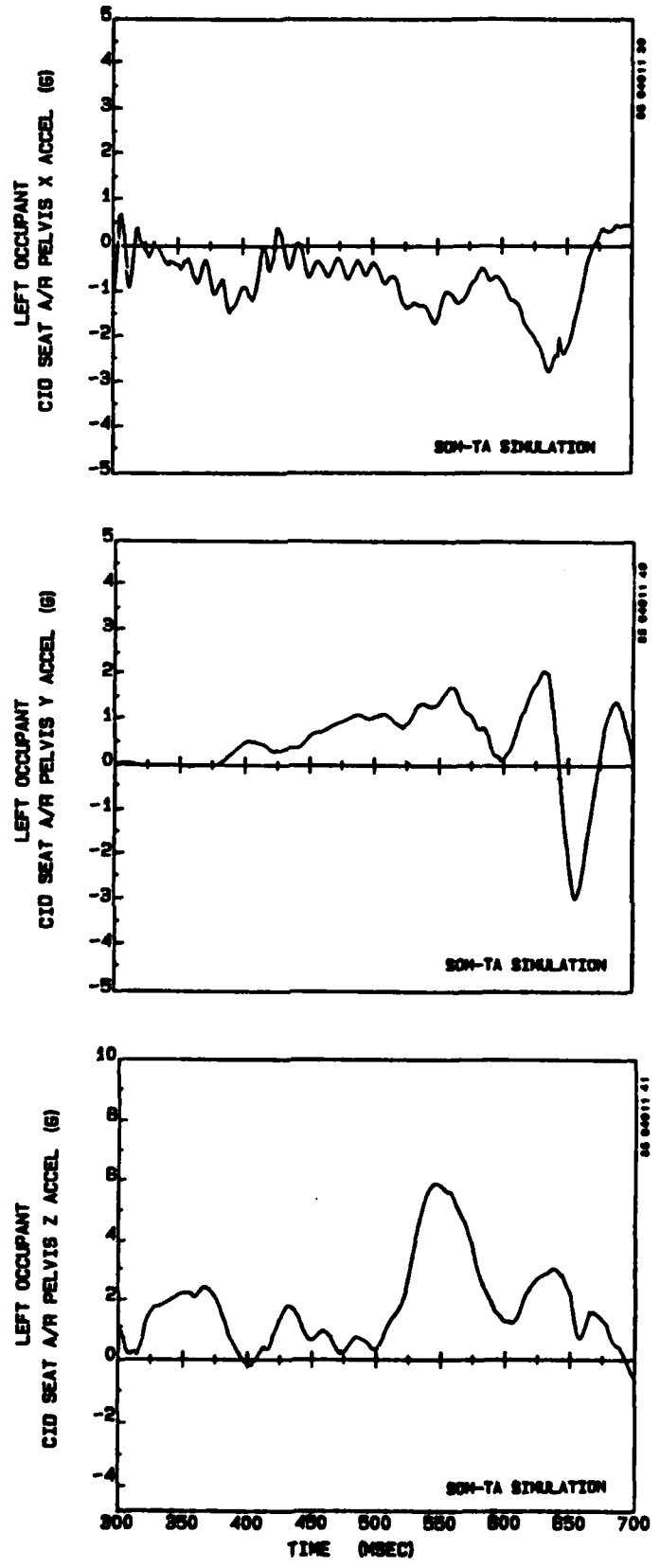

Figure F-22. Weberlite 4000 seat (A/R) left occupant head accelerations.

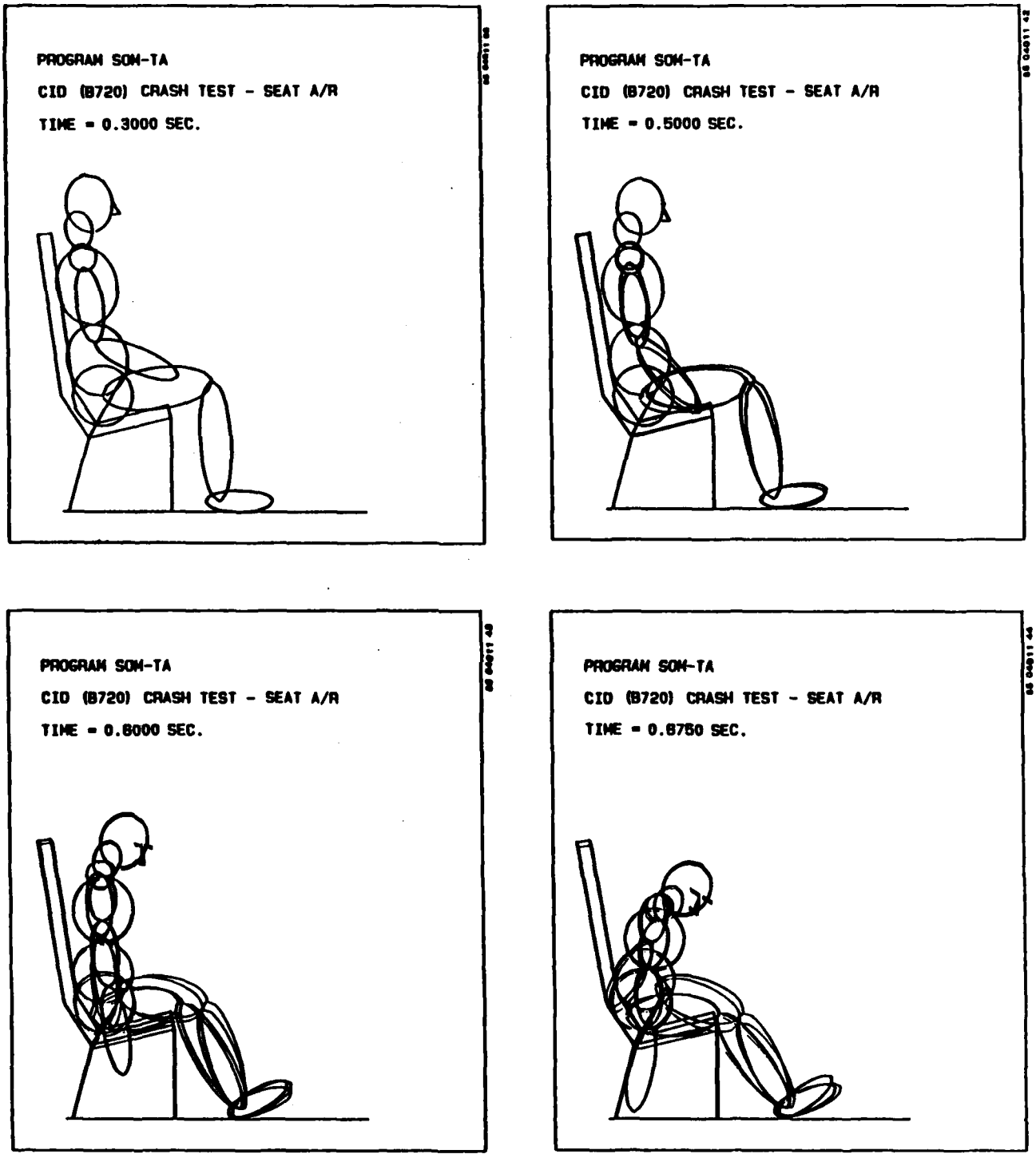

Figure F-23. Weberlite 4000 seat (A/R), Program SOM-TA predicted occupant response (side view).

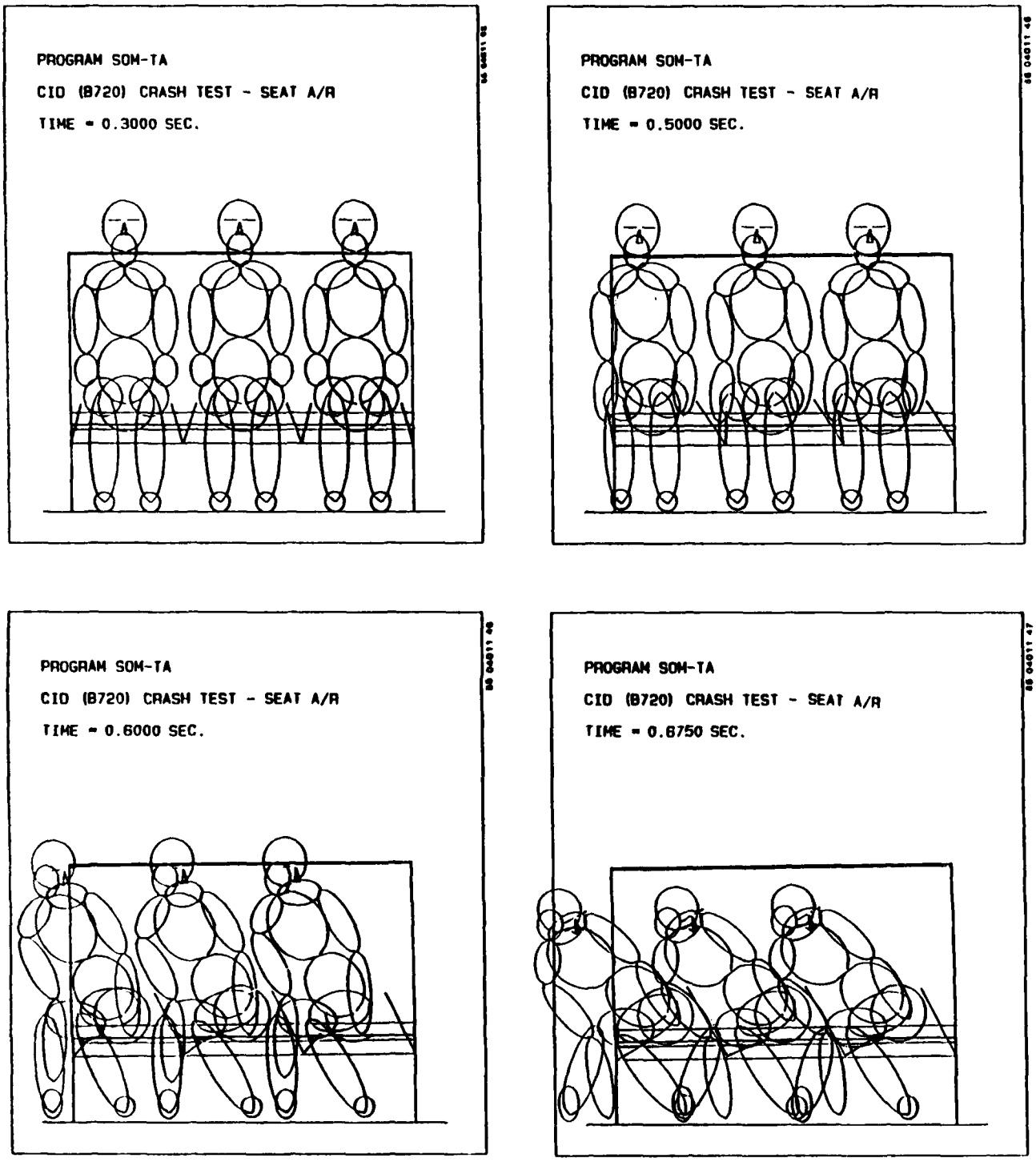

Figure F-24. Weberlite 4000 seat (A/R), Program SOM-TA predicted occupant response (front view).

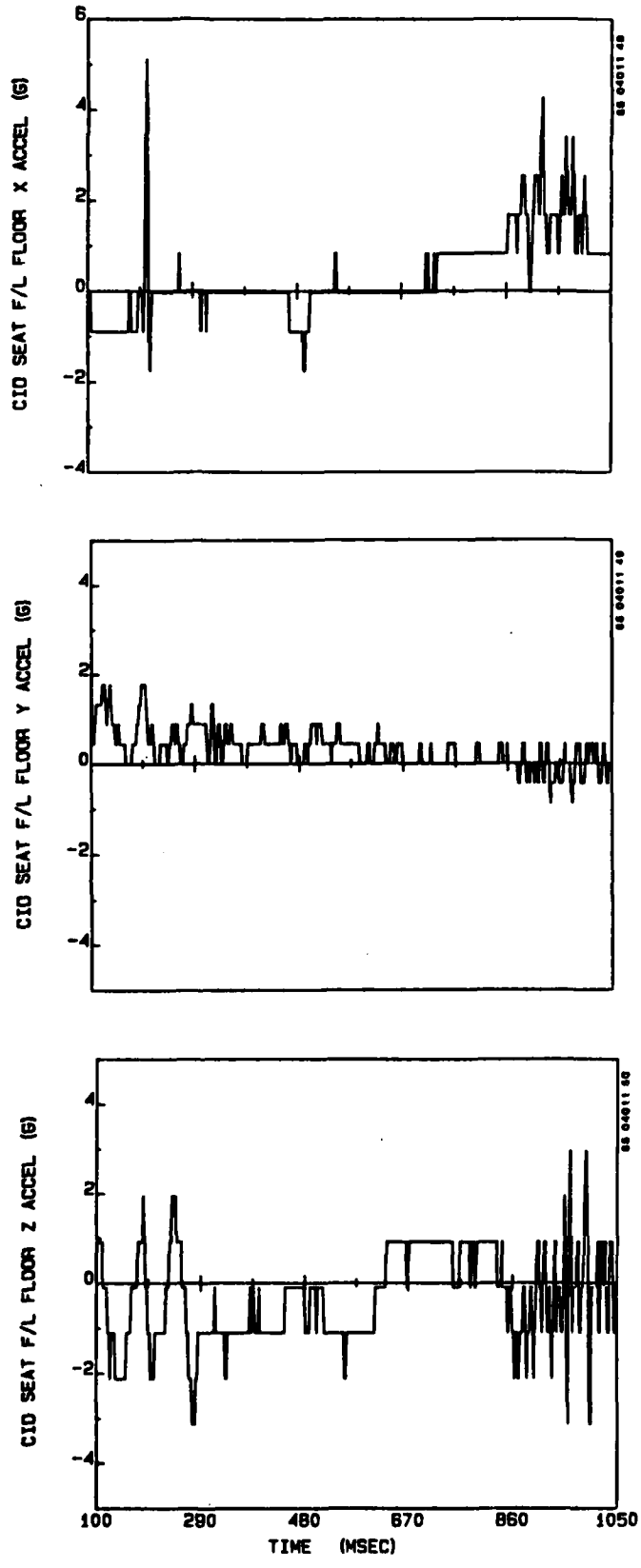

Figure F-25. Modified UOP 901 seat (F/L) floor accelerations.

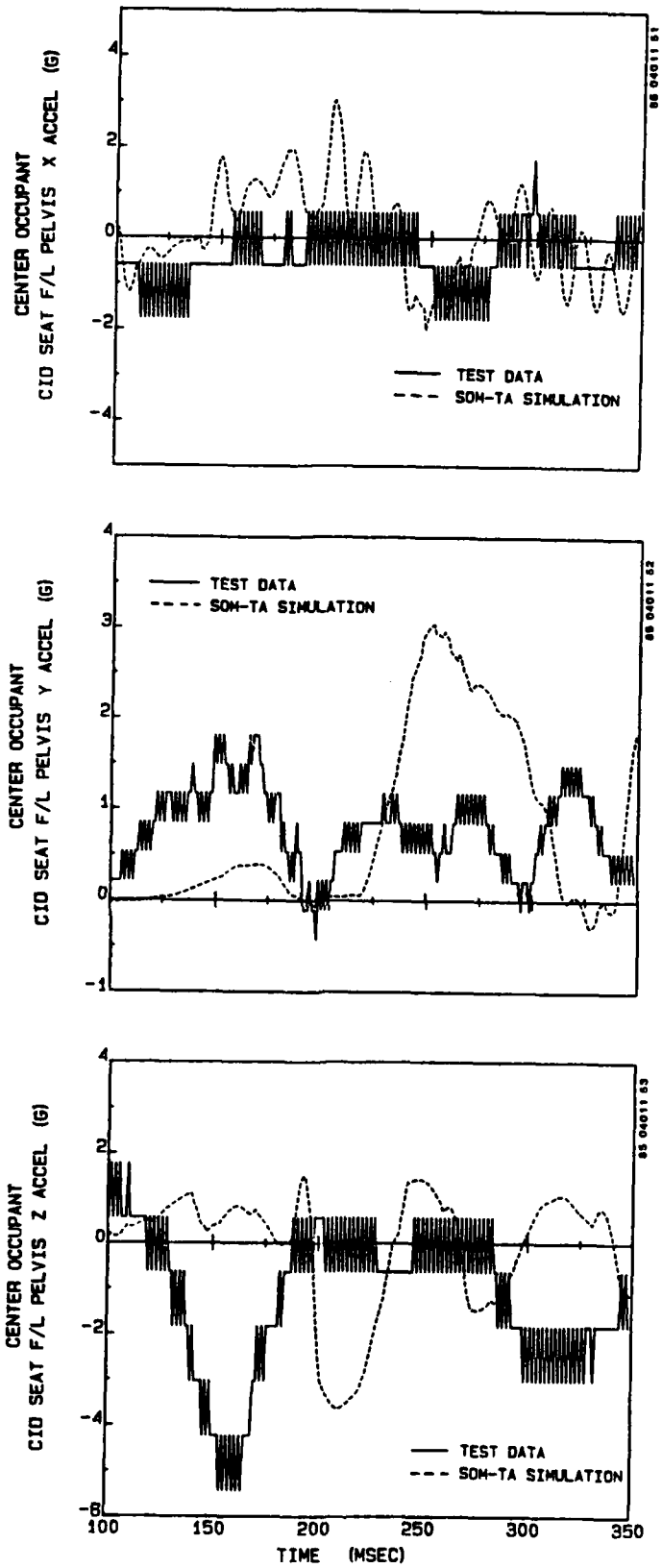

Figure F-26. Modified UOP 901 seat (F/L) center occupant pelvis accelerations.

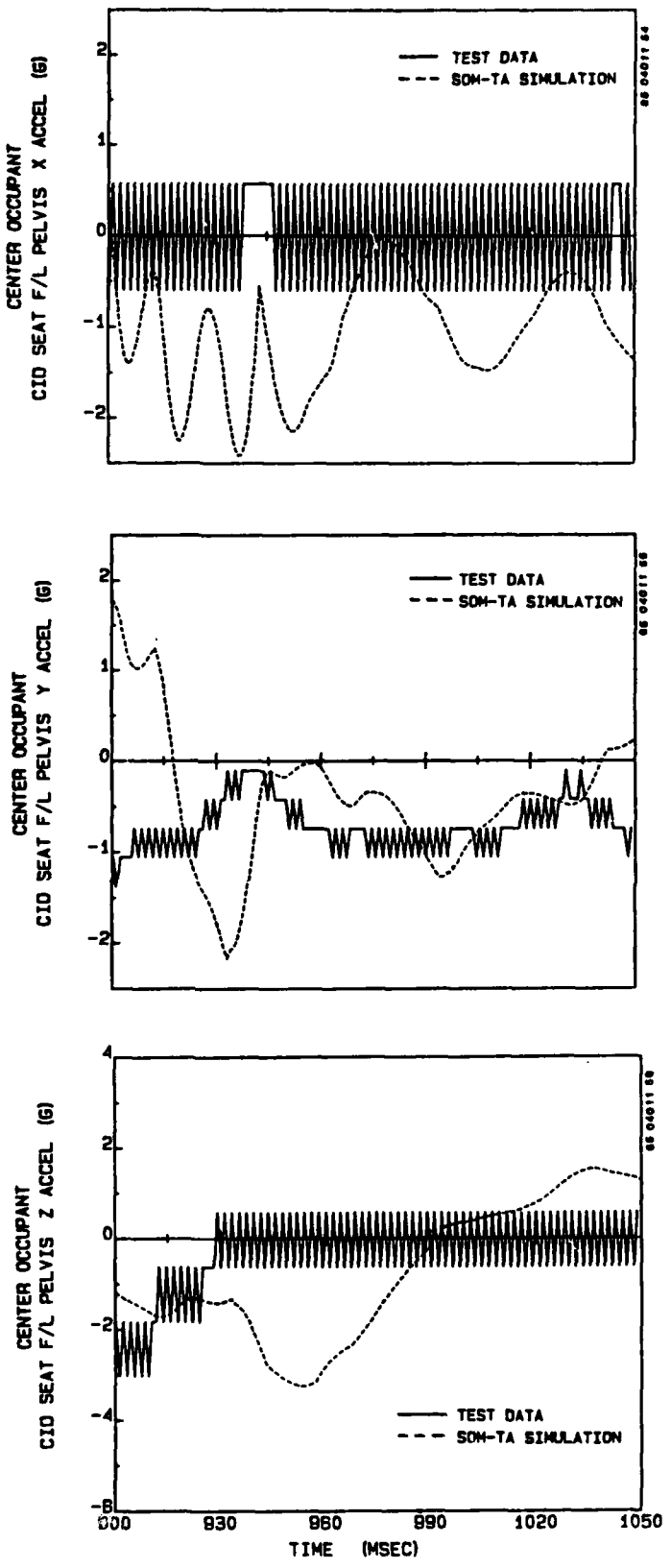

Figure F-26 (contd). Modified UOP 901 seat (F/L) center occupant pelvis accelerations.

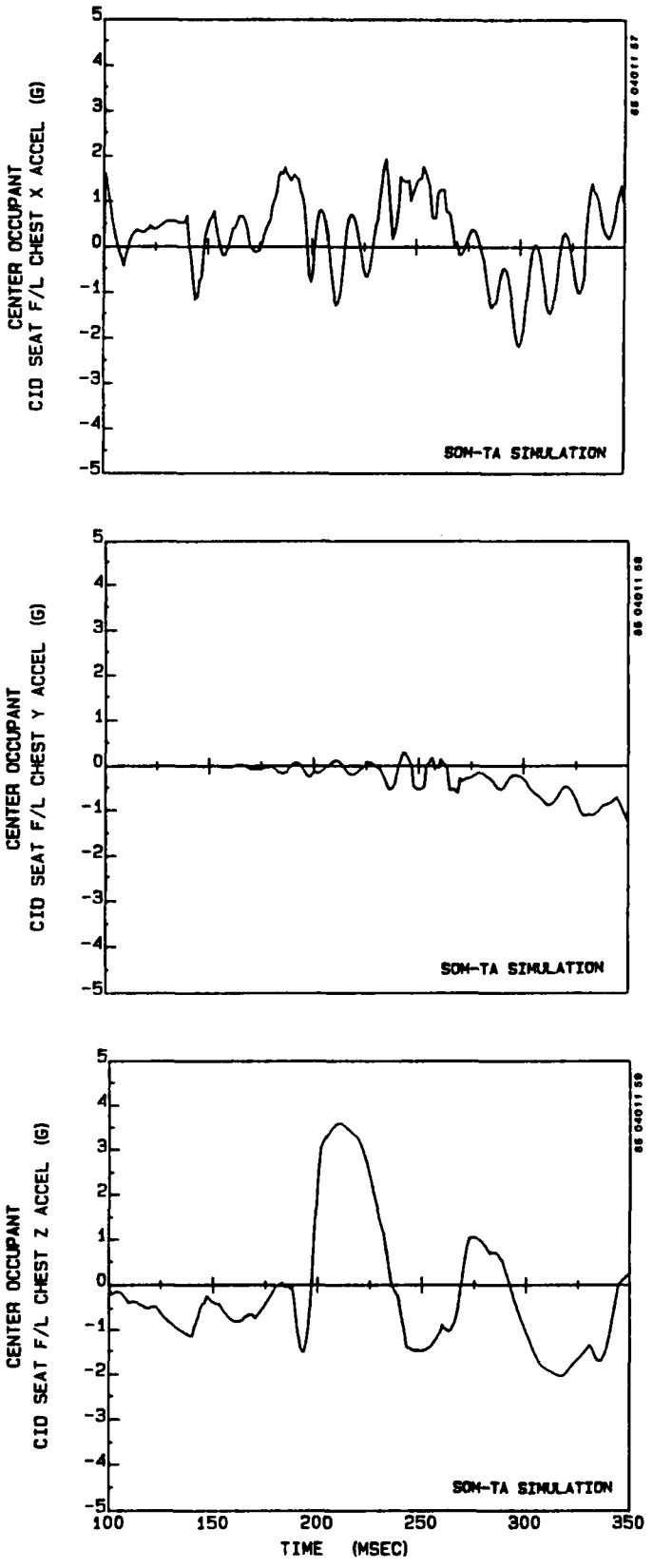

Figure F-27. Modified UOP 901 seat (F/L) center occupant chest accelerations.

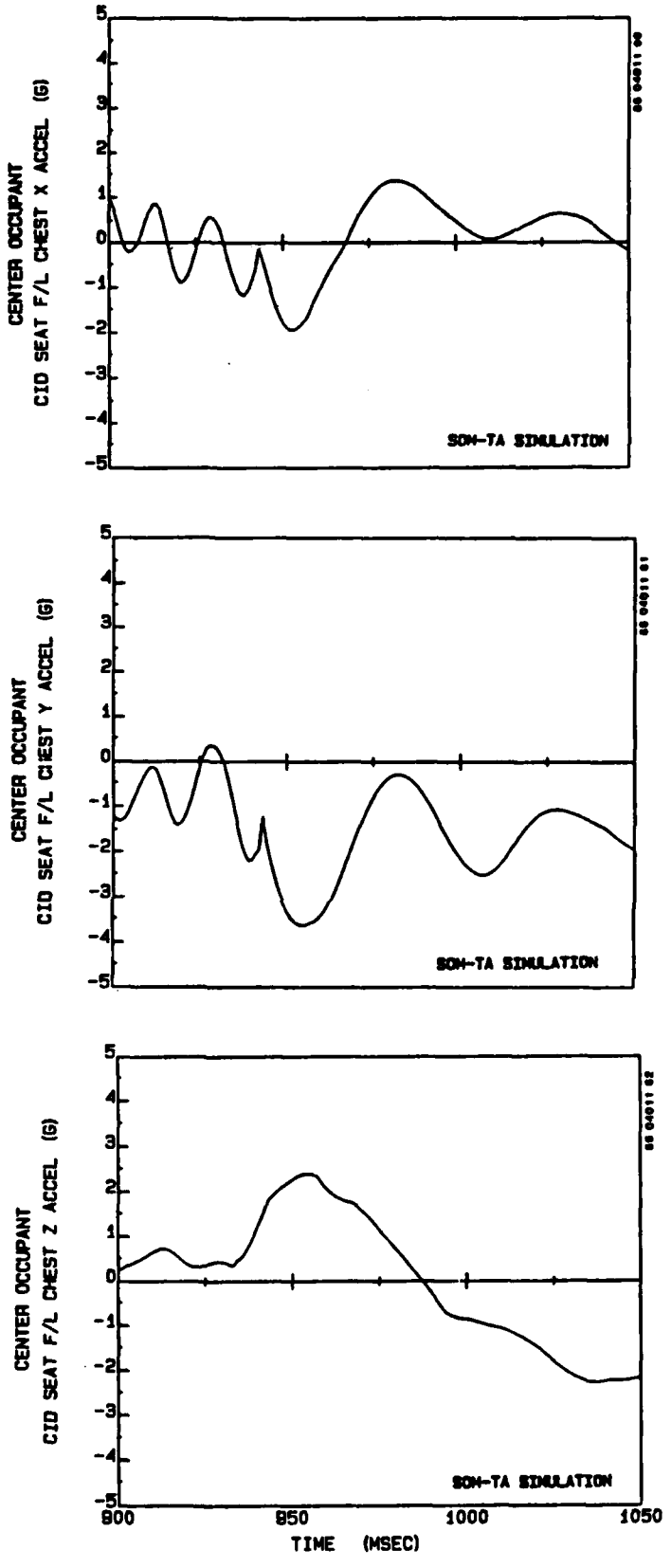

Figure F-27 (contd). Modified UOP 901 seat (F/L) center occupant chest accelerations.

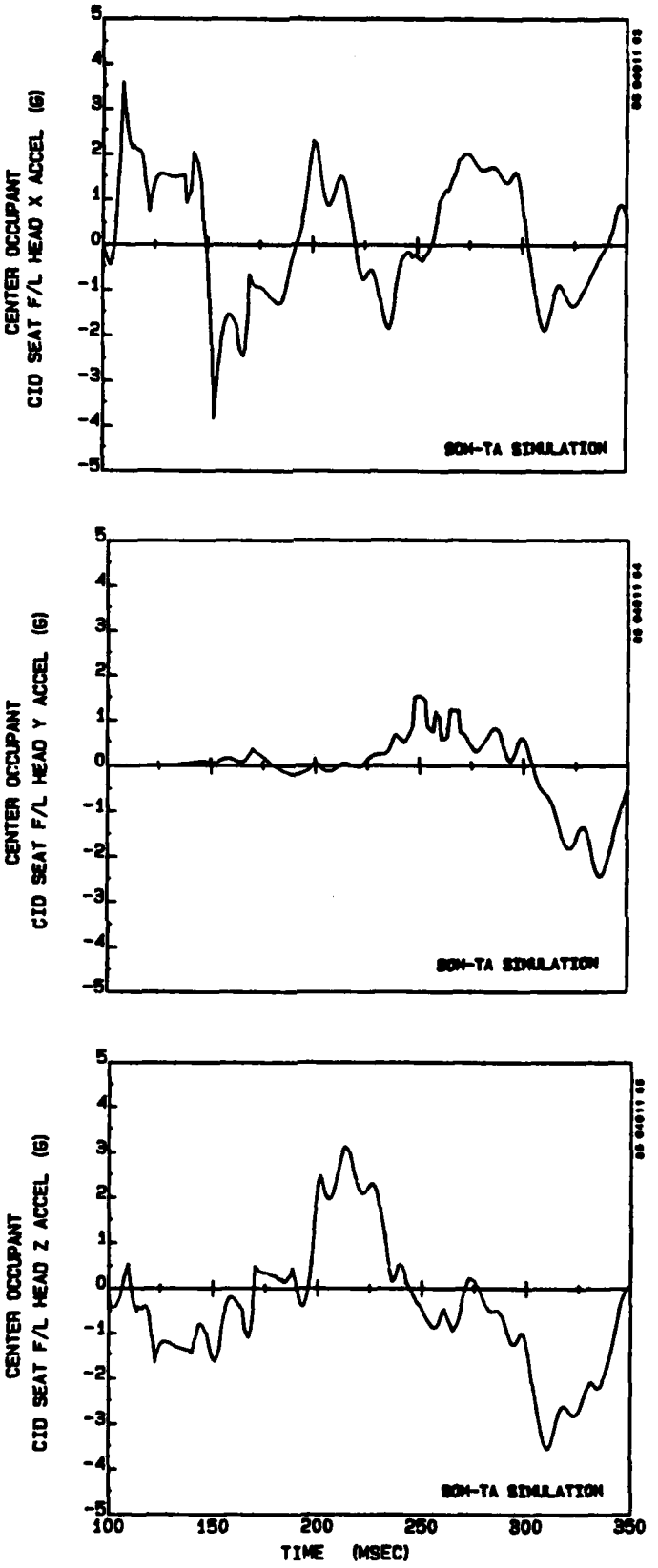

Figure F-28. Modified UOP 901 seat (F/L) center occupant head accelerations.

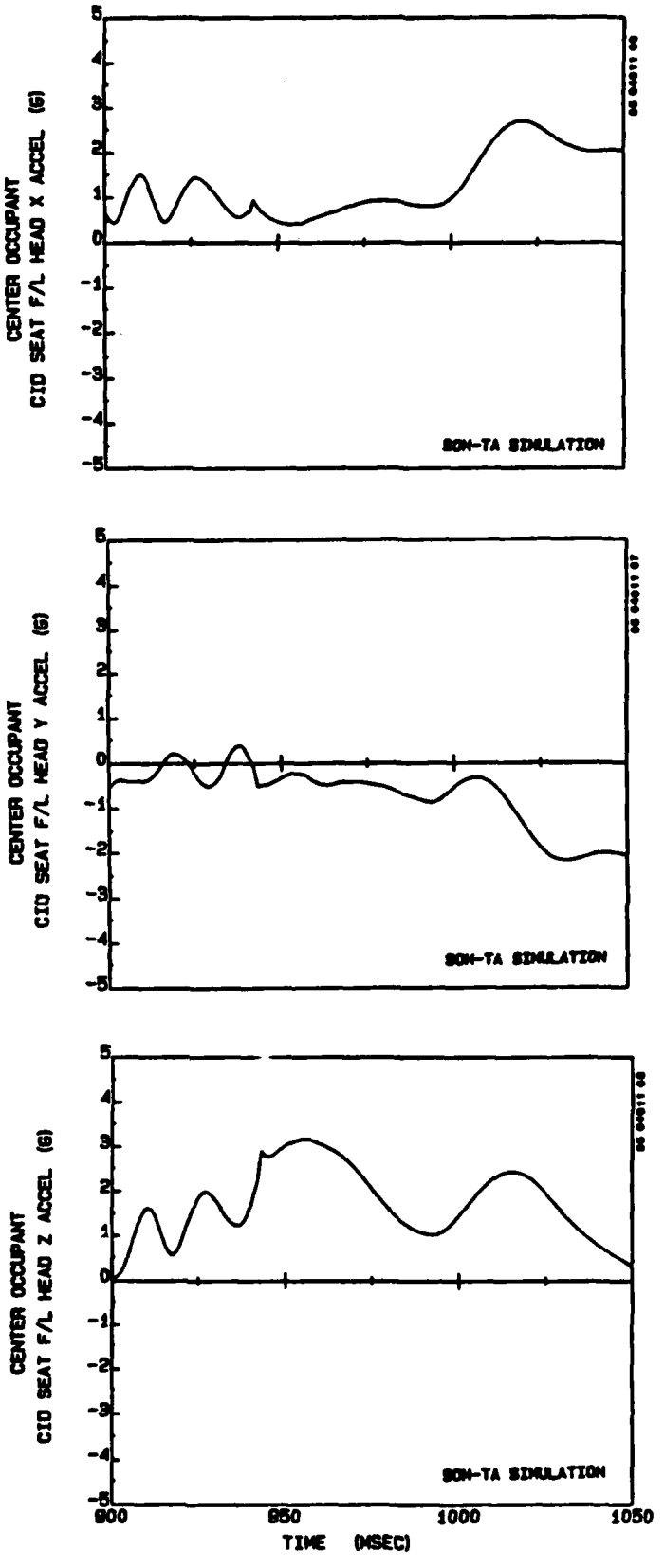

Figure F-28 (contd). Modified UOP 901 seat (F/L) center occupant head accelerations.

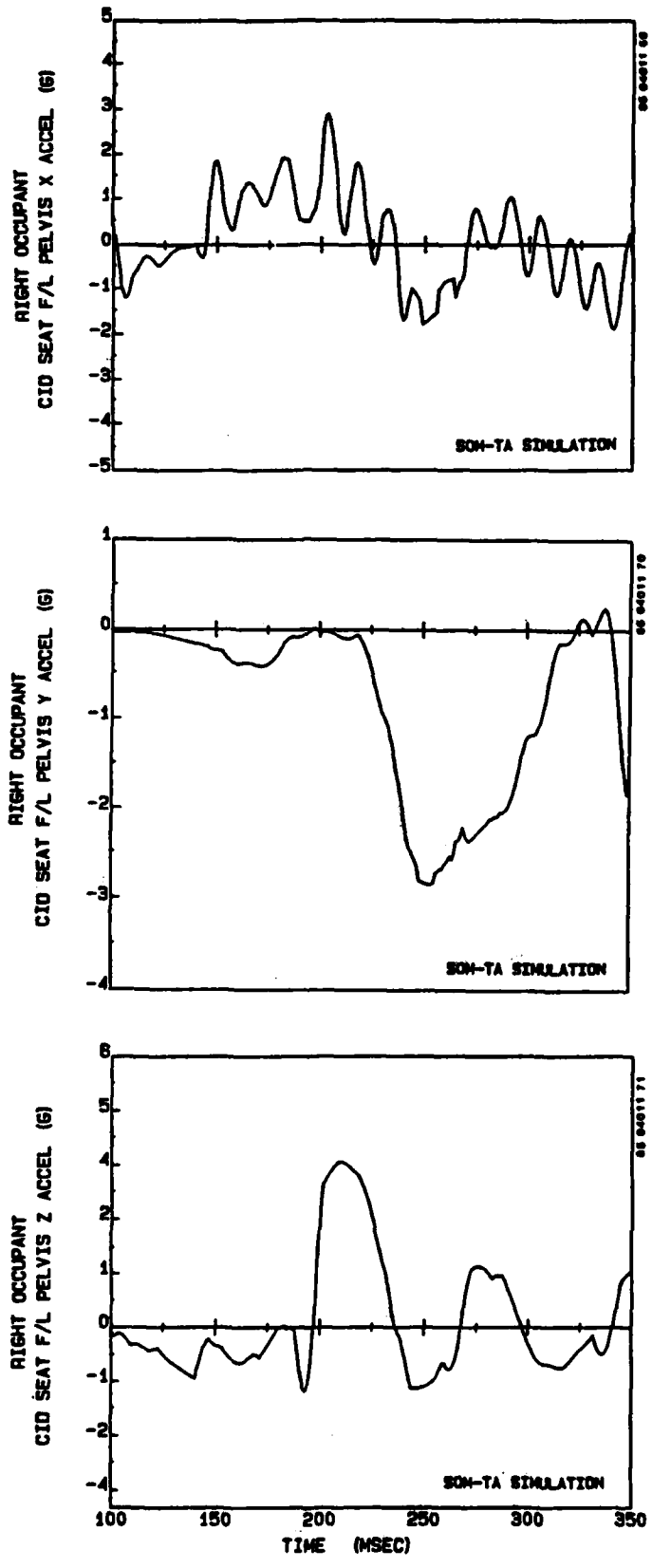

Figure F-29. Modified UOP 901 seat (F/L) right occupant pelvis accelerations.

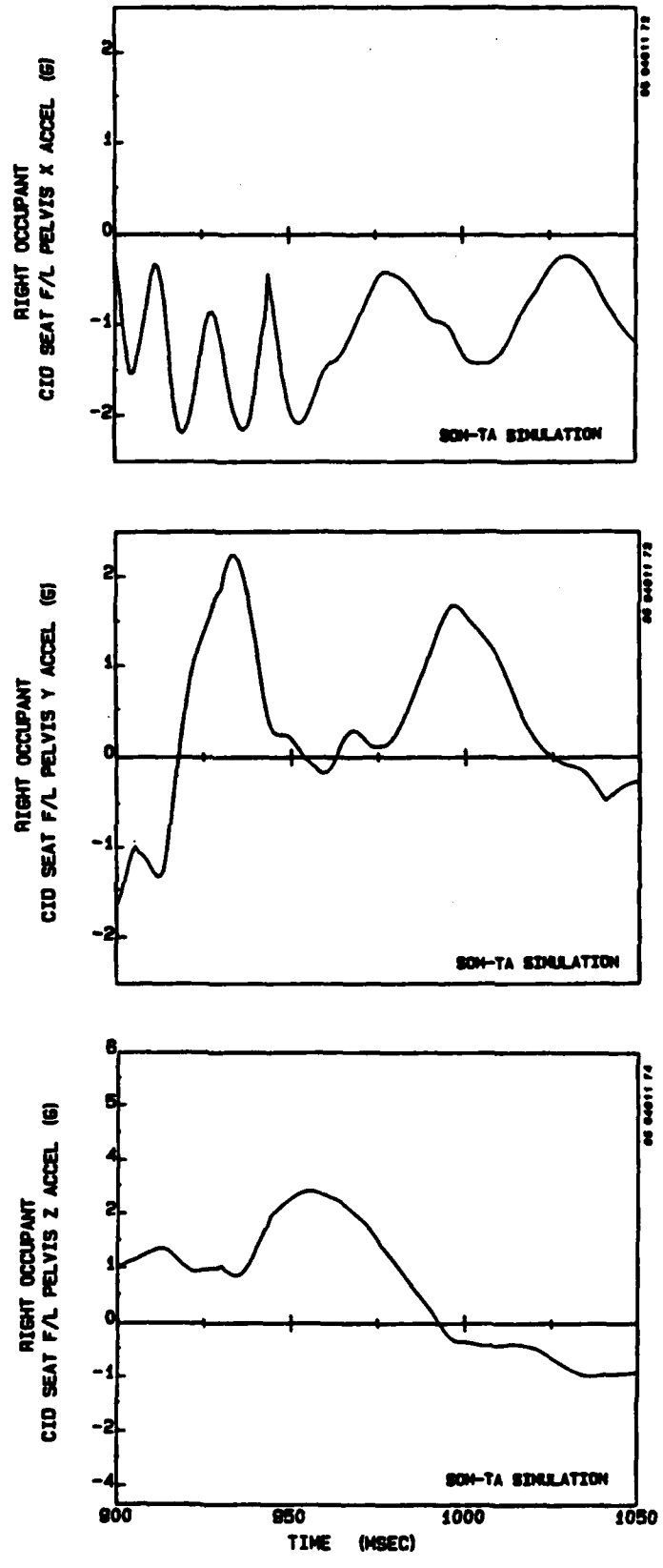

Figure F-29 (contd). Modified UOP 901 seat (F/L) occupant pelvis accelerations.

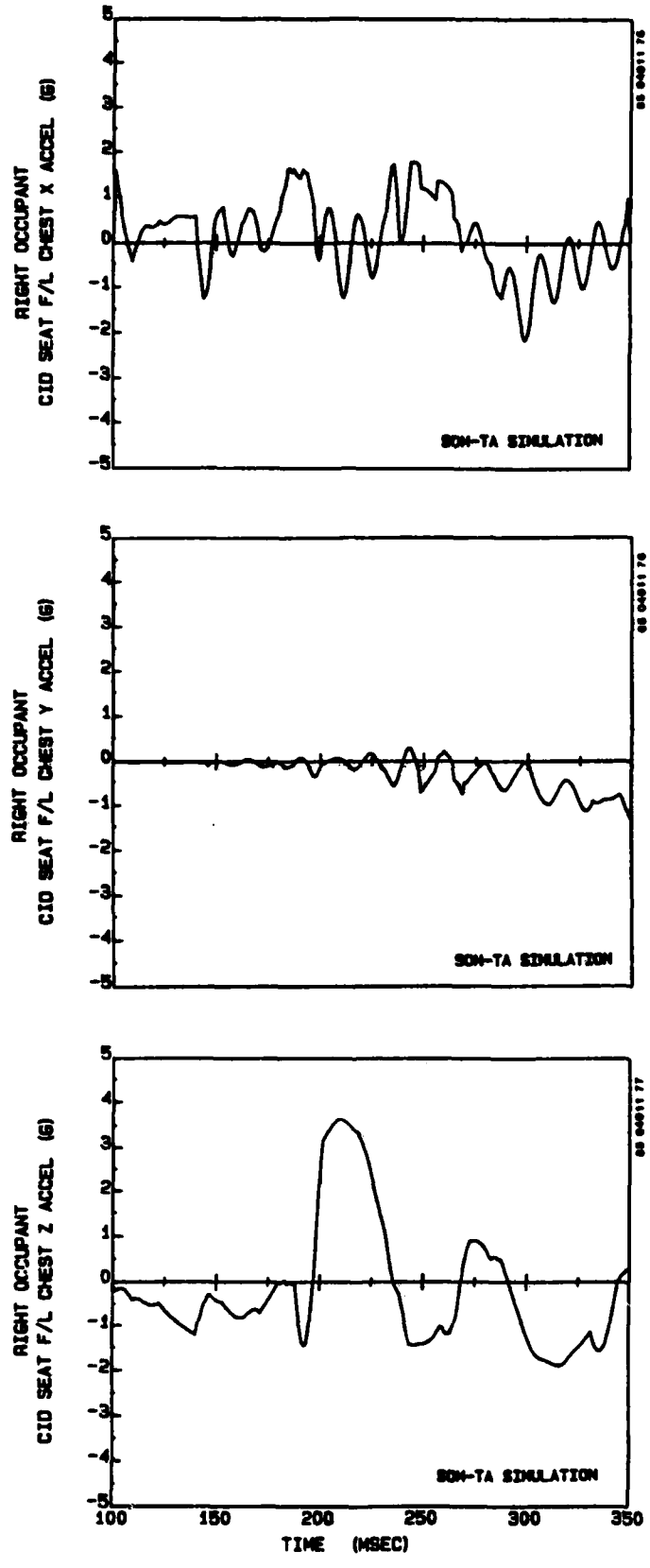

Figure F-30. Modified UOP 901 seat (F/L) right occupant chest accelerations

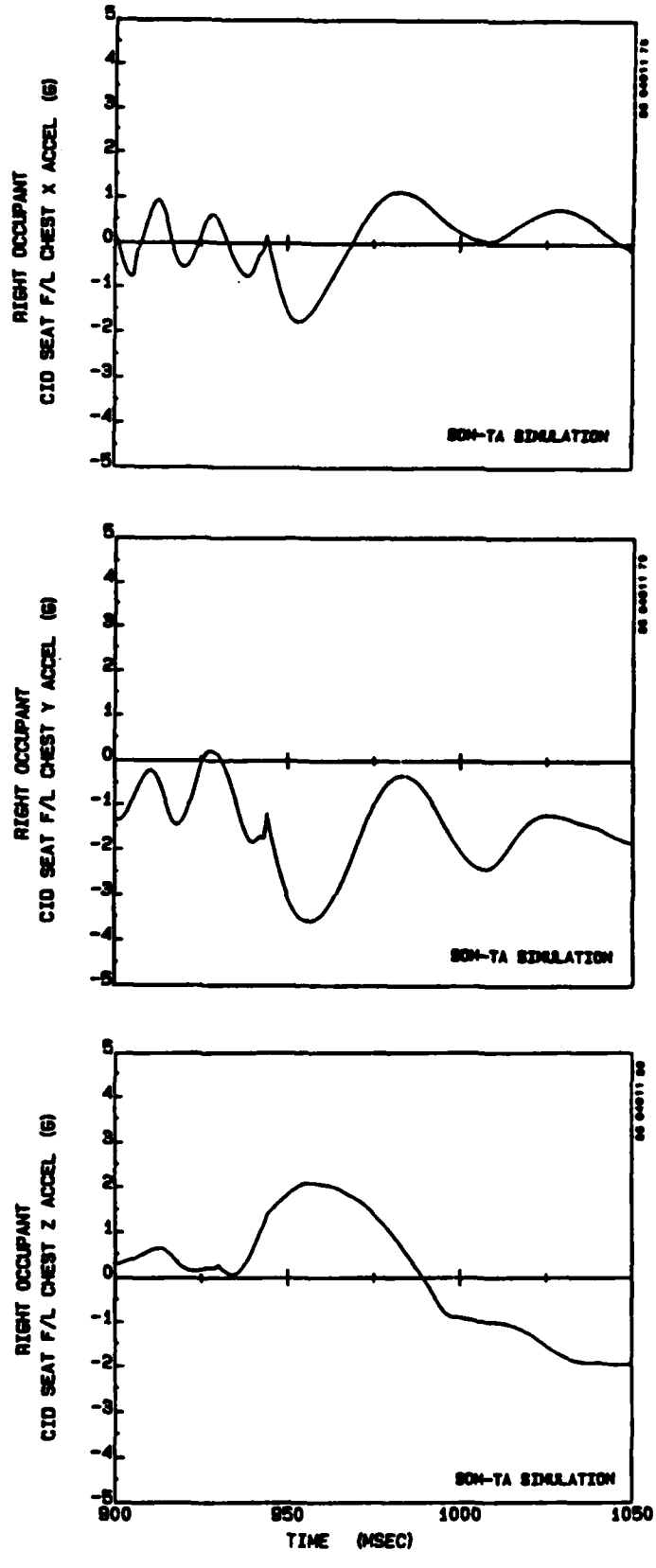

Figure F-30 (contd). Modified UOP 901 seat (F/L) right occupant chest accelerations.

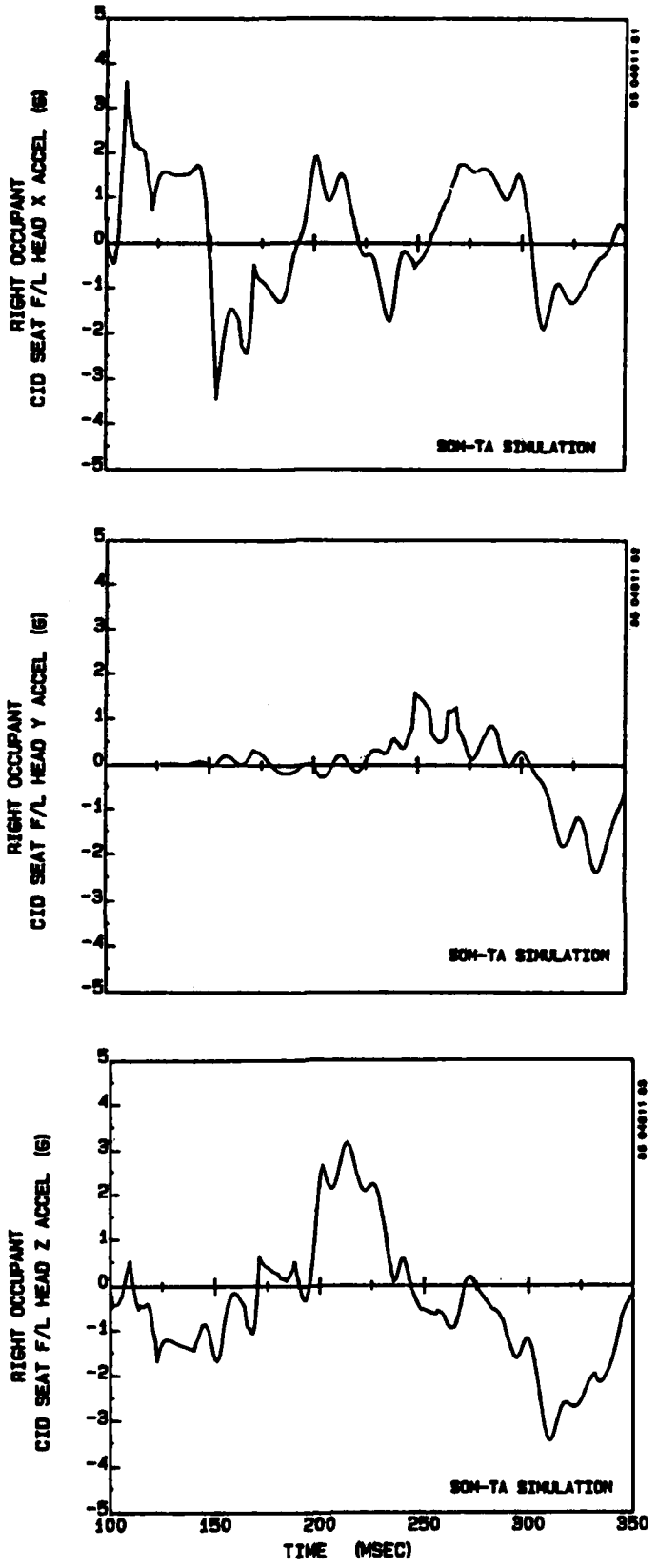

Figure F-31. Modified UOP 901 seat (F/L) right occupant head accelerations.

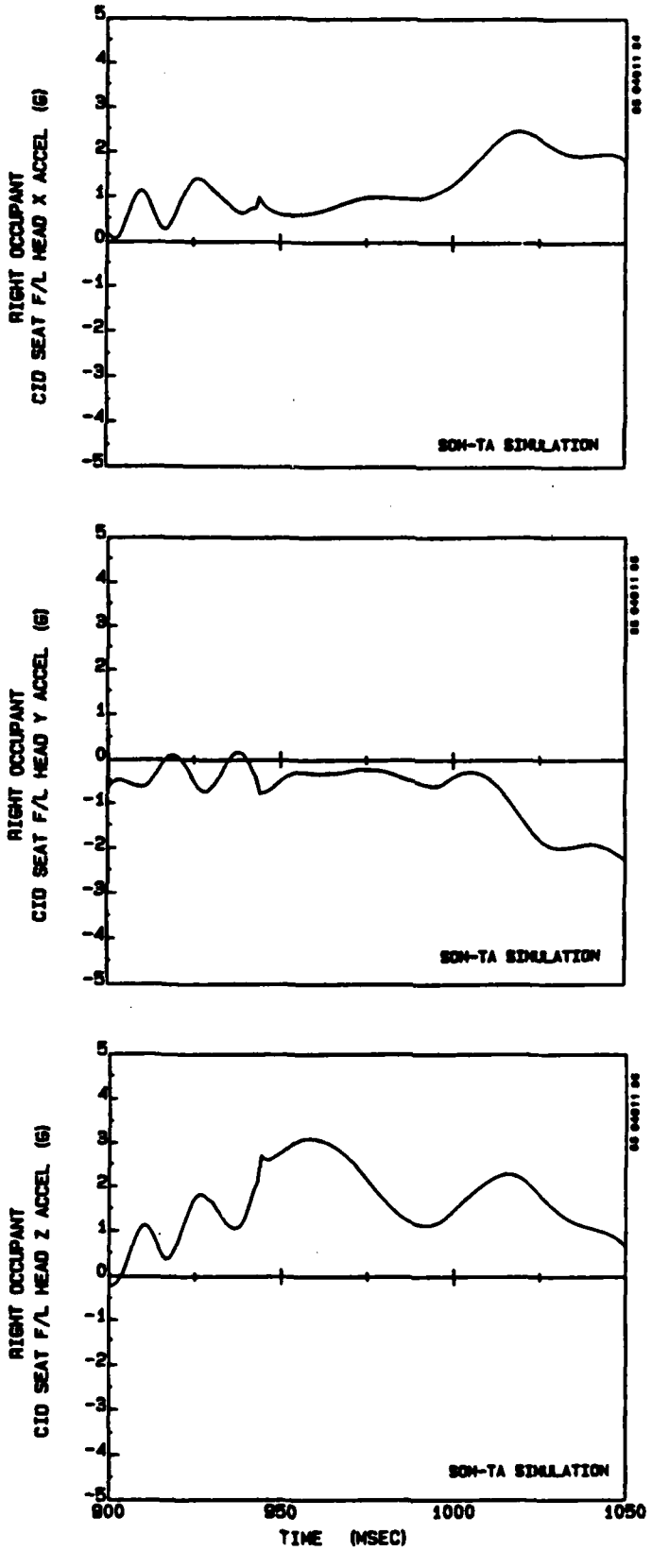

Figure F-31 (contd). Modified UOP 301 seat (F/L) right occupant head accelerations.

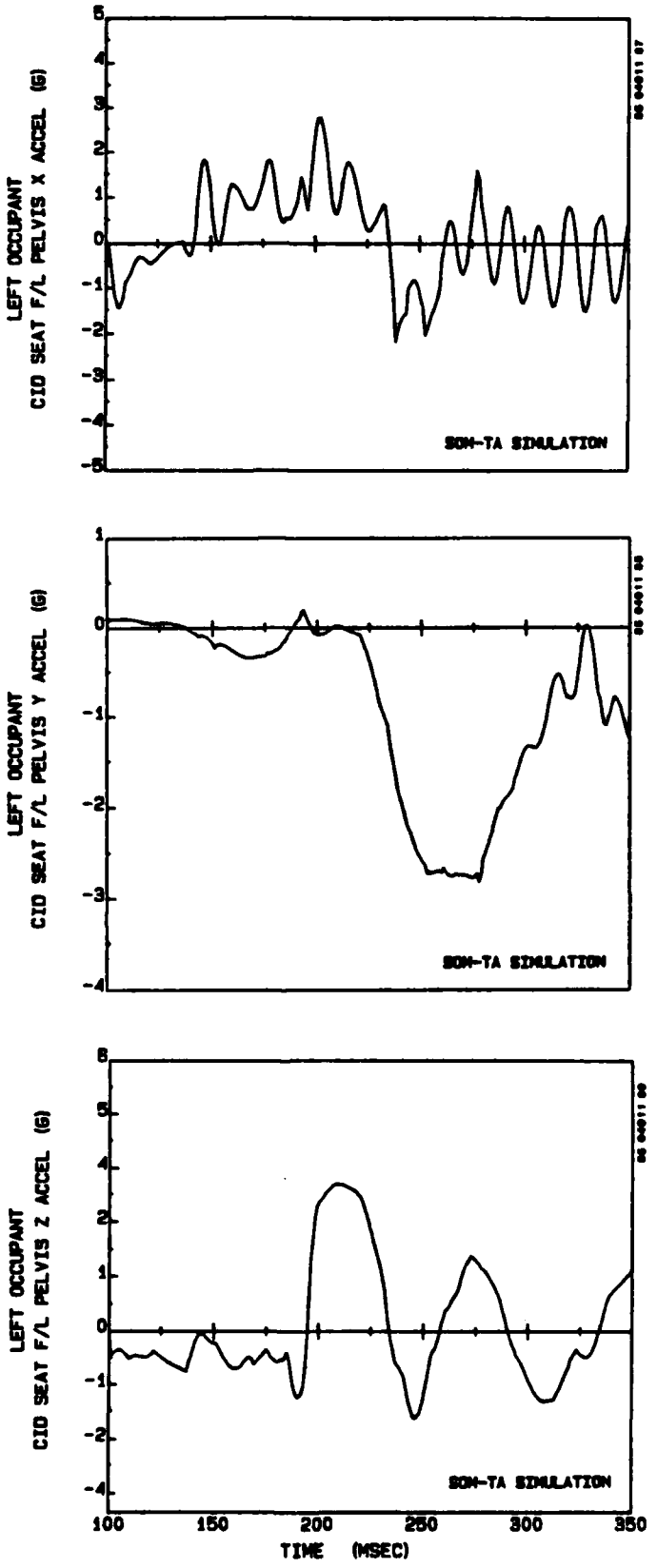

Figure F-32. Modified UOP 901 seat (F/L) left occupant pelvis accelerations.

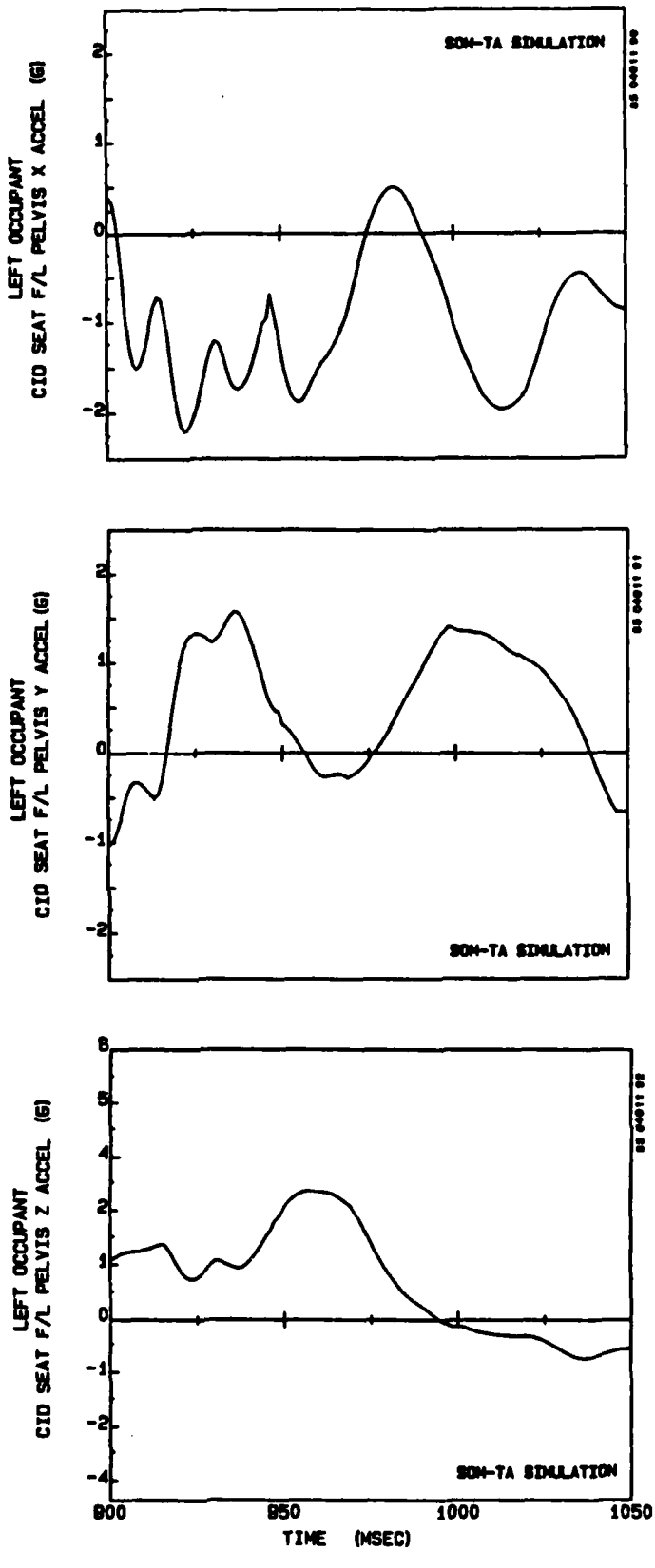

Figure F-32 (contd). Modified UOP 901 seat (F/L) left occupant pelvis accelerations.

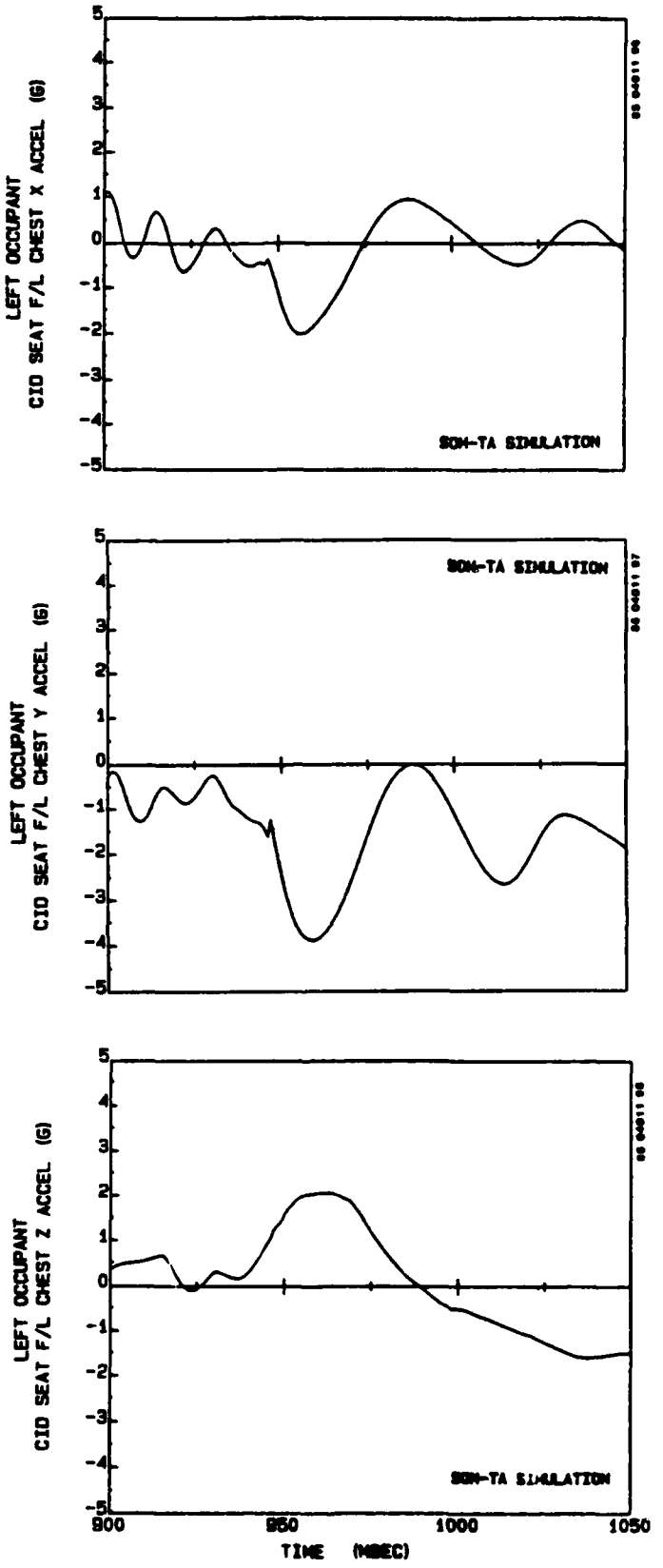

Figure F-33 (contd). Modified UOP 901 seat (F/L) left occupant chest accelerations.

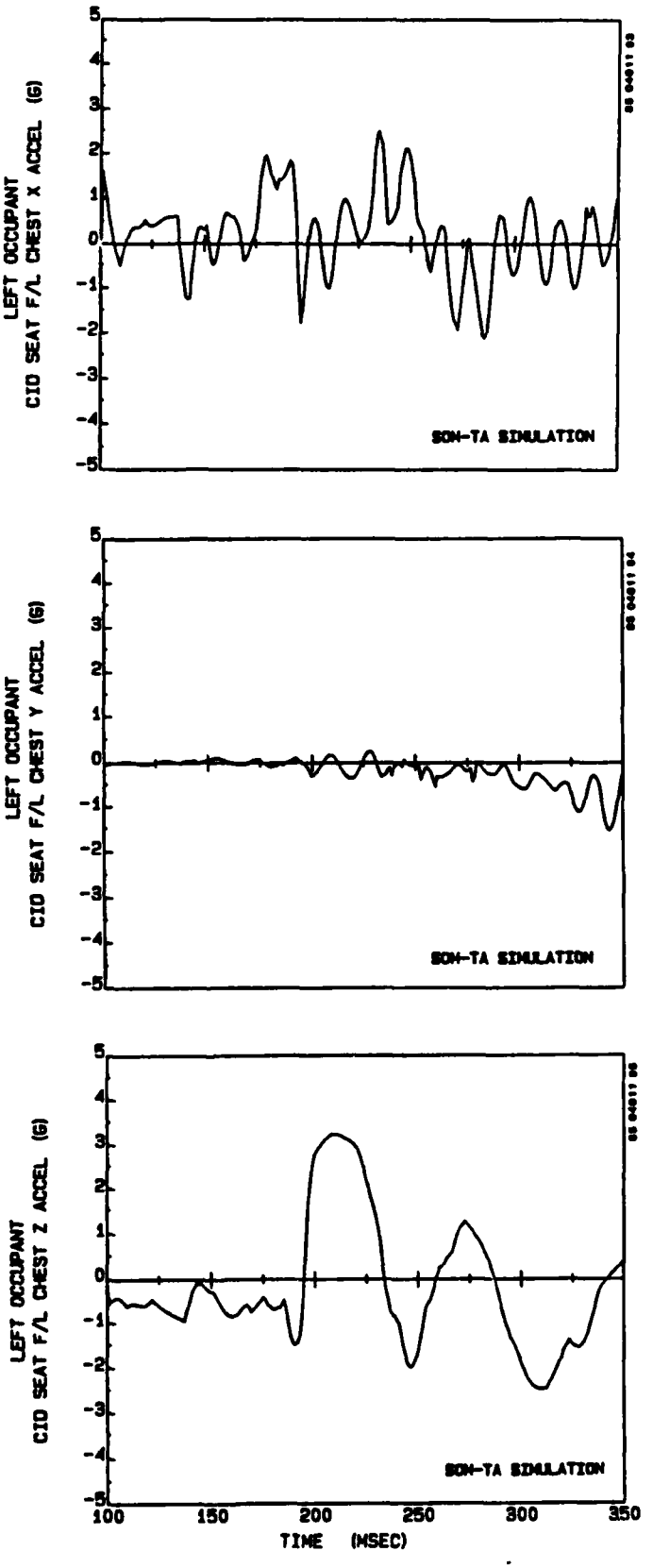

Figure F-33. Modified UOP 901 seat (F/L) left occupant chest accelerations

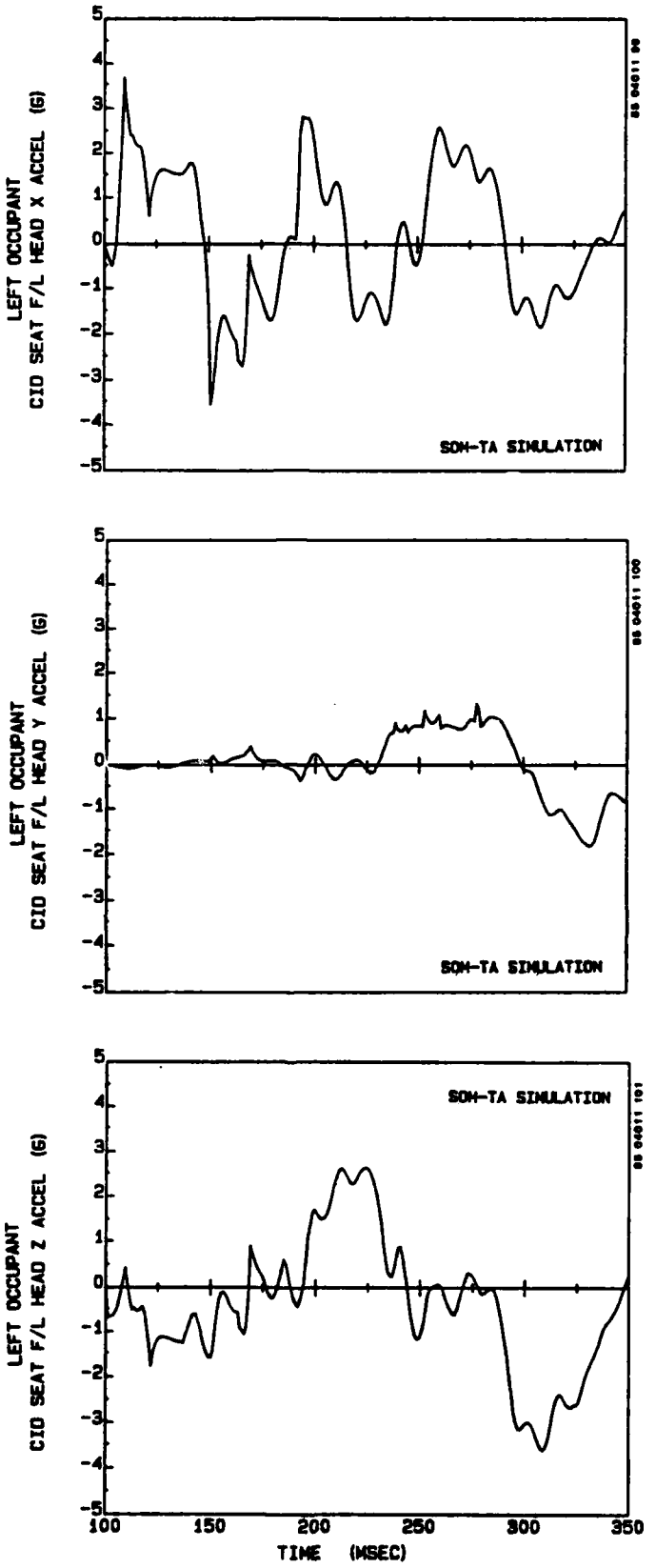

Figure F-34. Modified UOP 901 seat (F/L) left occupant head accelerations.

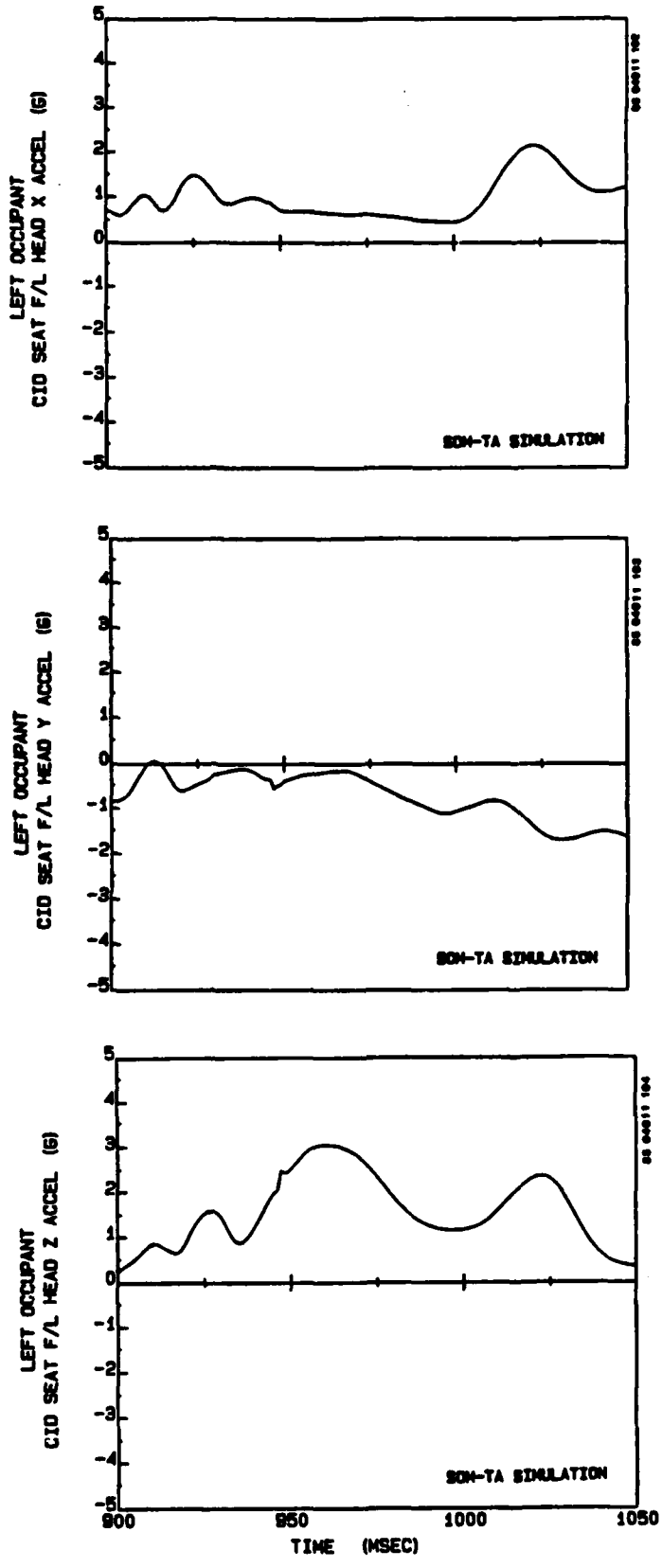

Figure F-34 (contd). Modified UOP 901 seat (F/L) left occupant head accelerations.

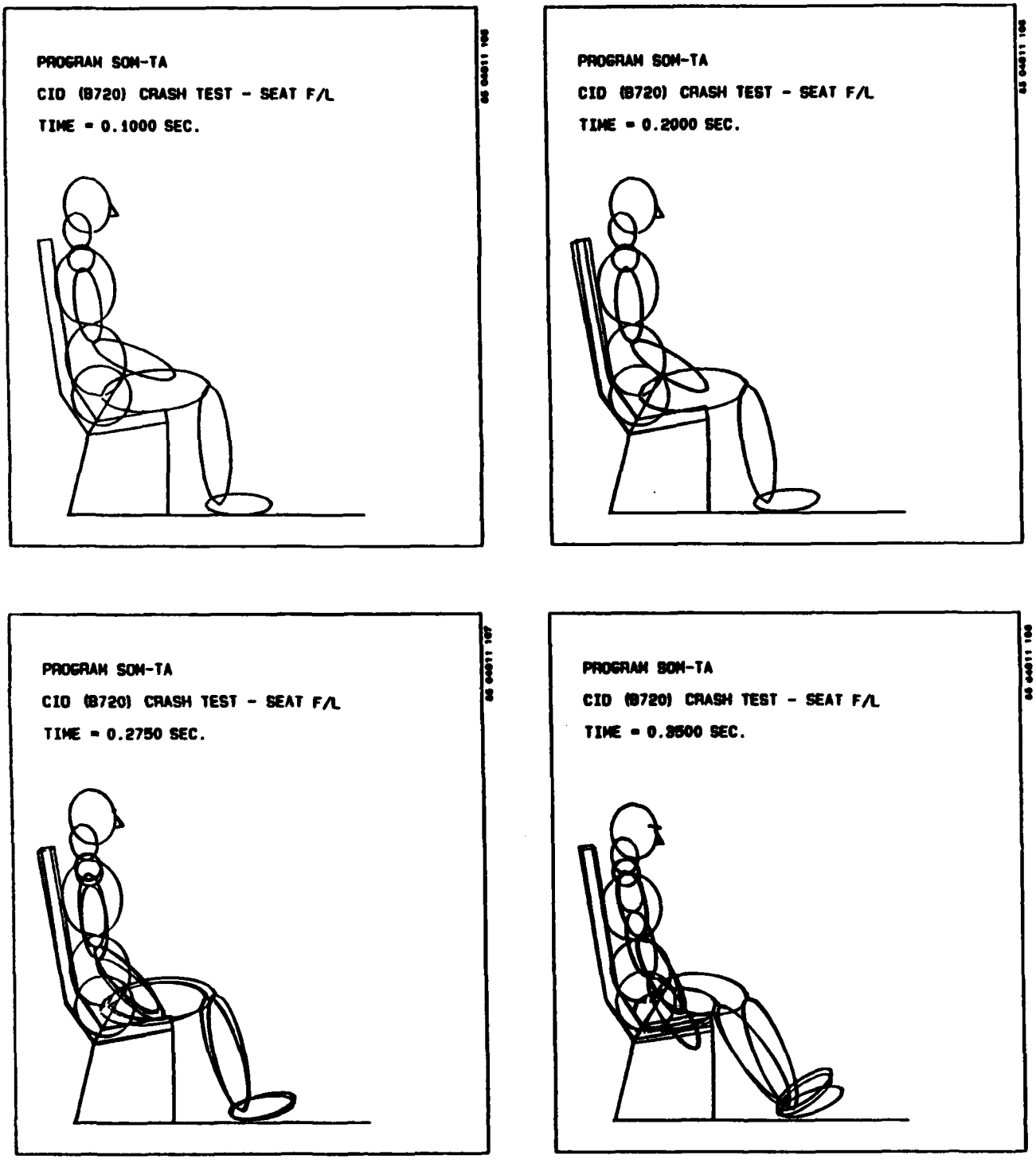

Figure F-35. Modified UOP 901 seat (F/L), Program SOM-TA predicted occupant response (side view).

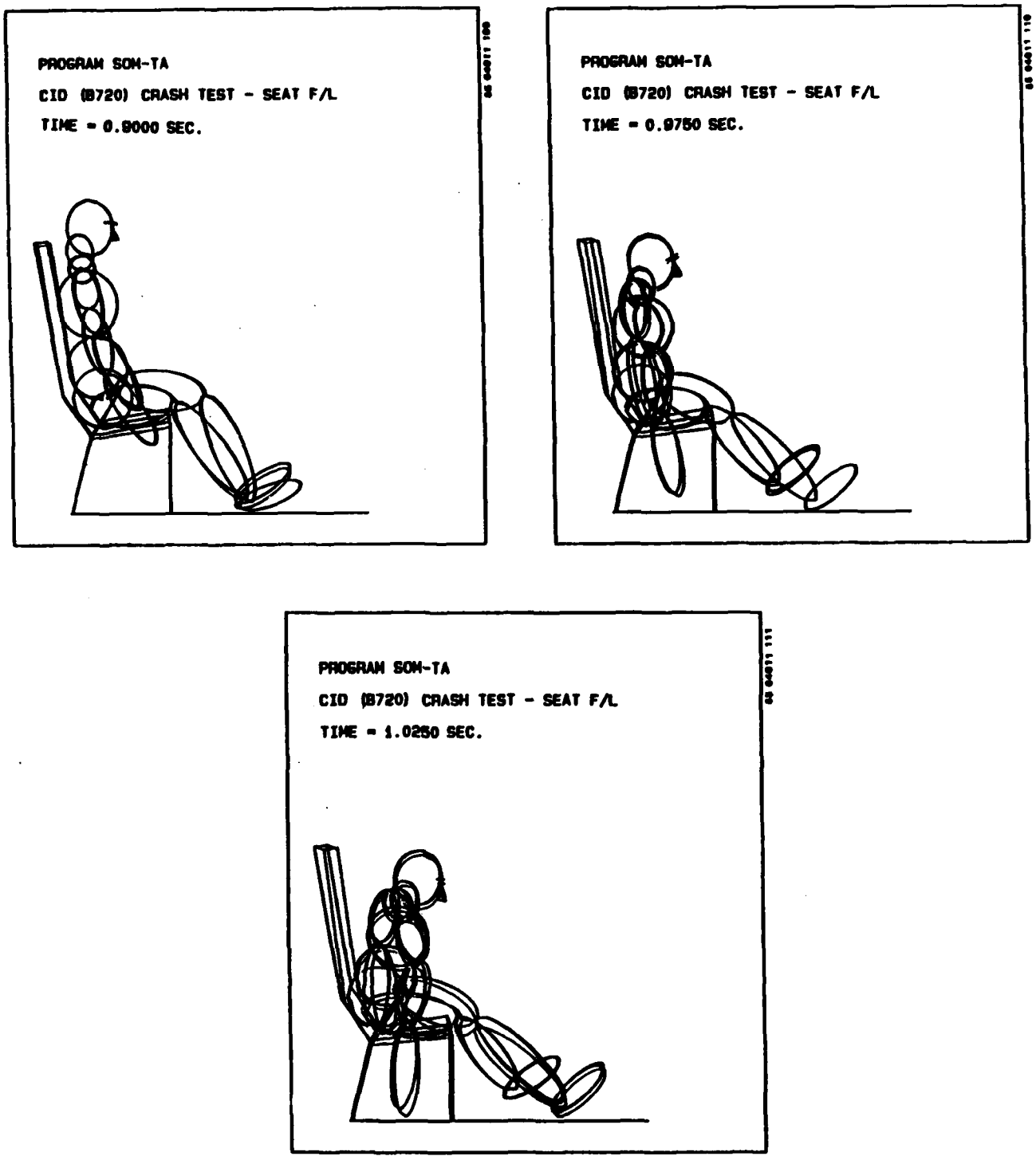

Figure F-35 (contd). Modified UOP 901 seat (F/L), Program SOM-TA predicted occupant response (side view).

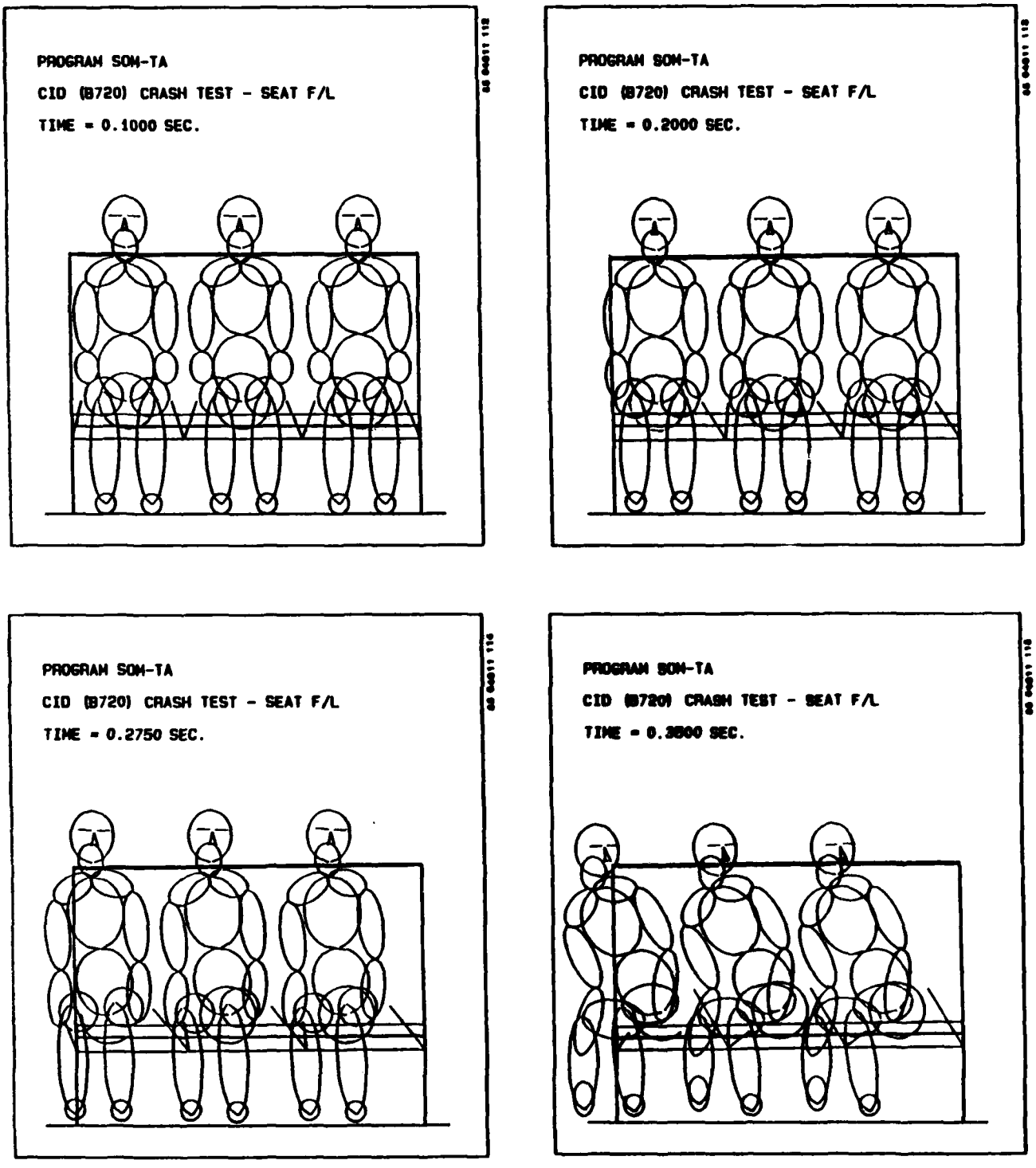

Figure F-36. Modified UOP 901 seat (F/L), Program SOM-TA predicted occupant response (front view).

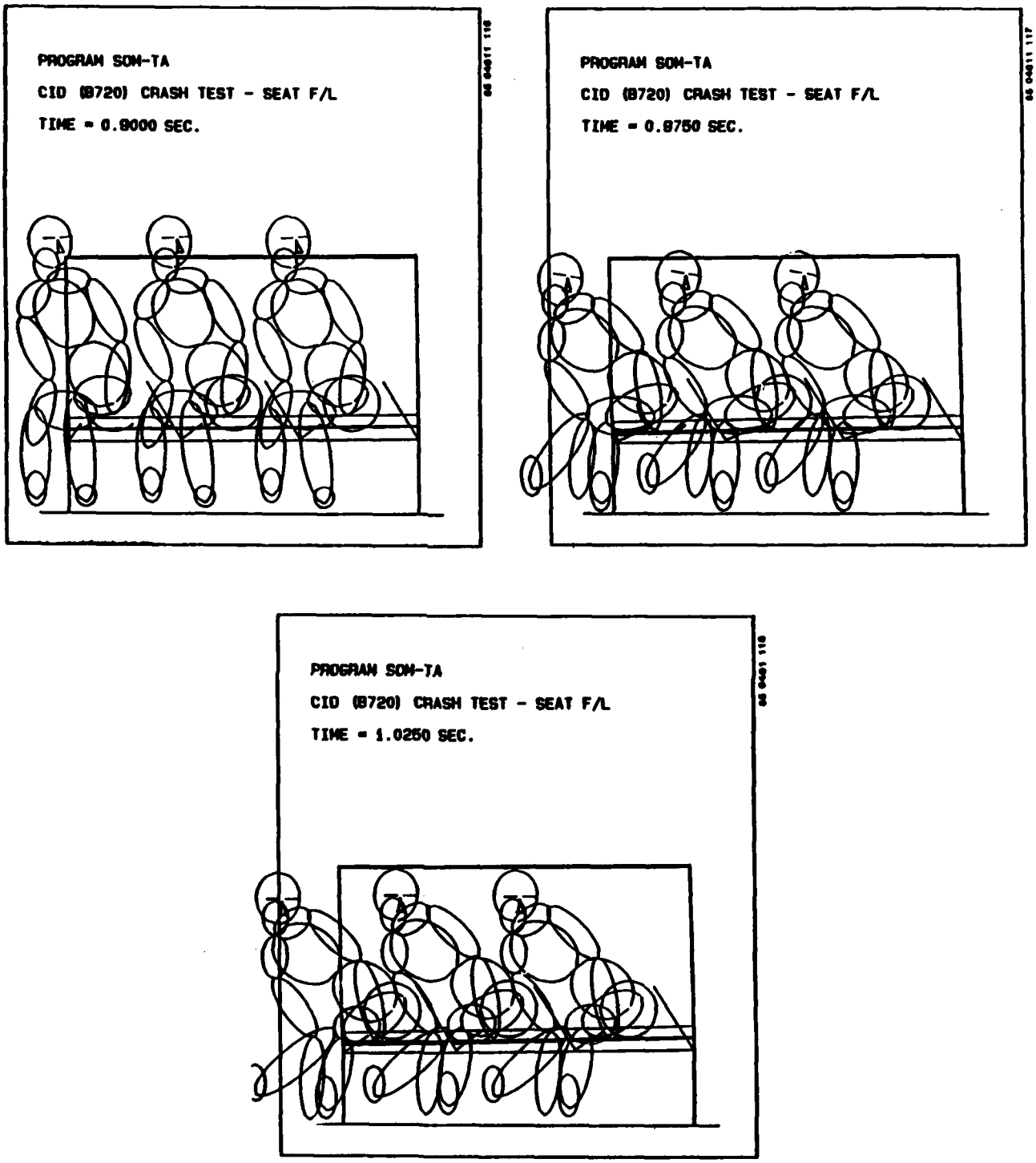

Figure F-36 (contd). Modified UOP 901 seat (F/L), Program SOM-TA predicted occupant response (front view).

APPENDIX G

STANDARD DISTRIBUTION LIST

Region Libraries

Alaska	AAL-64
Central	ACE-66
Eastern	AEA-62
Great Lakes	AGL-60
New England	ANE-40
Northwest-Mountain	ANM-60
Western-Pacific	AWP-60
Southern	ASO-63d
Southwest	ASW-40

Center Libraries

Technical Center	ACT-64
Aeronautical Center	AAC-44.4

Civil Aviation Authority
Aviation House
129 Kingsway
London WC2B 6NN England

Embassy of Australia
Civil Air Attache
1601 Mass Ave. NW
Washington, D. C. 20036

Scientific & Tech. Info FAC
Attn: NASA Rep.
P.O. Box 8757 BWI Aprt
Baltimore, Md. 21240

DOT-FAA AEU-500
American Embassy
APO New York, N. Y. 09667

Headquarters (Wash. DC)

ADL-1
ADL-32 (North)
APM-1
APM-13 (Nigro)
ALG-300
APA-300
API-19
AAT-1
AWS-1
AES-3

OST Headquarters Library

M-493.2 (Bldg. 10A)

University of California
Sers Dpt Inst of Trsp Std Lib
412 McLaughlin Hall
Berkely, CA 94720

British Embassy
Civil Air Attache ATS
3100 Mass Ave. NW
Washington, DC 20008

Dir. DuCentre Exp DE LA
Navigation Aerineene
941 Orly, France

Northwestern University
Trisnet Repository
Transportation Center Lib.
Evanston, Ill. 60201

DISTRIBUTION LIST

GOVERNMENT	No. of Copies
FAA NATIONAL HEADQUARTERS 800 Independence Ave., SW Washington, DC 20591 ATTN: Thomas McSweeney, AWS-100 (2) Phil Akers, AWS-120 (2) Raymond Ramaskis, AWS-300 (2) Leo Weston, AWS-340 (10) Angelo Masstrulo, AWS-340 (50)	66
FAA CENTRAL REGION HEADQUARTERS 601 East 12th Street Federal Building Kansas City, MO 64106 ATTN: John Reebling, ACE-250 (2) Walter Horn, ACE-115C (2)	4
FAA ALASKAN REGION HEADQUARTERS 701 C Street, Box 14 Anchorage, AL 99513 ATTN: Paul Donohoe, AAL-250 (2)	2
FAA MIKE MONRONEY AERONAUTICAL CENTER P.O. Box 25082 Oklahoma City, OK 73125 ATTN: Lyle Combs, AAC-950 (2)	2
FAA WESTERN-PACIFIC REGION HEADQUARTERS P.O. Box 92007 Worldway Postal Center Los Angeles, CA 90009 ATTN: William Sullins, AWP-250 (2)	2

FAA SOUTHWEST REGION HEADQUARTERS 2
P.O. Box 1689
Fort Worth, TX 76101

ATTN: George House, ASW-250 (2)

FAA SOUTHERN REGION HEADQUARTERS 2
3400 Norman Berry Drive
P.O. Box 20636
Atlanta, GA 30320

ATTN: George Mattern, ASW-250 (2)

FAA NORTHWEST MOUNTAIN REGION HEADQUARTERS 2
17900 Pacific Highway South
C-68966
Seattle, WA 98168

ATTN: Stanley Magnuson, ANM-250 (2)

FAA NEW ENGLAND REGION HEADQUARTERS 2
12 New England Executive Park
Burlington, MA 01803

ATTN: Gerald Nash, ANE-250 (2)

FAA GREAT LAKES REGION HEADQUARTERS 2
O'Hare Lake Office Center
2300 East Devon Avenue
Des Plaines, IL 60018

ATTN: Roger Gordon, AGL-250 (2)

FAA EASTERN REGION HEADQUARTERS 2
JFK International Airport
Fitzgerald Federal Building
Jamaica, NY 11430

ATTN: Arvid Hanson, AES-250 (2)

FAA EUROPEAN OFFICE HEADQUARTERS — 2
15 Rue de la Loi (3rd Floor)
B-1040 Brussels, Belgium
c/o American Embassy APO, NY 09667

ATTN: Joseph Pontecorvo, AEU-250 (2)

DOT TRANSPORTATION SYSTEMS CENTER — 20
Kendall Square
Cambridge, MA 02142

ATTN: Steve Bobo, DTS-48 (20)

FAA LOS ANGELES AIRCRAFT CERTIFICATION OFFICE — 2
4344 Donald Douglas Drive
Long Beach, CA 90808

ATTN: Anthony Bonano, ANM-130L (2)

USAF FLIGHT DYNAMICS LAB. — 8
Wright Patterson AFB, OH 45433

ATTN: Paul Wagner, AFWAL/FIEM (2)
Igors Skribliss, AFWAL/FIEM (2)
Avar Peterson, AFWAL/FIEM (2)
Bruce Tremblay, ASD/ENFE (2)

NATIONAL AERONAUTICS AND SPACE ADMINISTRATION — 2
Mail Stop 497
Langley Rearch Center
Hampton, VA 23665

ATTN: John Tanner (2)

CIVIL AVIATION AUTHORITY — 2
CAA Brabazon House
Redhill, Surrey U.K. RH1SQ

ATTN: Roger Christmas (2)

NONGOVERNMENT

ATTN: Thomas Dwenger 2
Goodyear Tire Company
1144 East Market STreet
Akron, OH 44316

ATTN: Richard R. Batten 2
TWA
KC International Airport
Kansis City, MO 64195

ATTN: Harry Davis 2
TATCO
7775 N.W. 12th Street
Miami, FL 33120

ATTN: Yukio Tadokoro 2
C/O Harry Davis, TATCO
7775 N.W. 12th Street
Miami, FL 33120

ATTN: Dave Lundquist 2
American Airlines
P.O. Box 582809
Tulsa, OK 74158-2809

ATTN: Gregory L. Felder 2
B.F. Goodrich
500 S. Main Street
Akron, OH 44318

ATTN: Ronald L. Olds 2
Michelin Tire Corp.
Patewood Exec. Park
P.O. Box 19001
Greenville, SC 29602

ATTN: Neal Billeran
McDonnell Douglas Corp.
3855 Lakewood Blvd.
Mail Code 36-94
Long Beach, CA 90846

2

ATTN: Prof. S. K. Clark
Mech. Eng./Appl. Mech.
315 Auto Lab.
University of Michigan
Ann Arbor, MI 48109

2

ATTN: W. E. Dunning
C1-250, Mail Code 36-94
Douglas Aircraft Co.
3855 Lakewood Blvd.
Long Beach, CA 90846

2

ATTN: Stanley Glen Mays
Sir Treads Inc.
P.O. Box X
5075 Pine Tree Street
Forest Park, GA 30051

2

ATTN: Dave Zitzman
Goodyear Tire & Rubber Co.
1144 E. Market Street
Akron, OH 44316

2

ATTN: W. C. Shaver
Air Treads, Inc.
1864 Sullivan Road
College Park, GA 30337

2

ATTN: Carl Topinka
Eng. Dept. 178
Cessna
P.O. Box 7704
Wichita, KS 67277

2

ATTN: W. W. Witt
United Air Lines/SFOEG
San Francisco National Airport
San Francisco, CA 94128 — 2

ATTN: Charles Westlund
1250 Knoxville Avenue
Long Beach, CA 90815 — 2

ATTN: Yosekui Okado
Bridgestone Research Inc.
P.O. Box 66120
Washington, DC 22035 — 2

☆ U.S. GOVERNMENT PRINTING OFFICE: 1986—605-071/40075

END

10-86

DTIC